



Investigation of candidate risk genes for neuropsychiatric disease *in vitro* and *in vivo* using ENU mutagenesis

A thesis presented for the degree of

Doctor of Philosophy

Eleanor Hobbs BSc

St Cross College

Word count: 49,674 words (approx.)

Abstract

Schizophrenia is a complex mental disorder characterised by positive symptoms such as hallucinations and psychosis, negative symptoms such as avolition and anhedonia, and cognitive defects. Schizophrenia risk has a genetic component, and it is likely that this is caused by interaction between numerous genes with individually small effects. Environment also plays a role; factors associated with schizophrenia include drug use, prenatal stressors and living environment.

Candidate genes linked to schizophrenia have been identified through recent GWAS of human populations with the disorder, including *ANK3, TCF4* and *CACNA1C.* GWAS associations alone are not sufficient to identify these as definitive risk genes for the disease. In order to validate these findings, animal models (in particular the mouse) can be used to study the effect of mutations in these genes of interest. Knockouts of these genes in the mouse are lethal, so we have used the ENU mutagenesis DNA archive at MRC Harwell to screen for additional allelic variants expressing more subtle and varied behavioural phenotypes. Endophenotypes associated with schizophrenia and bipolar disorder, such as anxiety, cognitive deficits and sensorimotor gating deficits, can be characterised in these mutants and, together with molecular characterisation, this can validate these genes as risk factors. While mutations in *Ank3* and *Tcf4* proved to be non-functional, two mutations in *Cacna1c* have been associated with anxiety phenotypes and differences in EEG power spectra, as well as causing a cardiac phenotype.

Acknowledgements

I would like to thank my supervisors, Dr Patrick Nolan and Dr Michael Parsons, for the opportunity to work on this project within the Neurobehavioural Genetics group. Their guidance and training have been invaluable and I have been able to learn new and challenging techniques and skills, as well as beginning and developing my scientific career.

I would like to thank everyone who I have worked with within the course of my DPhil, especially the members of the Neurobehavioural Genetics group past and present and particularly Dr Gareth Banks and Dr Inés Heise for their guidance and Michelle Stewart for her immeasurable phenotyping knowledge. I would also like to express my gratitude to the animal technicians who looked after my mice, particularly Greg Joynson and Lucie Vizor. I would also like to thank the students at MRC Harwell, whose support and friendship help make the Unit a welcoming and exciting place to work.

I would like to thank the Medical Research Council and the University of Oxford for their funding and support of my DPhil. I would also like to acknowledge the Brain and Behaviour Research Foundation, whose funding also supported this work, and Valter Tucci and Glenda Lassi, who contributed both funding and experimental data to this project.

Finally, I would like to thank my family and Ross, who have given me love, support, and encouragement throughout.

Statement of Work

The EEG experiments in this work were carried out in collaboration with Dr Valter Tucci and Dr Glenda Lassi from the Istituto Italiano di Tecnologia. Data were analysed by Ilaria Cosentini.

My colleague Dr Gareth Banks coordinated and assessed the circadian data and Dr Inés Heise assessed sleep screen data. Sara Wells and the team from Ward 4 in the Mary Lyon Centre took care of the mouse welfare. Echocardiogram and electrocardiogram were carried out and analysed by Dr Heather Cater, Thomas Nicol, and the phenotyping team in the MLC.

Archive screening of *Cacna1c* was carried out by Tom Nicols and screening of *Tcf4* was carried out by Dr Michael Parsons.

Table of Contents

Abstract i

Acknowledgements ii

Statement of Work iii

Table of Contents iv

Table of Figures xii

Abbreviations xvi

1 Introduction 1

1.1 Schizophrenia 1

1.1.1 Incidence, Prevalence and Mortality 1

1.1.2 Clinical presentation and symptoms 4

1.1.3 Treatment of schizophrenia 9

1.1.4 Co-morbidity 10

1.1.5 Pathophysiology 12

1.2 Aetiology of schizophrenia 16

1.2.1 Environmental component 17

1.2.2 Genetic component 18

1.2.3 Genetic hits for schizophrenia 20

1.2.4 Genome-wide association studies 21

1.2.5 Validation of GWAS results 23

1.3 Animal models of psychiatric disease 23

1.3.1 General limitations of mouse models 24

1.3.2 Can we make a schizophrenic mouse? 25

1.3.3 Construct validity 26

1.3.4 Face validity 28

1.3.5 Predictive validity 32

1.3.6 Limits of traditional knock-out models 33

1.4 ENU mutagenesis 34

1.4.1 Large-scale mutagenesis screens 34

1.5 Investigation of three candidate genes 39

1.6 Project Overview and Aims 40

1.7 *ANK3* 42

1.7.1 Overview of the *ANK* gene family 42

1.7.2 Protein Structure of 480/270kDa Ankyrin$_G$ 46

1.7.3 Ankyrin$_G$ in the axon initial segment 49

1.7.4 Ankyrin$_G$ in the node of Ranvier 54

1.7.5 Ankyrin$_G$ potentially plays other roles in the nervous system 55

1.7.6 GWAS identify ankyrin$_G$ as a risk factor for psychiatric disease 55

1.7.7 Knocking out *Ank3* causes homozygous lethality 57

1.7.8 Hypothesis 58

1.8 *TCF4* 59

1.8.1 Helix-loop-helix proteins 59

1.8.2 TCF4's role in lymphopoiesis and EMT 62

1.8.3 TCF4 in neurodevelopment 62

1.8.4 Haploinsufficiency of TCF4 causes Pitt-Hopkins Syndrome 63

1.8.5 Common variants in TCF4 are associated with schizophrenia 64

1.8.6 Novel mutations in *Tcf4* identified using ENU mutagenesis 66

1.8.7 Hypothesis 67

1.9 *CACNA1C* 68

1.9.1 Nomenclature of Ca_v Channels 68

1.9.2 Subunits of the Ca_v1 channel complex 70

1.9.3 The α_1 subunit 70

1.9.4 Localisation of $Ca_v1.2$ in the brain 70

1.9.5 Structure of the $Ca_v1.2$ subunit 71

1.9.6 Voltage Gating of $Ca_v1.2$ 72

1.9.7 Calcium-dependent inactivation of $Ca_v1.2$ 72

1.9.8 Cleavage and autoregulation of $Ca_v1.2$ 77

1.9.9 Calcium influx triggers changes in transcription 78

1.9.10 *CACNA1C* identified as risk factor in neuropsychiatric disease 81

1.9.11 Timothy Syndrome is caused by a gain of function mutation 82

1.9.12 Studies in mouse 83

1.9.13 ENU mutations discovered in the IQ domain of *Cacna1c* 85

1.9.14 Hypothesis 87

2 General Methods 89

2.1 Animal husbandry 89

2.2 Primary Phenotyping Battery 89

2.2.1 SHIRPA 89
2.2.2 Open Field 90
2.2.3 Acoustic Startle and Prepulse Inhibition (PPI) 91
2.2.4 Fear Conditioning 94
2.2.5 Circadian Phenotyping 96
2.2.6 Video tracking as a correlate of sleep 97
2.3 Secondary Phenotyping Battery 101
2.3.1 Light-Dark Box 101
2.3.2 Elevated Nought Maze 101
2.4 Heart phenotyping 103
2.4.1 Echocardiogram 103
2.4.2 Electrocardiogram (ECG) 104
2.5 Molecular Studies 105
2.5.1 Genomic DNA extraction from embryonic and adult tissue 105
2.5.2 Agarose gel electrophoresis 105
2.5.3 Purification of PCR Products 105
2.5.4 Gel extraction 105
2.5.5 Two-step reverse transcription 106
2.5.6 TOPO Cloning 107
2.5.7 Plasmid amplification and midiprep 108
2.5.8 Site-directed mutagenesis (SDM) 109
2.6 Tissue culture 110

2.7 Statistical analyses 110

2.8 *Ank3* 111

2.8.1 The ENU-mutagenised archive 111

2.8.2 Screening of the ENU-mutagenised DNA archive using PCR 111

2.8.3 Sequence alignments and conservation analysis 113

2.8.4 Site-directed mutagenesis 113

2.8.5 Re-derivation of mutation 114

2.8.6 Genotyping Assays 114

2.8.7 Behavioural Phenotyping 115

2.8.8 Sleep and Circadian Screens 115

2.9 *Tcf4* 116

2.9.1 Sequence alignments and conservation analysis 116

2.9.2 Site-directed mutagenesis of *Tcf4* 116

2.9.3 Prediction of post-translational phosphorylation 117

2.9.4 Luciferase reporter gene assays 118

2.9.5 Re-derivation of mutation 122

2.9.6 Genotyping Assays 122

2.9.7 Behavioural Phenotyping 123

2.9.8 Sleep and Circadian Screens 123

2.10 *Cacna1c*^{Q1625STOP} 124

2.10.1 Genotyping Assay 124

2.10.2 Timed matings to assess perinatal lethality 125

2.10.3 Behavioural Phenotyping 125
2.10.4 Secondary Behavioural Phenotyping 126
2.10.5 Sleep and Circadian Screens 126
2.10.6 EEG Recording 126
2.11 *Cacna1c*^{G1616D} 129
2.11.1 Genotyping Assay 129
2.11.2 Behavioural Phenotyping 130
2.11.3 Echocardiogram 130
2.11.4 Electrocardiogram (ECG) 130
2.11.5 Secondary Behavioural Phenotyping 130
2.11.6 Sleep and Circadian Screens 131
2.11.7 EEG Recording 131
3 *Ank3* 132
3.1 Introduction 132
3.2 Results: Archive Screen 132
3.2.1 Archive screen identifies three novel non-synonymous mutations 132
3.2.2 Sequence analysis of novel mutations 133
3.2.3 *In vitro* cloning of *Ank3* proved unsuccessful 134
3.2.4 ENU-induced mutation *Ank3*^{D1056G} was chosen for re-derivation 134
3.3 Results: Phenotyping 138
3.3.1 *Ank3*$^{D1056G/D1056G}$ mice are viable to adulthood 138
3.3.2 *Ank3*$^{D1056G/D1056G}$ mice show no behavioural phenotype 139

3.4 Discussion 148

4 *Tcf4* 150

4.1 Introduction 150

4.2 Results 151

4.2.1 *In vitro* prioritisation 151

4.2.2 *Tcf4*$^{S275R/S275R}$ mice are viable to adulthood 156

4.2.3 *Tcf4*$^{S275R/S275R}$ mice show no behavioural phenotype 156

4.3 Discussion 165

5 *Cacna1c*^{Q1625STOP} 168

5.1 Introduction 168

5.2 Results 169

5.2.1 *Cacna1c*$^{Q1625STOP/Q1625STOP}$ animals die before weaning 169

5.2.2 *Cacna1c*$^{Q1625STOP/+}$ animals show behavioural phenotypes 169

5.2.3 Circadian Rhythms and Sleep in *Cacna1c*$^{1625STOP/+}$ mice 183

5.3 Discussion 191

6 *Cacna1c*^{G1616D} 201

6.1 Introduction 201

6.2 Results: *Cacna1c*^{G1616D} 203

6.2.1 *Cacna1c*$^{G1616D/G1616D}$ animals are viable to P21 203

6.2.2 *Cacna1c*$^{G1616D/G1616D}$ mice have changes in anxiety and learning .. 204

6.2.3 *Cacna1c*$^{G1616D/G1616D}$ mice display cardiac defects 214

6.2.4 Circadian Rhythms and Sleep in *Cacna1c*$^{1625STOP/G1616D}$ mice..... 218

6.3 Discussion 225

7 Discussion 232

7.1 Validity of ENU-induced single point mutations 232

7.1.1 Construct validity 232

7.1.2 Face validity 235

7.2 Limitations 240

7.2.1 Using the mouse to model psychiatric disorders 240

7.2.2 Impact of background strain and congenicity 240

7.2.3 Predictive Validity 243

7.3 Future Directions 243

7.3.1 Gene editing 244

7.3.2 Gene x environment interactions 245

7.4 Concluding Remarks 246

8 Bibliography 247

Table of Figures

Figure 1 Age of onset of schizophrenia. 4

Figure 2 Dimensional spectrum of affective and non-affective psychosis. 5

Figure 3 Mechanism of ENU mutagenesis 37

Figure 4 ENU mutagenesis and archive generation 38

Figure 5 Project overview 41

Figure 6 Ankyrin domains and homology. 44

Figure 7 Alignment of human ANK3 transcripts showing the main domains. 45

Figure 8 Isoforms of ankyrin$_G$. 46

Figure 9 Establishment of neuronal polarity and formation of the AIS 50

Figure 10 Ankyrin$_G$ forms a subcellular scaffold at the AIS. 51

Figure 11 bHLH Proteins. 61

Figure 12 Phylogeny of Ca_v α1 subunits. 69

Figure 13 Schematic of Ca_v1.2 channel and associated subunits 71

Figure 14 Co-ordination of Ca^{2+} by a canonical EF-hand. 74

Figure 15 Mechanism of CDI. 76

Figure 16 Cleavage of the distal C-terminus of Ca_v1.2 by calpain. 78

Figure 17 Calcium signalling leads to induction of immediate-early genes. 80

Figure 18 The IQ Domain and *Cacna1c*^{Q1625STOP} mutation. 86

Figure 19 IQ domain of Ca_v1.2 and the *Cacna1c*^{G1616D} mutation. 87

Figure 20 Open Field Arena 91

Figure 21 Trial types of the acoustic startle & pre-pulse inhibition test. 94

Figure 22 Timing of tones, shocks, and inter-trial intervals in fear conditioning. 96

Figure 23 Circadian Screening 97

Figure 24 Sleep set-up with light-tight chambers and individual cages. 100

Figure 25 Schematic drawing illustrating the timeline of the sleep screens. 100
Figure 26 Secondary tests of anxiety 102
Figure 27 Settings for analysis of ECG recordings using LabChart 8. 104
Figure 28 Zappo colour scheme 113
Figure 29 Difference Curves identify novel mutations in exons of Ank3. 136
Figure 30 Novel mutations identified in the ENU-mutagenised DNA archive are in conserved regions. 138
Figure 31 Survival at 21 days post-birth. 138
Figure 32 *Ank3*$^{D1056G/D1056G}$ mice do not show any behavioural differences. 144
Figure 33 Unconditioned response to the cue. 145
Figure 34 *Ank3*$^{D1056G/D1056G}$ mice show no change in circadian period or rhythmicity. 146
Figure 35 *Ank3*$^{D1056G/D1056G}$ mice show no differences in sleep screens. 147
Figure 36 Sequence alignment of TCF4. 154
Figure 37 Dual-reporter gene assays show differences in transcriptional activation. 155
Figure 38 Survival of homozygous *Tcf4*$^{S275R/S275R}$ mice. 156
Figure 39 Behavioural Phenotyping of *Tcf4*$^{S275R/S275R}$ mice. 161
Figure 40 Unconditioned response to the cue. 162
Figure 41 *Tcf4*$^{S275R/S275R}$ mice show no change in circadian period or rhythmicity. ... 163
Figure 42 S *Tcf4*$^{S275R/S275R}$ mice show no differences in sleep screens. 164
Figure 43 The IQ Domain and *Cacna1c*^{Q1625STOP} mutation. 168
Figure 44 Homozygous *Cacna1c*$^{Q1625STOP/Q1625STOP}$ mice do not survive to weaning. 172
Figure 45 Locomotor activity in the SHIRPA test. 173
Figure 46 *Cacna1c*$^{Q1625STOP/+}$ animals have increased anxiety and reduced exploratory behaviour. 175

Figure 47 Light-Dark Box and Elevated Nought Maze validate the anxiety phenotype 176
Figure 48 *Cacna1c*$^{Q1625STOP/+}$ animals show mild changes in startle response. 178
Figure 49 *Cacna1c*$^{Q1625STOP/+}$ mice show differences in freezing. 180
Figure 50 Unconditioned response to the cue. 180
Figure 51 The *Cacna1c*^{Q1625STOP} mutation does not cause defects in heart function. 182
Figure 52 *Cacna1c*$^{Q1625STOP/+}$ mice show no difference in circadian period. 183
Figure 53 Minor differences in immobility revealed by a video-tracked Sleep Screen. 186
Figure 54 EEG Recordings show a reduction in delta frequencies in *Cacna1c*$^{Q1625STOP/+}$ mice. 189
Figure 55 Delta power is decreased in *Cacna1c*$^{Q1625STOP/+}$ mice. 190
Figure 56 IQ domain of $Ca_v1.2$ and the *Cacna1c*^{G1616D} mutation. 202
Figure 57 *Cacna1c*$^{G1616D/G1616D}$ mice are viable to P21. 203
Figure 58 Locomotor activity in the SHIRPA test 206
Figure 59 *Cacna1c*$^{G1616D/G1616D}$ mice show mildly reduced anxiety in Open Field. 208
Figure 60 *Cacna1c*$^{G1616D/G1616D}$ mice show a trend towards increased anxiety in other tests of anxiety. 209
Figure 61 Acoustic Startle PPI and Fear Conditioning of *Cacna1c*$^{G1616D/G1616D}$ mice 212
Figure 62 Unconditioned response to the cue. 213
Figure 63 The ECG wave. 216
Figure 64 Heart defects in *Cacna1c*$^{G1616D/G1616D}$ revealed using echocardiogram and electrocardiogram. 217
Figure 65 *Cacna1c*$^{G1616D/G1616D}$ mice have normal circadian rhythms. 218

Figure 66 *Cacna1c*$^{G1616D/G1616D}$ mice have a shortened latency to immobility after LP2 onset. 221

Figure 67 *Cacna1c*$^{G1616D/G1616D}$ mice have a small but significant decrease in theta frequencies. 223

Figure 68 Delta power is normal in *Cacna1c*$^{G1616D/G1616D}$ mice. 224

Abbreviations

ACC	anterior cingulate cortex
ADHD	attention-deficit hyperactivity disorder
AIS	axon initial segment
AMPAR	α-amino-3-hydroxy-5-methyl-4-isoxazolepropionic acid receptor
ANK	ANKYRIN
ASD	autism spectrum disorder
BD	bipolar disorder
BDNF	brain-derived neurotrophic factor
bHLH	basic helix-loop-helix
CaM	calmodulin
CaMK	calmodulin kinase
Ca_v	Voltage-gated calcium channel
CBT	cognitive behavioural therapy
CCAT	calcium-channel associated transcription regulator
CDI	calcium-dependent inactivation
CNS	central nervous system
CNV	copy number variant
CREB	CRE-binding protein
CRY1	Cryptochrome-1
CT	circadian time
DALY	disability-adjusted life years
DD	death domain
DHP	dihydropyridine
DISC1	disrupted-in-schizophrenia 1
DLPFC	dorsolateral prefrontal cortex
dpc	days *post coitum*
DSM-V	*Diagnostic and Statistical Manual of Mental Disorders , 5th Edition*
ECG	electrocardiogram
EEG	electroencephalogram
EMG	electromyography
ENU	N-ethyl-N-nitrosourea
eQTL	expression quantitative trait locus
GABA	γ-Aminobutyric acid
GWAS	genome-wide association study
ID	intellectual disability
ID1-3	inhibitor of DNA-binding 1-3
IEG	immediate early gene
IgG	immunoglobulin-G
Indel	insertion-deletion
iPSC	induced pluripotent stem cell
IVC	individually ventilated cage
IVF	in vitro fertilisation
LTD	long-term depression
LTP	long-term potentiation
MAPK	mitogen-activated protein kinase
MATH1	mammalian atonal homolog 1

MBD	membrane-binding domain
MHC	major histocompatibility complex
miR137	micro-RNA 137
NIR	near infra-red
NLS	nuclear localisation signal
NMD	nonsense-mediated decay
NMDAR	N-methyl-D-aspartate receptor
NrCAM	neuronal cell adhesion molecules
NSCaTE	N-terminal Spatial Ca2+-transforming element
PCP	phencyclidine
PGK	phosphoglycerate kinase
PHS	Pitt-Hopkins Syndrome
PNS	peripheral nervous system
PPI	pre-pulse inhibition
pRGP	postnatal radial glial progenitor
RNAi	RNA interference
SAGA	SPT-ADA-GCnS-acetyltransferase
SBD	spectrin-binding domain
SCN	suprachiasmatic nucleus
SD	sleep deprivation
SHIRPA	SmithKline Beecham, Harwell, Imperial College, Royal London Hospital, phenotype assessment
shRNA	short hairpin RNA
siRNA	silencer RNA
SMR	standard mortality ratio
SNP	single nucleotide polymorphism
SWA	slow wave activity
TAD	transcriptional activation domain
TCF4	transcription factor 4
TS	Timothy Syndrome
VDI	voltage-dependent inactivation
VGCC	voltage-gated calcium channel
ZT	zeitgeber time

1 Introduction

Schizophrenia is a complex, heterogeneous disorder that affects behavioural and cognitive domains. It has a high burden both on individuals and on medical services. Schizophrenia arises through disruption of neurodevelopment caused by genetic and environmental factors. Defects in the dopaminergic system are associated with psychotic symptoms, but other brain regions and circuits are involved in negative and cognitive defects and the precise location, timing and nature of these is less clear. Genome-wide association studies have identified genetic variants associated with the disorder, and mouse models act as genetic tools to investigate these variants and genes.

1.1 Schizophrenia

1.1.1 Incidence, Prevalence and Mortality

The incidence of schizophrenia (the probability of occurrence in a population) varies depending on multiple factors including sex, ethnicity, place, and migration status. A review of incidence in England between 1950 and 2009 found an average incidence rate of 15.2 people per 100,000 person-years, with an increased incidence in several minority groups including the black Caribbean, black African and South Asian populations (Kirkbride et al., 2012, Tortelli et al., 2015). Incidence is higher in men with a male:female risk ratio of 1.4 (Kirkbride et al., 2006, McGrath et al., 2008). Incidence is dependent on socio-economic factors including levels of income inequality (Burns et al., 2014) and urbanicity (Pedersen and Mortensen, 2001) although the specific risk-modifying factor is still unclear.

Prevalence is a measure of how many people have a disease at a specific point in time (point prevalence), during a particular period (period prevalence) or have ever had the disease in their lifetime (lifetime prevalence). Meta-studies of schizophrenia research found that for schizophrenia the prevalence (median per 1000 people) varied across the globe (Saha et al., 2005, Simeone et al., 2015), but global averages were 4.6 (point), 3.3 (period), and 4.0 (lifetime) patients per 1000 (Saha et al., 2005). Prevalence was found to be higher in migrant populations and positively correlated with latitude, but there were no differences seen by sex or by urbanicity. Least-developed countries were also found to have a lower prevalence compared to emerging and developed countries (Saha et al., 2005, McGrath et al., 2008). Why the observed incidence and the prevalence findings differ is still an ongoing question in schizophrenia research and is probably due to multiple aetiological and outcome differences.

Mental and behavioural disorders account for 8.6 million years of life lost to premature mortality, which was equivalent to 232,000 deaths in 2010 (Whiteford et al., 2013, Chesney et al., 2014). Mental and substance abuse disorders are the leading cause of years lived with disability worldwide, and schizophrenia accounts for 7.4% of disability-adjusted life years (DALYs) (Whiteford et al., 2013). The all-cause standard mortality ratio (SMR) in schizophrenia is 2.6%, meaning that patients with schizophrenia are over twice as likely to die as a person in the general population (Saha et al., 2007, Chesney et al., 2014). This higher mortality risk translates into approximately 15 years reduction in life expectancy (Chesney et al., 2014). While suicide is associated with the highest SMR of 12.9%, many patients with schizophrenia also have at least one chronic co-morbid condition including diabetes,

cardiovascular disease or metabolic syndrome (Mitchell and Malone, 2006), and most major causes-of-death categories are elevated in patients (Saha et al., 2007).

1.1.1.1 Age of Onset

The peak of incidence of schizophrenia in men and women is in early adulthood (20-29 years), and there is a second peak in women between 30 and 39 years (Figure 1) (van der Werf et al., 2014). Early adulthood follows adolescence, which is a critical period of neurodevelopment (Paus et al., 2008) during which the brain undergoes structural changes. Grey matter, which increases during childhood and peaks around puberty onset, declines in the frontal and parietal lobe during adolescence (Giedd et al., 1999). It has been hypothesised that the brain undergoes synaptic pruning, and that schizophrenia arises due to a developmental disturbance or over-pruning (Feinberg, 1982, Keshavan et al., 1994). White matter, on the other hand, increases in volume into adulthood and regions of the brain go through differential functional maturation, with sensorimotor areas maturing first followed by regions involved in executive function and visual processing (Paus, 2005, Paus et al., 2008). Schizophrenia appears to exaggerate the normal adolescent brain changes; in early-onset cases, there is progressive grey matter volume loss, as is usually seen in adolescence (Sporn et al., 2003, Kyriakopoulos and Frangou, 2007). Another change observed in adolescence is a decrease in slow-wave sleep, and these decreases are larger in patients with schizophrenia (Keshavan et al., 1998).

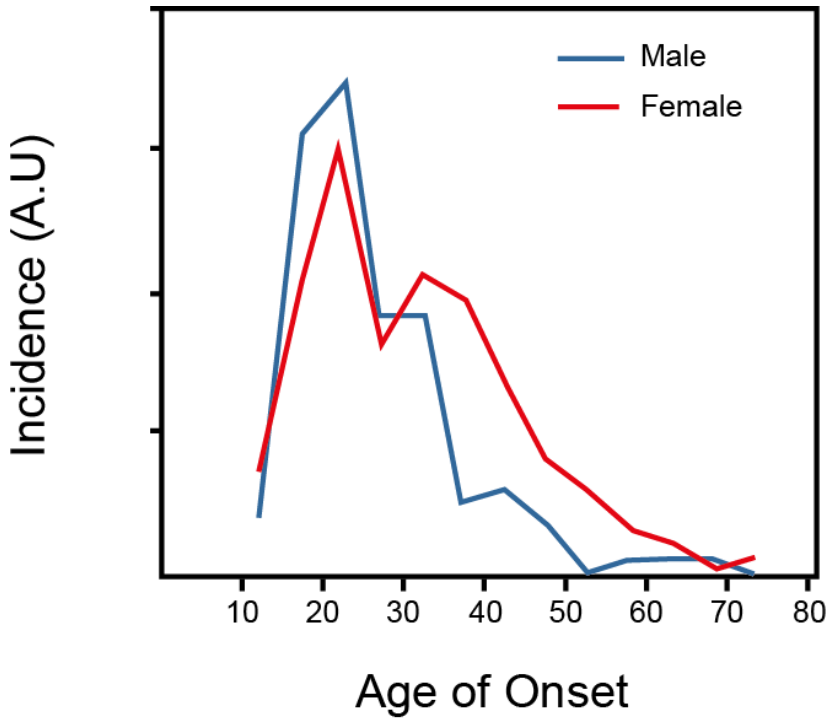

Figure 1 Age of onset of schizophrenia.

Incidence is highest between the ages of 20 and 30. Although many studies have measured age of onset in cohorts, there are no data for age of onset worldwide. Adapted from Sham et al. (1994)

1.1.2 Clinical presentation and symptoms

According to the 5th edition of the *Diagnostic and Statistical Manual of Mental Disorders (*DSM-V)(American Psychiatric Association, 2013) schizophrenia is characterised by positive symptoms (delusions, hallucinations and psychosis), negative symptoms (impaired motivation, reduction in spontaneous speech, and social withdrawal) and cognitive impairment, summarised in Table 1 (American Psychiatric Association, 2013, Tandon et al., 2013b). The disorder usually presents during late adolescence and is often preceded by a prodromal or pre-psychosis phase. Positive symptoms often recede and are amenable to treatment by antipsychotics, while negative symptoms and cognitive impairment are chronic conditions and their pathophysiology is less well understood (reviewed in Owen et al. (2016)). A diagnosis of schizophrenia is based on medical history and mental state,

and there are no diagnostic tests or biomarkers that are currently available. It is also becoming clear that the borders of a schizophrenia diagnosis are not clear-cut. Psychosis can occur in both non-affective (schizophrenia) and affective disorders (bipolar disorder with psychosis), and a diagnosis is made based on the presence of negative or affective symptoms (Figure 2) (van Os and Kapur, 2009). Many patients present with a degree of both negative and affective symptoms, or show varying symptoms at different points in their life. Some effort has been made to accommodate this overlap, for example, the diagnosis of schizotypal disorder, which has elements of both schizophrenia and bipolar disorder, but this only goes some way to addressing the cross-boundary symptoms (van Os and Kapur, 2009). It has also been shown that up to 8% of the general population experience attenuated hallucinations and delusions, suggesting that the border between schizophrenia and 'wellness' is also blurred (Owen et al., 2016).

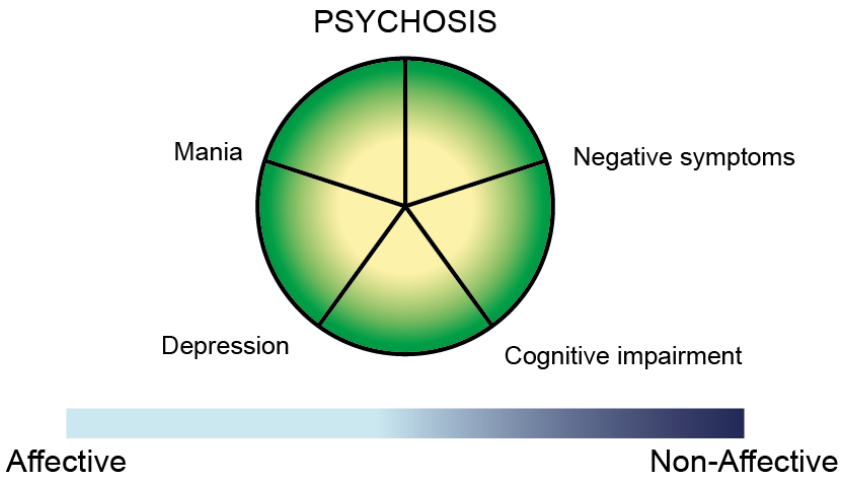

Figure 2 Dimensional spectrum of affective and non-affective psychosis.

Patients diagnosed with psychosis are assessed on five dimensions of psychopathology. If scores are weighted towards non-affective symptoms, the patient will be diagnosed with schizophrenia if all other clinical criteria are met.

Criteria	Details
Criterion A. Characteristic symptoms:	Two (or more) of the following, each present for a significant portion of time during a 1-month period (or less if successfully treated).
	At least one of these should include 1–3 1. Delusions 2. Hallucinations 3. Disorganised speech 4. Grossly disorganised or catatonic behaviour 5. Negative symptoms (i.e., diminished emotional expression or avolition)
Criterion B. Social/occupational dysfunction:	For a significant portion of the time since the onset of the disturbance, one or more major areas of functioning, such as work, interpersonal relations, or self-care, are markedly below the level achieved prior to the onset
Criterion C. Duration of 6 months.	This 6-month period must include at least 1 month of symptoms (or less if successfully treated) that meet Criterion A (i.e., active-phase symptoms) and may include periods of prodromal or residual symptoms.
Criterion D. Schizoaffective and mood disorder exclusion.	Schizoaffective disorder and depressive or bipolar disorder with psychotic features have been ruled out
Criterion E. Substance/general medical condition exclusion:	The disturbance is not attributed to the direct physiological effects of a substance or another medical condition.
Criterion F. Relationship to Global Developmental Delay or Autism Spectrum Disorder.	If there is a history of autism spectrum disorder or another communication disorder of childhood onset, the additional diagnosis of schizophrenia is made only if prominent delusions or hallucinations are also present for at least 1 month

Table 1 Diagnostic criteria for schizophrenia as described in the DSM-V

(Adapted from Tandon et al. (2013b))

1.1.2.1 Positive Symptoms

A schizophrenia diagnosis is usually based on the presence of positive symptoms including paranoid delusions or hallucinations (usually auditory), which are characterised by their bizarre content and mood-incongruence. Reality distortion and psychosis are generally observed during adolescence or early adulthood, although there may have been prodromal changes beforehand (Tandon et al., 2009, American Psychiatric Association, 2013, Owen et al., 2016). Of schizophrenia symptom domains, positive symptoms are the most responsive to antipsychotic medication, all of which act on the dopaminergic system as discussed below.

1.1.2.2 Negative Symptoms

Negative symptoms of schizophrenia are observed in two-thirds of patients with the disorder (Rabinowitz et al., 2013) and can be divided into two main domains: reduced emotional expression (including blunted affect and speech poverty) and reduced motivation and pleasure (anhedonia, avolition and apathy) (Tandon et al., 2009, Carbon and Correll, 2014). These domains also lead to social withdrawal and typically do not respond to antipsychotics. A higher burden of negative symptoms is associated with a negative treatment response and disease outcome and also correlates with the length of undiagnosed psychosis (Galderisi et al., 2013, Chang et al., 2013).

1.1.2.3 Cognitive Deficits

Cognitive impairments are highly prevalent to varying degrees in patients with schizophrenia and in premorbid patients (Keefe et al., 2005) and manifest in a generalised manner across domains as well as in specific cognitive functions (Lencz et al., 2006, Dickinson et al., 2008, Galderisi et al., 2009). There have been deficits

identified in episodic memory (Ranganath et al., 2008, Reichenberg and Harvey, 2007), information processing (Dickinson et al., 2007), verbal fluency (Henry and Crawford, 2005) and working memory (Barch and Smith, 2008, Dickinson et al., 2007). Cognitive impairments are also observed at a lower level of impact in non-psychotic relatives of patients with schizophrenia (Trandafir et al., 2006, Whalley et al., 2007, Smith et al., 2008), suggesting a continuum of symptoms which are genetically linked and discussed further in 1.2.

1.1.2.4 Impact of schizophrenia on quality of life

Although the prevalence of schizophrenia is on average less than 1%, it has a large impact on society due to the many functional impairments and the variable efficacy of treatment and diversity in outcome leading to reduced productivity and associated homelessness, unemployment and medical care. It is estimated to cost £11.8 billion a year in the United Kingdom (The Schizophrenia Commission, 2012). Unemployment is high, with less than a fifth of patients in full employment (Thornicroft et al., 2004, Rosenheck et al., 2006), and a higher cognitive impairment and worse negative symptoms are associated with a decreased likelihood of employment (Giugiario et al., 2012). Much of the burden of care falls upon family and support for carers is lacking (The Schizophrenia Commission, 2012). As well as this, patients often face stigma and discrimination. Antipsychotics also cause weight gain and increased cardiovascular risk (Foley and Morley, 2011), and patients have a low rate of diagnosis and treatment of other health problems including diabetes, hypertension and dyslipidaemia (Briskman et al., 2012).

1.1.3 Treatment of schizophrenia

1.1.3.1 Anti-psychotics

Antipsychotic medication is the first-line treatment offered to patients during their first episode of psychosis (Howes et al., 2009a, NICE, 2014). Symptoms usually respond after one to two weeks, although a third of patients show treatment resistance (Howes et al., 2009a). All licensed antipsychotics target and block dopamine receptors (Howes et al., 2009a). Typical antipsychotics were developed in the 1950s after the antipsychotic properties of reserpine were discovered to be due to its blocking of dopamine reuptake and subsequent dopamine dissipation (Carlsson et al., 1957). Typical antipsychotics (Carlsson and Lindqvist, 1963, Howes et al., 2009a) reduce the positive symptoms of schizophrenia but also cause multiple side effects mostly through extrapyramidal dopaminergic pathways, including stiffness, tardive dyskinesia, parkinsonism and akathisia (restless leg syndrome), as well as sexual effects and hyperprolactinaemia (Howes et al., 2009a).

Atypical or second-generation antipsychotics such as chlorpromazine are less likely to cause extrapyramidal side effects compared to haloperidol (a first-generation anti-psychotic), but have other effects such as weight gain, higher risk of stroke, tardive dyskinesia and neuroleptic malignant syndrome (Ucok and Gaebel, 2008, Howes et al., 2009a). Another atypical antipsychotic, clozapine, is used in treatment-refractory schizophrenia (Siskind et al., 2016) but can cause agranulocytosis, so patients must be monitored closely (Siskind et al., 2016). Clinical response to all antipsychotics correlates with D2 receptor binding and there is a threshold of occupancy of approximately 50%, above which efficacy is observed (Howes et al., 2009a). Unfortunately, a higher occupancy is also associated with a higher risk of

side effects and individual patient differences also influence the efficacy of treatment (Howes et al., 2009a). The dopaminergic system and its role in schizophrenia are discussed more in 1.1.5.2.

1.1.3.2 Psychological treatments

Alongside antipsychotics, patients are often encouraged to undergo psychological treatments including cognitive behavioural therapy (CBT). CBT can involve cognitive remediation, aiming to train patients to compensate for cognitive deficits, or cognitive training, which targets the underlying mechanisms of brain plasticity (Vinogradov and Schulz, 2016). Behavioural therapy has a modest benefit and can target sources of distress such as auditory hallucinations (Chadwick et al., 2016) and internalised stigma (Morrison et al., 2016). CBT may also be a promising intervention in individuals at high risk of developing psychosis (van der Gaag et al., 2012, Ising et al., 2016).

1.1.4 Co-morbidity

1.1.4.1 Psychiatric co-morbidity

Anxiety and depression are often observed in patients with schizophrenia and are associated with a poorer clinical outcome (Buckley et al., 2009, Braga et al., 2013, Tsai and Rosenheck, 2013). A small percentage of patients with intellectual disability (ID) have co-occurring schizophrenia, associated with greater disability and higher mortality rate (Tandon et al., 2009). 50% of people with schizophrenia also have a substance abuse disorder, and it is often difficult to distinguish between substance-induced or schizophrenic psychosis (Tandon et al., 2009). Substance use can also limit the effectiveness of antipsychotics and lead to worsening of psychosis, as well

as being a risk factor for the development of schizophrenia as discussed in section 1.2.1.

1.1.4.2 Medical co-morbidity

As detailed above, people with schizophrenia have a reduced life expectancy and greater risk of mortality than the general population. Some of this risk is due to suicide, but the majority of risk is caused by co-morbidity with chronic illnesses including cardiovascular disease and diabetes. Two-thirds of patients with schizophrenia die of coronary heart disease compared to half of the general population (Hennekens et al., 2005) due to increased risk factors such as smoking, obesity, alcohol consumption and hypertension (Newcomer, 2007, Megna et al., 2011, Laursen et al., 2012, Laursen et al., 2014). These have been shown to be underdiagnosed and undertreated (Briskman et al., 2012) and contribute to the increased mortality in people with schizophrenia. Antipsychotics also contribute to weight gain and obesity, and these conditions are linked to an increased healthcare burden (Cooper et al., 2016, Chwastiak et al., 2009).

1.1.4.3 Sleep and circadian rhythm disruption

Sleep or circadian disruptions are observed in up to 80% of patients with schizophrenia (Cohrs, 2008, Pritchett et al., 2012, Jagannath et al., 2013b). Circadian rhythms are 24-hour endogenous rhythms that in mammals arise from a transcriptional-translational feedback loop, wherein transcription factors CLOCK and BMAL1 drive expression of clock genes, which then feed, back and self-regulate their own expression. This process occurs in all cells and is synchronised by the suprachiasmatic nucleus (SCN), located in the ventral hypothalamus. The SCN is entrained by the light-dark cycle via the retina. Sleep homoeostasis is also important

in determining sleep and is sleep/wake-dependent – sleep pressure builds up over periods of wake and dissipates during sleep. Sleep disruption leads to cognitive problems including defects in memory consolidation and is caused by complex changes in brain region and neurotransmitter pathways.

Patients with schizophrenia have reported reduced sleep efficiency, reduced sleep time and increased sleep latency (Cohrs, 2008) and some studies have also observed differences in slow wave sleep (Feinberg et al., 1969, Kupfer et al., 1970, Sekimoto et al., 2007, 2011). Circadian disruptions have also been seen in patients with schizophrenia such as abnormal phasing, fragmentation and instability of rest-activity rhythms (Martin et al., 2001, Martin et al., 2005, Wulff et al., 2006, Wulff et al., 2009) and patients with co-morbid schizophrenia and sleep disruption often score badly on quality of life clinical subscales (Cohrs, 2008). It has been hypothesised that brain disorders and sleep disruption share a mechanistic origin and that some pathologies observed in schizophrenia arise from the disturbance of sleep mechanisms (Wulff et al., 2010) and, if this is the case, treatment and stabilisation of sleep may be an avenue to reduce the symptoms of schizophrenia.

1.1.5 Pathophysiology

1.1.5.1 Structural changes in the brain

In medicated patients, reductions in intracranial and total brain volumes are observed (Haijma et al., 2013). As described in 1.1.1.1, this is mostly due to grey matter reductions in patients with schizophrenia, and greater reductions are associated with a longer duration of illness and medication state. Grey matter reductions have been observed in multiple regions including the superior temporal gyrus and frontal, temporal and parietal lobes (Haijma et al., 2013, Vita et al., 2012).

First-generation antipsychotics are associated with a greater loss of grey matter compared to second-generation medications (Vita et al., 2015). White matter integrity is also disrupted in naïve first-episode patients (Lyu et al., 2015, Zhang et al., 2016) and a smaller effect is also observed in siblings of patients (Lyu et al., 2015). Increased ventricular volume has also been observed at disease onset (Vita et al., 1997, De Peri et al., 2012) and in patients with chronic schizophrenia (Vita et al., 1997, Shenton et al., 2001) but this is not observed in all patients (Shenton et al., 2001, John et al., 2015). There are as yet no anatomical or functional abnormalities identified that are specific to all schizophrenia cases (White et al., 2015, Linden, 2012) and this is probably due to the heterogeneous nature of schizophrenia and its overlapping borders with other psychiatric disorders and with the non-disease state (Owen et al., 2016).

1.1.5.2 The dopamine hypothesis

The proposed role of the dopaminergic system in schizophrenia is based on the action of antipsychotics in binding and blocking the D2/3 dopamine receptors, and the ability of dopaminergic system-activating drugs such as amphetamine to induce psychosis (Bonoldi and Howes, 2013, Howes and Murray, 2014). Dopamine is produced in neurons of the substantia nigra and ventral tegmental regions, and dopaminergic neurons then project to the nigrostriatal, mesolimbic and mesocortical systems. The dopaminergic system is important in regulating extrapyramidal movement and cognitive functions including motivation and reward associations (Luo and Huang, 2016). It has now been shown that there are only small alterations in D2/3 receptor expression and dopamine transporter availability in patients (Howes et al., 2012). Pre-synaptically, however, increased dopamine synthesis capacity, increased dopamine release and subsequently a higher baseline concentration of

dopamine have been observed in the striatum of patients with schizophrenia (Lyon et al., 2011, Howes et al., 2012) and molecular imaging has suggested presynaptic dysfunction as the basis of disease (Howes et al., 2009a, Lyon et al., 2011, Howes et al., 2012).

Dopamine concentration increase is also observed in prodromal patients who go on to develop psychosis (Howes et al., 2009b, Howes et al., 2011a, Howes et al., 2011b, Egerton et al., 2013). Levels of dopamine release are associated with disease state – a greater release is observed during acute psychosis and correlates with severity (Laruelle et al., 1999, Howes et al., 2011a). The dopamine hypothesis does not explain all the symptoms of schizophrenia; as discussed in 1.1.3.1 up to a third of patients do not respond to non-clozapine antipsychotics (Howes et al., 2009a, Mortimer et al., 2010) and treatment-resistant schizophrenia does not respond to depletion of presynaptic dopamine (Remington et al., 2012). Treatment-resistant patients also do not show an increase in striatal dopamine but do show an increase in glutamate (Demjaha et al., 2012, Demjaha et al., 2014). In terms of negative and cognitive symptoms of schizophrenia, clinical effects of antipsychotics are modest (Murphy et al., 2006) and treatment can worsen negative symptoms (Kim et al., 2013). Dopamine increase can also reduce negative symptoms (Laruelle et al., 1999) and it is thought that there are regionally selective changes in dopamine synthesis that must be taken into account when prescribing antipsychotics (Laruelle, 2014).

1.1.5.3 Glutamatergic signalling

Excitatory neurons in the brain are primarily glutamatergic, and make up 60-80% of the brain's metabolic activity (Kew and Kemp, 2005). One class of ionotropic glutamate receptor is the N-methyl-D-aspartate receptor (NMDAR). Drugs including phencyclidine (PCP) and ketamine are NMDAR antagonists and have been shown to

reproduce positive, negative and cognitive symptoms of schizophrenia such as poverty of speech and deficits in working memory and executive processing (Krystal et al., 1994, Lahti et al., 1995a, Lahti et al., 1995b, Malhotra et al., 1996, Umbricht et al., 2000, Parwani et al., 2005, Howes et al., 2015). This suggests that changes in NMDA receptor function may underlie symptoms of schizophrenia. Some studies have found an increase in NMDAR in post-mortem brains of patients, although findings have been inconsistent (McCullumsmith et al., 2012, Howes et al., 2015). It is thought that localisation of NMDAR may be aberrant and there may also be differences in glutamate transporter expression in patients with schizophrenia (Hammond et al., 2014). NMDAR antagonists have also been shown to cause cognitive deficits and hyperglutamatergic signalling in rodent (Harris et al., 2003, Kim et al., 2011, Featherstone et al., 2012) and primate models (Linn et al., 2007).

NMDA receptor full agonists such as glycine and D-serine reverse the effects of PCP in rodents and primates (Javitt et al., 2004, Linn et al., 2007), and are also suggested to be effective therapeutics in patients with schizophrenia (Heresco-Levy and Javitt, 2004, Javitt, 2010). Development of novel therapies targeting the glutamatergic system has produced mixed results (Javitt, 2010, Howes et al., 2015). *In vivo* human studies have shown that first-episode patients and patients with increased clinical or familial risk of developing schizophrenia have an increased glutamine concentration (measured as a correlate of glutamate) in the anterior cingulate cortex (Bustillo et al., 2010, Egerton et al., 2012, Tandon et al., 2013a) and, although data from patients with chronic schizophrenia has been mixed, some work has shown that these patients also have increases in glutamine (Bustillo et al., 2014). Alongside the increased glutamate levels observed in patients with treatment-resistant schizophrenia, these studies strongly link glutamatergic dysfunction with

schizophrenia. It is not clear, however, whether this means that there are subtypes of schizophrenia or if the glutamatergic and dopaminergic systems are integrated. The downstream effects of glutamatergic dysfunction are also not definitive; it is hypothesised that NMDAR hypofunction (as caused by antagonists such as PCP) causes a decrease in inhibitory γ-Aminobutyric acid (GABA)-ergic interneuron function, in turn causing cortical disinhibition and an increase in pyramidal neuron firing (Homayoun and Moghaddam, 2007).

1.2 Aetiology of schizophrenia

Schizophrenia has a significant genetic component. First-degree relatives of a patient have a higher risk of also developing the disorder than second-degree relatives, and monozygotic twins have a greater risk than dizygotic twins (Fischer et al., 1969, Kendler and Robinette, 1983, Onstad et al., 1991, Cannon et al., 1998, Cardno et al., 1999, Ingraham and Kety, 2000). A meta-analysis of twin studies found that schizophrenia is approximately 80% heritable (Sullivan et al., 2003). This study also supported schizophrenia as a complex trait with a polygenic, non-Mendelian inheritance (Risch, 2000, Sullivan et al., 2003) and environmental aetiological influences (Sullivan et al., 2003). It is now widely accepted that schizophrenia is a neurodevelopmental disorder wherein brain development pre- or perinatally or during adolescence is perturbed (Weinberger, 1987, Marenco and Weinberger, 2000, Owen et al., 2011, Piper et al., 2012, Rapoport et al., 2012) due to additive or interactive effects between susceptibility genes and environmental factors. Structural abnormalities in the brains of patients and the observation of a prodromal phase in patients at risk of schizophrenia are further evidence that schizophrenia is the result of a pathophysiological process across infancy and adolescence, culminating in a psychotic episode and diagnosis (Marenco and Weinberger, 2000).

1.2.1 Environmental component

Environmental insults can occur pre- or perinatally, or during childhood. Maternal infection and immunoglobulin-G (IgG) concentration are associated with increased risk; infections including influenza (Brown et al., 2004, Brown, 2012), *Toxoplasma gondii* (Brown et al., 2005, Mortensen et al., 2007, Pedersen et al., 2011), rubella (Brown et al., 2001) and genitourinary infections (Brown et al., 2011) all increase risk in offspring. Malnutrition is also a significant risk factor. Longitudinal studies of children born during or after famines in Holland and China found that malnutrition during early or mid-gestation increased the risk of schizophrenia two-fold (Susser et al., 1996, Xu et al., 2009, Lumey et al., 2011). Malnutrition is also a risk factor for mood disorders (Lumey et al., 2011). Perinatally, complications in pregnancy and labour can increase risk, as can placental pathology (Geddes et al., 1999, Rapoport et al., 2012).

The premorbid risk is increased by social factors including urbanicity and minority group position. Urbanicity is a causal factor in schizophrenia (Pedersen and Mortensen, 2001). Urban populations also have an increased prevalence of mood and anxiety disorders (Peen et al., 2010). First- and second-generation immigrant populations have an increased risk of schizophrenia (Cantor-Graae and Selten, 2005, Bourque et al., 2011) as do minority groups without recent migration (Bresnahan et al., 2007). The incidence of psychosis in ethnic minorities increases as the proportion of the minority in the population falls (Boydell et al., 2001) and migration itself has been associated with a greater risk of developing schizophrenia (Tarricone et al., 2016). Similar to urban environments, it is thought that this increased risk is due to social adversity and discrimination (Morgan et al., 2010, van Os et al., 2010).

Childhood adversity and trauma can include household poverty, separation of family, death of a parent, neglect and abuse. Meta-analyses of trauma research have shown that childhood adversity is associated with a 2 to 4-fold increase in risk for psychosis depending on the type of trauma (Varese et al., 2012, Morgan and Gayer-Anderson, 2016). Although many of these studies were retrospective and dependent on patient recall of abuse, longitudinal studies are now focussing on identifying adversity before a psychosis diagnosis. These have shown that bullying (both perpetration and victimisation) increases risk (Arseneault et al., 2011, Wolke et al., 2014) as does maltreatment by an adult (Arseneault et al., 2011) and sexual assault (Cutajar et al., 2010).

50% of patients with schizophrenia also have a co-morbid substance abuse disorder (Tandon et al., 2009) and many substances including alcohol and cannabis can also induce psychosis (Thoma and Daum, 2013). It is difficult to disentangle causal factors, particularly as patients who have a co-morbid substance abuse disorder are usually excluded from experimental cohorts.

1.2.2 Genetic component

As described above, genetic factors are a substantial but not exclusive source of risk for schizophrenia. Schizophrenia is a polygenic disorder and most variants are predicted to have modest effects at the population and individual level (Craddock et al., 2007, International Schizophrenia et al., 2009, Escudero and Johnstone, 2014, Kavanagh et al., 2015). There are also some rare variants associated with the disorder, discussed below.

To identify common variants associated with schizophrenia and other psychiatric disorders, genome-wide association studies (GWAS) have been widely used. These

studies involve the identification of multiple single nucleotide polymorphisms (SNPs) in patients (in this case with schizophrenia) and controls to assess whether an allelic variant is more prevalent in cases compared to controls. In initial GWAS studies, replication of associations was unreliable due to low cohort sizes (reviewed in Girard et al. (2012)). More recently, larger studies and meta-analyses have added statistical power and enabled replication of loci. Over 100 loci have now been identified (Schizophrenia Working Group of the Psychiatric Genomics, 2014), and some of the strongest hits are discussed on page 20.

Rare variants are also associated with schizophrenia. Patients have a higher burden of large (>100kb) rare (<1% frequency) copy number variants (CNVs), and multiple recurrent and *de novo* CNVs have been associated with increased risk of the disorder (International Schizophrenia Consortium, 2008, Xu et al., 2008, Malhotra and Sebat, 2012, Purcell et al., 2014, Rees et al., 2014). *De novo* SNPs and insertion-deletion (indel) events have also been associated with increased risk (Purcell et al., 2014). It is not yet clear what the net contribution of these mutations is, but given that schizophrenia is associated with a reduction in fecundity (Bundy et al., 2011) it is likely that rare variants are selected against while variants that confer small individual risk can become common in a population (Rees et al., 2011, Kavanagh et al., 2015).

It is now becoming clear that genetic risk is pleiotropic – alleles can affect multiple phenotypic traits and do not necessarily map onto well-defined domains. Common variants are pleiotropic both at the level of individual SNPs and at the polygenic level. The genetic relationship between five psychiatric disorders (schizophrenia, bipolar disorder, depression, autism spectrum disorder [ASD] and attention-deficit hyperactivity disorder [ADHD]) has been estimated from genome-wide SNPs;

schizophrenia and bipolar disorder were found to have a high genetic correlation while bipolar disorder, schizophrenia and ADHD each had a moderate correlation with depression (Cross-Disorder Group of the Psychiatric Genomics et al., 2013). Risk loci have also been identified that have a shared effect on the five diagnoses, implicating calcium signalling in particular (Cross-Disorder Group of the Psychiatric Genomics, 2013). CNVs also have pleiotropic effects (Owen et al., 2011) and are associated with autism and ID (Malhotra and Sebat, 2012, Fromer et al., 2014, Kenny et al., 2014).

This pleiotropy, combined with the heterogeneity and overlapping borders both between psychiatric diseases and between disease-wellness, suggests that existing diagnostic criteria are not a useful way to stratify patients for further research. A combination of polygenic risk and clinical symptoms may be more relevant; a study by Ruderfer et al. (2014) used a case-control analysis to create polygenic risk scores for patients with schizophrenia or bipolar disorder. This showed that, when directly compared, risk scores for these disorders were significantly different and also that there was a significant correlation between a bipolar polygenic risk score and mania in the schizophrenia cohort (Ruderfer et al., 2014)

1.2.3 Genetic hits for schizophrenia

Although genetic studies of schizophrenia are far from discovering all the underlying factors that may contribute to increased risk, multiple associations are beginning to converge on particular domains and biological processes.

Rare variants including CNVs, SNPs and indels that are significantly associated with schizophrenia have been identified in synaptic proteins, including voltage-gated calcium channels, neuregulin and interacting proteins, and glutamatergic system

proteins (Kenny et al., 2014, Hall et al., 2015). *De novo* mutations are overrepresented among NMDA receptor protein complexes (Fromer et al., 2014), and neurodevelopmental pathways are also implicated (Walsh et al., 2008).

1.2.3.1 DISC1

DISC1 (Disrupted-in-schizophrenia-1) is a unique case of direct genetic association with schizophrenia. A translocation between chromosome 1 and chromosome 11 identified in a large Scottish pedigree was associated with mental disorders (Millar et al., 2000, Blackwood et al., 2001) and was shown to directly disrupt *DISC1* and its protein, DISC1. DISC1 is a scaffolding protein involved in brain development, neurogenesis and neuronal proliferation, differentiation and signalling (Brandon et al., 2009). Other mutations in *DISC1* have now been associated with schizophrenia and also with bipolar disorder and depression (Brandon et al., 2009). It remains the strongest genetic association observed in schizophrenia.

1.2.4 Genome-wide association studies

The first generation of GWAS of schizophrenia illustrated the polygenic and complex aetiology of the disorder. No associations were replicated at first (reviewed in Girard et al. (2012)). With increased numbers and more power, however, associations were observed and replicated in genes involved in synaptic plasticity such as glutamate receptor genes (*GRM3, GRIN2A, GRIA1*), voltage-gated calcium channels (*CACNA1C, CACN2B, CACNA11*), and the dopamine D2 receptor encoded by *DRD2* (Schizophrenia Psychiatric Genome-Wide Association Study, 2011, Ripke et al., 2013, Schizophrenia Working Group of the Psychiatric Genomics, 2014, Hall et al., 2015).

Interestingly, the strongest association identified so far is with multiple SNPs in the major histocompatibility complex (MHC), a complex of cell surface proteins involved in immune response (Li et al., 2010, de Jong et al., 2012, Schizophrenia Working Group of the Psychiatric Genomics, 2014). *ITIH3/4,* another hit, encodes inter-alpha-trypsin inhibitor heavy chains 3 and 4, which are involved in the inflammatory immune response. Together these hits implicate immunity and inflammation in the aetiology of schizophrenia.

Association has also been observed with SNPs in the micro-RNA miR137 (Schizophrenia Psychiatric Genome-Wide Association Study, 2011, Ripke et al., 2013). This is a brain-enriched RNA known to be involved in neurodevelopment and mediation of synaptic plasticity (Wright et al., 2013, Olde Loohuis et al., 2016, Santos et al., 2016). It has many targets which have also been associated with schizophrenia (Kim et al., 2012, Kwon et al., 2013, Wright et al., 2015, Xia et al., 2015), including *CACNA1C* and *TCF4* which will be discussed later in this work (Li et al., 2010, Schizophrenia Psychiatric Genome-Wide Association Study, 2011, Hamshere et al., 2013, Guan et al., 2014, Schizophrenia Working Group of the Psychiatric Genomics, 2014, Li et al., 2015b).

As described above, GWAS are making it clear that genetic risk for psychiatric disease is pleiotropic. Partial overlap in schizophrenia and bipolar disorder associations has been illustrated through joint GWAS analysis of combined schizophrenia and bipolar disorder cohorts, which has found SNPs in calcium-channel gene *CACNA1C* and scaffolding protein *ANK3* (Schizophrenia Psychiatric Genome-Wide Association Study, 2011, Yuan et al., 2012), which are described in more detail below. SNPs in MHC complex genes are also associated with both schizophrenia and bipolar disorder (Williams et al., 2011).

In summary, GWAS have shown that the contribution of common variants to schizophrenia risk is substantial but highly polygenic. Larger sample sizes have identified more high-confidence variants, but no common variants that individually contribute a substantially higher risk have been identified. Finally, cross-disorder analysis has shown that there is genetic overlap, particularly between adult-onset psychiatric disorders such as schizophrenia and bipolar disorder.

1.2.5 Validation of GWAS results

GWAS are extremely useful for identifying novel gene variants that are associated with schizophrenia, particularly where hypothesis-driven approaches have had little success (Collins et al., 2012). Variants identified are not always causal; many are intronic or intragenic, and SNPs may be proxies for causal loci. The indirect association could be with another SNP, a set of interacting SNPs, a haplotype, indel, CNV or another genetic variant (Corvin et al., 2010). To investigate and validate GWAS hits for schizophrenia, we turn to transgenic manipulation of model organisms – in this case, the mouse.

1.3 Animal models of psychiatric disease

Historically, organisms such as flies and worms have been used for large-scale genetic screens. While they are very useful in this regard, the large evolutionary timespan means they do not share many structures and organs with humans that are affected by disease. Teleost fish such as zebrafish have also been used as model organisms, particularly in development, but these have limited applicability to mammalian genetics.

In the early 21st century the human genome was sequenced alongside parallel sequencing of genomes from model organisms (Venter et al., 2001, Cavalli-Sforza,

2005). Rodents such as *Rattus norvegicus* (rat) and *Mus musculus* (mouse) share approximately 95% genomic homology of coding regions with *Homo sapiens*. They also have a similar number of genes and extensive synteny. *M. musculus* is useful to researchers, as the genomes of many inbred strains have now been sequenced. Practically, mice are relatively cost-effective as they are small and easy to handle, feed and transport. They also age quickly and are physiologically similar to humans, allowing analysis of development, adulthood and ageing over two or three years. The mouse has historically been used as a model organism not only because of the extensive homology between human and mouse genomes but also because the mouse genome is uniquely amenable to manipulation. In the late 1970s, transgenic mice were created via injection of plasmids into blastocysts (Gordon et al., 1980), and this method is still used today, albeit with some refinements. Other methods of creating transgenic animals include homologous recombination in embryonic stem cells and subsequent transfer into embryos, and recombinant virus infection of embryos (reviewed in Jones (2011)). Mice are used as a model organism in neuroscience and behavioural research as they display measurable endophenotypes of complex behaviours such as anxiety, depression, and fear (Nguyen and Xu, 2008).

1.3.1 General limitations of mouse models

Although mice are a very useful model organism, care must be taken that results are not accepted without caveats. Although most coding regions in the mouse are homologous to human genes, conservation of non-coding regions is much lower (Batzoglou et al., 2000). It is becoming clear that there are important roles for non-coding regions and that a higher proportion of the genome is transcribed into RNA than previously realised (Rosenthal and Brown, 2007, Yue et al., 2014).

There are many experimental conditions to consider when using and reporting mouse models of disease. The genetic background of a mouse can influence phenotype. This is due to modifier loci or gene variants that are present in some strains but not others, and can cause interstrain phenotypic variability (Gingrich and Hen, 2000, Mestas and Hughes, 2004). Although most studies will use back-crosses (mating of a mouse mutant to a wild-type inbred strain) to eliminate a mixed genetic background, areas of the chromosome adjacent to the mutation of interest are likely to remain with the mutation and these could also affect phenotype (Crusio, 2004). Reporting of genetic background is also important for reproducibility. Selection marker genes can have an effect on gene expression. A neomycin resistance cassette under the control of the phosphoglycerate kinase (pGK) promoter is often used to produce null mutations, but it has been shown that in some cases disruption of a gene via pGK NEO minigene insertion can reduce the expression of nearby genes (Gingrich and Hen, 2000). Sometimes no obvious phenotype is observed, and this can be due to compensation by other proteins or isoforms that differ between mouse and human. Finally, environment can play a role and may confound results. For example, a gene may affect maternal behaviour which in turn can affect behaviour in offspring (Gingrich and Hen, 2000), and if some litters are raised by homozygous dams they will appear to have a behavioural phenotype. Environment can also affect phenotypes in mutant animals; enrichment has been shown to rescue an effect of NMDA receptor knockout on learning (Rampon et al., 2000).

1.3.2 Can we make a schizophrenic mouse?

Although targeted genetic manipulation of the mouse genome is becoming increasingly accessible, models of complex human psychiatric disorders have remained elusive. One reason for this is that positive symptoms, such as

hallucinations and delusions, are reliant on self-reporting and are difficult to establish convincingly in mice. There are correlates that are more easily tested, including memory, sensorimotor gating, and anxiety (described on page 29), but these may also be approximations of human symptoms. Another question is whether one animal can model all symptoms of a disorder, particularly as diagnoses in human patients is based on multiple domains and do not necessarily map onto specific abnormalities in molecules, synapses, cells or biological processes.

Animal models are unlikely to recapitulate the full extent of a specific psychiatric diagnosis, and individual phenotypes may not map directly onto symptoms. Instead, they are better viewed as experimental tools with which we can link genomic discoveries with mental processes and their underlying neural mechanisms.

Animal models are evaluated according to three criteria: construct validity, face validity, and predictive validity. These aim to judge whether the model corresponds to the disorder in humans (Chadman et al., 2009, Nestler and Hyman, 2010).

1.3.3 Construct validity

Construct validity considers the disease relevance with regard to the method of model construction. Ideally, human aetiology would be completely recreated, and symptoms, behaviour, and neural features can be observed. In the case of penetrant mutations with Mendelian inheritance, this can be implemented using genetic manipulation. For example, a mouse model with a knock in of the humanised *DISC1* mutation (described on page 21) displays hyperactivity and deficits in spatial memory, two phenotypes linked to schizophrenia (Pletnikov et al., 2008). Other methods, such as altering protein expression or function or perturbing neural circuits, can also produce phenotypes that appear similar to symptoms of schizophrenia. It is

often not easy to know whether these are legitimate models of disease states or whether they are close phenocopies.

Concerning the common variants that make up a substantial proportion of the genetic risk in schizophrenia, there are issues with the recapitulation of variants in the mouse. Firstly, the penetrance of these variants is very low and not all people who carry a variant will display a phenotype. Therefore one variant alone is unlikely to cause a phenotype in a mouse model. Secondly, genetic variants are pleiotropic and many hits are associated with more than one psychiatric diagnosis. It is unknown what factors combine to link a variant to schizophrenia or another disorder, but other genes, developmental events and epigenetics, or environmental factors could all play a role. Thirdly, there are large numbers of common variants present in each case or control, meaning that each patient has a different genetic route to their diagnosis combined with a unique environmental effect. Therefore any mouse modelling a single variant has low construct validity. It is possible to produce polygenic risk scores so a combination of variants could be studied, but the problem remains that results would only apply to a subset of patients. Finally, each SNP is only associated with a small increment of risk. If only one variant is studied, the effect may be so small that genetic background will dominate and no phenotype will be observed. Focus has therefore been mostly on penetrant mutations such as deletions, or on mutations that disrupt one gene completely or partially.

Disease symptoms can also be induced in rodent models by exposing them to environmental risk factors such as maternal infection and neglect. For instance, infection of pregnant mice at mid-gestation results in offspring with hippocampal and cortical abnormalities and changes in expression of presynaptic genes. These mice also show deficits in social interaction and pre-pulse inhibition, which as discussed

below are relevant to schizophrenia. An on-going issue is that there is no consensus on the threshold of environmental exposure required; in the case of maternal infection, many studies use differing concentrations of virus (Patterson, 2009). Alongside this, environmental factors also lack specificity and cause an increased risk of many psychiatric disorders.

To increase construct validity of genetic models, research is now moving towards gene x environment interaction models. In such studies, mice with transgenic manipulation of a gene of interest also undergo environmental stress, designed to model risk factors. Alongside the appropriate control groups, this allows comparison of effects of the gene manipulation, environmental risk, and the interaction between the two (Burrows et al., 2011).

1.3.4 Face validity

Face validity is based on the recapitulation in the mouse model of the anatomical, biochemical, neuropathological and behavioural features of the human disorder. There are no biomarkers for schizophrenia and diagnosis is based on behavioural symptoms. In animal models, behavioural features are often used as a correlate of the disorder and the underlying neuropathological features are then determined. As discussed above, behavioural features are not exact or specific, and one mouse model is unlikely to recapitulate all the features of schizophrenia. The disease is therefore broken down into individual components and domains known as endophenotypes.

Endophenotypes are intended to reflect the effects of genetic predisposition to disease, even in the absence of diagnosable pathology. Theoretically, they are determined by fewer genes compared to the number of variants that predispose

individuals to schizophrenia, and should be as simple as possible, well-defined, and quantifiable (Gottesman and Gould, 2003). There are some considerations to take into account when linking endophenotypes to a disorder (Turetsky et al., 2007). Firstly, the endophenotype must associate with the disorder in the population, and represent a robust, stable, and reproducible impairment that survives re-testing. Endophenotypes should also be present independent of a disease state. Secondly, an endophenotype is highly heritable, allowing intra- and inter-familial variance to be attributed to genetic factors. Thirdly, within families, the endophenotype should segregate with illness, but can also be evident in non-affected family members. The purpose of an endophenotype is to be quantifiable, and ideally, it should be attributable to a discrete and well-understood neurobiological mechanism.

1.3.4.1 Endophenotypes of psychiatric disease

Many feasible endophenotypes have been determined in studies of psychiatric disease, alongside behavioural tests to investigate them. Domains include anxiety, locomotor activity, depression, social interactions, cognition and memory (summarised in Chadman et al. (2009)). Of particular interest in schizophrenia are endophenotypes of sensorimotor processing and memory deficits.

1.3.4.1.1 Sensorimotor processing

Deficits in sensorimotor processing are consistently observed in patients with schizophrenia and also in their clinically unaffected relatives (Braff et al., 2001). Deficits can be assessed using neuropsychological methods such as pre-pulse inhibition (PPI) of a startle response. A loud noise or bright light will elicit a reflexive startle response in humans or animals. If a weaker pre-pulse is administered prior to the startling stimulus, the startle response is attenuated. It has generally been found

that in patients with schizophrenia, the attenuation of the startle response is deficient, meaning that they startle just as much whether or not there is a pre-pulse (Braff et al., 2001). PPI testing requires no prior training or specific preparation of subjects, and set-up can be automated so researcher bias can be minimised. Testing of rodents is relatively high-throughput so PPI is useful as a first-line screen in behavioural testing.

There are some drawbacks of sensorimotor gating as an endophenotype of schizophrenia. Evidence for translation of the neural circuits involved in PPI (Braga et al., 2013) across species is contradictory. In rodents, strain-dependent differences in PPI suggest that there is a genetic link. Dopamine agonists such as amphetamines reduce PPI in both humans and some rodent strains. On the other hand, administration of ketamine (an NMDA receptor antagonist) disrupts PPI in rodents but increases PPI in clinically normal patients (reviewed in Turetsky et al. (2007)), suggesting there may be some differences in the underlying neural circuits. PPI deficits are also common to other psychiatric disorders including bipolar disorder (Perry et al., 2001), obsessive-compulsive disorder (Swerdlow et al., 1993, Pittenger et al., 2016), seizures (Pouretemad et al., 1998), Huntingdon's disease (Swerdlow et al., 1995), and Alzheimer's disease (Grillon et al., 1992, Ueki et al., 2006). Other confounds include hearing deficits (which are strain-dependent). It has also been suggested that PPI is actually state-related and is more affected when a patient is in an acute psychotic state and that it can change with medication state (Amann et al., 2010). Startle response in animals is also dependent on weight as it is measured using a movement-sensitive pad (Tarantino et al., 2000).

1.3.4.1.2 Memory

One test that can be used in animal models is the novel object recognition test, which utilises the tendency of rodents to focus on new objects in their environment. An animal is exposed to two objects in a sampling trial. Next, the animal is exposed to a new group of objects that contains one of the familiar objects and a novel object. The time that the animal spends exploring the new object compared to the old is a measure of how well it remembers the familiar object. This paradigm has an advantage in not requiring deprivation or avoidance, and there is no training period required. Animals can also be recorded using video, which makes the test high-throughput. Locomotor activity must be taken into account, and also objects must carry equal salience as rodents show preferences for some types of objects over others.

Another useful paradigm for studying memory is cued and contextual fear conditioning. Animals learn to associate a non-aversive context and cue (for example a tone) with an aversive stimulus such as a foot shock. Animals undergo a conditioning trial where the cue precedes the aversive stimulus. After a period of time (often 24 hours) the freezing in response to the context or cue is taken as a measure of how well the animal has remembered the association. This is a relatively quick and simple experiment, and both the test and measurement of freezing can be automated. It is relatively high-throughput and quick, taking 2-3 days to administer. Finally, as the test is not reward-based, no food deprivation is required. On the other hand, any aversive stimulus is stressful to animals. Care must be taken that other behavioural tests are not influenced by fear conditioning (for example by carrying the test out last in a battery). Results can also be confounded by differences in mechanosensation and pain response.

1.3.4.1.3 Anxiety

Approximately 40% of patients with schizophrenia also have a co-morbid anxiety disorder. To test anxiety in rodents, the approach/avoidance conflict can be utilised. Rodents will explore novel environments, but also avoid brightly-lit, open areas (Bailey and Crawley, 2009) and the conflict between these two drives is thought to be analogous to anxiety. To measure this, paradigms such as Open Field, in which the animal is placed in a square arena, or Elevated Plus or Nought Maze, which consist of raised platforms with closed and open areas, can be used. These give the animal a choice between exploring the open 'anxiogenic' areas or centre of the arena or the closed areas/periphery. These tests are affected by classic anxiolytic drugs such as benzodiazepines, which increase the time a mouse spends exploring open areas (Prut and Belzung, 2003). These tests are high-throughput, and recording and scoring can be completely automated. Care must be taken that animals do not have locomotor defects or problems with vision, as this can confound results. The Open Field test can also be useful in identifying psychomotor hyperactivity, an endophenotype of bipolar disorder (Bauer et al., 1991, Einat, 2006, Perry et al., 2010). This is useful when studying genetic models of psychiatric disease as many genes are associated with both schizophrenia and bipolar disorder (Bauer et al., 1991, Einat, 2006, Perry et al., 2010, Schizophrenia Psychiatric Genome-Wide Association Study, 2011).

1.3.5 Predictive validity

Another measure by which a model can be validated is predictive, or pharmacological, validity. This judges whether the model responds to treatment in a way that predicts treatment effects in human patients. In the case of neuropsychiatry, this is often difficult as there is a poor therapeutic standard. As discussed on page 9,

the targets of antipsychotic drugs were identified *post hoc* (Carlsson et al., 1957, Carlsson and Lindqvist, 1963). Antipsychotics also have the greatest effect on positive symptoms, which are difficult to measure in animal models, and are not effective in some patients. Behavioural screens have been developed to screen for new drugs, but these often treat the mouse as a 'black box' and behaviour as the only output. This means that the underlying mechanism is unknown and may not reflect the pathophysiology of human disease, and also does not take into account the therapeutic mechanism of any reference compound. One example of this is in anxiety; benzodiazepines are anti-anxiogenic, and Open Field is then accepted as a 'test of anxiety' because it responds to benzodiazepines –however, there are factors that are dissimilar when compared to human anxiety treatment response (Ennaceur, 2014). Benzodiazepine response is often used as a comparison point for novel drugs, but not all anti-anxiety drugs have an effect in Open Field (Ennaceur, 2014) and this approach could lead to premature dismissal of novel compounds.

1.3.6 Limits of traditional knock-out models

Many transgenic mouse models study the effect of a complete gene knock-out, as this is relatively simple to carry out via targeted homologous recombination or by using gene-editing technology. One issue that often arises is lethality or developmental effects, either prenatally or perinatally. It is estimated that up to 55% of genes in the mouse are essential (Liao and Zhang, 2007) and knock-outs can cause lethality or sub-viability One method of combating developmental lethality is to use lines with a conditional mutation that can be induced either tissue-specifically or at a certain time point, for example in adulthood. There are still problems with using this method to create knock-out alleles; null mutations in mouse also often result in different phenotypes to those observed in humans, and this is associated with

changes in adaptation at the protein sequence, but not gene-expression, level (Liao and Zhang, 2008). Homology between mouse and human is also reduced in the non-coding regions (Batzoglou et al., 2000). In schizophrenia, the genetic risk is increased by many variants each with an incremental effect, and negative and cognitive deficits are not always overwhelming. It is possible that a complete knockout of a susceptibility gene will result in a mouse with severe deficits in multiple domains. Consequently, knock-out models may lack both construct and face validity. One other approach, utilised in this work to generate novel mouse models, is to use chemical mutagenesis in a reverse-genetics approach.

1.4 ENU mutagenesis

1.4.1 Large-scale mutagenesis screens

In the late 1990s, large-scale chemical mutagenesis screens were carried out on many model organisms including the mouse (Nolan et al., 1997, Nolan et al., 2000b, Nolan et al., 2002). This involved mutagenesis followed by phenotypic screening to identify novel mutations in a forward-genetics approach. Alongside the phenotype-driven method, an archive of mutagenised genetic material and sperm was also created.

1.4.1.1 ENU mutagenesis

N-ethyl-*N*-nitrosourea, or ENU, is a potent chemical mutagen (Figure 3) that causes small intragenic lesions by introducing single base pair changes. ENU can transfer an ethyl group to oxygen or nitrogen radicals in DNA, causing mispairing and base substitution (Nolan et al., 1997, Justice et al., 1999). The mutation rate is highest in pre-meiotic spermatogonial stem cells, with a single locus mutation frequency of 6 – 1.5 x 10^{-3} per 1000 treated genome (Justice et al., 1999). Practically,

this means that one mutation will be observed for any given locus in one of 175-655 gametes screened (Justice et al., 1999, Nolan et al., 2000b). ENU predominantly causes substitutions in A/T pairs, and the majority of these are missense mutations (Justice et al., 1999). This is an advantage of ENU mutagenesis as it can produce a range of alleles including loss of function, viable hypermorphs, antimorphs, and gain-of-function (Justice et al., 1999, Nolan et al., 2000b, Coghill et al., 2002, Nolan et al., 2002) and, as it causes single point mutations, this may have more construct validity for models of psychiatric disease.

In order to generate F_1 animals for dominant phenotype screens, mutagenised BALB/c male mice were mated to wild-type C3H/HeH females. F_1 (BALB/c x C3H/HeH) offspring were then screened (Nolan et al., 1997, Justice et al., 1999, Nolan et al., 2000b, Nolan et al., 2002). Following phenotypic screening batteries, sperm from F_1 males (heterozygous for novel ENU-induced mutations) was cryopreserved alongside DNA samples (Figure 4)(Thornton et al., 1999). The phenotype-driven approach is not hypothesis-driven, and can identify novel genes that, when mutated, cause phenotypes. An alternative approach is gene-driven and utilises the DNA from F_1 males (in parallel with the cryopreserved genetic material) for the screening of a selected gene for ENU-induced mutations (Coghill et al., 2002, Quwailid et al., 2004).

The DNA was archived and made available for gene-driven studies (Coghill et al., 2002, Quwailid et al., 2004). The DNA archive at MRC Harwell contains samples from over 10,000 mice. Pilot studies estimated that the functional mutation rate in the archived material was 1/1.82Mbp (Coghill et al., 2002, Quwailid et al., 2004), and this means that, if over 5000 samples are screened, there is almost 100% chance of finding a functional mutation at a given locus (Coghill et al., 2002, Quwailid et al.,

2004). A gene of interest can be screened using high-throughput PCR combined with a hybridisation step. Heating amplified samples to 95°C and slowly cooling to 24°C allows hybridisation of duplexes. Any mutated locus will be heterozygous so will form a heteroduplex. A high resolution intercalating melt dye is also included., which is then used to detect heteroduplexes (Wittwer et al., 2003). When mutations are identified they can be verified using sequencing and the corresponding cryopreserved sperm sample is then retrieved for *in vitro* fertilisation (IVF). The recovery process for these animals is also reliable and produces a high recovery rate (Thornton et al., 1999, Coghill et al., 2002, Quwailid et al., 2004).

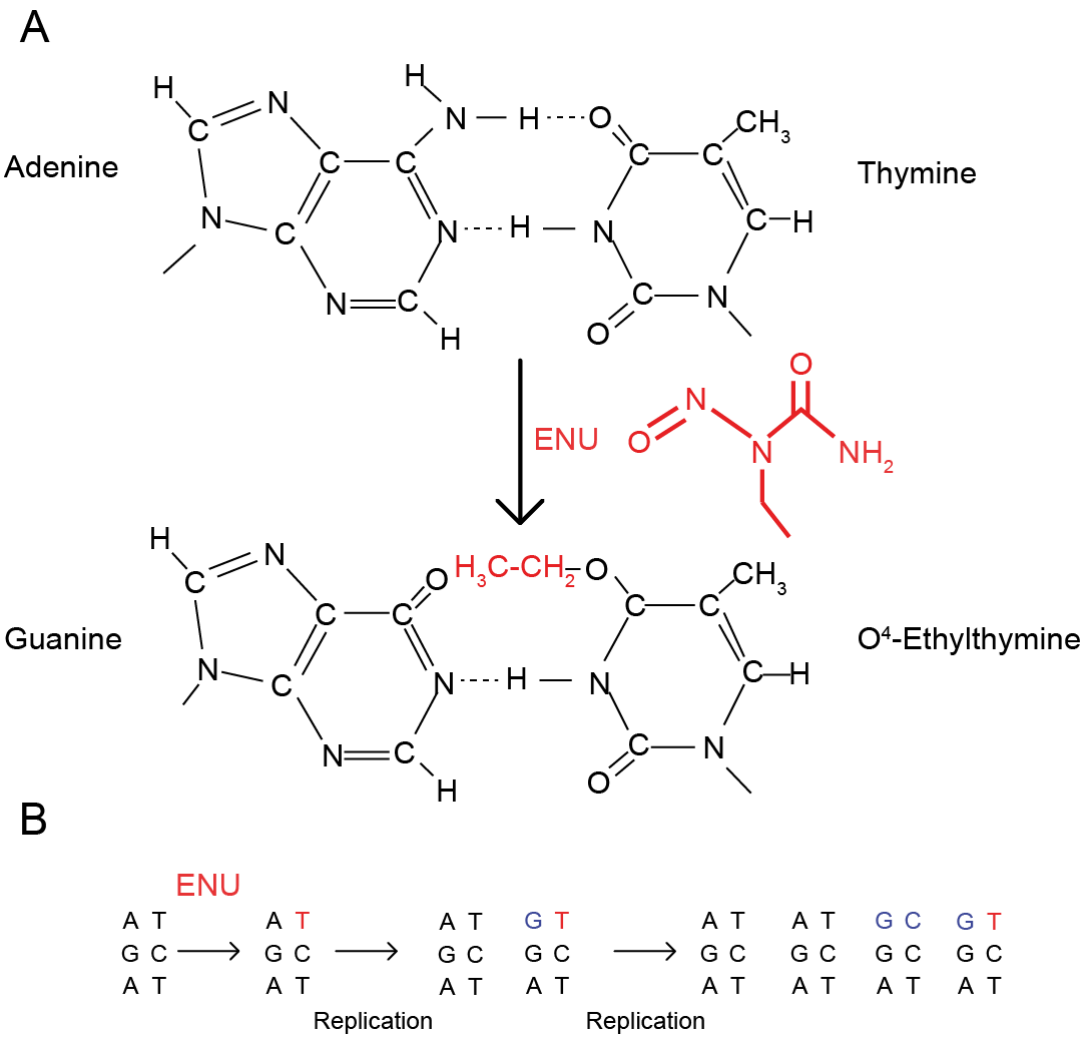

Figure 3 Mechanism of ENU mutagenesis

(A) Methylation of a thymine residue by ENU. (B) Mechanism of base-pair substitution induced by ENU. Red indicates O^4 adduct and blue indicates base substitution. Adapted from Noveroske et al. (2000).

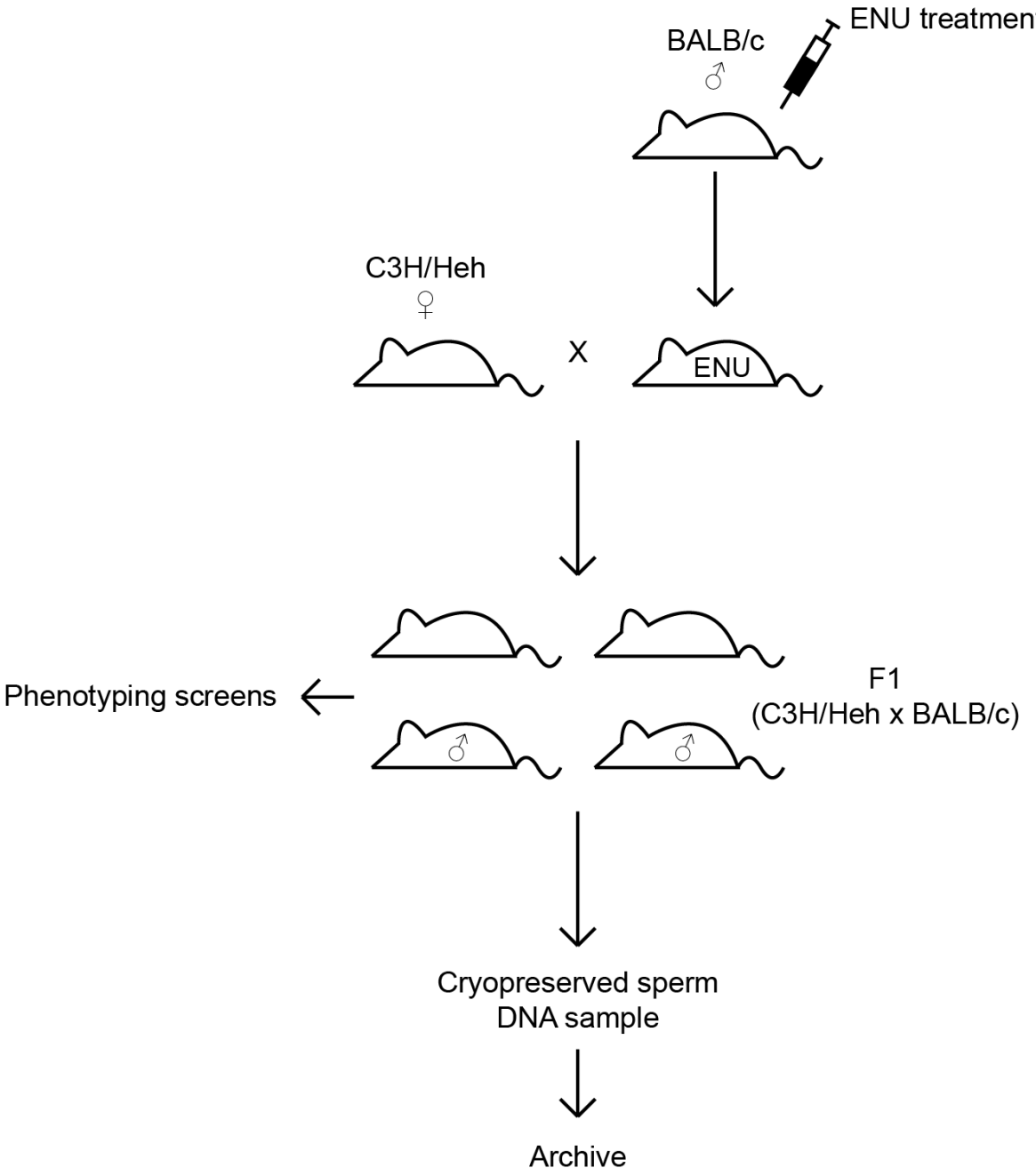

Figure 4 ENU mutagenesis and archive generation

1.5 Investigation of three candidate genes

As discussed on page 20, multiple schizophrenia associations have now been replicated. Three genes identified through GWAS were chosen for further investigation using a reverse-genetics approach and behavioural phenotyping battery. These genes were *Ank3, Tcf4,* and *Cacna1c.* These are described in detail in 1.7, 1.8, and 1.9.

Briefly, loci in *ANK3* and *CACNA1C* have been identified in GWAS of both schizophrenia and bipolar disorder (Ferreira et al., 2008, Schizophrenia Psychiatric Genome-Wide Association Study, 2011, Wirgenes et al., 2014), while *TCF4* has been associated with schizophrenia (Hamshere et al., 2013, Li et al., 2010, Stefansson et al., 2009, Steinberg et al., 2011). *ANK3* encodes ankyrin$_G$, an axonal scaffolding protein that is required for the trafficking ion channels and action potential propagation (Sobotzik et al., 2009, Gasser et al., 2012). TCF4 is a transcription factor involved in pontine nucleus development (Flora et al., 2007) and immune system development (Quong et al., 2002, Ross et al., 2003). Finally, *CACNA1C* encodes $Ca_v1.2$, a subunit of a voltage-gated calcium channel that is implicated in long-term potentiation (LTP) (Langwieser et al., 2010, Moosmang et al., 2005), , hippocampal neural survival (Lee et al., 2016) and elongation of the cardiac QT interval (Splawski et al., 2004, Wemhoner et al., 2015). *CACNA1C* and *TCF4* are also targets of miR-137, which, as described above, has been identified in GWAS of schizophrenia (Kwon et al., 2013, Wright et al., 2013). This suggests that they are part of a neuronal pathway that may be perturbed in patients.

1.6 Project Overview and Aims

The overall project pipeline is summarised in Figure 5. My part in the investigations into each gene began at different points along the timeline and more detail is included in later sections.

In brief, domains of interest in each gene are identified using literature searches and online genomic databases. The ENU-mutagenised DNA archive at MRC Harwell can be screened for mutations in these domains, followed by confirmation of the mutation. If more than one mutation is identified, *in vitro* and *in silico* prioritisation allows a choice of the allele to re-derive. The corresponding sperm sample was then used for IVF of C57BL/6J female ova.

Mutant cohorts are then tested using a phenotyping battery designed to identify neurological, behavioural and sensorimotor phenotypes (described in section 2.2). This included a broad dysmorphology screen, Open Field, Acoustic Startle PPI, and Context- and Cue-dependent Fear Conditioning. These tests are high-throughput and have relative ease of use. If mice display phenotypes in these tests, further investigation is warranted.

Investigation of these three genes will help to further the study and validation of schizophrenia-associated genes through the identification of novel missense mutations and a behavioural phenotyping battery. If this is successful, this could produce models of schizophrenia endophenotypes with high face validity, which could be utilised to study the neural underpinnings of the behavioural domain. Further to this, neural correlates of some behaviours are still unknown. If behavioural phenotypes are observed in mutant mice it could help to identify genes that are involved in neurodevelopment.

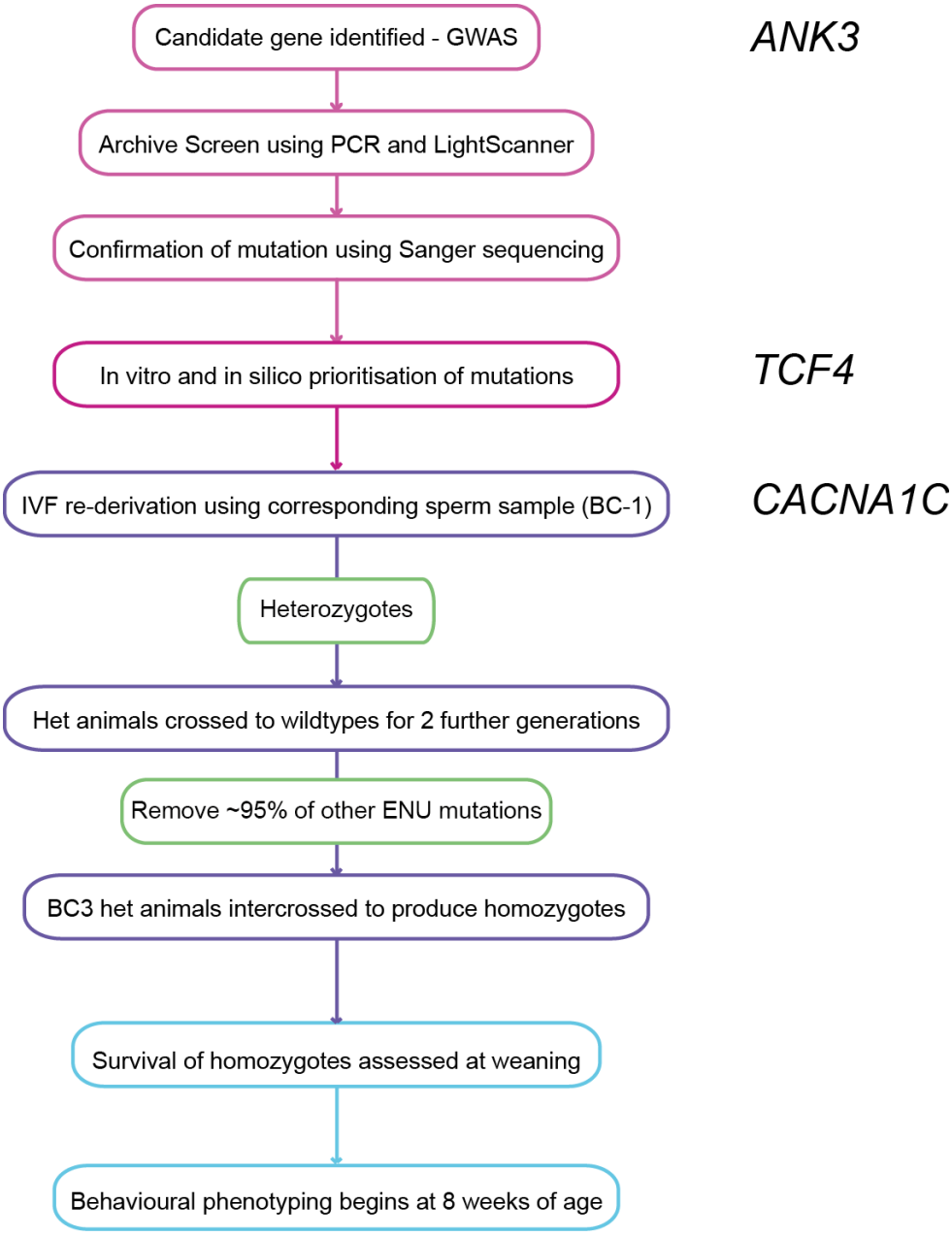

Figure 5 Project overview

1.7 *ANK3*

Ankyrins are intracellular proteins that act as adaptors to link membrane-bound proteins to the intracellular cytoskeleton and target them to specific membrane domains (reviewed in Mohler et al. (2002b)). Brain-specific isoforms of ankyrin$_G$ are important for the development and maintenance of the axon initial segment (1.7.3) and nodes of Ranvier (1.7.4) and are associated with axonal function and disease. Some animal models have been described (1.7.7) but there are currently no good models of more subtle mutations that could validate *ANK3* as a risk factor for psychiatric disease.

1.7.1 Overview of the *ANK* gene family

In mammals, there are three ankyrin genes *ANK1*, *ANK2* and *ANK3*; these encode ankyrin$_R$, ankyrin$_B$ and ankyrin$_G$ respectively. *ANKYRIN1 (ANK1)* was the first identified member of the ankyrins (Podgorski et al., 1988, Lambert et al., 1990); it encodes ankyrin$_R$ and is expressed in erythrocytes. *ANKYRIN2 (ANK2)* was then identified in foetal brain (Tse et al., 1991), adult brain, and heart (Otto et al., 1991). There are well-conserved orthologues in invertebrates – *dank1* and *dank2* in *D. melanogaster* and *unc44* in *C. elegans*, suggesting that these genes arose early in metazoan development. The ankyrin family of proteins contain a conserved membrane-protein-binding domain (MBD), a spectrin-binding domain (SD) and a less well-conserved C-terminal region, shown in Figure 6A (Mohler et al., 2002b).

ANKYRIN3 (*ANK3)* was identified as a novel and separate gene by its restricted distribution in neurons to axon initial segment (AIS) and nodes of Ranvier, and was cloned from foetal brain (Kordeli et al., 1995) and mouse brain and kidney (Peters et al., 1995) using the conserved spectrin-binding regions of *ANK1/2* as probes. Kordeli et al. (1995) identified a 480kDa protein containing 4377 amino acids that contained

an ANK repeat region and spectrin-binding region, conserved between ankyrin$_R$, ankyrin$_B$ and the novel protein. However the protein contained a novel serine-rich domain and an unconserved C-terminal region, as shown in Figure 6B and C. Peters et al. (1995) located the gene encoding this protein on chromosome 10 in both human and mouse, showing that it is encoded by a separate gene to *ANK1* and *ANK2* (8p11 and 4q25-27 respectively). They also identified the unconserved C-terminus with <30% homology to *ANK1/2*, although some areas of this region resembled the cytoplasmic domain of the tumour necrosis factor (TNF) receptor. Ankyrin$_B$ is expressed throughout the brain and nervous system, while ankyrin$_G$ is limited to nodes of Ranvier and the axon initial segment in CNS and PNS. Ankyrin$_G$ is also the major form of ankyrin in the kidney and cardiac, skeletal and smooth muscle (Peters et al., 1995, Kordeli et al., 1995).

There appear to be developmental- and tissue-specific isoforms of ankyrin$_G$: in brain two isoforms of 480 and 270kDa were identified and recognised by a probe targeted to the serine-rich domain whereas in the kidney a 190kDa isoform was identified (Peters et al., 1995) and in muscle a shorter still isoform was identified that lacks the repeat domain (Gagelin et al., 2002). 33 transcripts appear on Ensembl as shown in Figure 7; these include the giant isoforms (480- and 220-kDa) found in brain (ANK3-001) as well as shorter isoforms formed through splice variation. Many of these are processed transcripts with unknown function. While the giant isoforms are well characterised *in vitro*, any models of disease will need to take the range of isoforms throughout development and tissue into consideration. Isoforms may also differ in their homology to mouse *Ank3*; the 480-kDa isoforms are 92% homologous but shorter isoforms in human may not directly map onto an isoform in mouse.

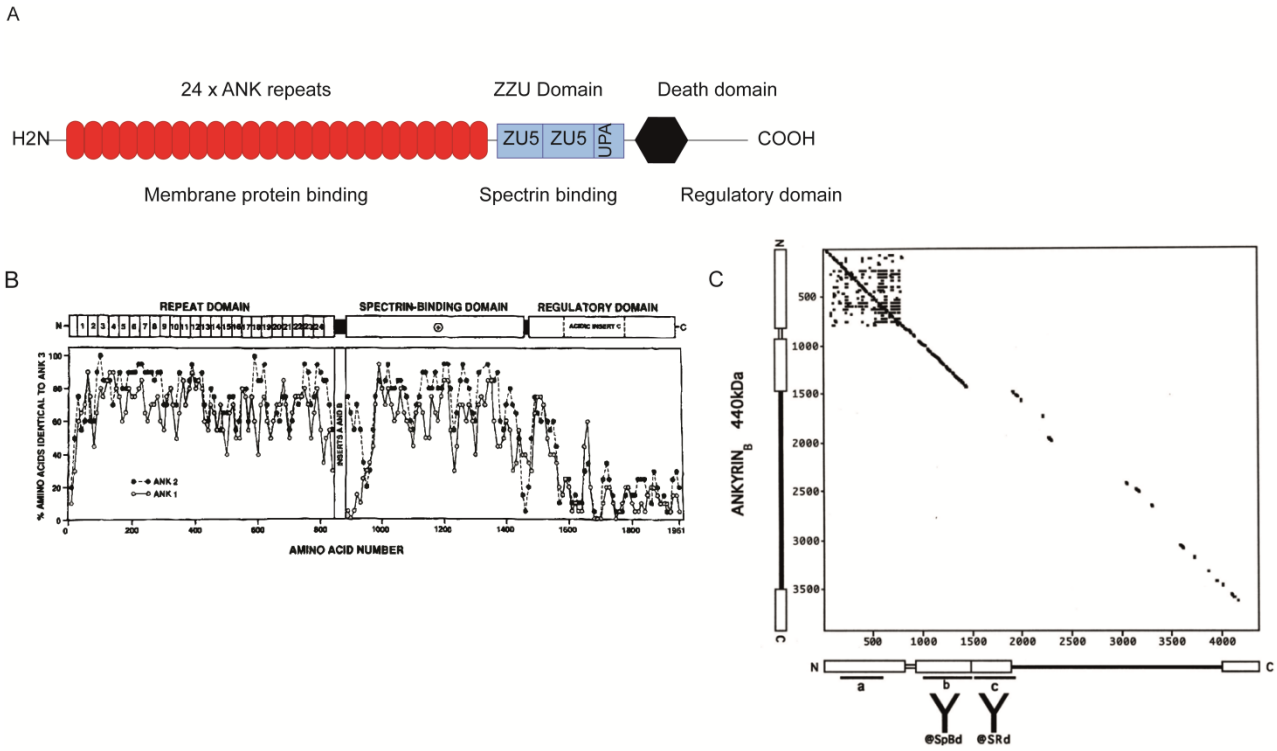

Figure 6 Ankyrin domains and homology.

(A) Canonical ankyrin domains include the ANK-repeat membrane-binding domain, the ZZU spectrin-binding domain, a death domain and a C-terminal regulatory domain. (B) When compared to mouse ankyrin$_R$ and human ankyrin$_B$, 190-kDa mouse ankyrin$_G$ shows high homology in the ANK repeat region and SBD and much lower homology (<30%) in the regulatory domain (Peters et al., 1995). (C) A dot matrix alignment of the derived amino acid sequence of 480-kDa ankyrin$_G$ against that of 440-kDa ankyrin$_B$. Each dot represents a minimum identity of 60% over a window of 8 residues (adapted from Kordeli et al. (1995)).

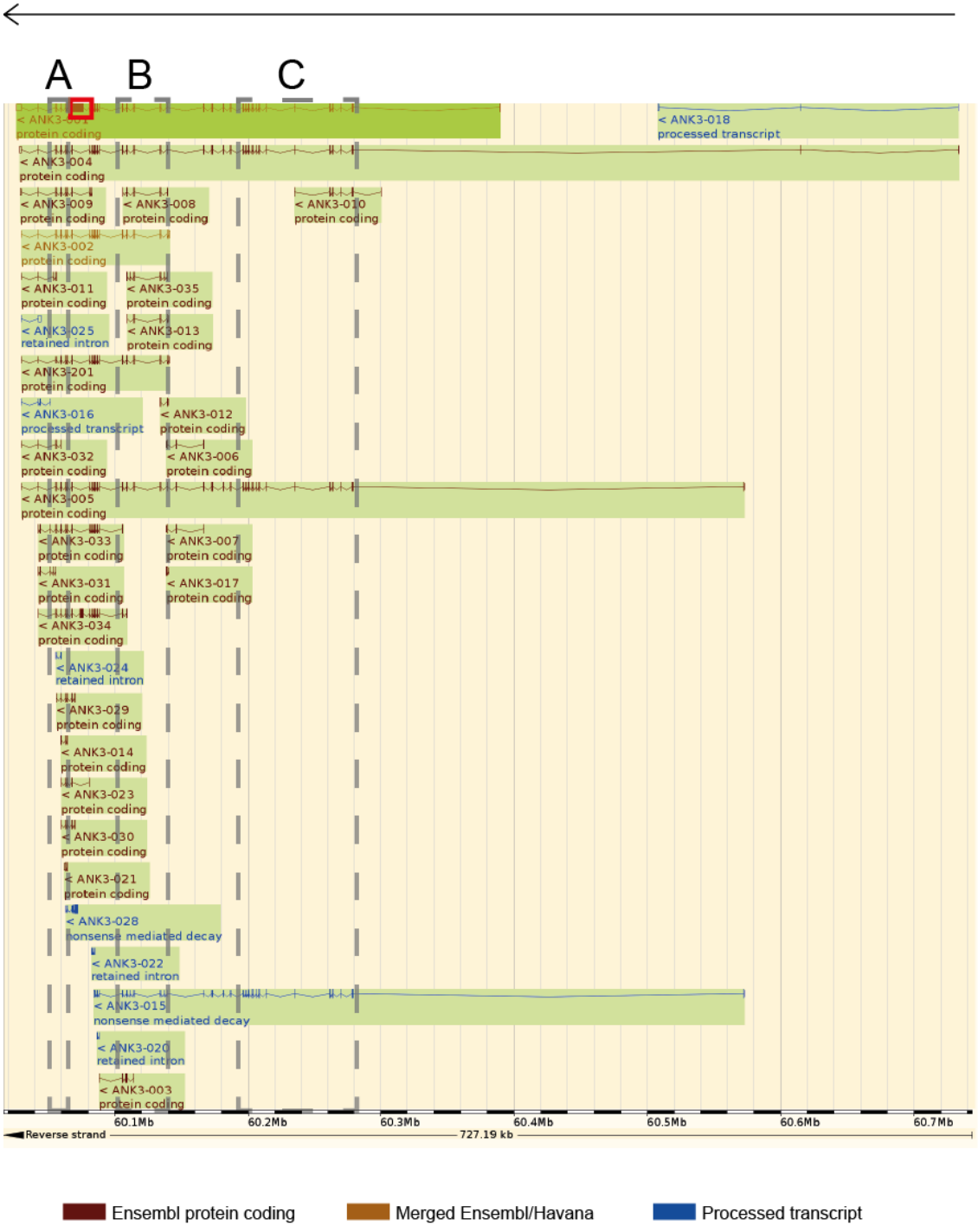

Figure 7 Alignment of human ANK3 transcripts showing the main domains.

Not all transcripts contain (A) the Death domain; (B) the spectrin-binding domain; or (C) the ANK repeat domain. Shown in red is the serine-rich region only present in 480- and 270-kDa brain-specific transcripts. Adapted from http://www.ensembl.org/Homo_sapiens/Gene/Splice?db=core;g=ENSG00000151150;r=10:60026298-60733490;t=ENST00000355288

1.7.2 Protein Structure of 480/270kDa Ankyrin$_G$

As described, these giant isoforms have a close homology to other ankyrins in their membrane-binding domain and spectrin-binding domain, while containing a large serine-rich region and varying in their regulatory domains. The most common isoforms are shown in Figure 8.

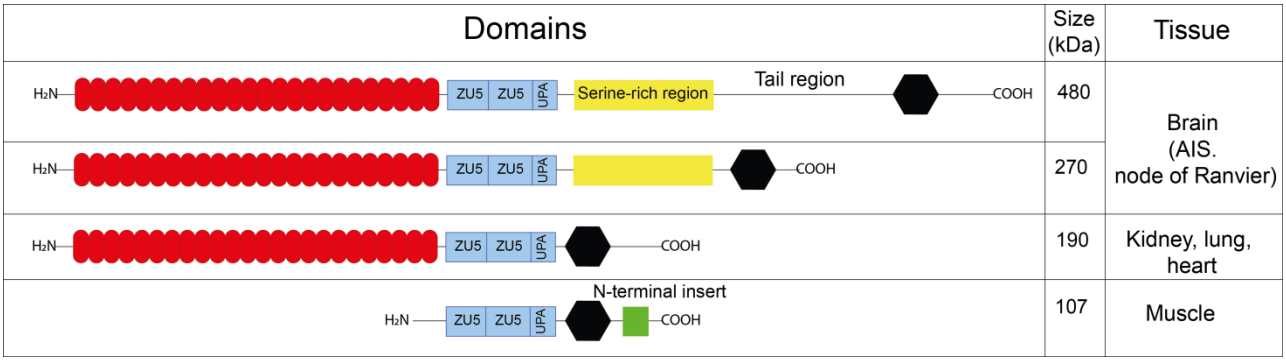

Figure 8 Isoforms of ankyrin$_G$.

Tissue-specific isoforms of ankyrin$_G$ contain unique regions such as the serine-rich region in 490/270-kDa brain-specific ankyrin$_G$ and an N-terminal insert in a muscle-specific isoform which also does not contain the ANK repeat region (reviewed in Rubtsov and Lopina (2000) and Cunha and Mohler (2006))

1.7.2.1 Membrane-binding domain (MBD)

The N-terminus of ankyrin$_G$ contains an 89kDa ANK repeat domain consisting of 24 copies of a 33 amino acid motif (except repeat 5, which only contains 29 a.a.). This covers a.a. residues 1-873 and has 57% and 71% homology to ankyrin$_R$ and ankyrin$_B$ respectively (Kordeli et al., 1995, Peters et al., 1995). This region is involved in recognising and binding membrane channel proteins (Michaely and Bennett, 1992). Each repeat forms a broken α-helix joined to the next repeat by an exposed perpendicular loop. Specificity of each ankyrin for different proteins is thought to arise from the non-conserved residues at the tips of these loops (Michaely and Bennett, 1992, Sedgwick and Smerdon, 1999). The whole domain forms a multivalent left-handed helix and contains multiple regions that can bind targets with diverse

sequences potentially simultaneously to co-ordinate multiprotein complexes (Wang et al., 2014).

The MBD of ankyrin$_G$ has been shown to bind ion channels via a common binding motif found in Na$_v$ channel orthologues in vertebrates including Na$_v$1.2 (Bouzidi et al., 2002) and Na$_v$1.6 (Gasser et al., 2012) and potassium channels KCNQ2 and KCNQ3 (Rasmussen et al., 2007, Pan et al., 2006). Ankyrin$_G$ is required for normal clustering of Na$_v$ channels at the AIS and nodes of Ranvier (Srinivasan et al., 1988, Zhou et al., 1998, Susuki et al., 2013). The MBD also binds neuronal cell adhesion molecules (NrCAM) and neurofascin both *in vitro* (Dubreuil et al., 1996, Zhang et al., 1998) and *in vivo* in *D. melanogaster* (Hortsch et al., 1998) and rat (Davis et al., 1993, Davis and Bennett, 1994, Davis et al., 1996) to form membrane-spanning complexes.

1.7.2.2 Spectrin-binding domain (SBD)

Downstream of the ANK repeat region, ankyrin$_G$ contains a highly conserved spectrin-binding domain, consisting of two ZU5 domains and a UPA domain (ZZU). Each ZU5 domain contains ~150 a.a. and folds into a β-strand-rich structure. This domain is conserved between all three ankyrin proteins, although they vary in their affinity for different isoforms of spectrin. Detailed functional studies have not been carried out in ankyrin$_G$, but in ankyrin$_B$, only the first ZU5 (ZU5$_N$) domain is required for spectrin binding (Wang et al., 2012). Mutations in the second ZU5 (ZU5$_C$) and the UPA domain of ankyrin$_B$ give rise to inherited cardiac arrhythmia in patients (Hashemi et al., 2009) but spectrin binding remains intact (Mohler et al., 2004), so these regions must have other functions – potentially regulation of binding or stabilisation of binding to membrane channels by the N-terminal ANK3 repeat region.

Ankyrin$_G$ specifically binds to βIV-spectrin, which in turn binds actin, linking ankyrin$_G$ to the cytoskeleton. βIV-spectrin was identified in a binding assay and confirmed to be enriched at axon initial segments and nodes of Ranvier (Berghs et al., 2000) and to co-localise with ankyrin$_G$ and sodium channels (Komada and Soriano, 2002).

1.7.2.3 Serine-rich region

The 270- and 480kDa isoforms of ankyrin$_G$ are characterised by a serine-rich region downstream of the SBD (Kordeli et al., 1995). This region is 46kDa and 35% of residues are serine or threonine. Serine-rich regions are found in a huge range of protein families with different functions, and serine residues can undergo post-translational modifications including phosphorylation (important for signalling) and glycosylation. The function of this region is unknown but it has been shown that this region is glycosylated and that the 480kDa isoform is also modified by *O*-linked *N*-acetylglucosamine residues (Zhang and Bennett, 1996). This and other *O*-GlcNac-glycosylated proteins are enriched at nodes of Ranvier, suggesting that this potentially aids in targeting or binding.

1.7.2.4 C-terminal and 'death' domain (DD)

The human ankyrin$_G$ death domain (DD) resembles the DD found in type 1 tumour necrosis factor receptor and *in vitro* the death domain of the kidney-specific 190-kDa isoform has been shown to interact with Fas, a pro-apoptotic molecule (Del Rio et al., 2004). When isolated, the domain folds into six α-helices and three 3_{10}-helices. These form a hydrophobic pocket on the surface of the protein. The C-terminal tail then curves to allow an upstream residue, Phe100, to fit into the pocket, which anchors the flexible tail region to the core domain (Liu et al., 2014). There is little known about the death domain in other isoforms of ankyrin$_G$ including in the brain,

although it is speculated to have a regulatory function possibly through protein interactions. The C-terminal domain of ankyrins enables selective binding of target proteins as shown using ankyrin$_B$/ankyrin$_G$ chimeras (Mohler et al., 2002a).

1.7.3 Ankyrin$_G$ in the axon initial segment

The axon initial segment (AIS) is a subcellular domain close to the neuronal cell body that is 30-60µm long and defined by the clustering of Na_v channels (reviewed in Bender and Trussell (2012), Yoshimura and Rasband (2014)). In cultured hippocampal neurons, the AIS can be detected 3-4 days after dissection as shown in Figure 9 (Grubb and Burrone, 2010b, Normand and Rasband, 2015). A high concentration of ion channels gives the AIS a low threshold for membrane depolarisation and allows integration of synaptic events into a new action potential. The AIS is capable of fine-tuning neuronal excitability; it can relocate and change length to compensate for chronic alterations in activity (Grubb and Burrone, 2010a). AIS formation does not require input from glial cells (Hedstrom and Rasband, 2006).

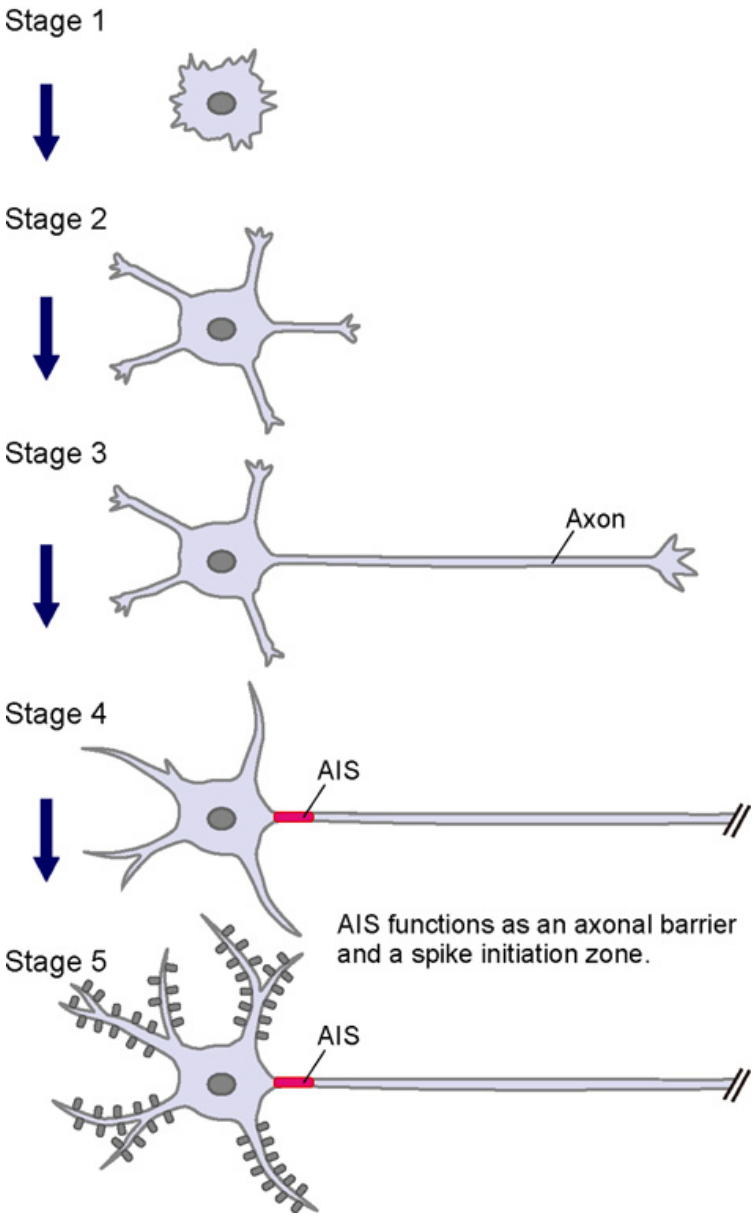

Figure 9 Establishment of neuronal polarity and formation of the AIS

Cultured pyramidal neurons from a rodent hippocampus acquire their characteristic polarised morphology in five successive stages. The first step in neuronal polarisation is initial axon formation in the transition from stage 2 to stage 3. The AIS is formed from stage 3 to stage 4. The AIS maintains neuronal polarity and regulates action potential initiation. Adapted from Yoshimura and Rasband (2014).

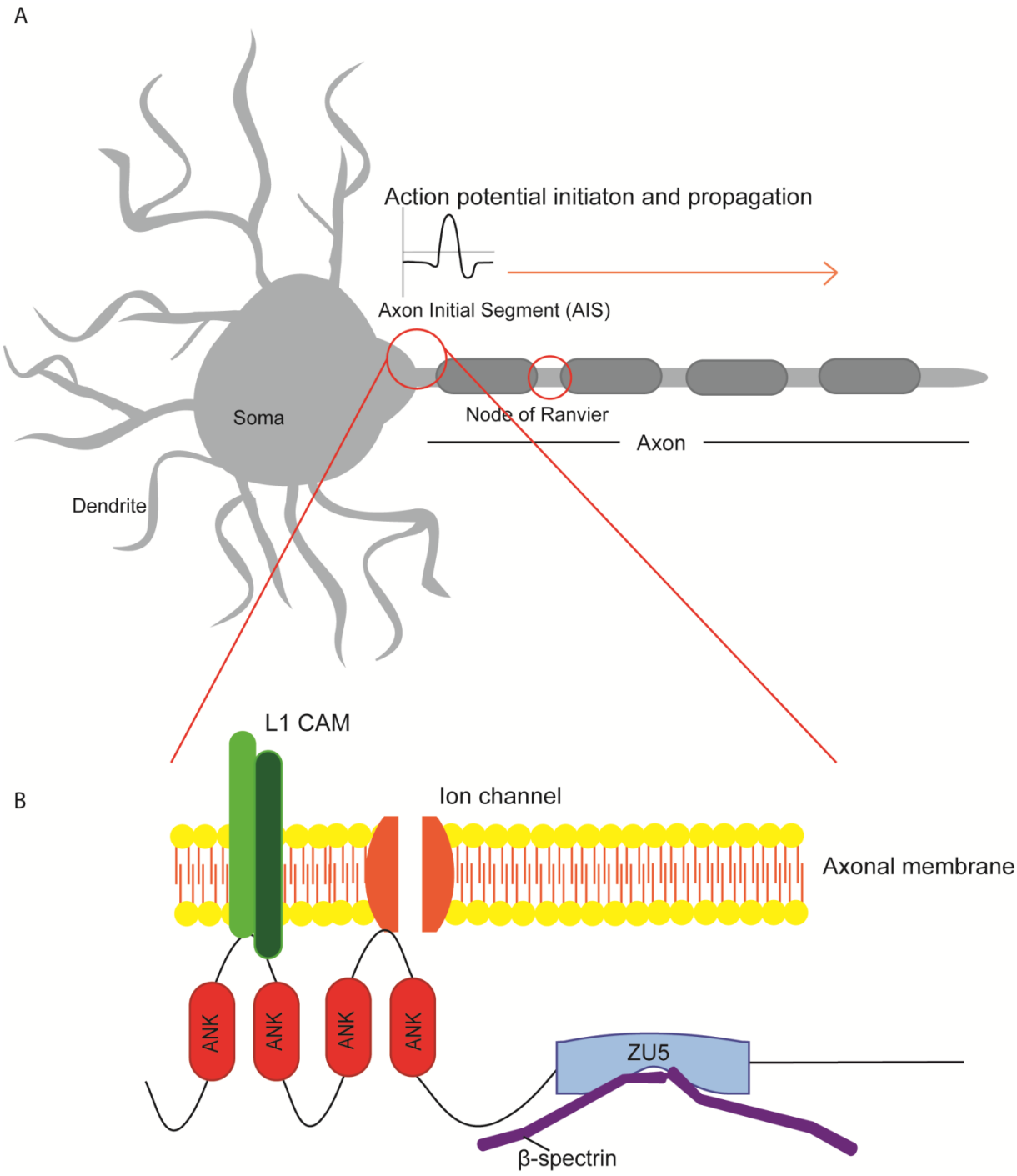

Figure 10 Ankyrin$_G$ forms a subcellular scaffold at the AIS.

(A) Ankyrin$_G$ is localised to the AIS and nodes of Ranvier (circled in red). (B) Co-ordination of NrCAMs such as L1 CAM, transmembrane ion channels and βIV-spectrin by ankyrin$_G$.

Ankyrin$_G$ co-ordinates assembly of βIV-spectrin, Na$_v$ channels and L1 CAMs at the AIS (Figure 10A and B) (Jenkins and Bennett, 2001) and is required for maintenance of the AIS. *In vitro*, siRNA knockdown of ankyrin$_G$ causes axons in hippocampal neurons to take on a more dendritic identity, with cytoplasmic proteins redistributing into axons and the formation of postsynaptic spines (Hedstrom et al., 2008), and this also occurs *in vivo* in ANK3$^{-/-}$ neurons (Sobotzik et al., 2009). Some polarity remains in these neurons – a single axon on the basal cell pole is distinct from dendrites on the apical side, which is consistent with the later finding that axon specification and AIS formation precede clustering of ankyrin$_G$ (Galiano et al., 2012).

Ankyrin$_G$ is required to target both Na$_v$ channels and βIV-spectrin to the AIS: Purkinje neurons in *Ank3*$^{-/-}$ mice show deficiencies in Na$_v$ channel trafficking (Zhou et al., 1998) and ankyrin$_G$ has been shown to preclude βIV-spectrin at the AIS (Yang et al., 2007). In neurons from 3-month old βIV-null mice both ankyrin$_G$ and Na$_v$ fail to localise to the AIS (Komada and Soriano, 2002) which suggests that ankyrin$_G$ and βIV-spectrin are both required for AIS formation and maintenance. βIV-spectrin alone cannot, however, localise ankyrin$_G$ to the AIS *in vitro,* and when early time points were studied in βIV-null neurons it emerged that the AIS formed even in the absence of spectrin (Yang et al., 2007). Therefore it can be hypothesised that βIV-spectrin is required for the maintenance of the AIS after the AIS has formed and that ankyrin$_G$ is required for βIV-spectrin's targeting to the AIS.

As well as targeting Na$_v$ channels and βIV-spectrin to the AIS, ankyrin$_G$ is important for filtering and restriction of proteins to the correct neuronal compartment. In neurons 5 days *in vitro* (DIV), large ~70kDa dextrans were restricted from the axon but this restriction was disrupted after siRNA knockdown of ankyrin$_G$. This filter is selective – synaptic vesicle protein VAMP2 was trafficked through to the axon,

whereas dendritic NR2B (an NMDA receptor subunit) was restricted to the soma (Song et al., 2009).

Both ankyrin$_G$ and ankyrin$_B$ (the other ankyrin expressed in brain) bind neurofascin so this cannot be the cause of location-specific clustering. *In vitro,* it has been shown that multiple domains of ankyrin$_G$ are required. The size and glycosylation of the serine-rich domain contribute to its restriction, and the serine-binding and C-terminal tail domains alone *in vitro* are targeted to the axolemma, showing that these regions are important for locating ankyrin$_G$ to the AIS (Zhang and Bennett, 1998).

Immunohistochemically, AIS can be identified by co-staining for ankyrin$_G$ and ankyrin$_B$; they are mutually exclusive within the neuron with ankyrin$_B$ expressed at the distal tip of the axon and ankyrin$_G$ at the proximal region, and it is expressed before ankyrin$_G$ in development. The spectrin-binding domain of ankyrin$_B$ targets it to axons and overexpression of ankyrin$_B$ restricts ankyrin$_G$ to shorter portions of the axon. Conversely, if ankyrin$_G$ is overexpressed ankyrin$_B$ accumulates into dense aggregates in the distal tip. Further to this, if αII-spectrin or βII-spectrin (the isoforms expressed in the distal axon) are overexpressed, the AIS becomes longer as ankyrin$_B$ is more efficiently localised to the distal tip. Knockdown of ankyrin$_B$, αII-spectrin or βII-spectrin *in vitro* causes ankyrin$_G$ to diffuse through the axon instead of clustering at the proximal region or in some cases form a 'fragmented AIS' co-localised with other AIS proteins throughout the axon. *In vivo*, *Ank2*$^{-/-}$ neurons retain a normal AIS; however knockouts of *Spna2* or *Spnb2* (αII-spectrin or βII-spectrin respectively) in neurons caused a similar fragmentation of ankyrin$_G$ localisation showing that they are essential for restriction of ankyrin$_G$ to the AIS (Galiano et al., 2012).

Surprisingly, it has also been shown that in some cases ankyrin$_G$ is not necessary for AIS formation. *Nestin-Cre/Ank3$^{F/F}$* mice, with exons 23 and 24 floxed out in neurons, did not survive past birth (Ho et al., 2014), as expected from previous studies. However, when a *Cre*-specific to peripheral sensory neurons (*Advilin-Cre*) or retinal ganglion cells (*Six3-Cre*) was used, ankyrin$_G$ was absent from nodes but mice survived to P14 and no impairment in rotarod performance when tested up to 2 years old (Ho et al., 2014). A compensatory mechanism was found wherein ankyrin$_R$ (the erythrocyte form) and βI-spectrin (its binding partner in erythrocytes) was expressed at nodes in ankyrin$_G$-deficient neurons, and this was enough to rescue Na$_v$ channel localisation. Ankyrin$_R$ is not required for normal channel clustering (Ho et al., 2014) but ankyrins are required, as double knockouts of ankyrin$_G$ and ankyrin$_R$ using these Cre drivers were lethal by P3 and Na$_v$ clustering was completely absent (Ho et al., 2014).

1.7.4 Ankyrin$_G$ in the node of Ranvier

Along the length of myelinated axons, Na$_v$ channels cluster at regular unmyelinated regions allowing 'jumping' of action potentials, known as saltatory conduction (Salzer, 1997, Lambert et al., 1997). These unmyelinated regions are the nodes of Ranvier and are 1-2μm long, flanked by paranodal regions. In the peripheral nervous system (PNS), the myelinating glial cells are Schwann cells whereas in the central nervous system (CNS) instead they are oligodendrocytes. During development (rat embryonic day 15), ankyrin$_G$, Na$_v$ channels and spectrin are diffuse along the length of the axon. During myelination, ankyrin$_G$ redistributes to clusters with Na$_v$ channels, neurofascin and NrCAMs (Lambert et al., 1997).

1.7.5 Ankyrin$_G$ potentially plays other roles in the nervous system

Although it is now widely accepted that ankyrin$_G$ is important for AIS and nodal structure and function, it may also play other, unknown functions in neurons – particularly if different isoforms have differing roles. 190kDa ankyrin$_G$ is upregulated in a subpopulation of postnatal radial glial progenitors (pRGPs) during formation of the subventricular zone stem cell niche and after shRNA knockdown the pRGPs failed to differentiate (Paez-Gonzalez et al., 2011). Further to this, the 480/270-kDa brain-specific isoforms of ankyrinG are necessary for embryonic neural progenitor proliferation, and knockdown of these causes an increase in proliferation by reducing cell-cycle exit (Durak et al., 2015) and is accompanied by an increase in canonical Wnt signalling. Knockdown of 190-kDa ankyrin$_G$ using RNAi in mature cortical neuron culture causes a 20% reduction in amplitude of excitatory post-synaptic currents as well as an 18% reduction in spine area and density (Smith et al., 2014). This suggests that a short isoform (190kDa) of ankyrin$_G$ increases the stability of AMPA receptors (Smith et al., 2014). These studies suggest that different isoforms of ankyrin$_G$ could play a part in development, stem cell niche and proliferation, and synaptic excitation and LTP.

1.7.6 GWAS identify ankyrin$_G$ as a risk factor for psychiatric disease

There have been multiple SNPs identified in *ANK3* as being associated with schizophrenia, bipolar disorder, or both (supporting the theory that common genetic mechanisms are shared across disorders). There are two distinct clusters of SNPs that have been identified, at the 5' end and the 3' end of the gene, which are independently associated with BD (Ferreira et al., 2008, Schulze et al., 2009). At the 5' end, rs10761482 was associated with schizophrenia alone in European and Chinese populations (Athanasiu et al., 2010, Yuan et al., 2012, Nie et al., 2015) while

rs10994338 (Liu et al., 2011), rs1938526 (Smith et al., 2009) and rs10994338 (Chen et al., 2013) were associated with BD, and rs10994359 (Schizophrenia Psychiatric Genome-Wide Association Study, 2011) and rs10994336 (Ferreira et al., 2008, Tesli et al., 2011, Schulze et al., 2009, Scott et al., 2009, Liu et al., 2011, Yuan et al., 2012) were associated with both schizophrenia and BD.

Although many of the SNPs have not been confirmed as functional, some such as rs10994336 have been well-characterised; healthy controls carrying the risk allele T showed lower novelty seeking and a high startle reactivity (Roussos et al., 2011), alterations in white matter integrity in the anterior limb of the internal capsule and altered decision-making (Linke et al., 2012), and a decreased lateral temporal cortical activation in the temporal gyrus (Delvecchio et al., 2015). At the 3' end of *ANK3*, rs9804190 was associated with bipolar disorder independently of the 5'-end SNPs (Schulze et al., 2009, Smith et al., 2009, Tesli et al., 2011) and carriers of the risk allele showed changes in working memory regional activation (Delvecchio et al., 2015). Studies of blood mRNA expression of ankyrin$_G$ showed that patients with schizophrenia or BD have reduced levels of *ANK3* mRNA, with this effect being larger in BD than in schizophrenia (Wirgenes et al., 2014). None of the associated SNPs has been identified as expression quantitative trait loci (eQTLs) for ankyrin$_G$ expression or of other genes.

Although single nucleotide changes confer a very slight susceptibility to disease, larger disruptions have been identified in patients with autism spectrum disorder (ASD). A balanced translocation disrupting all isoforms of ankyrin$_G$ was found in a patient with attention-deficit hyperactivity disorder (ADHD), autism and sleeping problems as well as a consanguineous family presenting with moderate intellectual disability (ID) and ADHD-like symptoms who had a truncating frameshift in the gene

(Iqbal et al., 2013). Whole-exome sequencing of patients with ASD identified a novel mutation c4705T>G, pS1569A in two unrelated patients (Bi et al., 2012). This is yet more evidence that ASD, BD and schizophrenia all share some molecular foundation and it may be that different levels of gene disruption give rise to the spectrum of neuropsychiatric disorders. Nevertheless, it is still unclear what the mechanism behind this susceptibility is, and so in order to validate *ANK3* as a risk gene we turn to animal models.

1.7.7 Knocking out *Ank3* causes homozygous lethality

A constitutive knockout using β-actin-Cre as a driver to flox exons 22 and 23 (just upstream of the spectrin-binding domain) eliminated the 190-, 270- and 480-kDa isoforms and caused homozygotes to die before birth (Jenkins et al., 2013). Knocking out *Ank3* in the cerebellum via a targeted disruption of exon 1b causes a progressive ataxia in P16 mice, as well as a loss of Purkinje neurons and deficiencies in action potential initiation and neuron firing. Homozygous mice also had a smaller cerebellum with a thin molecular layer, and the number of Purkinje cells decreased by 60%. Some homozygous animals died prematurely (Zhou et al., 1998). Heterozygous cerebellar-specific knockout males showed decreased anxiety in the Elevated Plus Maze and a higher preference for sugar, which was reversed by treatment with lithium (Leussis et al., 2013). This was replicated using *Ank3* RNAi in the hippocampal dentate gyrus; injection of an shRNA led to decreased anxiety and this was again reversed by lithium. A second shRNA increased activity in the light phase, raising the possibility that this could link bipolar disorder risk genes and the circadian and sleep disruption often seen in BD patients. These models are all severe – whole brain region knockouts are enough to cause premature death and a visible ataxia phenotype while knockouts of all brain-specific isoforms are lethal – while

ideally a model for endophenotypes of BD or schizophrenia would survive to adulthood for behavioural testing. In order to find mutations with small behavioural effects, we utilise ENU mutagenesis as described in 1.4.

1.7.8 Hypothesis

Novel mutations in *Ank3* found via a genetic screen of ENU-mutagenised DNA and re-derived can be intercrossed to produce homozygous mutant animals. The mutation has the potential to have a range of effects dependent on whether it is a functional null, hypomorph, dominant negative or gain of function, and these may affect domains altered in BD or schizophrenia patients such as anxiety, memory, and startle response and prepulse inhibition. We are most likely to see effects in Na_v channel and βIV-spectrin localisation and AIS specification as $ankyrin_G$ is essential for these functions.

1.8 *TCF4*

TCF4 encodes a transcription factor TCF4, which has many other identifiers (SEF2-1B, SEF2, ITF2, FECD3, bHLHb19, SEF-2, SEF2-1D, PTHS, TCF-4, SEF2-1A, SEF2-1, BHLHB19, E2-2, ITF-2) and is involved in lymphopoiesis and neurodevelopment. It is not to be confused with TCF7L2, a member of the T-cell factor family, which is involved in Wnt signalling and has been called Tcf4 in a number of publications. TCF4 is a helix-loop-helix protein, able to form dimers and bind DNA to activate gene transcription, and common variants have been associated with schizophrenia.

1.8.1 Helix-loop-helix proteins

Basic helix-loop-helix (bHLH) proteins are well-conserved throughout vertebrates, *D. melanogaster* and yeast, and are involved in a range of functions including sex determination and neurogenesis in *Drosophila*, myogenesis, and lymphopoiesis (reviewed in Murre et al. (1994)). Class I contains TCF4, TCF12 (also known as HEB), and TCF3 (also known as E2A) which are ubiquitously expressed and also known as E-proteins. These proteins form dimers with other tissue-specific bHLH proteins and bind DNA.

The helix-loop-helix (HLH) domain contains hydrophobic residues on one side of the helix and is required for homo- and heterodimerisation (Murre et al., 1989a, Voronova and Baltimore, 1990, Quong et al., 1993). When dimerised, the basic DNA-binding domains then bind promoter or enhancer elements at a conserved Ephrussi-box (E-box) consensus sequence 5'-GCANNTG-3' (Figure 11A) (Murre et al., 1989b, Henthorn et al., 1990a). Dimers interact with the DNA major groove perpendicular to each other on opposite sides of the DNA (Ferre-D'Amare et al., 1993). Heterodimers

usually cause transcriptional activation although some binding partners (ID1-3) lack the DNA-binding domain and act as repressors (Bertrand et al., 2002) (Figure 11A-B).

TCF4 was first identified as binding to the immunoglobulin enhancer μE5/κ2 E-box motifs (Henthorn et al., 1990a, Henthorn et al., 1990b) and is expressed in developing and adult brain, with a peak in late prenatal life (Rannals et al., 2016), and in the immune system (https://genevisible.com/tissues/HS/UniProt/P15884, Hruz et al. (2008)). It is involved in lymphopoiesis and neurogenesis, described below, via recruitment of transcription factor IIB (TFIIB) (Pscherer et al., 1996) or by modulation of chromatin via recruitment of the SPT-ADA-GCnS-acetyltransferase (SAGA) complex (Massari et al., 1999).

The *TCF4* gene (Figure 11C) transcribes multiple splice variants. The gene contains 41 exons in total and 21 of these are alternative and mutually exclusive 5' exons situated throughout the gene (Sepp et al., 2011). In total, *TCF4* could encode up to 18 isoforms. All isoforms contain the bHLH domain (encoded by exon 19) and transactivational domain (TAD) 2 (exons 14-16) (Sepp et al., 2011), while only the isoforms with the longest N-termini contain TAD1 (exons 3-6). In between TAD1 and TAD2, there is a nuclear localisation signal (NLS) (Sepp et al., 2011). TCF4 also contains regulatory domains, including a C domain required *in vivo* for heterodimerisation (Goldfarb et al., 1998) and a conserved self-contained transcriptional repressor domain (Herbst and Kolligs, 2008) (Figure 11C). In this introduction, the focus will be on TCF4-B, the longest isoform and the most widely studied. The overall structure of *TCF4* is conserved in the mouse genome; exons 3-20 have 92% identity homology (Sepp et al., 2011).

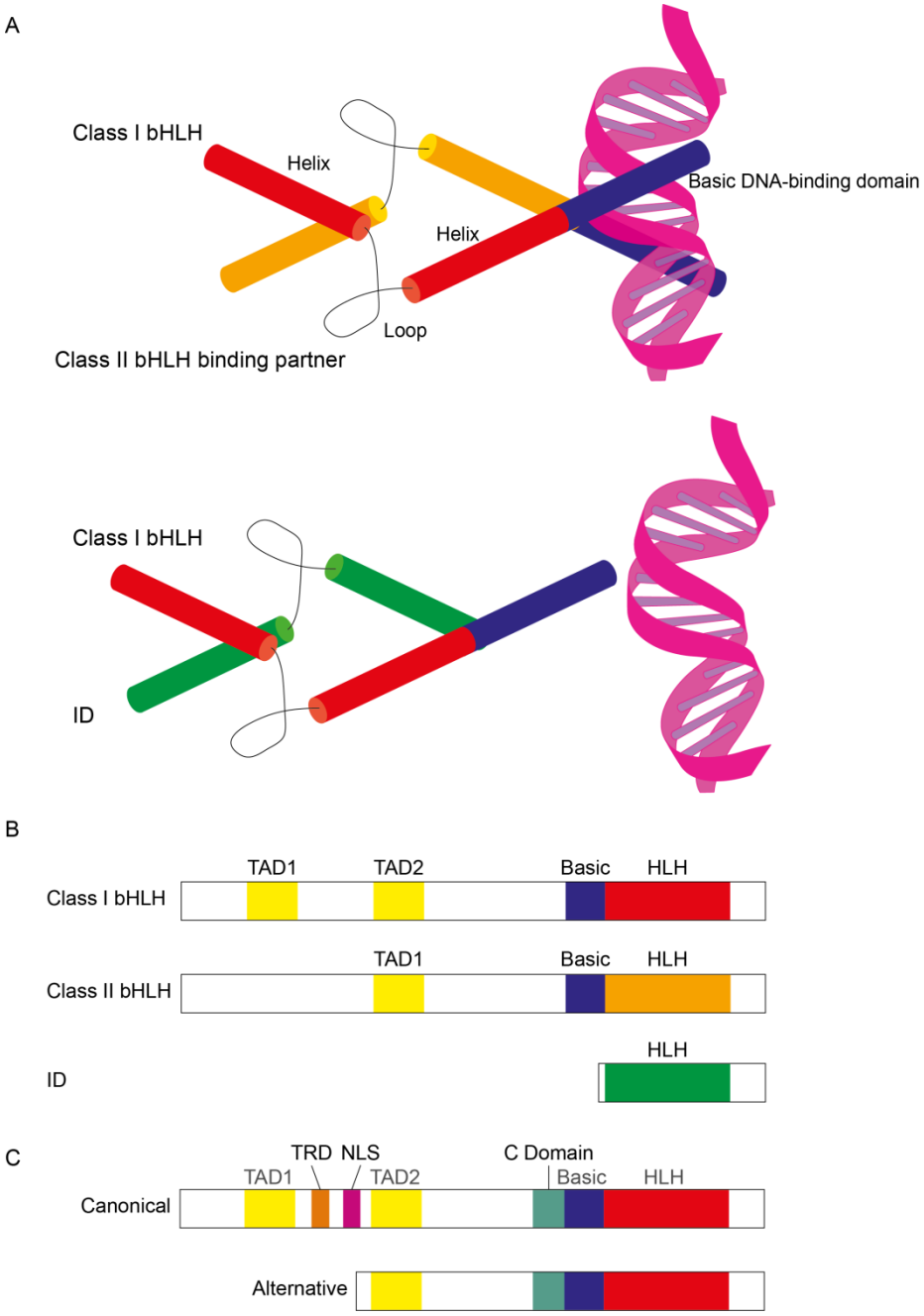

Figure 11 bHLH Proteins.

(A) Schematic of dimerisation between a class I and a class II bHLH protein (top) and subsequent DNA binding via the basic domain. When bound to an ID protein lacking a DNA-binding domain (bottom) binding is inhibited. (B) Schematic showing domains of Class I and Class II bHLH proteins and IDs. (C) Overview of TCF4, showing both canonical and alternative start sites. bHLH – basic helix loop helix, TAD – transactivational domain, TRD – transcriptional repressor domain, NLS – nuclear localisation signal.

1.8.2 TCF4's role in lymphopoiesis and EMT

TCF4 is involved in the development of T- and B-lymphocytes (Bergqvist et al., 2000, Quong et al., 2002). However, it is not essential; in a knock-out mouse model (*Tcf4*$^{-/-}$), while homozygous animals were observed at a low frequency and died perinatally, they were still able to produce B-cells albeit a reduced quantity (Zhuang et al., 1996). This study showed that a double heterozygote lacking a copy of another bHLH protein TCF3 (*Tcf4*$^{+/-}$*E2A*$^{+/-}$) produced fewer B-cells than the homozygous *Tcf4*$^{-/-}$ animals, suggesting that a combined dosage of these and another E-protein TCF12 is required for normal B-cell development. TCF4 has also been shown to be essential for maintenance of mature plasmacytoid dendritic cells (Cisse et al., 2008, Ghosh et al., 2010) and epithelial-mesenchymal transition (EMT) (Cano and Portillo, 2010).

1.8.3 TCF4 in neurodevelopment

E-proteins and tissue-specific bHLH proteins are essential for neurodevelopment (Bertrand et al., 2002, Powell and Jarman, 2008). Proneural bHLH factors are expressed in neural progenitors and throughout development, co-ordinating cell cycle exit, migration, and terminal differentiation to produce specific neuronal subpopulations (Farah et al., 2000, Schwab et al., 2000, Ge et al., 2006). In the brain TCF4 interacts with MATH1 to regulate differentiation of a subset of neuronal progenitors in the hindbrain and *Tcf4*$^{-/-}$ mice have disrupted pontine nucleus development (Flora et al., 2007). This role is specific to TCF4; knock-outs of TCF3 and TCF12 do not show hindbrain defects (Flora et al., 2007). The repressive proteins DNA-binding protein inhibitor (ID)1 and ID2 are also expressed during neurogenesis *in vivo* and *in vitro* (Duncan et al., 1992, Neuman et al., 1993, Einarson and Chao, 1995). TCF4 prevents S phase entry, keeping neural progenitors in a proliferative state (Ross et al., 2003) and this function is opposed by ID2 which

promotes S-phase entry and cell division (Neuman et al., 1993). Prevention of S phase occurs downstream of Zac1, a zinc finger protein that activates expression of TCF4 in the cerebellum. This then upregulates $p57^{Kip2}$, keeping cells in G1 phase (Chung et al., 2011, Schmidt-Edelkraut et al., 2014).

1.8.4 Haploinsufficiency of TCF4 causes Pitt-Hopkins Syndrome

First described in 1978 (Pitt and Hopkins, 1978), Pitt-Hopkins Syndrome (PHS) is a rare autosomal dominant syndrome caused by mutations in *TCF4*. PHS patients display severe intellectual disability (ID) and psychomotor delay, facial abnormalities and breathing problems including apnoea and hyperventilation, and some also have epilepsy or microcephaly. PHS is caused by a haploinsufficiency of TCF4 via a deletion or mutation that disables the DNA binding domain and acts in a dominant negative manner (Amiel et al., 2007, Brockschmidt et al., 2007, Zweier et al., 2007). A range of causative mutations have been discovered, most in the basic domain (de Pontual et al., 2009). Breakpoint disruptions which leave a partially functional DNA-binding domain give rise to a less severe form of the syndrome (mild ID and facial abnormalities) (Kalscheuer et al., 2008). It is not yet clear what pathways are involved downstream of TCF4 in PHS; it has been shown that TCF4 may modulate the expression of neurexin-1 and contactin-associated protein-like-2 (CNTNAP2) in a variable and context-specific manner, suggesting that these form a regulatory network (Forrest et al., 2012). In an *in vivo* model of PHS, suppression of *Tcf4* expression in mouse and rat prefrontal neurons caused an attenuation in neuronal spiking due to an increased afterhyperpolarisation. This study also identified two ion channels SCN10a and KCNQ1 which were upregulated in these models, suggesting that TCF4 regulates neuronal excitability via repression of these genes (Rannals et al., 2016).

Hemizygous deletion of the 18q chromosome arm has also been associated with a higher incidence of neurodevelopmental disorders such as autism and attention-deficit hyperactivity disorder (ADHD) (O'Donnell et al., 2010). Balanced translocations and copy number variants (CNVs) that disrupt *TCF4* have also been associated with autism (Talkowski et al., 2012), linking alterations in *TCF4* to diverse clinical consequences.

1.8.5 Common variants in TCF4 are associated with schizophrenia

Multiple SNPs in *TCF4* have been associated with schizophrenia, with rs9960767 being the first identified (Stefansson et al., 2009). This SNP has been associated with an increase in adolescent paranoia (Sieradzka et al., 2014) and changes in verbal declarative memory (Lennertz et al., 2011), as well as disrupted sensorimotor gating of PPI (Quednow et al., 2011, Quednow et al., 2012). Another SNP in intron 3 of *TCF4*, rs17512836 (Schizophrenia Psychiatric Genome-Wide Association Study, 2011, Hamshere et al., 2013), has been associated with a decrease in P300 amplitude suggesting defects in attention and working memory (Hall et al., 2014). Two SNPs have been identified with strong linkage (rs4309482 and rs12966547)(Steinberg et al., 2011, Schizophrenia Psychiatric Genome-Wide Association Study, 2011) and these have also been associated with decreased verbal fluency (Wirgenes et al., 2012) and an earlier age of onset (Chow et al., 2016). Other SNPs have been identified but not yet replicated (International Schizophrenia et al., 2009, Aberg et al., 2013) and others have been identified only in a Han Chinese population (Li et al., 2010, Li et al., 2016). No schizophrenia-associated SNPs have been shown to be eQTLs (Wirgenes et al., 2012). Studies of expression have produced contrasting results; Wirgenes et al. (2012) observed an increase in

blood mRNA in patients with schizophrenia, while in post-mortem brains no changes have been observed (Umeda-Yano et al., 2014).

Interestingly, a transgenic mouse model of TCF4 brain-specific overexpression (*Tcf4tg)* displays sensorimotor gating defects and reduced fear-conditioned and trace memory (Brzozka et al., 2010, Brzozka and Rossner, 2013). Patients displaying these endophenotypes have been shown to have structural changes in the anterior cingulate cortex (ACC) and malfunction in cortical and hippocampal networks (Szeszko et al., 2000, Quintana et al., 2004) and this was also observed in the transgenic mice (Brzozka and Rossner, 2013). This suggests a role for TCF4 in connectivity between the ACC and hippocampus.

TCF4 may also play a role in circadian rhythms. *Tcf4tg* mice show an increase in the circadian gene *mPer2* at most time points in the hippocampus, and also changes in *Id2*, which is expressed in a circadian manner with a peak at the dark-light transition (Brzozka et al., 2010). This implicates *Tcf4* in circadian gene expression profiles in the brain. *Cryptochrome1* (*Cry1)* is a key component of the circadian clock with multiple E-box motifs in its promoter (Hardin, 2004, Fustin et al., 2009). Cell lines from PHS patients have decreased *Cry1* expression, and siRNA knockdown of *Tcf4* in SH-SY5Y cells altered circadian expression pathways (Mullegama et al., 2014). *Id2* has also been shown to be involved in circadian rhythms; *Id2*$^{-/-}$ mice show abnormally rapid entrainment and an increase in the magnitude of phase shift, as well as disrupted rhythms in constant darkness in some animals (Duffield et al., 2009). It is also expressed in the SCN and may act with *CLOCK* and *BMAL*, two pieces of the core circadian machinery that are also bHLH proteins (Ko and Takahashi, 2006). TCF4 expression has not been studied extensively in circadian networks and it may be that it plays a role in modulation of transcription alongside other bHLH proteins.

Overall, TCF4 appears to act as an integrator of bHLH protein networks during neurodevelopment and changes in TCF4 expression also affect plasticity and information processing in adulthood. It was therefore chosen for further investigation using a reverse genetics approach.

1.8.6 Novel mutations in *Tcf4* identified using ENU mutagenesis

Two non-synonymous mutations were identified in *Tcf4* through screening of the ENU-mutagenised archive as described previously (Parsons, unpublished data). Both mutations affect serine residues in a putative serine-rich region. This spans residues 181 - 371 (in mouse) in between the NLS and TAD2 and is predicted by PROSITE (Sigrist et al., 2002, Sigrist et al., 2013). Serines make up over 25% of residues in this region but there are no publications on its structure or function. $Tcf4^{S189G}$ causes a serine-glycine substitution and $Tcf4^{S275R}$ causes a serine-arginine change.

1.8.6.1 Post-translational modifications of serine residues

Post-translationally, serines can be reversibly phosphorylated, with the phosphate group donated by ATP. Phosphoserines are one of the most prevalent modifications observed (Prabakaran et al., 2012). The phosphoryl group is dianionic at physiological pH (Johnson, 2009), and can form hydrogen bonds. In binding sites, phosphorylation can reinforce conformational states, often through forming hydrogen bonds with arginine residues or polar amino acid side chains. Phosphorylation can also promote disorder-to-order transitions and conformational changes that lead to protein association (Johnson, 2009). Modifications encode the prevailing physiological and cellular conditions, and these can vary with tissue or cell type, cell state, or location of the protein within the cell (Prabakaran et al., 2012). The serine-rich region of TCF4 contains many putative modification sites, and these could

expand the function of the protein and confer functional plasticity (Prabakaran et al., 2012).

1.8.7 Hypothesis

Through *in silico* and *in vitro* methods these two mutations will be prioritised for re-derivation and behavioural phenotyping. We hypothesise that these residues may undergo post-translational modification, for example, phosphorylation, and that their mutation will cause changes in dimerisation of TCF4 both alone and with heterodimer binding partners, and therefore affect activation of transcription. Once prioritised and re-derived, we expect that animals will show neurodevelopmental defects. If an allele functions as a null we may see severe psychomotor delay and morphological changes as in Pitt-Hopkins Syndrome. On the other hand, if they are a gain of function we may see defects in sensorimotor gating and fear-conditioned learning, as observed in *Tcf4tg* mice (Brzozka et al., 2010, Brzozka and Rossner, 2013). Animals are likely to have circadian defects if a mutation causes changes in ID2 binding or mPER2 expression.

1.9 *CACNA1C*

CACNA1C encodes $Ca_v1.2$, an α_1 subunit of the post-synaptic voltage-dependent calcium channel expressed in the brain and heart. $Ca_v1.2$ is responsible for the voltage-dependence, calcium specificity, and calcium-dependent inactivation of the channel, mediated by cytoplasmic N- and C-terminal domains and four transmembrane pore-forming regions.

1.9.1 Nomenclature of Ca_v Channels

There are three families of voltage-gated calcium channels characterised by their physiological and pharmacological properties (reviewed in (Catterall, 2000)). Each family is defined by similarities in the amino acid sequence of the α subunit and named in order of discovery (Table 2) (Ertel et al., 2000). Each family (Ca_{v1}, Ca_v2 and Ca_v3) has 80% intrafamily similarity, whereas between families there is 52% (Ca_v1 vs. Ca_v2) or 28% (Ca_v vs. $Ca_v1/2$) sequence similarity (Figure 12) (Catterall et al., 2005). Ca_v1 channels are known as L (long-lasting)-type, and have a high voltage of activation, large single channel conductance and slow voltage-dependent inactivation (VDI), and were first characterised as dihydropyridine (DHP)-sensitive channels in rabbit skeletal muscle (Tanabe et al., 1987).

Name	Former Names	Gene Name and Human Chromosome	Primary Tissues
$Ca_v1.1$	α_{1S}	CACNA1S; 1q31-32	skeletal muscle
$Ca_v1.2$	α_{1C}	CACNA1C; 12p13.3	brain, heart, pituitary, adrenal
$Ca_v1.3$	α_{1D}	CACNA1D; 3p14.3	brain, pancreas, kidney, ovary, cochlea
$Ca_v1.4$	α_{1F}	CACNA1F; Xp11.23	retina
$Ca_v2.1$	α_{1A}	CACNA1A; 19p13	brain, cochlea, pituitary
$Ca_v2.2$	α_{1B}	CACNA1B; 9q34	brain, nervous system
$Ca_v2.3$	α_{1E}	CACNA1E; 1q25-31	brain, cochlea, retina, heart, pituitary
$Ca_v3.1$	α_{1G}	CACNA1G; 17q22	brain, nervous system
$Ca_v3.2$	α_{1H}	CACNA1H; 16p13.3	brain, heart, kidney, liver
$Ca_v3.3$	α_{1I}	CACNA1I; 22q12.3-13-2	brain

Table 2 Nomenclature of calcium channels (Ertel et al., 2000)

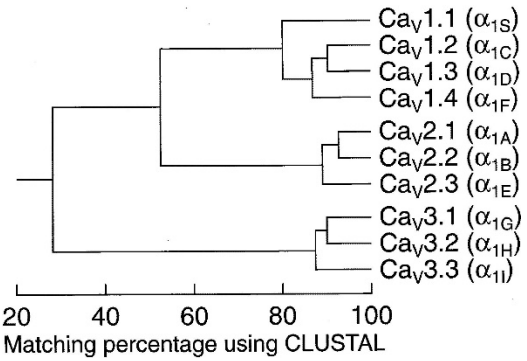

Figure 12 Phylogeny of Ca_v α1 subunits.

Only the membrane-spanning segments and the pore loops (~350 amino acids) of human Ca_v subunits are compared. First, all sequence pairs were compared, which clearly defines three families with intrafamily sequence identities above 80% (CaV1.m, CaV2.m, CaV3.m). Then, a consensus sequence was defined for each family, and these three sequences were compared to one another, with interfamily sequence identities of ~52% (CaV1.m versus CaV2.m) and 28% (CaV3.m versus CaV1.m or CaV2.m) (from Ertel et al. (2000)

1.9.2 Subunits of the Ca_v1 channel complex

Ca_v channels are heteromultimeric and generally contain α_1, β, γ and $\alpha_2\delta$ subunits (Catterall et al., 2005) although the $Ca_v1.2$ channel in neurons does not have a γ subunit associated (Cooper et al., 1987). The α_1 subunit is sufficient for voltage-dependent current and calcium-dependent inactivation (CDI), but with low expression levels and abnormal kinetics (Tanabe et al., 1987, Perez-Reyes et al., 1989).

1.9.3 The α_1 subunit

The α_1 subunit contains approximately 2000 amino acids and is similar to the pore-forming subunit of the voltage-gated sodium channel. The Ca_v1 L-type subunit was identified in rabbit skeletal muscle (Tanabe et al., 1987) and a homologous 170kDa peptide was found in cardiac tissue (Cooper et al., 1987) as well as in lung (Biel et al., 1990). In rat brain, distinct α_1 subunits with related and conserved transmembrane domains were identified and designated α_1A to D. Subunit α_1C showed 75% homology to the skeletal channel and 97% homology to the cardiac channel (Snutch et al., 1990). When nomenclature of Ca_v channels was standardised this became $Ca_v1.2$ (Ertel et al., 2000).

1.9.4 Localisation of $Ca_v1.2$ in the brain

Antibodies raised against skeletal muscle Ca_v were found to stain hippocampus, cortex and cerebellum with strong staining clustered at the base of dendrites (Ahlijanian et al., 1990). This was also shown in hippocampal pyramidal neurons (Westenbroek et al., 1990). An antibody against $Ca_v1.2$ immunoprecipitated 75% of L-type DHP-sensitive channels from rat cerebral cortex and hippocampus (Hell et al., 1993), showing that this is the dominant subtype present in these areas. This also showed that the $Ca_v1.2$ subunit localised to neuronal cell bodies and major proximal

dendrites in clusters. $Ca_v1.2$ was also identified in cortex, hippocampus, thalamus, hypothalamus, caudate putamen and amygdala (Splawski et al., 2004).

1.9.5 Structure of the $Ca_v1.2$ subunit

The $Ca_v1.2$ subunit contains four domains I-IV that span the plasma membrane, each containing six transmembrane segments (S1-6) as shown in Figure 13. S4 acts as a voltage sensor; every third residue is positively charged allowing a conformational change under an electric field (Tanabe et al., 1987). The pore loops between S5 and S6 line the pore and confer Ca^{2+} selectivity (Catterall, 2000).

The C-terminus of $Ca_v1.2$ is cytoplasmic and contains multiple putative regulatory elements including one EF-hand (Babitch, 1990) and calmodulin-binding domains (Figure 13). (Zühlke and Reuter, 1998) This region is essential for calcium-dependent inactivation of $Ca_v1.2$, discussed in 1.9.7.

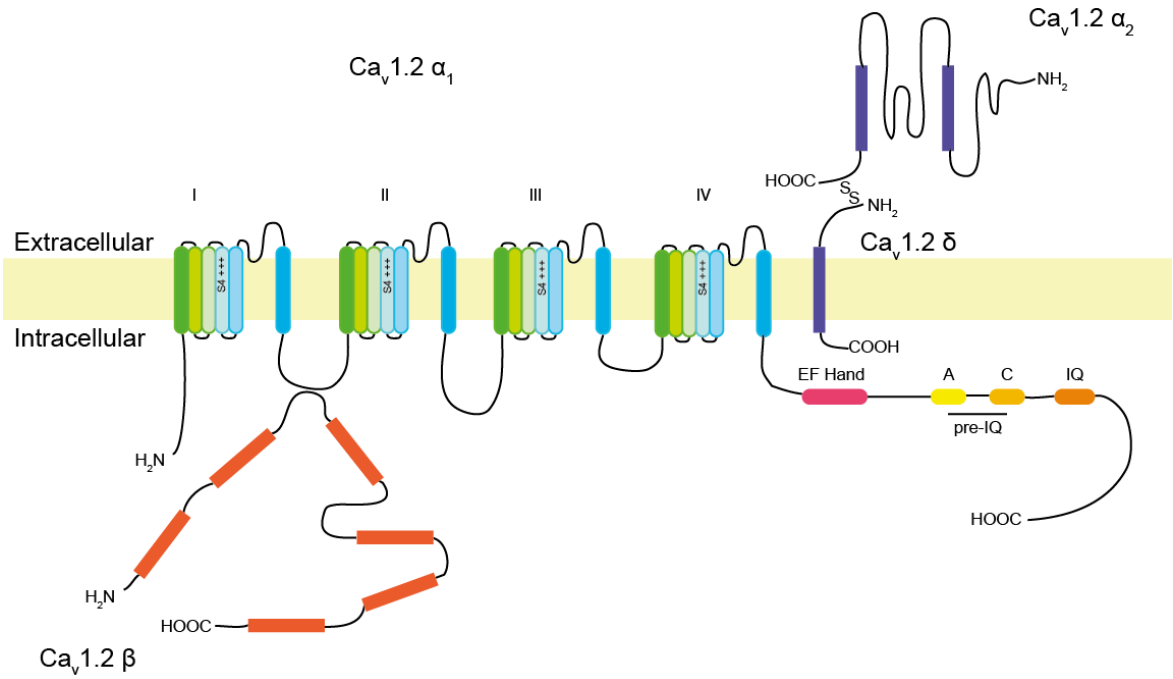

Figure 13 Schematic of $Ca_v1.2$ channel and associated subunits

1.9.6 Voltage Gating of $Ca_v1.2$

Activation of $Ca_v1.2$ channels is voltage-dependent and occurs at ~ -30mV (Lipscombe et al., 2004), sensed by the S4 coil as discussed above. Voltage-dependent inactivation (VDI) is slow compared to calcium-dependent inactivation (CDI) (reviewed in Tuckwell (2012)).

1.9.7 Calcium-dependent inactivation of $Ca_v1.2$

$Ca_v1.2$ is inactivated by Ca^{2+} entry (Eckert and Chad, 1984). An increase in Ca^{2+} concentration causes a physical conformational change in the channel (Imredy and Yue, 1994) and the resistance of $Ca_v1.2$ CDI to calcium-chelating buffers suggests that the critical region for CDI is close to the channel mouth (Neely et al., 1994, Hofer et al., 1997). Several regions in the proximal third of the C-terminus were identified as potential mediators of CDI: a putative EF-hand motif, A and C-peptides, and a calmodulin-binding consensus IQ domain (Figure 13).

1.9.7.1 The EF-Hand

A putative EF hand domain was identified downstream of the last transmembrane domain and shown to be conserved between α_1 subunits (Babitch, 1990) suggesting that it may have an important role in channel function. EF hands are helix-loop-helix structures found in Ca^{2+}-binding proteins including calmodulin (reviewed in Gifford et al. (2007)). EF hands contain 29 amino acid residues (9 forming the E helix, a 9-residue loop, and an 11-residue F-helix) and are rich in negatively charged glutamic and aspartic acid residues. The loop forms a pentagonal bipyramidal structure that co-ordinates one Ca^{2+} ion between seven ligands. Five of these co-ordinating groups are provided by the 9-residue loop while two come from a carboxylate ligand in the second helix (Figure 14). The structure is stabilised through numerous hydrogen bonds allowing several negatively-charged oxygen atoms to be in close proximity.

Unusually in $Ca_v1.2$ there is only one EF-hand domain; canonically the domains occur in pairs that stabilise the secondary structure.

EF-hand binding to calcium was supported by chimera experiments exchanging the EF-hand of $Ca_v1.2$ (which undergoes CDI) and Ca_v 2.3 (which does not) (de Leon et al., 1995). These appeared to show that the EF-hand of $Ca_v1.2$ conferred CDI to $Ca_v2.3$, and vice versa. Further studies failed to replicate these effects in $Ca_v1.2/2.3$ EF-hand chimeras, and a triple mutation designed to eradicate calcium binding showed no change in CDI (Zhou et al., 1997). This study also created $Ca_v1.2/2.3$ chimeras using a ~140-a.a segment immediately following the EF-hand, which was able to confer CDI onto $Ca_v2.3$. This, along with work by Zühlke and Reuter (1998), indicated that multiple regions in the C-terminal tail were involved in CDI including the EF-hand, two hydrophilic residues downstream and an IQ consensus sequence (associated with calmodulin binding). It has now been shown that the EF hand is required for CDI, but not necessarily through direct calcium binding (Peterson et al., 2000).

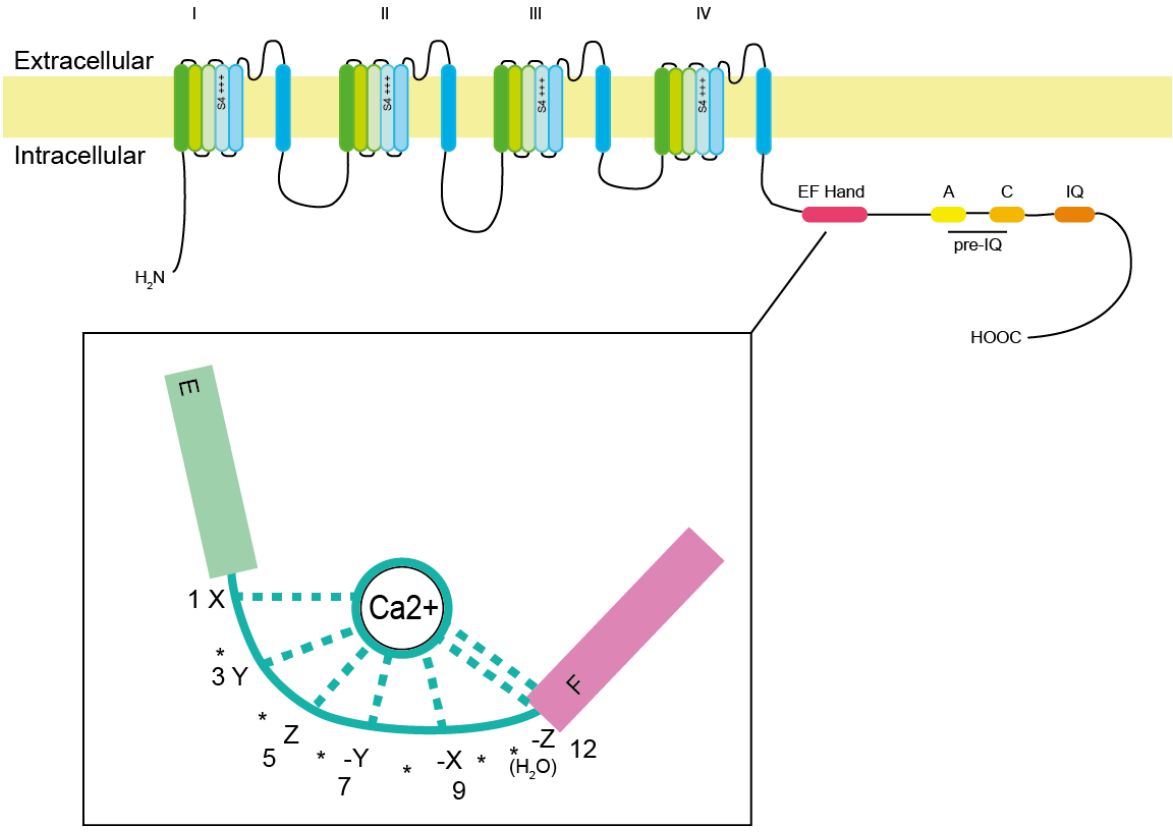

Figure 14 Co-ordination of Ca^{2+} by a canonical EF-hand.

Schematic of $Ca_v1.2$ showing the C-terminal location of EF-hand downstream of S6 of TM domain IV. The EF hand loop co-ordinates Ca^{2+} in a pentagonal bipyramidal structure between seven ligands.

1.9.7.2 A, C and IQ motifs downstream of the EF-hand

Multiple non-contiguous peptide sequences that are necessary for CDI were identified through systematic deletions (Zühlke and Reuter, 1998). One of these was an IQ (isoleucine-glutamate) motif, which is a calmodulin (CaM)-binding motif.

1.9.7.2.1 Calmodulin

Calmodulin (CaM) is ubiquitous and well-conserved throughout the animal, plant, fungi and protozoan kingdoms. It responds to changes in Ca^{2+} concentration, coupling it to downstream signalling and synchronising the cellular response (reviewed in Haeseleer et al. (2002)). CaM has two lobes (C-terminal and N-terminal), each of which contains a pair of EF hands, and the lobes are connected by

a central helix. When Ca^{2+} binds, it causes a conformational change; CaM opens and exposes binding sites in the central linker, which then bind target peptides. The structural flexibility of this central linker allows recognition and binding to many diverse peptides (Halling et al., 2006).

1.9.7.2.2 The IQ domain binds CaM in a Ca^{2+} dependent manner

Mutation of the isoleucine (I) residue had varying effects: mutation to alanine removed CDI and unmasked a strong facilitation effect, while mutation to glutamate removed both CDI and facilitation effects (Zühlke et al., 1999). These results suggest that the same CaM molecule may act as a Ca^{2+} sensor for both positive and negative regulation of channel activity. A mutant Ca^{2+}-insensitive CaM with a dominant negative effect ablates both positive and negative regulation, indicating that binding of CaM to $Ca_v1.2$ is not Ca^{2+}-dependent (Zühlke et al., 2000). The IQ domain was therefore posited as a tethering site for CaM.

1.9.7.2.3 Other peptides identified as tethering sites for CaM

Further work using a Ca^{2+}-insensitive CaM (CaM_{234}) showed that the IQ domain alone could not bind either in the presence of Ca^{2+} or in EGTA (a calcium-chelating agent) (Pitt et al., 2001). This study identified two non-contiguous peptide stretches able to bind CaM and CaM_{234}; the first was a type A motif (IKTEG) and the second was designated the C motif (LLDQV). It was also shown that tethering in a Ca^{2+} concentration similar to resting cytoplasmic concentration required both of these sequences and that the N-terminal of CaM binds constantly to the A-peptide. A model was put forward wherein the N-terminal lobe of CaM constitutively binds the A motif and the C motif sits between the lobes as it can bind to either. When CaM binds Ca^{2+}, this causes a conformational change in CaM exposing binding sites and allowing IQ to interact with the C-terminus (Figure 15)(Pitt et al., 2001, Xiong et al., 2005).

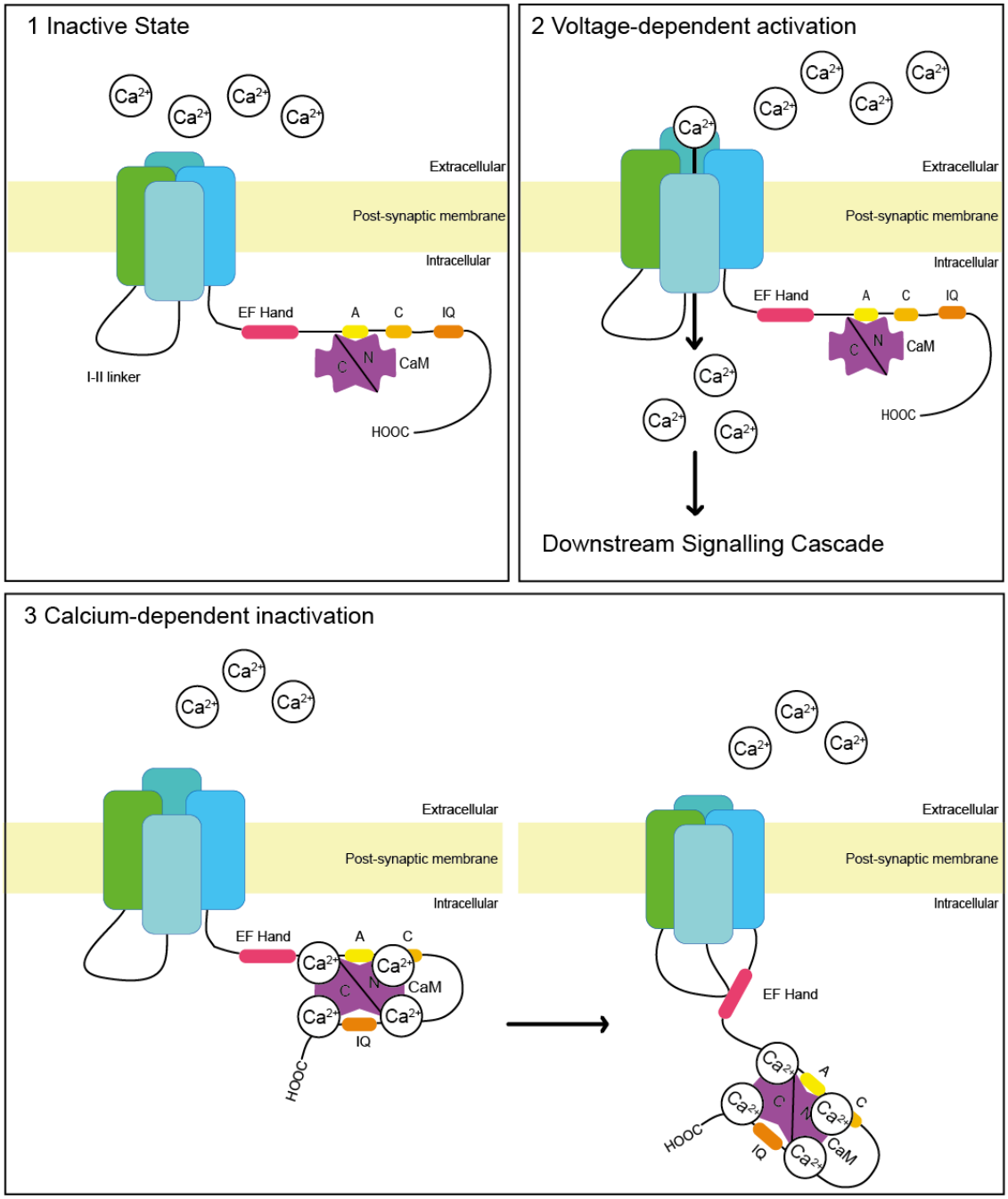

Figure 15 Mechanism of CDI.

1. At resting potential, the pore of $Ca_v1.2$ is closed and the channel is inactive. CaM is constitutively bound to the A motif. 2. When depolarised, the channel activates and Ca^{2+} enters the cell. 3. As the concentration of Ca^{2+} increases, Ca^{2+} binds CaM and causes a conformational change, allowing it to bind the IQ domain. This leads to inactivation of $Ca_v1.2$ via a proposed interaction between the EF-hand and the I-II intracellular linker.

1.9.7.3 The N-terminal of $Ca_v1.2$ and its role in CDI

A CaM-binding site was identified in the cytosolic N-terminus of $Ca_v1.2$, termed the *N*-terminal *S*patial *Ca*$^{2+}$-*t*ransforming *e*lement (NSCaTE) (Dick et al., 2008). A second site was identified and both sites were found to be involved in CDI (Simms et al., 2014). A recent paper showed that the N-terminal and the proximal C-terminal domain interact in a CaM-independent manner, and that Ca^{2+} weakens this interaction (Benmocha Guggenheimer et al., 2016).

1.9.8 Cleavage and autoregulation of $Ca_v1.2$

$Ca_v1.2$ is truncated in many tissues, and when purified from the heart and reduced only around 10-15% of transcripts are full-length (240kDa); the remainder is cleaved to around 190kDa. The full-length channel is cleaved by proteases including calpain I (De Jongh et al., 1994) and expression of a truncated protein *in vitro* can increase currents by up to 10-fold (Hell et al., 1996, Gao et al., 2001). In hippocampal neurons, proteolysis is induced by calcium entry through NMDA receptors (Hell et al., 1996). The cleaved fragment re-associates with and inhibits the truncated channel (Gao et al., 2001) (Figure 16) and is required for survival (Fu et al., 2011). Inhibition is Ca^{2+}-dependent and is relieved by Ca^{2+}/CaM, enabling an increase in the dynamic range of calcium transients (Crump et al., 2013).

The 3' end of *CACNA1C* also produces a *c*alcium-*c*hannel *a*ssociated *t*ranscription regulator (CCAT), which is encoded by a cryptic promoter in exon 46 of *CACNA1C* (Gomez-Ospina et al., 2006, Gomez-Ospina et al., 2013). Expression of CCAT is independent of $Ca_v1.2$ expression and is differentially regulated during development and in different cell types, with expression increasing during development (Gomez-Ospina et al., 2013). The expression and cleavage of multiple

proteins increase the diversity of the proteome and allow developmental and cell diversity in regulation of $Ca_v1.2$ and other proteins (Gomez-Ospina et al., 2006).

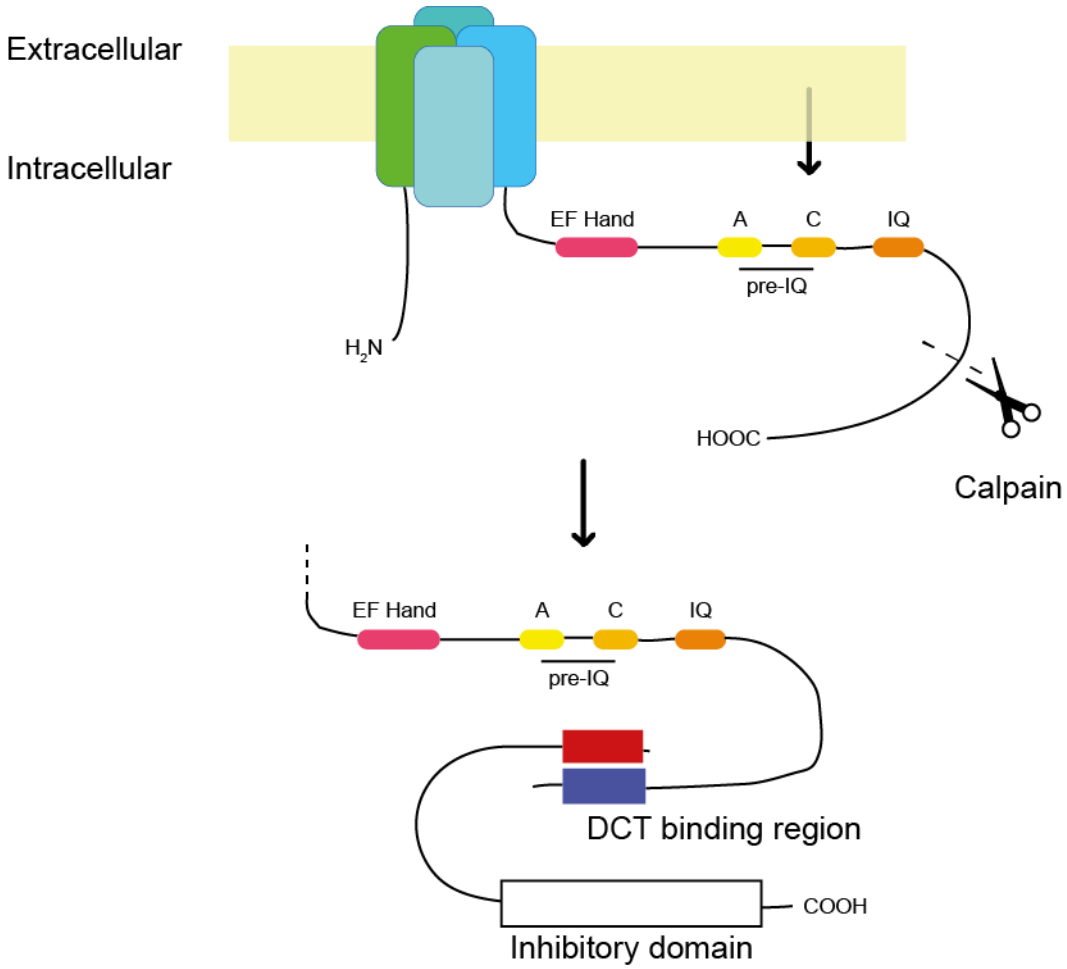

Figure 16 Cleavage of the distal C-terminus of $Ca_v1.2$ by calpain.

1.9.9 Calcium influx triggers changes in transcription

Activation of expression of the 'immediate early' gene (IEG) *c-fos* is induced by neurotransmitters and is one transcription factor that allows coupling of environmental signals to long-term changes in neuronal function. Basal expression of *c-fos* and other IEGs is suppressed by VGCC antagonists, although there is not much change in current or synaptically-induced Ca^{2+} currents (Murphy et al., 1991). This suggests that although the contribution of $Ca_v1.2$ to calcium transients is small, it plays a key role in coupling synaptic excitation to activation of gene transcription.

A motif 5'-(TGACGTTT)-3' similar to the cAMP-response element (CRE) 5'-(TGACGTCA)-3' was identified in the promoter of *c-fos* and termed the calcium-response element (CaRE) (Sheng et al., 1990). Depolarisation causes phosphorylation of the CRE-binding protein (CREB) and CREB was shown to bind CaRE. Multiple kinases are capable of phosphorylating CREB including cAMP-dependent kinase. However, increasing cAMP levels does not increase *c-fos* expression, suggesting that this is not the pathway through which *c-fos* is regulated (Sheng et al., 1990). *In vitro*, CREB is a substrate for CaMKII and acts as a Ca^{2+}-regulated transcription factor (Greenberg et al., 1992, Wheeler et al., 2008) (Figure 17).

Another example of downstream regulation through calcium influx through $Ca_V1.2$ is through brain-derived neurotrophic factor (BDNF), which modulates synaptic activity. This also has multiple CaRE motifs in its promoter; some of these sites respond to CREB while others are bound by a separate but similar factor (identified as a calcium-responsive transcription factor) (Tao et al., 1998, Tao et al., 2002). As well as the CaMKII pathway, calcium influx and Ca^{2+}/CaM is also necessary for the activation of the mitogen-activated protein kinase (MAPK)/Erk pathway (Dolmetsch et al., 2001) (Figure 17).

Long-term, the regulation of transcription allows maintenance of homeostatic plasticity though LTP and LTD. Increase in Ca^{2+} and signalling through CaM kinase kinase (CaMKK) and CaMKII lead to decreased AMPAR and NMDAR responses (Goold and Nicoll, 2010, Lee and Chung, 2014).

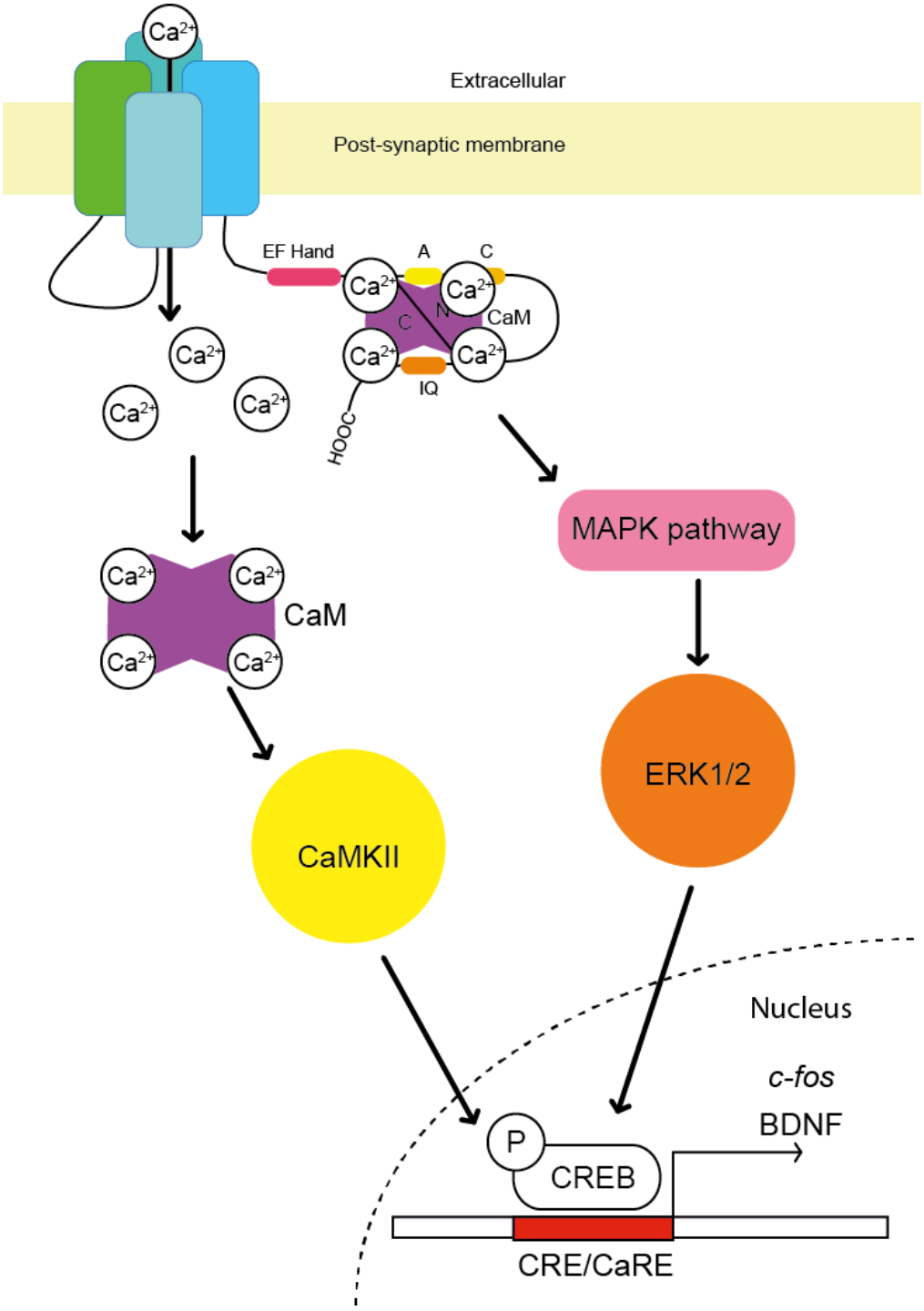

Figure 17 Calcium signalling leads to induction of immediate-early genes.

Signalling cascades converge on CREB and CaRF (calcium-responsive factors) which bind CRE/CaRE and activate transcription.

1.9.10 *CACNA1C* identified as risk factor in neuropsychiatric disease

A SNP in intron 3 of *CACNA1C*, rs1006737, is associated with bipolar disorder (Sklar et al., 2008, Ferreira et al., 2008, Green et al., 2013) and schizophrenia (Jiang et al., 2015, Nie et al., 2015) as well as being identified in meta-analyses combining populations of both disorders (Schizophrenia Psychiatric Genome-Wide Association Study, 2011). The SNP has also been associated with autism (Li et al., 2015a) and major depressive disorder (Liu et al., 2011), suggesting that it may be a shared genetic risk factor across the psychiatric disorder spectrum. Carriers of the risk allele have high startle reactivity and lower extraversion (Roussos et al., 2011) as well as impaired performance in alerting, orienting, and facial recognition (Thimm et al., 2011, Soeiro-de-Souza et al., 2012, Nieratschker et al., 2015). Carriers also show higher anxiety and a lower contextual mood (Pasparakis et al., 2015) and impaired memory (Hori et al., 2012, Zhang et al., 2012). Reduction of hippocampal activation during memory recall was observed in healthy carriers, as well as decreased activation of the dorsolateral prefrontal cortex (DLPFC) (Erk et al., 2010, Erk et al., 2014b, Krug et al., 2014). This allele also modulates amygdala function (Jogia et al., 2011) with a significant increase of activation during emotional processing observed in BD patients (Tesli et al., 2013) and an association of the risk allele with increased amygdala volume (Lancaster et al., 2016)

The rs1006737 SNP is a quantitative trait locus for *CACNA1C* expression (Eckart et al., 2016) and the risk allele is associated with decreased *CACNA1C* expression in the superior temporal gyrus (which shows a reduction in grey matter in patients with BD). However, this study also reported trends in the opposite direction in the dorsolateral prefrontal cortex (DLPFC), showing a region-specific effect of rs1006737. This study also showed that rs4765905, another SNP associated with BD and

schizophrenia (Schizophrenia Psychiatric Genome-Wide Association Study, 2011), is in high linkage disequilibrium with rs1006737 (Eckart et al., 2016). The risk allele C of this SNP showed stronger binding compared to the G allele, suggesting a functional effect of these SNPs.

Other SNPs have been identified as risk factors for psychiatric disorders including rs4765905 (Psychiatric GWAS Consortium Bipolar Disorder Working Group, 2011) and rs7297582 (Liu et al., 2011). These have not been replicated so far. Other SNPs in intron 3 have been associated with narcolepsy (Shimada et al., 2010) and sleep latency and quality (Byrne et al., 2013, Parsons et al., 2013). These support the involvement of calcium signalling in a diverse range of disorders and may underlie the co-morbidity of psychiatric disease and sleep disorders.

1.9.11 Timothy Syndrome is caused by a gain of function mutation

Timothy Syndrome, a multisystem disorder with symptoms including a long QT interval, arrhythmias, polydactyly, autism and other developmental impairments, is caused by *de novo* mutations in *CACNA1C*. Classic TS (TS1) results from a G406R mutation in exon 8a (an alternatively-spliced exon) (Splawski et al., 2004) and atypical or type 2 TS (TS2) is caused by the same mutation but in exon 8 (highly expressed in brain and heart) as well as a G402S mutation (Splawski et al., 2005). Both of these mutations disrupt the link between activation and inactivation, causing an ablation of VDI and leading to sustained membrane depolarisation and an overload of Ca^{2+} in the heart (Depil et al., 2011). A mouse model of TS2 showed that mice homozygous or heterozygous for the G406R mutation die before weaning; heterozygous animals with a neomycin cassette in exon 8a survived to adulthood possibly due to blunted expression of the mutant channel (Bader et al., 2011) These mice displayed autism-like endophenotypes including impaired social interactions

and vocalisation, restricted and perseverative behaviour, and enhanced cued and contextual memory following fear conditioning, as well as self-injurious scratching (Bader et al., 2011, Bett et al., 2012). However, the heart function of these mice has not been studied.

Other gain-of-function mutations have been identified in *CACNA1C* that cause long QT syndromes and heart defects but without the multisystem symptoms of Timothy Syndrome (Fukuyama et al., 2014, Wemhoner et al., 2015). This variation in symptoms makes it clear that the function of $Ca_v1.2$ in the brain and heart, and how changes in calcium influx can impair this, is not completely understood. Mutations in the mouse *Cacna1c* gene have been used to elucidate the function of $Ca_v1.2$, including whole-body constitutive knock-out, heterozygous knockout and conditional tissue-specific knock-out models.

1.9.12 Studies in mouse

A whole-body knockout of *Cacna1c* in the mouse either by insertion of a *Neo* cassette into exon 3 or by floxing out exons 14 and 15 causes embryonic lethality. *Cacna1c*$^{-/-}$ embryos die between 12.5 and 14.5dpc due to a loss of cardiac function (Seisenberger et al., 2000). A heart-specific adult knockout also causes homozygous lethality, but heterozygous animals show no change in cardiac function or survival (Rosati et al., 2011). In order to study the function of *Cacna1c* in adult animals either heterozygous knockouts or conditional, tissue-specific knockouts have been used. Behavioural tests have produced contradictory results as detailed below.

Heterozygous knockout animals (*Cacna1c*$^{+/-}$) show reduced exploratory behaviour in the Open Field and decreased response to anti-depressants (Dao et al., 2010, Bader et al., 2011). In these studies, sex differences were observed in these mice,

with only female animals also showing decreased risk taking and increased anxiety in multiple tests and a decreased startle response at high dB levels (Dao et al., 2010). While this suggests a sex difference, in another study both heterozygous males and females showed increased anxiety in the elevated plus maze (Lee et al., 2012).

A CNS-specific knockout of *Cacna1c* caused no changes in Open Field or locomotor activity, unlike the heterozygous knockout. It also did not recapitulate acute pharmacological blocking of $Ca_v1.2$ by isradipine, which impairs acquisition of auditory fear memory (Langwieser et al., 2010). Animals with conditional knockout of *Cacna1c* in the hippocampus and cerebral cortex survive to adulthood and show a loss of late-phase LTP (L-LTP), impairment of hippocampal spatial memory and reduced activation of the MAPK pathway (Moosmang et al., 2005). Neurons from these mice showed an increase in the minimal depolarisation required to initiate an action potential (AP) train and increased latency to first AP, as well as a reduction in initial spiking frequency (Lacinova et al., 2008). Anxiety was also increased in a forebrain-specific conditional knockout as well as after AAV-Cre-mediated prefrontal cortex-specific knockout (Lee et al., 2012). *Cacna1c* is involved in hippocampal neuron survival; forebrain-specific knockout causes a decrease in hippocampal BDNF expression and a decrease in cell proliferation (Lee et al., 2016).

$Ca_v1.2$ has also been shown to play a role in circadian rhythms and sleep. Calcium and membrane depolarisation are important for clock regulation and adaptation, and some clock genes such as *Per1* and *Per2* are regulated by CREB. *Cacna1c* is expressed rhythmically in the SCN with a peak at late night (CT18) (Schmutz et al., 2014). CNS-specific KO of *Cacna1c* did not cause any changes in free-running, period, onset of activity or any other circadian parameters. CNS-KO mice did, however, show a defect in phase adjustment; a light pulse in early

subjective night (CT14) caused a normal phase delay in both WT and CNS-KO animals but after a pulse in late night (CT22) CNS-KO animals had a reduced phase advance compared to WT. REV-ERBα, a transcription factor also involved in the circadian clock, acts as a repressor of *Cacna1c* expression in a circadian fashion, binding the promoter during the day (ZT4) but not at night (ZT16) (Schmutz et al., 2014). Treatment of cells with lithium (a treatment for bipolar disorder) leads to proteosomal degradation of REV-ERBα and amplification of circadian rhythms (Yin et al., 2006) and fibroblasts from patients with bipolar disorder show a weaker amplification after lithium treatment (McCarthy et al., 2013). Knockdown of $Ca_V1.2$ also eliminates lithium's ability to amplify rhythms suggesting that *CACNA1C* genotype may underlie the attenuated response in bipolar disorder (McCarthy et al., 2016).

EEG recordings from *Cacna1c*$^{+/-}$ mice show that they do not spend more or less time asleep or in REM (rapid-eye-movement sleep) or non-REM (NREM) over 24 hours, although they show a small increase in REM and NREM only in the dark phase (Kumar et al., 2015). In wake and REM they showed a reduction in beta and gamma frequencies (20-64Hz) and in NREM there was a trend towards more SWA. *Cacna1c*$^{+/-}$ also had defects in the homeostatic REM sleep recovery process after sleep deprivation (Kumar et al., 2015).

1.9.13 ENU mutations discovered in the IQ domain of *Cacna1c*

The Harwell ENU-mutagenised archive was screened for mutations in *Cacna1c.* The pore-forming region was avoided, as mutations in this area could be too severe to study in adulthood. Two mutations were identified in the IQ domain and re-derived as described as described in 1.5 (Parsons, unpublished data). These were

Cacna1c^{Q1625STOP} and *Cacna1c*^{G1616D}. Mice were re-derived using IVF, backcrossed for three generations and intercrossed.

1.9.13.1 Cacna1c^{Q1625STOP}

The *Cacna1c*^{Q1625STOP} mutation causes a premature stop codon to replace the glutamine residue Q1625. This is the 'Q' residue of the IQ motif in mouse $Ca_v1.2$ (ENSMUST00000078320) and is invariable throughout CaM-binding IQ motifs (while the I residue can vary) (Rhoads and Friedberg, 1997) (Figure 18).

1.9.13.2 Cacna1c^{G1616D}

The *Cacna1c*^{G1616D} mutation is also within the IQ domain of mouse $Ca_v1.2$. It is predicted to cause a glycine to aspartic acid change as shown in Figure 19A-B.



Figure 18 The IQ Domain and *Cacna1c*^{Q1625STOP} mutation.

Aligned sequences from human and mouse Cav1.2 and the truncation caused by the Cacna1cQ1625STOP mutation (top)

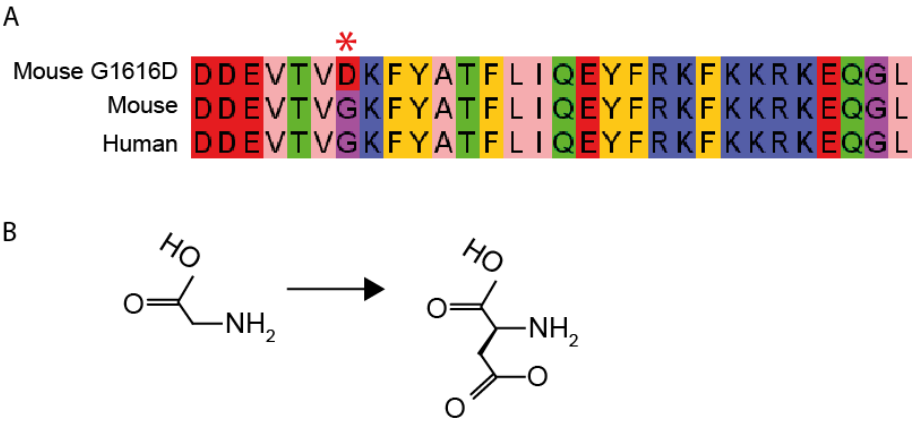

Figure 19 IQ domain of $Ca_V1.2$ and the *Cacna1c*^{G1616D} mutation.

(A) Alignment of the IQ domain from mouse and human $Ca_V1.2$ showing the location of the missense mutation G1616D. (B) Skeletal formula showing the amino acid structures of glycine and aspartic acid.

1.9.14 Hypothesis

The two mutations (one missense and one truncation) identified in *Cacna1c* will produce two alleles that could have a range of potential effects. Previous studies have indicated that truncations cause degradation of the protein and therefore we hypothesise that this mutation could cause loss of function as a result of nonsense-mediated decay. Knock-out of *Cacna1c* in the mouse causes homozygous lethality before birth and therefore if *Cacna1c*^{Q1625STOP} leads to a loss of function we would expect to see perinatal lethality when this allele is homozygous. As discussed above, previous studies have shown that reductions in *Cacna1c* expression *in vivo* lead to increased anxiety and reduced exploratory behaviour, so we could expect to recapitulate these phenotypes. Additionally, heterozygous knock-out of *Cacna1c* has an effect on beta and gamma frequencies during REM sleep and causes defects in sleep recovery, which could also be expected if *Cacna1c*^{Q1625STOP} is a functional null allele.

The *Cacna1c*^{G1616D} mutation (evaluated in Chapter 6) could have a more subtle and complex effect; if it produces a functional protein there may be changes in the gating and Ca^{2+} influx. It may cause a reduction in Ca^{2+} influx, in which case we could expect to see similar phenotypes to null alleles and the allele could cause perinatal lethality, increased anxiety and defects in sleep recovery. On the other hand, if this mutation causes a gain of function we could expect a Timothy Syndrome-like phenotype including defects in heart function and a long QT, facial dysmorphology or syndactyly, and if the allele causes complete ablation of inactivation it may lead to complete lethality in any carriers of the allele. A less severe gain of function could cause a lengthened QT interval but allow survival, and animals carrying the allele could show changes in anxiety or exploratory behaviour possibly in the opposite direction to that seen in knock-out models.

Therefore, this reverse genetics approach will allow an insight into subtle point mutations in the protein that may link it to endophenotypes of psychiatric disease.

2 General Methods

2.1 Animal husbandry

All procedures, unless otherwise stated, were performed under Project License 30/3206. All procedures were carried out in compliance with the Animals (Scientific Procedures) Act 1986. All colonies were bred and maintained in individually ventilated cages (IVCs) under controlled light (light 7a .m. to 7 p.m., dark 7 p.m. to 7 a.m.), temperature (21°C ± 2°C) and humidity (55% ± 10%) conditions, with food and water *ad libitum*. For genotyping and identification purposes all animals underwent an ear biopsy at post-natal day 21. Gene-specific genotyping assays are detailed in the corresponding sections of this chapter.

2.2 Primary Phenotyping Battery

Cohort sizes, sex and any other line-specific details are included in the corresponding chapter. In general, cohorts underwent a primary phenotyping battery designed to identify differences in anxiety, cognition, sensorimotor, sleep and circadian domains.

2.2.1 SHIRPA

The purpose of the modified SHIRPA battery (**S**mithKline Beecham, **H**arwell, **I**mperial College, **R**oyal London Hospital, **p**henotype **a**ssessment) is to examine mice for obvious physical characteristics, behaviours and morphological abnormalities. The screen is modified from Rogers et al. (1997) and provides a behavioural profile of the mouse via observation.

Mice were allowed to acclimatise to the phenotyping room for a period of 30 minutes prior to testing. Throughout the test, any vocalisation, aggression, salivation

or unexpected behaviours were noted. Each mouse was placed in a clear cylinder over a wire grid and observed for activity and tremors. The mouse was transferred out of the cylinder by removing the metal plate/grid whilst positioning over an arena, and transfer arousal was recorded. Locomotor activity was recorded as the number of $10cm^2$ squares the mouse moved through in the first 30 seconds in the arena. Mice were allowed to move freely around the arena while gait and tail elevation were observed. A click box emitting a 20kHz, 90dB tone burst was then held ~30cm above the arena to test for the Preyer reflex (startle response to auditory stimuli manifested by an ear flick). The mouse was then approached from the front with a bent finger, aiming to touch the mouse on the back of the neck rather than on the face and a record was taken whether the mouse moved away before the finger touched the mouse, when the finger touched the mouse or if the mouse did not move at all. The mouse was picked up by the tail and observed for limb grasping and trunk curl. Contact righting reflex was tested by placing the mouse in a small transparent tube that was turned quickly so the mouse was fully upside down. The researcher was blind to genotype. Responses were recorded in Excel; locomotor activity was quantified while all other responses were qualified as present/not present.

2.2.2 Open Field

The open field test is used to measure anxiety and exploratory behaviour, based on the natural tendency of an animal to explore and to protect itself using avoidance which translates to a normal animal spending more time in the periphery of the Open Field arena than in the centre (the most anxiogenic area)(Bailey, 2009).

Arenas with an area of 44cm x 44cm were constructed in grey Perspex. by the MRC Harwell Workshop. Animals were transported to the phenotyping suite and left undisturbed for 30 minutes before the test. Four mice at a time were placed in

separate square arenas, with light levels set between 150 and 200 lux in each arena. Each mouse is placed in the middle of a peripheral zone of the arena facing the wall and allowed to freely explore the apparatus, with the experimenter out of the animal's sight. Mice were video-tracked using Ethovision (Noldus, Wageningen, Netherlands, EthovisionXT version 8.5) for 30 minutes. For analysis, each open field arena is divided into a peripheral zone measuring 8 cm from the edge of the arena walls, and an 11 x 11cm central zone (Figure 20).

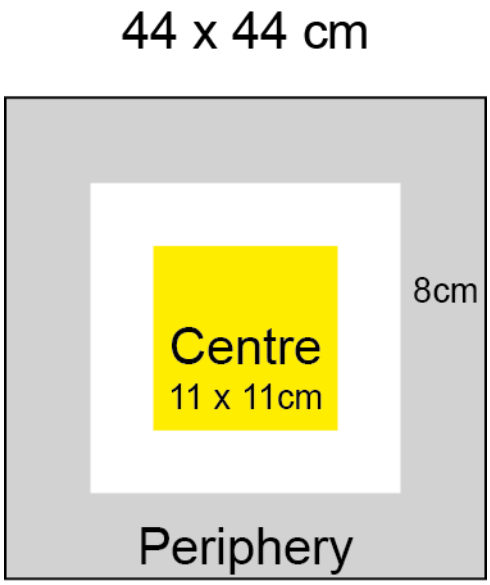

Figure 20 Open Field Arena

2.2.3 Acoustic Startle and Prepulse Inhibition (PPI)

The acoustic startle response is characterised by an exaggerated flinching response to an unexpected strong auditory stimulus (pulse). This response can be attenuated when it is preceded by a weaker stimulus (pre-pulse) and is the principle underlying pre-pulse inhibition (PPI). PPI has been described in numerous species, including mice and humans and provides an operational measure of sensorimotor gating reflecting the ability of an animal to successfully integrate and inhibit sensory information. Several clinical studies have shown that a number of human disorders

have impaired PPI including schizophrenia and autism (Braff et al., 2001, Amann et al., 2010).

The experimental apparatus consists of an outer attenuated chamber that serves to prevent external noise or vibrations interfering with the experiment. Within this chamber a load cell platform that records the startle response is linked to the transducer and amplifier, which calibrates the load cell platform. An animal holder rests upon the load cell platform. A sound generator and the appropriate software regulate pulses from the amplifier.

2.2.3.1 PPI Procedure

Mice were transported to the phenotyping suite and left undisturbed for a minimum of 30 minutes. Cages were not changed on the day of the experiment. Mice were individually placed onto the load cell platform inside the sound attenuated acoustic chamber and the door was closed and secured.

Sessions were initiated with a 5 minute acclimation period (only background noise (BN) is on). BN was set at 45 decibels (dB). The session was then continued by presentations of different trial types, each presented 6-10 times in pseudorandom order, with an inter-trial interval (ITI) varying randomly between 20 and 30 seconds.

Trials included:

a. Different pre-pulse trials of 20 ms duration of white noise stimuli, which were presented alone (PP1, PP2, PP3, or PP4 dB) or preceded the pulse by 50-120 ms (PP1 + pulse, PP2 + pulse, PP3 + pulse, or PP4 + pulse) to derive the pre-pulse inhibition response. The intensities of the pre-pulse were kept at levels above the BN so to not elicit a significant startle

response on their own. Intensities of the pre-pulse were 55, 65, 70 and 75 dB. Results are presented from 65dB, 70dB, and 75dB trials only.

b. Startle pulse trials where 110-120 dB/40-60 ms of white noise is presented alone.
c. No stimulus (NOSTIM) trials in which only background noise is presented to measure baseline movement of the animal in the chamber.

Startle response was recorded every millisecond for 65-100 ms after the onset of startle, i.e. 40-60 ms during the startle plus 25-40 ms after the startle ended; 65-100 ms from the end of the previous ITI for NOSTIM (Figure 21). Data were exported as Access files for detailed analysis.

The maximal peak amplitude is used to determine the acoustic startle response. Basal startle responses S and PP-S are calculated respectively as the average responses to the pulses presented alone and the average responses to the combined pre-pulse-pulses. The amount of pre-pulse inhibition (PPI) is calculated as a percentage score for each acoustic pre-pulse trial type: % PPI= 100 x (S – PPi_S)/S.

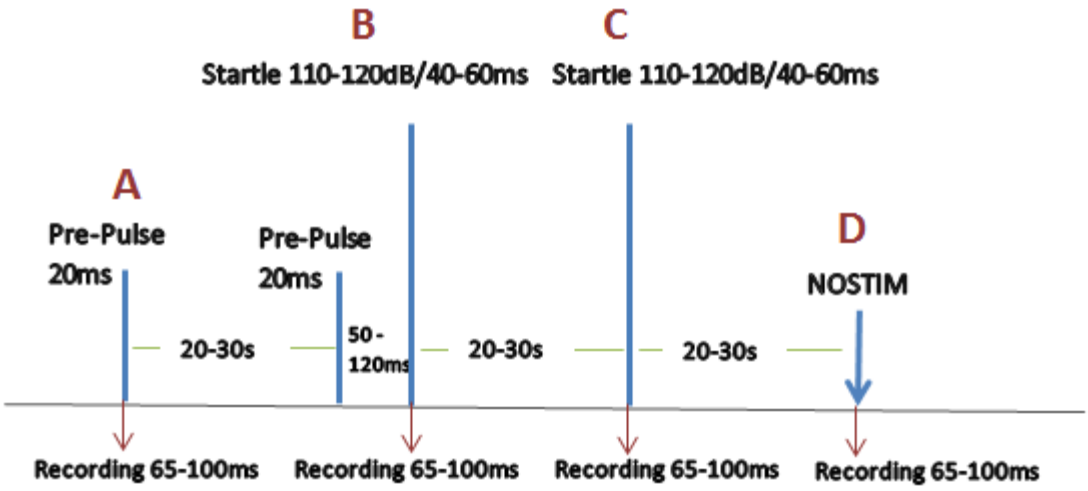

Figure 21 Trial types of the acoustic startle & pre-pulse inhibition test.

A: pre-pulse alone (PP1, PP2, PP3 and PP4), B: startle preceded by pre-pulse (PP1_S, PP2_S, PP3_S and PP4_S), C: startle alone and D: NOSTIM.

Retrieved from https://www.mousephenotype.org/impress/protocol/176/7 (Accessed 22/08/16)

2.2.4 Fear Conditioning

Fear conditioning is a behavioural test in which mice learn to predict aversive events, in this case, a foot shock (Crawley, 2006). Studies have shown that the amygdala is involved in the conditioned response to cue and context, while the hippocampus is involved in the conditioned response to context only (Phillips and LeDoux, 1992, Pape et al., 2005, Maren et al., 2013). On day one mice were placed individually into square arenas with metal grid floors (Ugo Basile, Italy), with lux in each arena set at 26 +/- 1. A conditioning protocol was performed using AnyMaze software (Stoelting, Wood Dale, IL, USA) and consisted of 150s baseline recording, a 5s 90db tone, immediately followed by a 0.5s 0.5mA shock. The tone and shock were repeated twice more at 150s intervals to reinforce association (Figure 22). 150s after the last shock the mice were removed and placed back in their home cage. Video tracking was recorded throughout the test. Arenas were cleaned with 70% alcohol

and dried between each trial. On day two, mice were placed back in the same arena to assess response to context. Mice were video tracked for 300s; no tones or shocks were administered. Four hours after the context trial, mice were placed in round arenas, with a plastic floor, black and white walls (custom-made by MRC Harwell Workshop), with lux reduced to 16 and scent of vanillin added to the top of the arena. Mice were video tracked for 180s with no tones or shocks and then for a further 180s with a 5s tone sounding every 60s.

At all times mice were video tracked using AnyMaze software (Version 4.5, Stoelting, USA) and time freezing calculated using AnyMaze freezing detection. Time spent freezing was then converted into a percentage of time. Baseline freezing was recorded during the time in conditioning trial before any tones or shocks (150s); context-dependent percentage freezing was measured over the whole trial (300s) and cue-dependent percentage freezing was measured from the tone onset to the end of the trial (180-360s). The increases in context-dependent percentage freezing compared to baseline were calculated by subtracting the baseline or pre-cue percentage from the learnt freezing percentage response. Freezing in the cue-dependent test was compared at baseline and after each cue for 10 seconds. Unconditioned response to the cue was measured by comparing percentage time spent immobile in the 5 seconds before the first tone in the conditioning session and during the 5 seconds after tone onset.

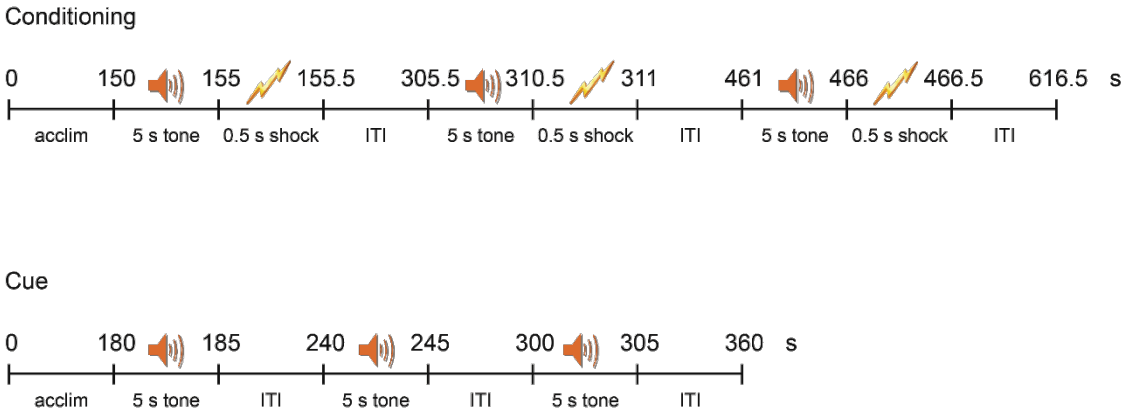

Figure 22 Timing of tones, shocks, and inter-trial intervals in fear conditioning.

Schematic drawing of the tone, shocks, and inter-trial intervals (ITI) in the fear conditioning test for the conditioning (top) and the cued test (bottom).

2.2.5 Circadian Phenotyping

Wheel-running activity was used to assess entrainment to light-dark (LD) cycles and free-running period in constant light conditions (Banks and Nolan, 2011). Mice were individually housed in light-tight, ventilated chambers (Figure 23A). Each cage contained running wheels and bedding, and no other environmental enrichment. Light levels were set to ~150 lux. Mice had access to food and water *ad libitum*. The light regime comprised entrainment to a 12:12h light/dark (LD) cycle and was followed by a 4h light pulse (LP) during night time at ZT16 on day 4 with further 2 days under LD conditions. To assess the internal circadian rhythm of the animals they were subsequently kept under constant conditions in constant darkness (DD). Wheel-running activity was recorded by ClockLab software (Actimetrics, Wilmette, USA) and data were presented in double-plotted actograms (Figure 23B). Equipment, set-up and data analysis were according to Banks and Nolan (2011). This work was carried out by Gareth Banks and Greg Joynson.

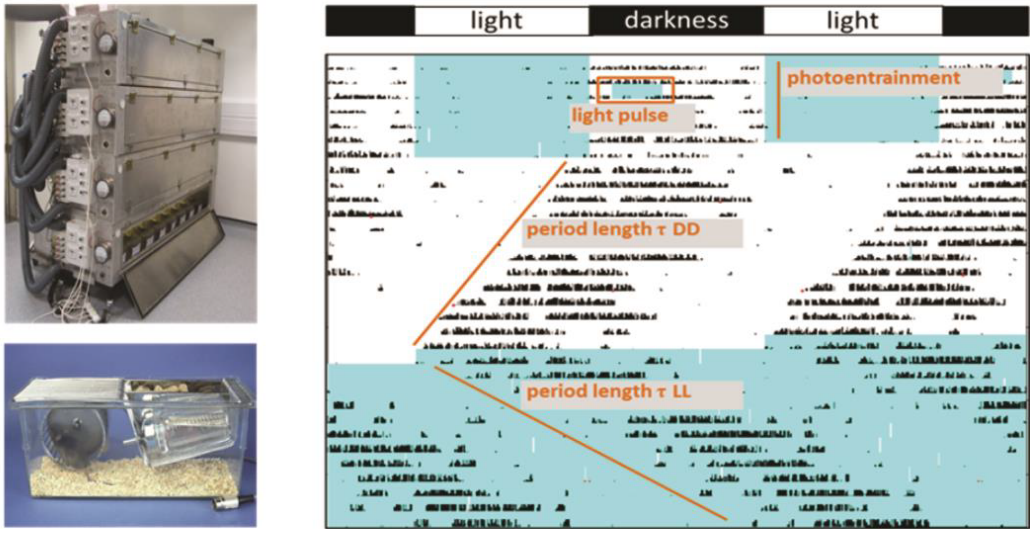

Figure 23 Circadian Screening

A) Light-tight chamber and a cage equipped with a running wheel. B) An example of a double plotted actogram highlighting different measures such as photoentrainment, period length in constant darkness and constant light and negative masking in form of an acute light pulse during the dark phase. From Heise (2015).

2.2.6 Video tracking as a correlate of sleep

Singly housed adult mice (min. 8 weeks of age) with food and water *ad libitum* were placed into ventilated, light-tight chambers which were also isolated from possible confounding external stimuli (Figure 24A). This set-up enabled for simultaneous recording of 32 cages. Light was provided by LED lamps on top of each cage and white light at 100 lux was routinely used (Figure 24B). During dark periods, infra-red light that is not perceived by mice but enables video visualisation was used. Lighting conditions were controlled by timer switches to pre-set conditions such as 12:12 h light/dark or light pulses during night at ZT16 (equivalent to 11pm). Miniature near infra-red video cameras (Sentient mini-night vision CCTV camera, Maplin, UK) were mounted above each cage to permit video recording of mice under either light or dark conditions. Cameras were fitted with a wide angle lens (Open Twenty four Seven Ltd, UK) (130°, 2.8mm) to enable the whole cage area to be viewed. To

prevent animals from hiding under the food hopper, access to that area was restricted by introducing a custom-made metal plate directly under the food hopper. In some circumstances, glare from NIR LEDs occurred due to reflected light from the cage bars. This was reduced by using tracing paper (W H Smith, UK) as a diffusor that covered the lights but leaving the camera free. In addition, areas surrounding the cages in the light-tight chambers were painted white to enhance the contrast of the cages and recorded area.

All cameras were connected to a 16-channel digital hard-drive recorder (Model VXM4B-16, Videcon, PLC) with video data recorded at 5 frames per second.

Video data from the 12:12h light/dark recording after habituation (Figure 10 red marking for 12:12 LD) and the second light pulse of the video-tracking data were transferred to perform video tracking using AnyMaze (Version 4.5, Stoelting, USA). Routinely, screens consisted of five days with mice entering the screen on Mondays.

Even though a habituation period of full 12 hours in darkness and full 12 hours in light was included in the screens, a potential effect of novelty and single housing of the mice cannot be excluded completely. Videos were recorded constantly during the whole time in the light-tight chambers. The first two and the last day consisted of 12 h light (starting at 7am, ZT0) and 12 h darkness (12:12 LD) with the first day to habituate and the second full day for comparison. During the dark phases on day 3 and day 4, a 1 h light pulse was given with only the second light pulse routinely analysed to obtain as consistent results as possible and to exclude false positives (Figure 25, red marking on LP2). Light acts as a zeitgeber and modulates sleep/wake timing by photoentrainment. An acute light pulse during night time will induce sleep in mice (Benca et al., 1998, Lupi et al., 2008). To test for anomalies in light-induced

sleep, an acute light pulse was used. As animals were not constantly awake during the dark phase in 12:12 LD (LD_{dark}), data from 30 min prior to the light pulse were included in the analysis as well as the light pulse itself and 2 h after the end of the light pulse.

As sleep was estimated by periods of immobility, settings of the AnyMaze software for the tracking and immobility detection were crucial. As tested before by Fisher and colleagues (Fisher et al., 2012) immobility detection with a setting of 95% sensitivity in AnyMaze for motion detection (to avoid to detect breathing as a movement) and an immobility detection onset after 40 seconds of immobility showed a very high correlation (>94%) with sleep as measured by EEG recordings.

24-hour light/dark recordings were analysed in hourly bins, whereas pre-, post-, and light pulse recordings were analysed in 10 min bins. Batch analysis and comparisons between animals were performed by using Microsoft Excel (version 2010) and specifically prepared macros for facilitating and speeding up the analysis.

Equipment, set-up, and data analysis were according to Heise et al. (2015) and carried out by Inés Heise.



Figure 24 Sleep set-up with light-tight chambers and individual cages.

(A) Photograph of the light-tight chamber seen from outside. (B) Light-tight chamber opened up with LED lights and cameras on top of the individual cages. From Heise (2015).

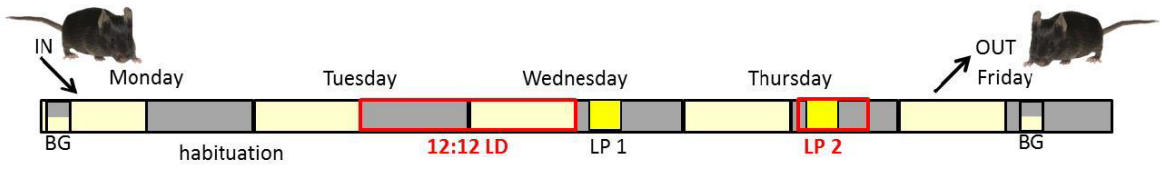

Figure 25 Schematic drawing illustrating the timeline of the sleep screens.

A background picture was taken before mice started the screen. Mice were transferred to sleep cages during the light period. The habituation period consisted of full 12 hours in darkness and 12 hours of light before the following 12 hours in dark and light were taken for analysis (marked in red). During the following night, a 1 hour light pulse (LP1) was given but not routinely analysed. On Thursday night a second light pulse (LP2) was administered and data were exported and routinely analysed. On Friday mice finished the screen and females were put back into groups. Again a background picture was taken after the screen without any mice in the cage. From Heise (2015).

2.3 Secondary Phenotyping Battery

Additional cohorts of two lines were put through a secondary phenotyping battery, which included further tests of anxiety. Cohorts were randomised and researcher was blind to genotype. All experiments were carried out in the light phase by the same researcher.

2.3.1 Light-Dark Box

The Light-Dark Box apparatus consists of two compartments, one dark and enclosed and one brightly-lit. Most mice exhibit a preference for the enclosed area (Bailey, 2009).

Mice were transported to the phenotyping suite and left undisturbed for a minimum of 30 minutes. Cages were not changed on the day of the experiment. Each mouse was individually tested. The experiments were carried out in the same room as Open Field (above), with light levels at 150-200 lux. Mice were placed in the dark area and recorded for 5 minutes. Due to the tracking software being unable to track mice when they begin in the dark area, transitions were manually scored. Duration in the light and dark areas was then calculated using Ethovision.

2.3.2 Elevated Nought Maze

Elevated Nought Maze is a modification of the Elevated Plus Maze which, similarly to Light-Dark Box, exposes the subject to a novel environment with protected enclosed areas and open, anxiogenic areas (Bailey, 2009).

Mice were transported to the phenotyping suite and left undisturbed for a minimum of 30 minutes. Cages were not changed on the day of the experiment. Each mouse was individually tested. The experiments were carried out in the same room as Open Field (above). Animals were placed in an enclosed area and recorded

for 5 minutes, and scored using Ethovision. Time spent in enclosed and open areas and total distance travelled were recorded.

2.3.2.1 Validation of the Elevated Nought Maze

The maze was constructed by the MRC Harwell Workshop and consisted of a raised circular track of 2cm width with a 1cm raised border on each edge. The maze was made from grey Perspex. Two-quarters of the maze were bordered with walls to create enclosed areas (Figure 26). In order to optimise the conditions of this test, a mixed-sex cohort of 20 wild-type C57BL6/J mice was tested with varying light levels. Light levels of 150 lux in the open areas and 80 lux in the dark were found to be optimal for anxiogenicity of the open areas.

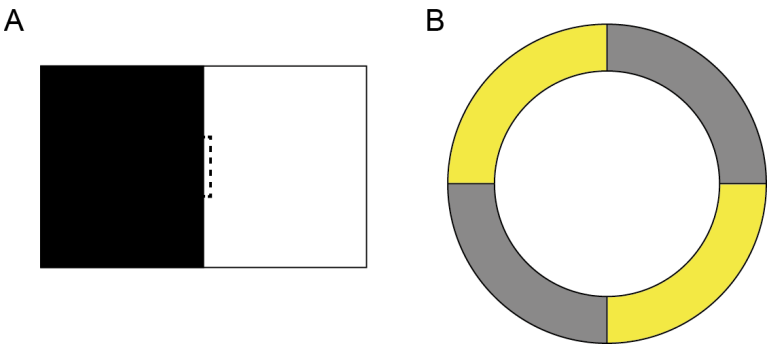

Figure 26 Secondary tests of anxiety

(A) The Light-Dark Box apparatus show the dark (black) and light (white) areas, connected by a small opening (dashed lines). (B) The Elevated Nought Maze showing division into open (yellow) and closed (grey) areas.

2.4 Heart phenotyping

Two mutant lines underwent an echocardiogram. One of these also had an electrocardiogram carried out to test for defects in cardiac function and electrical rhythm.

2.4.1 Echocardiogram

Echocardiograms are used to assess the functionality of the heart and the protocol is described at IMPReSS (https://www.mousephenotype.org /impress/protocol/109/8). Animals were placed in an induction chamber and anaesthetised. Hair was removed using cream on the area for imaging. The animal was then moved to the imaging platform and paws were taped to the ECG lead plates. A rectal probe was used to ensure body temperature was maintained at 36-37°C. Anaesthesia was managed during the procedure to ensure normal heart rate. Gel was applied onto the area to be imaged and probe attached. Images of the heart were taken in the short-axis mode with papillary muscles being the point of reference. Once the papillary muscles were parallel in B-Mode, M-mode was used to identify the centre of the left ventricle. 4 short loops of M-mode data were stored. The heart was then viewed two-dimensionally in the parasternal long-axis with the transducer placed vertically to the animal body on the left side of its sternum with the notch of transducer pointing to the animal head. Each animal had at least 3 short B-Mode, parasternal long axis view images captured. Once imaging was completed, animals were removed from the platform and allowed to recover atop a heating pad. Data were collected and analysed using VEVO 770 V3.0.0 software (FUJIFILM VisualSonics). This work was carried out by Barbara Nell and analysed by Heather Cater.

2.4.2 Electrocardiogram (ECG)

Anaesthetised mice were placed on the recording pad and electrical activity captured using a 2lead system with a sampling rate of 2k/s for 90 seconds. Data were analysed using the ECG analysis add-on for LabChart 8. The entire 90 seconds was analysed and only sections that are unusable due to noise or movement were excluded. Settings in LabChart 8 were as shown in Figure 27. This work was carried out by Thomas Nicol.

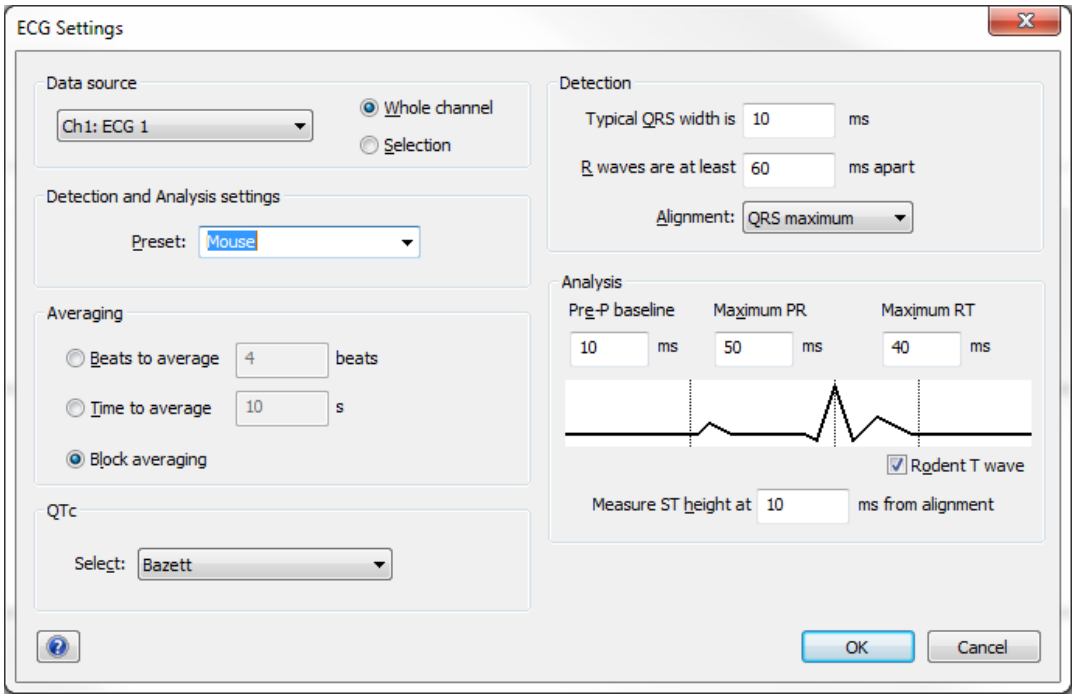

Figure 27 Settings for analysis of ECG recordings using LabChart 8.

2.5 Molecular Studies

2.5.1 Genomic DNA extraction from embryonic and adult tissue

Unless otherwise stated, tissue samples were degraded in 100-150µl 50mM sodium hydroxide (NaOH) at 95°C for 90 minutes. 10-15µl 1M Tris (pH5) was added to neutralise the solution. DNA was stored at -20°C.

2.5.2 Agarose gel electrophoresis

Agarose (Sigma-Aldrich) was dissolved in 1 X TAE (Tris-acetic acid-EDTA) buffer by boiling. When cooled to ~50°C, GelRed (Biotium) was added at a 1:10000 ratio. Gels were run at ~100mV for ~1 hour unless otherwise stated.

2.5.3 Purification of PCR Products

PCR products were isolated and purified using the QIAquick PCR Purification kit (Qiagen). 5 volumes Buffer PB was added to 1 volume of the PCR mixture and mixed. This was added to a QIAquick column in a collection tube and centrifuged for 60s. To wash, 0.75ml Buffer PE was added to the QIAquick column and centrifuged for 60s. Flow-through was discarded and the QIAquick column placed back in the same tube. This was centrifuged again for 1 min to remove residual wash buffer. Each QIAquick column was moved to a clean 1.5 ml microcentrifuge tube. To elute DNA, 40µl ddH_2O was added to the centre of the QIAquick membrane, incubated for 1 min and centrifuged.

2.5.4 Gel extraction

For fragments 70bp-10kb, the QIAquick® Gel Extraction Kit (Qiagen) was used. Sample bands were cut out of gels, transferred to a clean 1.5ml Eppendorf, and weighed. 3 volumes Buffer QG were added to 1 volume gel and incubated at 50°C for 10 min (or until the gel slice had completely dissolved). 1 gel volume of isopropanol

was added to the sample and mixed. To bind DNA, samples were added to QIAquick columns and centrifuged for 1 min. 500µl Buffer QG was added to the column and centrifuged for 1 min to remove all traces of agarose. To wash, 75µl Buffer PE was added to the column and centrifuged for 1 min. Flow-through was discarded and the columns centrifuged again to remove residual wash buffer. Columns were placed into a clean 1.5 ml microcentrifuge tube and 40µl ddH_2O added to the centre of the membrane. Columns stood for 1 min and were then centrifuged for 1 min to elute DNA.

2.5.5 Two-step reverse transcription

2.5.5.1 RNA extraction from tissue

To extract RNA from tissue the RNeasy® Mini Kit (Qiagen) was used. Up to 30mg of tissue was lysed and homogenised in buffer RL. After centrifuging for 3 minutes, the supernatant was transferred to a clean microcentrifuge tube. An equal volume of 70% ethanol was added to the lysate and mixed well by pipetting. Up to 700µl of the sample, including any precipitate, was transferred to an RNeasy Mini spin column placed in a 2 ml collection tube and centrifuged for 15 s at ≥8000 x g. 700µl Buffer RW1 was added to the RNeasy spin column and centrifuged for 15 s at ≥8000 x g. Two washes of 500µl Buffer RPE were added to the RNeasy spin column and centrifuged for 15s (first wash) and 2 minutes (second wash) at ≥8000 x g. The spin column was placed in a new 1.5 ml collection tube and 50µl RNase-free water was added directly to the spin column membrane. The columns were centrifuged for 1 min at ≥8000 x g to elute the RNA.

2.5.5.2 Reverse Transcription

First-strand cDNA was generated using SuperScript III Reverse Transcriptase (RT) (Invitrogen). 10µl RT Reaction Mix was combined with 2µl RT Enzyme Mix and

RNA on ice. Tubes were gently mixed and incubated at 25°C for 10 minutes, 50°C for 30 minutes, and finally terminated at 84°C for 5 minutes before chilling. 1µl *E. coli* RNase H was added and incubated at 37°C for 20 minutes to remove RNA. The concentration of cDNA was assessed using NanoDrop and cDNA stored at -20°C.

2.5.6 TOPO Cloning

2.5.6.1 Producing PCR Products

The pcDNA™3.1/V5-His TOPO® TA Expression Kit (Thermo Fisher) was used to clone DNA fragments into a mammalian expression vector. The following 50µl PCR was set up: 10-100 ng DNA Template, 5µl 10X PCR Buffer, 0.5µl 50mM dNTPs, 1 µl forward and 1µl reverse primers (100ng/µl), and ddH_2O added to a final volume of 49µl. 1µl *Pfu* polymerase (1 unit/µl) was then added to total volume 50µl. This was cycled at parameters depending on target DNA length and primer design. As *Pfu* polymerase has proofreading ability but leaves blunt ends, an A-overhang was then added as follows: PCR products were purified as described above; 24µl of purified DNA was added to 25µl Hotshot Master Mix (Clent Life Science) containing *Taq* polymerase, and 1µl dATP (10mM); Samples were incubated at 72°C for 20 minutes and TA cloned as soon as possible.

2.5.6.2 TA Cloning

4µl of PCR product and 1µl Salt Solution were added to 1µl pcDNA™3.1/V5-His TOPO® vector (Invitrogen) and incubated for 5 minutes at RT. Plasmid constructs were transformed into One Shot® TOP10 chemically competent cells. Cells were thawed on ice and 4µl plasmid vector added. Cells were incubated for 30 minutes on ice before a 30-second heat shock at 42°C. 250µl room temperature SOC medium was added and shaken (250rpm) at 37°C for 1 hour. 50µl and 200µl were spread on

ampicillin-selective LB plates and incubated at 37°C overnight. Positive colonies were cultured overnight in 4ml of LB medium containing 50µg/ml ampicillin.

2.5.6.3 DNA isolation by Miniprep

Plasmid DNA was then isolated by miniprep using the PureYield™ Plasmid Miniprep System (Promega Corp.). Briefly, 1.5ml of bacterial culture was centrifuged at 13000 x g for 30s. Supernatant was discarded and the pellet resuspended in 600µl ddH_2O. 100µl of Lysis Buffer was added and inverted to mix. 350µl cold Neutralisation Buffer was added, mixed by inverting, and samples were centrifuged for 3 minutes (13000g). Supernatant containing DNA was transferred to a PureYield™ Minicolumn, placed in a Collection Tube and centrifuged (13000g) at 15 seconds. 200µl of Endotoxin Removal Wash (ERB) was added to the minicolumn and centrifuged (13000 x *g*) for 15 seconds. 400µl of Column Wash Solution (CWC) was added to the minicolumn and centrifuged (13000g) for 30 seconds. The minicolumn was transferred to a clean 1.5ml microcentrifuge tube and 30µl of ddH_2O was added directly to the minicolumn matrix. This was kept for 1 minute at room temperature. Tubes were centrifuged for 15 seconds to elute the plasmid DNA. Eluted plasmid DNA was stored at –20°C.

2.5.7 Plasmid amplification and midiprep

Plasmids were transformed and plated as described above. For Midipreps, positive colonies were grown overnight in 100ml of LB medium containing 50µg/ml ampicillin. To isolate plasmid DNA, PureLink™ HiPure Midiprep Kit (Invitrogen) was used. Briefly, samples were centrifuged at 4500rpm for 15 minutes. Media was discarded and pellets were resuspended in R3 resuspension buffer containing 100µg/ml RNAse A. Cells were lysed in Lysis buffer L7 for 2 minutes at room temperature and neutralised using buffer N3. PureLink midi-columns were

equilibrated using buffer EQ1 before adding the sample lysates. Columns were washed twice with buffer W8 and DNA was eluted in 5ml elution buffer E4. 3.5ml isopropanol was added and incubated at room temperature for 5 minutes. Tubes were centrifuged (15,000g) at 4°C for 30 minutes. Isopropanol was removed and 3ml 70% ethanol added. Tubes were centrifuged again for 5 minutes. Ethanol was removed and the resulting DNA pellet air-dried for 10 minutes. Pellets were resuspended in ~200µl ddH_2O and concentration assessed by NanoDrop (Thermo).

2.5.8 Site-directed mutagenesis (SDM)

Primers for SDM were designed using the Agilent QuikChange Primer Design Tool (http://www.genomics.agilent.com/primerDesignProgram.jsp) to be between 25 and 45 bases in length, with a melting temperature (T_m) of ≥78°C. Reactions were set up as follows (QuikChange II XL Site-Directed Mutagenesis Kit, Agilent): 5 µl of 10X reaction buffer, 10 ng of dsDNA template, 20µl (125 ng) of forward oligonucleotide primer and of reverse oligonucleotide primer, 1µl of dNTP mix, 3µl of QuikSolution, and ddH_2O to a final volume of 50 µl. Then 1µl of PfuUltra HF DNA polymerase (2.5 U/µl) was added. Each reaction was cycled using the parameters in Table 3. *Dpn* digestion (1µl added to each reaction) was then used to remove the parental supercoiled dsDNA.

Samples were then transformed into XL10-Gold Ultracompetent Cells. Cells were thawed on ice and 45µl aliquoted per reaction. 2µl of the reaction mix was added and gently mixed before incubating for 30 minutes. Tubes were heat-shocked at 42°C for 30 seconds before adding 500µl pre-warmed SOC media. They were then incubated for 1 hour at 37°C with shaking at 250rpm. Two pre-warmed ampicillin-selective agar plates were spread with 250µl of the reaction mixture and incubated overnight at 37°C. Positive colonies were cultured overnight in 4ml of LB medium containing

50µg/ml ampicillin and plasmid DNA was isolated using Minipreps as described above. Sanger sequencing (Source Bioscience) was then used to confirm successful mutagenesis.

Step	Cycles	Temp	Time
1	1	95°	1 min
2	18	95°	50s
		60°	50s
		68°	1 min / kb
3	1	68°	7 mins

Table 3 Site-directed mutagenesis PCR

2.6 Tissue culture

HEK293T and NIH3T3 cell line cultures were maintained at 37°C, 5% CO_2 in Dulbecco's modified Eagle's medium (DMEM) + 1X PenStrep (penicillin-streptomycin antibiotic) + 1X foetal bovine serum (FBS). When 70-80% confluent, cells were washed in PBS and trypsinised in 0.05% trypsin (Gibco). Trypsin was quenched with DMEM before dilution into fresh DMEM.

2.7 Statistical analyses

Unless otherwise stated, statistical analyses were performed using GraphPad Prism version 6.00 for Windows (GraphPad Software, La Jolla California USA, www.graphpad.com). Differences were considered statistically significant at p-values < 0.05. Differences were considered to have a trend towards significance at $0.05 \leq$ p-values < 0.10. In all figures, bars show the mean of data and error bars show the standard error of the mean. Asterisks on figures indicate significant p-values: * signifies $p < 0.05$, ** signifies $p < 0.01$, and *** signifies $p < 0.001$.

2.8 *Ank3*

2.8.1 The ENU-mutagenised archive

As described in 1.4, the ENU DNA archive contains samples from over 10,000 F1 male mice, generated by mating mutagenised BALB/c males with wild-type C3H/HeH females. The archive was screened using pooled plates, each well containing DNA from four individuals (Quwailid et al., 2004). Once a mutation was identified, individual samples were requested and screened as described below.

2.8.2 Screening of the ENU-mutagenised DNA archive using PCR

Ensembl transcript ENSMUST00000054167, sequence build GRCm38 (Ensembl 71) was used as a template for primer design and exon IDs are listed in Table 4. Five exons were chosen from three functional domains of *Ank3 (*Table 4*)* and primers covering each exon and 20bp intronic sequence either side were designed using Primer3Plus (Untergasser et al., 2007) (Table 5). PCR conditions were optimised by using a PCR gradient with cycling parameters described in Table 6 and running products on a 1% agarose gel. The DNA archive was screened for mutants using PCR with reagents as described in Table 7 then melt curve analysis was carried out using a Lightscanner machine (Idaho Technologies). After amplification, samples were subjected to a temperature gradient from 80°C to 90°C to produce a melt curve. The fluorescence produced by LCGreen was measured; when LCGreen is bound to double-stranded DNA there is a high signal and as the sample is heated the DNA melts into single-stranded DNA and the fluorescent signal decreases. Mutants have significantly lower melting temperatures due to the presence of heteroduplex DNA, which is less stable due to base-pair mismatches and this was visualised on a plot of Δfluorescence against temperature.

Exon number	Ensembl Exon ID	Functional Domain
6	ENSMUSE00001288955	ANK repeat
13	ENSMUSE00001220057	ANK repeat
25	ENSMUSE00001255995	Spectrin-binding
27	ENSMUSE00000642806	Spectrin-binding
35	ENSMUSE00000642792	Death

Table 4 Ensembl exon identities.

Gene	Region	Exon	Forward Primer	Reverse Primer
AnkG	Membrane-binding	6	CCCACCTTGGCTGATCT	CCAAGGATGCGAAAGGC
	Membrane-binding	13	GTCTTGAGAGTTGCTGCTAAT	TTCCACCTCAGTTGCAGTTT
	Spectrin-binding	27	GATACAAAAAGAAATCATGTGGCT	CTTCACCCTGTCCCTGG
	Death	35	GTATCCCTGGGTGGCTC	GGTTGCCTCGTCCGACA
	Death	37	GTATCCCTGGGTGGCTC	TTTTCCTGATTTCATCGAACGATT

Table 5 Primer Sequences for archive screening

Step	Temperature (°C)	Time	
1	95	00:30	PCR Cycle Gradient
2	55 - 70	00:30	
3	72	00:30	
	PCR cycle x 44		
4	72	05:30	

Table 6 PCR cycling parameters for primer optimisation. A gradient step from 55-70°C was used.

Reagent	Volume per well (µl)
Hotshot Master Mix (Clent Life Science)	5
LC Green (Biofire)	1
10µM forward+backward primer mix	0.1
double distilled (dd) H_2O	1.9
Archive DNA (5ng/µl)	2

Table 7 PCR Reagent mix for archive screening

2.8.2.1 Confirmation of mutations

As the first archive screen was carried out on pooled DNA samples (4 per well), potential mutant pools were then isolated and screened separately as described above. Once individual mutant samples were identified, PCR was used to amplify the region using the same conditions as before but with no LCGreen. PCR products were

isolated as described (2.5.3) and sent to Source Bioscience for Sanger sequencing using screening primers (Table 5).

2.8.3 Sequence alignments and conservation analysis

Ankyrin$_G$ protein sequences for mouse, rat, rabbit, human, chimp, gorilla, frog, *C. elegans* and *D. melanogaster* were retrieved from Ensembl. The spectrin-binding domain and death domain from each was isolated and aligned using Clustal Omega (www.ebi.ac.uk/Tools/msa/clustalo/). Alignments used default settings as described in the literature (Sievers et al., 2011, McWilliam et al., 2013). ClustalO was also used to produce a percentage sequence identity matrix comparing sequence similarity between each organism and all other sequences. Alignments were then visualised using Jalview (Waterhouse et al., 2009) and the Zappo colour scheme to show side chain properties as described in Figure 28.

Aliphatic/hydrophobic	ILVAM
Aromatic	FWY
Positive	KRH
Negative	DE
Hydrophilic	STNQ
Conformationally special	PG
Cysteine	C

Figure 28 Zappo colour scheme

2.8.4 Site-directed mutagenesis

In order to prioritise mutations *in vitro* before re-derivation we obtained a 190kDa-ankyrin$_G$ construct from rat DNA, kindly provided by Peter Mohler. This was in the pEGFP plasmid (Clontech)(Mohler et al., 2002a). This was used to design primers for all detected mutations (Table 8) (Agilent, Sigma-Aldrich) and recombinant constructs were produced using SDM as described in 2.5.8. Part of this process took place at Ohio State University under the guidance of Peter Mohler and Faith Kline. This

process proved difficult as the *Ank3* gene is very large and repetitive and due to a lack of phenotype in re-derived animals this was not taken further.

AA Change	Primer Name	Sequence 5'>3'
N1046S	A3137G_F	CGTCCTTCGGAGCGAGAGCGGAGAGAC
	A3137G_R	GTCTCTCCGCTCTCGCTCCGAAGGACG
D1056G	A3167G_F	TGGAAGGAACATCAGTTTGGCAGTAAAAACGAAG ACCTC
	A3167G_R	GAGGTCTTCGTTTTTACTGCCAAACTGATGTTCCT TCCA
V1446A	T4337C_F	ATCAGGATGGCGATAGCAGCCGATCACCTGG
	T4337C_R	CCAGGTGATCGGCTGCTATCGCCATCCTGAT

Table 8 Primer IDs and sequences for site-directed mutagenesis of the ANK3-190kDa rat gene

2.8.5 Re-derivation of mutation

Sperm from the ENU archive was retrieved for *in vitro* fertilisation (IVF) of wild-type C57BL/6J ova. These were then implanted into pseudopregnant female WT mice to produce offspring. Ear biopsies were lysed as described in 2.5.1 and heterozygotes were identified by PCR and melt curve analysis as described in 2.8.2 above. Heterozygous mice were then backcrossed to WT C57BL/6J mice and this was repeated in the next generation. Once three generations of backcrosses had been completed, heterozygotes were intercrossed to produce homozygous animals.

2.8.6 Genotyping Assays

Colonies (ID: ANK3-D1056G-B6 and ANK3-D1056G-IC) were genotyped using a LightScanner LunaProbe assay using primers described in Table 9. Ear biopsies were lysed using TaqMan® Sample-to-SNP™ Kit (Thermo Fisher) and diluted 1/10, and reaction mixture (Table 10) underwent cycling parameters described in Table 11.

Primer ID	Sequence 5'>3'
ANK3 D1056G LS FOR	GAGAACTTATCGTCCTTCGG
ANK3 D1056G LS REV	CCTTCATCCATGCCATTGAG
ANK3 D1056G PROBE rev	GTCTTCGTTTTTACTGCCAAACTGATGTTC

Table 9 Primer IDs for genotyping ANK3-D1056G-B6 and ANK3-D1056G-IC mouse colonies

Reagent	Volume per well (µl)
HotShot master mix	5
LCGreen	1
Primer1 R(20ng/µl)	0.1
Primer2 F (20ng/µl)	0.5
Primer3 Pr R (20ng/µl)	0.5
DNA (1/10 dil)	2
ddH2O	0.9
TOTAL	**10**

Table 10 Reaction mixture for genotyping ANK3-D1056G-B6 and ANK3-D1056G-IC mouse colonies

Step	Temperature (°C)	Time	
1	95	02:00	
2	95	00:30	PCR Cycle
3	60	00:30	
4	72	00:30	
	PCR cycle x 55		
5	95	00:30	Hybridisation
6	25	00:30	
7	15	00:30	

Table 11 Cycling parameters for genotyping ANK3-D1056G-B6 and ANK3-D1056G-IC mouse colonies

2.8.7 Behavioural Phenotyping

10 *Ank3*$^{D1056G/D1056G}$ male mice were used for the primary phenotyping battery which included SHIRPA, Open Field, Acoustic Startle PPI and Fear Conditioning as described in 2.2. They were compared with 10 WT littermate controls. They entered the battery pipeline at 9 weeks of age. These animals were transferred to Project License 30/2890 as some cardiac phenotyping was also carried out (data not presented).

2.8.8 Sleep and Circadian Screens

8 *Ank3*$^{D1056G/D1056G}$ female mice and WT littermate controls went through a basic sleep and circadian screen as described (2.2.5-6). Sleep tracking took place at 9 weeks and circadian screening began after this at 12 weeks.

2.9 *Tcf4*

2.9.1 Sequence alignments and conservation analysis

TCF4 protein sequences for mouse, rat, rabbit, human, chimp, gorilla, cat, dog and frog were retrieved from Ensembl. Residues corresponding to human residues 121-360 from each were isolated and aligned using Clustal Omega (www.ebi.ac.uk/Tools/msa/clustalo/). Alignments used default settings as described in the literature (Sievers et al., 2011, McWilliam et al., 2013). Alignments were then visualised using Jalview (Waterhouse et al., 2009) and the Zappo colour scheme as described above.

2.9.2 Site-directed mutagenesis of *Tcf4*

A pcDNA™3.1/V5-His plasmid containing the *Tcf4* cDNA sequence (OTTMUST00000049842.3) was kindly supplied by Dr Mike Parsons. The S189G and S275R mutations were reproduced in this construct using site-directed mutagenesis as described in 2.5.8. Primers are described in Table 12 and each reaction was cycled using the parameters in Table 13. *Dpn* digestion (1µl added to each reaction, incubated at 37° for 1 hour) was then used to remove the parental supercoiled dsDNA.

Samples were then transformed and plasmid DNA was isolated using Minipreps as described in 2.5.8. Sanger sequencing (Source Bioscience) was then used to confirm successful mutagenesis (Table 14) and midi-preps were used to produce plasmid stocks (2.5.7).

Primer ID	Sequence
S189G_F	CGCTCCTTCAGCC**G**GCACTGCCGACTA
S189G_R	TAGTCGGCAGTGC**C**GGCTGAAGGAGCG
S275R_F	GGCAGACATCAACTCC**C**GTCTTCCTCCGATGTC
S275R_R	GACATCGGAGGAAGAC**G**GGAGTTGATGTCTGCC

Table 12 Primer sequences for SDM. Mutational base changes are bolded.

Step	Cycles	Temp	Time
1	1	95°	1 min
2	18	95°	50s
		60°	50s
		68°	9 mins
3	1	68°	7 mins

Table 13 Cycling parameters for SDM of *Tcf4*-pcDNA3.1/V5-His

Primer ID	Sequence
tcf4_Ex9F1	CAGCAGCCAGCACTTTC
tcf4_Ex9R1	AGTTCCTCTGTTTGCCATTATAC
tcf4_Ex11F1	CTCTAGGGAAAGCCCTAGC
tcf4_Ex11R1	AGTGCAAGGGTCCTTCATA

Table 14 Primer sequences for confirming mutagenesis. The S189G mutation falls within exon 9 and the S275R mutation is in exon 11.

2.9.3 Prediction of post-translational phosphorylation

The Group Prediction Software (GPS) v3.0 was used to predict phosphorylation of S189 and S275 in the mouse wild-type TCF4 (OTTMUST00000049842.3) (Xue et al., 2011, Liu et al., 2015). The full-length protein sequence was tested using the desktop software. The high threshold was used; this has a false positive rate of 2% so findings should be significant at the $p < 0.05$ level (Liu et al., 2015). Results were filtered to show the two serine residues of interest. To rank kinase predictions, the score (a measure of prediction strength) was divided by cut-off (the value under the threshold)(Liu et al., 2015).

2.9.4 Luciferase reporter gene assays

2.9.4.1 Cloning of TCF4 binding partners

TCF3, TCF12, ID1 and ID3 have been identified as binding partners of TCF4 (Loveys et al., 1996, Murakami et al., 2004, Ravasi et al., 2010). Cloning primers were designed using Primer3 Plus as described (Table 15). Two 40µl reactions were set up per gene: 4µl DNA template (mouse liver cDNA),1 µl forward and 1µl reverse primers (100ng/µl), and 14µl ddH_2O were added to 10µl 5X Phusion HF Buffer (NEB). 20µl Phusion® High-Fidelity DNA Polymerase was then added. Reactions were cycled as described in Table 15. After gel purification (2.5.4) an A-overhang was added as described in 2.5.6.1. 4µl of each PCR product was added to 1µl Salt Solution and 1µl pcDNA™3.1/V5-His TOPO® vector (Invitrogen) and incubated for 5 mins at RT. These constructs were then transformed, grown and purified as described in 2.5.6.2-3. Integration of DNA sequences was checked using Sanger sequencing (Source Bioscience) and T7F and BGHR primers. Once confirmed plasmids were midi-prepped as described in 2.5.7. Constructs containing *Clock* and *Bmal1* were already available in the lab (Parsons, unpublished data).

Primer ID	Sequence
TCF3_F_nat	CCTGGGTGGATGAACCAGTCTCAGAGAATGG
TCF3_R2	CAGGTGCCCGGCTGGGTT
TCF12_F_nat	GCTAGAAGTGGCTGAAGATGAATCCCCAGCAGCAG
TCF12_R	CAGATGACCCATAGGGTTGG
ID1_F_nat	TTCTCAGGATCATGAAGGTCGCCAGTGGC
ID1_R	GCGACACAAGATGCGATC
ID3_F_nat	CTCTCTATCTCTACTCTCCAACATGAA
ID3_R	TCAGTGGCAAAAGCTCCTCT

Table 15 Primer sequences for cloning of TCF4 binding partners

Step	Cycles		Temp	Time
1	1		98°	10s
2	30		98°	5s
		Tcf3	58.6°	15s
		Tcf12	68.7°	
		Id1	50.7°	
		Id3	50.7°	
			72°	1 min
3	1		72°	5 mins

Table 16 PCR parameters for cloning of TCF4 binding partners

2.9.4.2 Cell seeding

HEK293T cells (ECACC 12022001) were maintained as described (2.6). For transfection, cells were plated in 12-well plates at 2.5 x 10^5 cells/well. Briefly, cells were washed with PBS and trypsinised in 0.05% trypsin (Gibco). Trypsin was quenched with DMEM before centrifuging for 5 minutes at 800rpm. Media was removed and the cell pellet resuspended in 12mls complete DMEM. Cells were counted using a haemocytometer to calculate cells per ml. A dilution to be plated was then calculated as follows:

$$cells/ml = viable\ cell\ count \times 10^4$$

$$Total\ cell\ number\ required = {}^{cells}/_{well} \times 2 \times 10^5 \times 1.1$$

$$Cell\ suspension\ needed(ml) = Total\ cell\ number / {}^{cells}/_{ml}$$

$$Media = (No.of\ wells \times 1.1) - cell\ suspension$$

Cells were plated and incubated at 37°C, 5% CO_2 until 80-90% confluent.

2.9.4.3 Transfection

Cells were transfected using the jetPRIME system (Polyplus-transfection, NY, USA). Three technical replicates were used for each condition. Transfection

combinations are shown in Table 17. Empty pcDNA™3.1/V5-His vector (*Blank*) was used to keep total DNA concentration constant. A *Cry1-luc* construct was kindly provided by Mike Parsons; the promoter of *Cry1* contains multiple E-box motifs (Hardin, 2004) and so can be activated by bHLH dimers. Renilla luciferase was used as an internal control.

DNA (Table 17 + 100ng/well *Cry1-luc* + 5ng/well *Renilla*) was diluted into 75µl/well jetPRIME® buffer and mixed by vortexing. 2.2µl/well jetPRIME® was added, vortexed for 10s, and briefly centrifuged down before incubation at RT for 10 minutes. 81µl of transfection mix was added per well onto the cells. Plates were returned to the incubator and analysed after 24h.

		Heterodimers		
	Blank (1µg)	*Tcf4-wt/Tcf3*	*Tcf4-S189G/Tcf3*	*Tcf4-S275R/Tcf3*
Homodimers	*Tcf4-wt/lBlank*	*Tcf4-wt/Tcf12*	*Tcf4-S189G/Tcf12*	*Tcf4-S275R/Tcf12*
	Tcf4-S189G/Blank	*Tcf4-wt/Id1*	*Tcf4-S189G/Id1*	*Tcf4-S275R/Id1*
	Tcf4-S189G/Tcf4-wt	*Tcf4-wt/Id3*	*Tcf4-S189G/Id3*	*Tcf4-S275R/Id3*
	Tcf4-S275R/Blank	*Tcf4-wt/Clock*	*Tcf4-S189G/Clock*	*Tcf4-S275R/Clock*
	Tcf4-S275R/Tcf4-wt	*Tcf4-wt/Bmal*	*Tcf4-S189G/Bmal*	*Tcf4-S275R/Bmal*

Table 17 Transfection combinations.

Constructs were combined to study homodimerisation (boxes shaded in grey) and heterodimerisation. 500ng/well of construct was used to total 1µg; ICIL-Blank plasmid was used to keep concentration constant where only one construct was transfected or in the negative control.

2.9.4.4 Dual-Luciferase reporter assay

To analyse reporter gene activity the Dual-Luciferase Reporter Assay System (Promega, WI, USA) was used.

Growth medium was removed from cells and 1ml PBS added to gently wash the surface. This was removed before application of 250µl Passive Lysis Buffer (Promega). Plates were placed on a rocker for 15 minutes at RT before the transfer of the lysate to clean tubes. The lysate was then dispensed into luminometer plates; 20µl was added per well and 3 replicates were dispensed per lysate.

Assays for luciferase activity and Renilla activity were then carried out sequentially using a VarioskanFlash 4.00.53 luminometer (Thermo Scientific). Luciferase Assay Reagent II (LARII) was prepared by re-suspending lyophilised Luciferase Assay Substrate in 10ml of the supplied Luciferase Assay Buffer II. 1 volume of 50X Stop & Glo® Substrate was added to 50 volumes of Stop & Glo® Buffer just before use.

Before carrying out the experiment, injector lines were washed with 1500µl ddH_2O. Injectors were then primed using 800µl of LARII or Stop & Glo. SkanIt Software 2.4.5 RE for Varioskan Flash (Thermo Scientific) was used to identify samples and run the dual-injection protocol. The sample plate was inserted and samples identified. 100µl LARII was injected into each well, shaken for 5 seconds, and luciferase output measured. Stop & Glo® was then injected, shaken for 5 seconds, and renilla output measured. When finished, injectors were purged of reagents and washed with 4500µl ddH_2O.

Outputs were normalised by dividing the luciferase output by the renilla output. Results were then exported to Microsoft Excel for analysis. Technical replicates and then biological replicates were averaged to produce a grand mean. Each grand mean was then divided by the grand mean of the negative control (*Blank)* to study the

relative change in activation. GraphPad Prism 7 was used to carry out a 2-way ANOVA.

2.9.4.5 Statistics

Results were adjusted for multiple testing depending on comparison. *Tcf4wt* homodimerisation vs heterodimerisation underwent 2-way ANOVA with Sidak's test. *Tcf4* mutant constructs vs *Tcf4wt* homo- and heterodimerisation underwent 2-way ANOVA with Dunnett's test.

2.9.5 Re-derivation of mutation

Sperm from the ENU archive was retrieved for *in vitro* fertilisation (IVF) of wild-type C57BL/6J ova. These were then implanted into pseudopregnant female WT mice to produce offspring. Ear biopsies were lysed as described (2.5.1) and heterozygotes were identified by PCR using primers listed in Table 18. Heterozygous mice were then backcrossed to WT C57BL/6J mice and this was repeated in the next generation. Once three generations of backcrosses had been completed to eliminate approximately 88% of other ENU point mutations in the founder genome, heterozygotes were intercrossed to produce homozygous animals.

2.9.6 Genotyping Assays

Colonies (ID: TCF4-S275R-B6 and TCF4-S275R -IC) were genotyped using a LightScanner LunaProbe assay using primers described in Table 9. Ear biopsies were lysed using TaqMan® Sample-to-SNP™ Kit (Thermo Fisher) and diluted 1/10, and reaction mixture (Table 20) underwent cycling parameters described in Table 21.

Primer ID	Sequence 5'>3'
TCF4_exon11_F	AGACTAAGTATACCGTGACTGAAC
TCF4_exon11_R	ATGGAGCACTGGCTTCT

Table 18 Primer IDs for identifying heterozygous animals using melt-curve analysis

Primer ID	Sequence 5'>3'
TCF4 S275R LS FOR	TACCGTGACTGAACGTCTTCT
TCF4 S275R LS REV	GAGGTGCTGTAATGGTTTGTG
TCF4 S275R PROBE rev	GGAAGACGGGAGTTGATGTCTGC

Table 19 Primer IDs for genotyping TCF4-S275R-B6 and TCF4-S275R -IC mouse colonies

Reagent	Volume per well (µl)
HotShot master mix	5
LCGreen	1
Primer1 R(20ng/µl)	0.1
Primer2 F (20ng/µl)	0.5
Primer3 Pr R (20ng/µl)	0.5
DNA (1/10 dil)	2
ddH2O	0.9
TOTAL	**10**

Table 20 Reaction mixture for genotyping TCF4-S275R-B6 and TCF4-S275R -IC mouse colonies

Step	Temperature (°C)	Time	
1	95	02:00	
2	95	00:30	PCR Cycle
3	60	00:30	
4	72	00:30	
	PCR cycle x 55		
5	95	00:30	Hybridisation
6	25	00:30	
7	15	00:30	

Table 21 Cycling parameters for genotyping TCF4-S275R-B6 and TCF4-S275R -IC mouse colonies

2.9.7 Behavioural Phenotyping

10 *Tcf4*$^{S275R/S275R}$ male mice were used for the primary phenotyping battery, which included SHIRPA, Open Field, Acoustic Startle PPI and Fear Conditioning as described in 2.2. They were compared with 10 WT littermate controls. They entered the battery pipeline at 8 weeks of age.

2.9.8 Sleep and Circadian Screens

10 *Tcf4*$^{S275R/S275R}$ female mice and 10 WT littermate controls went through a basic sleep and circadian screen as described (2.2.5-6). Sleep tracking took place at 9 weeks and circadian screening began after this at 12 weeks.

2.10 *Cacna1c*^{Q1625STOP}

2.10.1 Genotyping Assay

Colonies (ID: CACNA1C-Q1466STOP-B6 and CACNA1C-Q1466STOP-IC) were genotyped using a LightScanner LunaProbe assay using primers as described in Table 22. Ear biopsies were lysed using TaqMan® Sample-to-SNP™ Kit (Thermo Fisher) and diluted 1/10, and reaction mixture (Table 23) underwent cycling parameters described in Table 24.

Primer ID	Sequence 5'>3'
CACNA1C-Q1466STOP-F	CCGTATGCCTTAGATGACGA
CACNA1C-Q1466STOP-R	GGGACAGTGCATTCCTTTG
CACNA1C-Q1466STOP-PrR	GAAGTACTCTTAGATCAGGAAGGTGGC

Table 22 Primer IDs for genotyping CACNA1C-Q1466STOP-B6 and CACNA1C-Q1466STOP-IC mouse colonies

Reagent	Volume per well (µl)
HotShot master mix	5
LCGreen	1
Primer1 R(20ng/µl)	0.1
Primer2 F (20ng/µl)	0.5
Primer3 Pr R (20ng/µl)	0.5
DNA (1/10 dil)	2
ddH2O	0.9
TOTAL	**10**

Table 23 Reaction mixture for genotyping CACNA1C-Q1466STOP-B6 and CACNA1C-Q1466STOP-IC mouse colonies

Step	Temperature (°C)	Time	
1	95	02:00	
2	95	00:30	PCR Cycle
3	60	00:30	
4	72	00:30	
	PCR cycle x 55		
5	95	00:30	Hybridisation
6	25	00:30	
7	15	00:30	

Table 24 Cycling parameters for genotyping CACNA1C-Q1466STOP-B6 and CACNA1C-Q1466STOP-IC mouse colonies

2.10.2 Timed matings to assess perinatal lethality

As no *Cacna1c*$^{Q1625STOP/Q1625STOP}$ homozygous animals were observed at postnatal day 21, timed matings were carried out. *Cacna1c*$^{Q1625STOP/+}$ x *Cacna1c*$^{Q1625STOP/+}$ intercrosses were mated and pregnant females were dissected at 9.5 or 14.5 days *post coitum* (dpc). Briefly, pregnant adult females were culled by cervical dislocation and embryos were surgically removed after confirmation of death. Embryos were placed into cold PBS and decapitated as soon as possible. A tail biopsy was taken from each embryo and these were genotyped as described above.

2.10.3 Behavioural Phenotyping

Due to homozygous lethality (described below), heterozygous *Cacna1c*$^{Q1625STOP/+}$ animals and littermate controls were used for phenotyping. Due to low numbers, mixed-sex cohorts were used for the primary phenotyping battery (SHIRPA, Open Field, Acoustic Startle PPI and Fear Conditioning, as described in 2.2). Each test was analysed for sex differences using a 2-way ANOVA. No sex differences were observed so results are presented from all animals. 6 *Cacna1c*$^{Q1625/+}$animals and 6 *Cacna1c*$^{+/+}$ littermate controls were used for primary phenotyping. These animals were transferred to Project License 30/2890 in order to carry out echocardiogram

studies. All 6 heterozygous animals and controls underwent echocardiogram as described in 2.4.1, carried out by Heather Cater.

2.10.4 Secondary Behavioural Phenotyping

An additional cohort was produced for secondary phenotyping battery including Light-Dark box, Elevated Nought Maze, and Acoustic Startle PPI (re-calibrated equipment) (protocols described in 2.3). 11 *Cacna1c*$^{Q1625STOP/+}$ females and 10 *Cacna1c*$^{Q1625STOP/+}$ males were screened with littermate controls. Animals were genotyped before weaning and randomised; researcher was blind to genotype.

2.10.5 Sleep and Circadian Screens

8 *Cacna1c*$^{Q1625STOP/+}$ female mice and 8 littermate controls went through a basic sleep and circadian screen as described (2.2.5-6). Sleep tracking took place at 9 weeks and circadian screening began after this at 12 weeks.

2.10.6 EEG Recording

2.10.6.1 Animals

9 *Cacna1c*$^{Q1625STOP/+}$ mice and 8 littermate controls, all males and aged 6 months, were subjected to a sleep assessment. Animals were individually housed in standard cages kept in a controlled environment with a 12-hour day-night cycle (lights on at 8 a.m.) within the animal facilities of the IIT (Istituto Italiano di Tecnologia, Genova, Italy). Animals had free access to water and standard rodent food pellets. All procedures were done under the Italian Policy (licence number 039, expires on 15/06/2015). Surgery and sleep deprivation was carried out by Glenda Lassi and data collection and analysis was carried out by Valter Tucci and Ilaria Cosentini.

2.10.6.2 Surgery and data acquisition

Mice were anaesthetised with Ketamine/Xilaxine, 90-150 K/ 7.5-16 X, and implanted with a transmitter that measures electroencephalography (EEG) and electromyography (EMG) (Data Sciences, F20-EET, Gold system). Leads from the transmitter were led, subcutaneously, to the skull, where holes were drilled to implant EEG-screw electrodes. The screws was then covered with dental acrylic. EMG electrodes were attached to the muscle in the nape of the neck. The animals were able to move freely while assessed in their home-cage environment. Dataquest A.R.T. software (DSI) was used to acquire the EEG data. EEG activity was sampled at 500 Hz with a filter cut-off of 50 Hz.

2.10.6.3 Protocol

A 10-day post-surgery period of recovery was given to the mice to ensure that they had completely recovered and that sleep architecture was fully restored. At the end of the recovery period, physiological signals were recorded uninterruptedly for 24 consecutive hours (sleep baseline). Then, mice were sleep deprived for 4 hours from 8am to 12pm; the animals were kept awake by gentle handling and brushing. Sleep deprivation (SD) was followed by a 20-hour recovery period during which the animal was left undisturbed.

The EEG and EMG signals were continuously acquired through all the protocol conditions and stored in a computer for the following analysis processes.

2.10.6.4 EEG analysis

EEG data recordings were imported into the SleepSign software package for staging and extrapolation of power spectrum values. Vigilance stages were analysed in 4-second epochs and identified based on the combination of EMG data and of the EEG power spectra. Epochs with artefacts were excluded from the analysis. Such

analysis was automatically performed with SleepSign software and then it was visually inspected and corrected.

We calculated the percentage of time spent in wakefulness and total sleep, considering 2-hour bins, in both light and dark phases. Spectral characteristics of the EEG were further analysed within the states of wakefulness, REM and NREM. Every epoch was sorted by stage and subjected to an FFT (Fast Fourier Transformation) with a resolution of 0,48Hz using Hanning window method. The analysis range 0,25-20Hz was divided into the canonical bands for the analysis: delta 0,25-5Hz, theta 5-9Hz, alpha 9-12Hz, beta 12-20Hz. Power spectra values of baseline and recovery were considered in 30-minute bins.

2.11 *Cacna1c*^{G1616D}

2.11.1 Genotyping Assay

Colonies (ID: CACNA1C-G1457D-B6 and CACNA1C-G1457D-IC) were genotyped using a LightScanner LunaProbe assay using primers as described in Table 25. Ear biopsies were lysed using TaqMan® Sample-to-SNP™ Kit (Thermo Fisher) and diluted 1/10, and reaction mixture (Table 26) underwent cycling parameters described in Table 27.

Primer ID	Sequence 5'>3'
CACNA1C-G1457D-F	TCAAGGTAACCTGGTGGGA
CACNA1C-G1457D-R	TTCCTTTGTGAGGGCTTGC
CACNA1C-G1457D-PrF	GGTCACAGTGGACAAGTTCTATGCC

Table 25 Primer IDs for genotyping CACNA1C-G1457D-B6 and CACNA1C-G1457D-IC mouse colonies

Reagent	Volume per well (µl)
HotShot master mix	5
LCGreen	1
Primer1 F(20ng/µl)	0.1
Primer2 R (20ng/µl)	0.5
Primer3 Pr F (20ng/µl)	0.5
DNA (1/10 dil)	2
ddH2O	0.9
TOTAL	**10**

Table 26 Reaction mixture for genotyping CACNA1C-G1457D-B6 and CACNA1C-G1457D-IC mouse colonies

Step	Temperature (°C)	Time	
1	95	02:00	
2	95	00:30	PCR Cycle
3	60	00:30	
4	72	00:30	
	PCR cycle x 55		
5	95	00:30	Hybridisation
6	25	00:30	
7	15	00:30	

Table 27 Cycling parameters for genotyping CACNA1C-G1457D-B6 and CACNA1C-G1457D-IC mouse colonies

2.11.2 Behavioural Phenotyping

9 *Cacna1c*$^{G1616D/G1616D}$ animals and 9 *Cacna1c*$^{+/+}$ littermate controls were used for the primary phenotyping battery including SHIRPA, Open Field, Acoustic Startle PPI and Fear Conditioning. Details of these tests are described in 2.2. These animals were transferred to Project License 30/2890.

2.11.3 Echocardiogram

A cohort of 10 *Cacna1c*$^{G1616D/G1616D}$males and 10 littermate controls underwent echocardiogram at 3 months of age as described in 2.4.1. This was on Project License 30/2890. This was carried out by Heather Cater and was blind to genotype.

2.11.4 Electrocardiogram (ECG)

The same cohort of 10 *Cacna1c*$^{G1616D/G1616D}$ males and littermates also underwent ECG recording, carried out by Tom Nicol as described in 2.4.2.

2.11.5 Secondary Behavioural Phenotyping

A new cohort was produced for secondary phenotyping battery including Light-Dark box, Elevated Nought Maze and Acoustic Startle PPI (re-calibrated equipment)

(details of tests in 2.3). 10 *Cacna1c*$^{G1616D/G1616D}$ females and 11 *Cacna1c*$^{G1616D/G1616D}$ males were screened with littermate controls. Animals were genotyped before weaning and randomised; researcher was blind to genotype.

2.11.6 Sleep and Circadian Screens

8 *Cacna1c*$^{G1616D/G1616D}$ female mice and WT littermate controls went through a basic sleep and circadian screen as described (2.2.5-6). Sleep tracking took place at 9 weeks and circadian screening began after this at 12 weeks.

2.11.7 EEG Recording

2.11.7.1 Animals

9 *Cacna1c*$^{G1616D/G1616D}$ mice and 7 littermate controls, all males and aged 6 months, were subjected to a sleep assessment. Animals were individually housed in standard cages kept in a controlled environment with a 12-hour day-night cycle (lights on at 8 a.m.) within the animal facilities of the IIT (Istituto Italiano di Tecnologia, Genova, Italy). Animals had free access to water and standard rodent food pellets. All procedures were done under the Italian Policy (licence number 039, expires on 15/06/2015).

2.11.7.2 Surgery, data acquisition and protocol

Surgery, data acquisition, protocol and data analysis were carried out as described in 2.10.6.

3 *Ank3*

3.1 Introduction

Ankyrin$_G$, as described in 1.7, is an adaptor protein that links membrane-bound proteins to the intracellular cytoskeleton and targets them to the axon initial segment (AIS). SNPs in *ANK3* have been associated with schizophrenia and bipolar disorder (1.7.6) and this work aims to identify novel mutations and study their effect on behavioural domains in the mouse.

Novel mutations in *Ank3* identified via a genetic screen of ENU-mutagenised DNA have the potential to produce a range of effects dependent on whether they are a functional null, hypomorph, dominant negative or gain of function, and these may affect domains altered in BD or schizophrenia patients such as anxiety, memory, and startle response and prepulse inhibition. We expected to see effects in Na_v channel and βIV-spectrin localisation and AIS specification as ankyrin$_G$ is essential for these functions. Exons were chosen for screening from the membrane-binding domain, spectrin-binding domain, and death domain.

3.2 Results: Archive Screen

3.2.1 Archive screen identifies three novel non-synonymous mutations

After screening the ENU-mutagenised archive for mutations in exons 13, 15, 27, 28 and 35 of *Ank3* (Figure 29A) three non-synonymous mutations were identified using high-resolution melt curve analysis. Two mutations were identified in exon 27 (Figure 29B), which is in the spectrin-binding domain, and one in exon 35 (Figure 29C) in the C-terminal regulatory/'death' domain. These were sequenced to identify the base and amino acid change (Figure 29D). The two mutations in exon 27 were

both an A to G base substitution, while the mutation in exon 35 was a T to C change. All three caused predicted amino acid substitutions: in exon 27, one mutation caused an asparagine to serine change at position 1046 (*Ank3*^{N1046S}) and the other caused an aspartic acid to glycine change at position 1056 (*Ank3*^{D1056G}). In exon 35, the mutation caused a valine to alanine change at position 1446 (*Ank3*^{V1446A}).

3.2.2 Sequence analysis of novel mutations

Spectrin-binding and death domain sequences from vertebrates (mouse, rat, rabbit, human, chimp, gorilla and frog) and invertebrates (*C. elegans* and *D. melanogaster*) were aligned using ClustalOmega and sequence conservation was visualised using JalView.

Mutations 1 (*Ank3*^{N1046S}) and 2 (*Ank3*^{D1056G}) in the spectrin-binding domain are both at highly conserved positions (Figure 30A), and the SBD is highly conserved between vertebrates (90-99% sequence identity) and somewhat conserved in invertebrates (~50%) (Figure 30B). The amino acid change in *Ank3*^{N1046S} (Figure 30C) does not result in a change to the polarity or charge of the side chain, although the addition of a hydroxyl group could allow new hydrogen bonds to form. In *Ank3*^{D1056G} (Figure 30D) there is a drastic change from a large, negatively charged side chain to no side chain at all which could affect steric hindrance or intramolecular bonds. This could thereby lead to a change in the ability of this region to interact with other proteins.

The death domain is less well conserved (Figure 30E). In vertebrates, there is ~75% sequence homology but invertebrates show much less conservation, suggesting that this region may have evolved a different or extra function in vertebrates (Figure 30F). *Ank3*^{V1446A} (Figure 30G) does cause a small change in size,

but both residues are hydrophobic. The loss of two carbon atoms could cause steric changes, however.

Based on conservation and amino acid change (summarised in Figure 30H), *Ank3*^{N1046S} and *Ank3*^{D1056G} were predicted to cause the largest changes in amino acid conformation or charge. In order to try to prioritise further, *in vitro* work was then carried out.

3.2.3 *In vitro* cloning of *Ank3* proved unsuccessful

To prioritise which of the three ENU mutations to re-derive, I attempted to clone the full-length mouse cDNA sequence. However, the full-length gene proved too long and repetitive to amplify successfully. This was repeated using primers targeted to smaller regions of the gene, but this was still unsuccessful mostly due to the highly repetitive ankyrin repeat regions. Being unsuccessful at cloning the gene in-house, we searched the literature for existing constructs. Professor Peter Mohler (Ohio State University, Columbus OH) generously supplied us with a construct that contained a 190-kDa isoform of rat *Ank3* with an N-terminal GFP tag. After SDM, Sanger sequencing showed that mutation and reproduction of the N1046S and the V1446A residues had been successful. However, when colonies supposed to have a mutated residue D1056G were sequenced it became clear that the SDM was unsuccessful, probably due to the length and repetitive region of the gene. Therefore, *in silico* analysis was used to prioritise the ENU mutations.

3.2.4 ENU-induced mutation *Ank3*^{D1056G} was chosen for re-derivation

Aspartic acid has an acidic, electrically-charged side chain, has a molecular weight of 133.10, and as shown in Figure 30D is a long chain that may play a role in steric conformation and tertiary structure of the full-length protein. A mutation to

glycine, which has no side chain, is likely to cause changes in conformation. As the *Ank3*^{D1056G} mutation was in the spectrin-binding domain, we conjectured that it could affect binding and targeting of Ank3 protein as spectrin binding has been shown to be necessary (see 1.7.2.2).

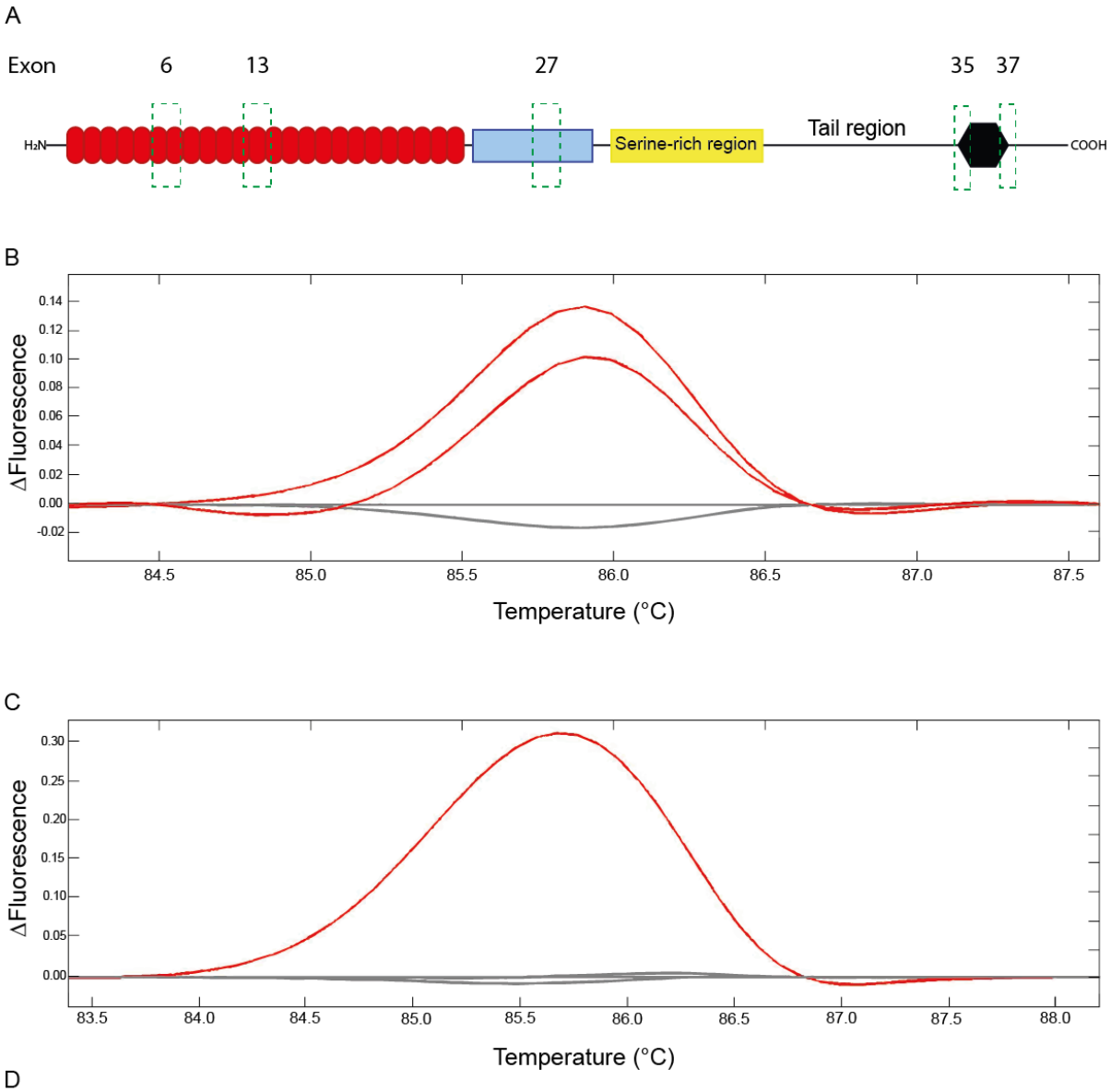

D

Region	Exon (bp)	Mutants found	Base change	AA change
Spectrin-binding domain	27 (248)	2	A>G	N1046S
			A>G	D1056G
Death domain	35 (147)	1	T>C	V1446A

Figure 29 Difference Curves identify novel mutations in exons of Ank3.

(A) A schematic showing the 5 exons of mouse *Ank3* screened. Heterozygous mutations cause a decrease in melting temperature, which can be identified by visualising temperature against Δfluorescence in B) exon 27 and C) exon 35 of *Ank3* in ENU-mutagenised samples. Mutations were identified and summarised in Table (D).

A

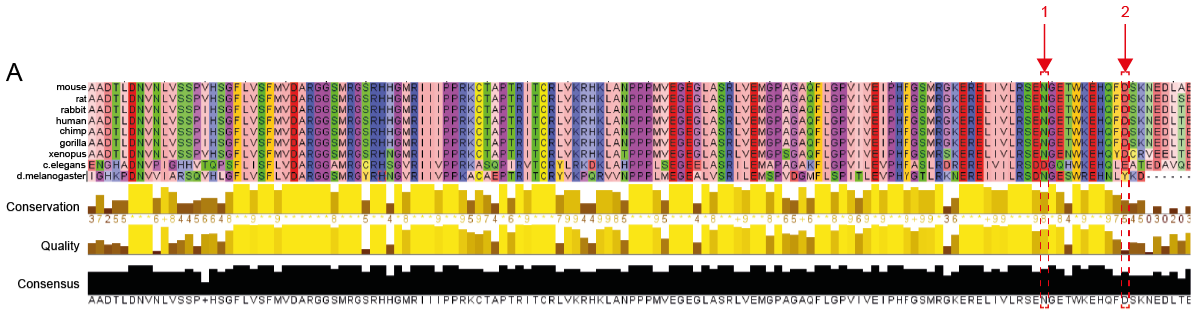

B

Percent Identity Matrix - created by Clustal2.1

vs	Mouse %	Human %
1: mouse	100.00	98.51
2: rat	99.07	98.02
3: rabbit	98.52	100.00
4: human	98.51	100.00
5: chimp	98.51	100.00
6: gorilla	98.51	100.00
7: xenopus	90.65	90.59
8: c.elegans	47.78	47.22
9: d.melanogaster	51.31	50.28

C

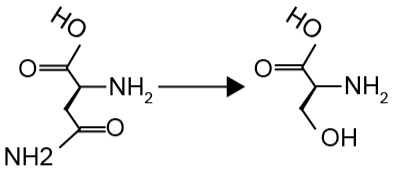

D

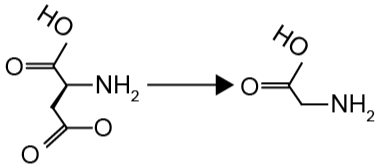

E

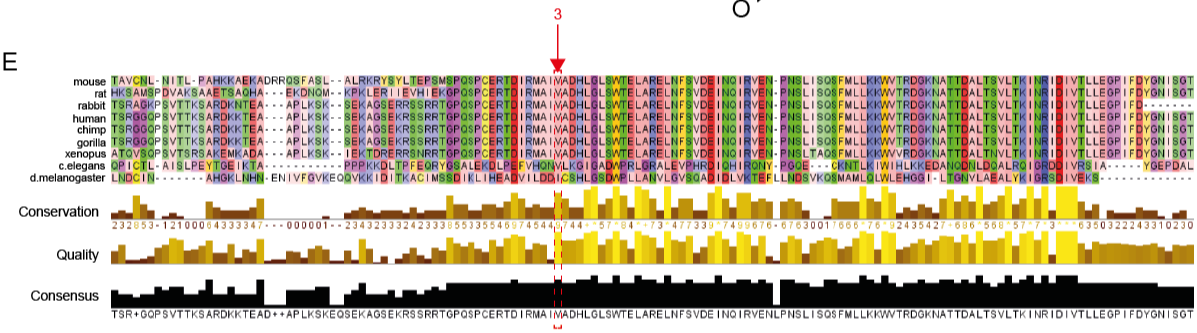

F

Percent Identity Matrix - created by Clustal2.1

vs	Mouse %	Human %
1: mouse	100.00	76.22
2: rat	75.16	75.90
3: rabbit	72.86	96.79
4: human	76.22	100.00
5: chimp	75.76	100.00
6: gorilla	75.76	100.00
7: xenopus	68.71	81.01
8: c.elegans	22.09	19.23
9: d.melanogaster	25.16	24.29

G

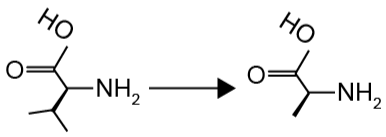

H

Region	Mutation	AA change	Predicted function
SBD	1	N1046S	Disrupt spectrin binding
	2	D1056G	Impaired channel function
DD	3	V1446A	Disrupted targeting Disrupted binding to apoptotic proteins

Figure 30 Novel mutations identified in the ENU-mutagenised DNA archive are in conserved regions.

(A) The spectrin-binding domain is well conserved in vertebrates and conserved in invertebrates (B). Skeletal formulae showing (C) Mutation 1 (*Ank3*^{N1046S}) and (D) mutation 2 (*Ank3*^{D1056G}). The death domain (E) is less well-conserved but still has ~75% homology in vertebrates (F). (G) Skeletal formula showing mutation3 (*Ank3*^{V1446A}). (H) summarises the mutations and their predicted effect on ankyrin$_G$ function.

3.3 Results: Phenotyping

3.3.1 *Ank3*$^{D1056G/D1056G}$ mice are viable to adulthood

At post-natal day 21 (P21), offspring from *Ank3*$^{D1056G/+}$ x *Ank3*$^{D1056G/+}$ intercross matings were weaned, biopsied and genotyped. There were 20 WT animals, 31 heterozygous *Ank3*$^{D1056G/+}$ animals and 20 homozygous *Ank3*$^{D1056G/D1056G}$ animals recorded (Figure 31A). This is not significantly different to the expected Mendelian ratio (X^2=1.141, ns) (Figure 31B). The homozygous mutation is therefore not lethal, either pre-or post-natally, and appears to have little or no effect on survival to weaning age. There was no observation of abnormal survival post-weaning.

A

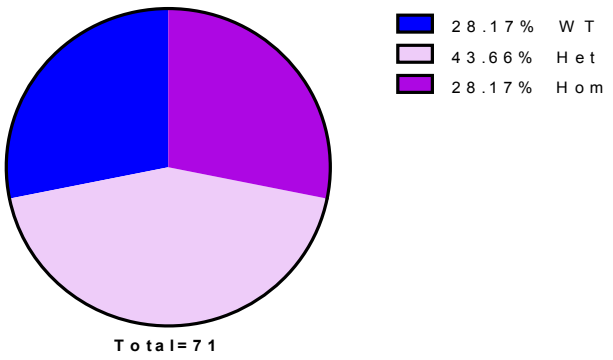

B

Chi-square	1.141
Degrees of freedom	2
P value (two-tailed)	0.5653
P value summary	**ns**

Figure 31 Survival at 21 days post-birth.

(A) Mendelian ratios were observed at P21 and (B) the X^2 test showed no significance.

3.3.2 *Ank3*$^{D1056G/D1056G}$ mice show no behavioural phenotype

A cohort of 10 *Ank3*$^{D1056G/D1056G}$ males and 10 *Ank3*$^{+/+}$ littermate controls underwent a primary phenotyping battery as described in 2.2. This battery consisted of SHIRPA, Open Field, Acoustic Startle PPI, and Fear Conditioning tests.

3.3.2.1 SHIRPA

Ank3$^{D1056G/D1056G}$ mice showed no obvious morphological or behavioural differences to *Ank3*$^{+/+}$ animals. They also did not show any differences in transfer arousal or locomotor activity and did not display any limb grasping or trunk curl.

3.3.2.2 Open Field

Over the whole 30-minute trial *Ank3*$^{D1056G/D1056G}$ mice showed no differences in duration spent in the centre (M = 106.6s ± 19.2, n=10) compared to *Ank3*$^{+/+}$ mice (M = 81.0s ± 10.1, n=10), t(18) = 1.177, ns (Figure 32A). There was no difference in frequency of entries into the centre between *Ank3*$^{D1056G/D1056G}$ (M = 67 ± 6, n=10) and *Ank3*$^{+/+}$ (M = 62 ± 8, n=10), t(18)=0.5797, ns (Figure 32B). They also showed no difference in total distance travelled (*Ank3*$^{D1056G/D1056G}$ M = 11969cm ± 765.4, n=10, *Ank3*$^{+/+}$ M = 11432cm ± 1174, n=10; t(18)=0.3834, ns) (Figure 32C).

3.3.2.3 Acoustic Startle PPI

There was no difference in the startle response between homozygous mutants (665.2 ± 84.25, n=10) and WT animals (M = 564.8 ± 83.47, n=10), t(18)=0.8468), ns (Figure 32D). After 2-way repeated measures ANOVA there was no significant interaction between genotype and PPI (Table 28). After correction for multiple testing, there was a trend towards an increased inhibition using the 75dB pre-pulse (p=0.0691) but in the context of the other phenotyping tests and lack of phenotype this was not considered a strong enough phenotype to investigate further (Figure 32E).

ANOVA table	SS	DF	MS	F (DFn, DFd)	P value
Interaction	176.9	2	88.47	F (2, 30) = 1.145	P=0.3318
Pre-Pulse	680.9	2	340.5	F (2, 30) = 4.406	P=0.0210
Genotype	1127	1	1127	F (1, 15) = 3.331	P=0.0879
Subjects (matching)	5075	15	338.3	F (15, 30) = 4.378	P=0.0003
Residual	2318	30	77.28		

Table 28 2-way RM ANOVA of pre-pulse decibel level interaction with genotype

3.3.2.4 Fear Conditioning

A two-way ANOVA of genotype and shock in the conditioning trial showed that all *Ank3*$^{+/+}$ and *Ank3*$^{D1056G/D1056G}$ mice had increased freezing after the first cue and shock, showing that genotype had no effect on the unconditioned response (Table 29, Figure 32F). The ratio of context freezing percentage to baseline percentage showed no difference (*Ank3*$^{+/+}$ (M = 18.34 ± 2.427, n=10), *Ank3*$^{D1056G/D1056G}$ (M = 20.00 ± 4.997, n=10), t(18) =0.2995, ns) (Figure 32G). Analysis of the baseline freezing in a novel arena showed no difference but response to cues 1 and 3 in the cue-dependent memory test trended towards being higher in *Ank3*$^{D1056G/D1056G}$ animals (2-way RM ANOVA, Figure 32H), and although there was a trend towards an effect of genotype (p=0.05) there was no interaction between genotype and time (Table 30).

We attempted to assess the unconditioned response to cue by comparing immobility in the 5s pre-tone and post-tone onset in the conditioning session. We would expect to see an increase in immobility as a response to the tone. However, we did not observe this in either wild-type or *Ank3*$^{D1056G/D1056G}$ animals (Figure 33A), and although there was a significant effect of genotype with *Ank3*$^{D1056G/D1056G}$ mice spending more time immobile (Figure 33B), it is difficult to confirm that animals could hear the cue tone.

ANOVA table	SS	DF	MS	F (DFn, DFd)	P value
Interaction	0.2351	1	0.2351	F (1, 18) = 0.004749	P=0.9458
Time	1381	1	1381	F (1, 18) = 27.9	P<0.0001
Column Factor	660.4	1	660.4	F (1, 18) = 4.379	P=0.0508
Subjects (matching)	2715	18	150.8	F (18, 18) = 3.047	P=0.0115
Residual	891.1	18	49.51		

Table 29 2-way RM ANOVA of freezing pre- and post-shocks

ANOVA table	SS	DF	MS	F (DFn, DFd)	P value
Interaction	605.3	3	201.8	F (3, 54) = 1.478	P=0.2308
Time	15024	3	5008	F (3, 54) = 36.68	P<0.0001
Genotype	3095	1	3095	F (1, 18) = 4.387	P=0.0506
Subjects (matching)	12697	18	705.4	F (18, 54) = 5.167	P<0.0001
Residual	7372	54	136.5		

Table 30 2-way RM ANOVA of freezing in the cue-dependent test

3.3.2.5 Ank3$^{D1056G/D1056G}$ mice do not show any circadian or sleep deficits

Both *Ank3*$^{+/+}$ and *Ank3*$^{D1056G/D1056G}$ female mice entrained to light in 12:12 LD (Figure 34A) showing that light input and response is intact. Free-running period in DD (τ_{DD}) showed no difference between *Ank3*$^{+/+}$ (M = 23.84 ± 0.04126, n=9) and *Ank3*$^{D1056G/D1056G}$ (M = 23.95 ± 0.04996, n=8), t(15) = 1.673, ns.

In sleep screens, there were no significant differences seen in immobility (as a correlate of sleep) over 24 hours (Table 31, Figure 35A), or averaged in the dark and light phase (Table 32, Figure 35B). There were also no differences in activity while the mice were awake shown by distance travelled over 24 hours (Table 33, Figure 35C) and averaged in light phase (Table 34, Figure 35D). There was a trend towards decreased distance travelled in the dark phase (Table 35), which could mean *Ank3*$^{D1056G/D1056G}$ animals have minor differences in movement. After a light pulse, both *Ank3*$^{+/+}$ and *Ank3*$^{D1056G/D1056G}$ mice showed an increase in immobility (Table 36, Figure 35E) but, although *Ank3*$^{D1056G/D1056G}$ mice appear to not be as immobile, this was non-significant after multiple comparison correction. Latency to immobility after

the light pulse was also similar between *Ank3*$^{+/+}$ (M = 917.8 ± 157.5, n=7) and *Ank3*$^{D1056G/D1056G}$ (M = 709.7 ± 109.8, n=8), t(13) = 1.106, ns (Figure 35F).

ANOVA table	SS	DF	MS	F (DFn, DFd)	P value
Interaction	14102	23	613.1	F (23, 322) = 1.143	P=0.2966
Time	242960	23	10563	F (23, 322) = 19.7	**P<0.0001**
Genotype	308.2	1	308.2	F (1, 14) = 0.7687	P=0.3954
Subjects (matching)	5613	14	401	F (14, 322) = 0.7476	P=0.7255
Residual	172692	322	536.3		

Table 31 2-way RM ANOVA measures - % Immobility over 24 hours

ANOVA table	SS	DF	MS	F (DFn, DFd)	P value
Interaction	0.7473	1	0.7473	F (1, 14) = 0.02057	P=0.8880
Time	16244	1	16244	F (1, 14) = 447.2	**P<0.0001**
Genotype	25.72	1	25.72	F (1, 14) = 0.7701	P=0.3950
Subjects (matching)	467.6	14	33.4	F (14, 14) = 0.9196	P=0.5612
Residual	508.5	14	36.32		

Table 32 2-way RM ANOVA measures - % Immobility in Dark and Light phase

ANOVA table	SS	DF	MS	F (DFn, DFd)	P value
Interaction	36485	23	1586	F (23, 322) = 1.142	P=0.2983
Time	598159	23	26007	F (23, 322) = 18.72	**P<0.0001**
Genotype	34210	1	34210	F (1, 14) = 2.682	P=0.1238
Subjects (matching)	178598	14	12757	F (14, 322) = 9.181	**P<0.0001**
Residual	447409	322	1389		

Table 33 2-way RM ANOVA measures - Distance travelled over 24 hours

ANOVA table	SS	DF	MS	F (DFn, DFd)	P value
Interaction	1997	1	1997	F (1, 14) = 2.025	P=0.1766
Time	36424	1	36424	F (1, 14) = 36.93	**P<0.0001**
Genotype	2851	1	2851	F (1, 14) = 2.681	P=0.1238
Subjects (matching)	14884	14	1063	F (14, 14) = 1.078	P=0.4452
Residual	13808	14	986.3		

Table 34 2-way RM ANOVA measures – Distance travelled in Dark and Light phase

	Ank3$^{+/+}$ M	*Ank3*$^{D1056G/D1056G}$ M	t	DF	Adjusted P Value
Dark	91.29	56.61	2.167	28	**0.0763**
Light	8.008	4.933	0.1921	28	0.9772

Table 35 Sidak's Test for multiple corrections - Distance travelled in Dark and Light

ANOVA table	SS	DF	MS	F (DFn, DFd)	P value
Interaction	7821	20	391.1	F (20, 280) = 1.031	P=0.4258
Time	176322	20	8816	F (20, 280) = 23.24	**P<0.0001**
Genotype	64	1	64	F (1, 14) = 0.2609	P=0.6174
Subjects (matching)	3434	14	245.3	F (14, 280) = 0.6464	P=0.8249
Residual	106240	280	379.4		

Table 36 2-way RM ANOVA measures – % Immobility after LP2

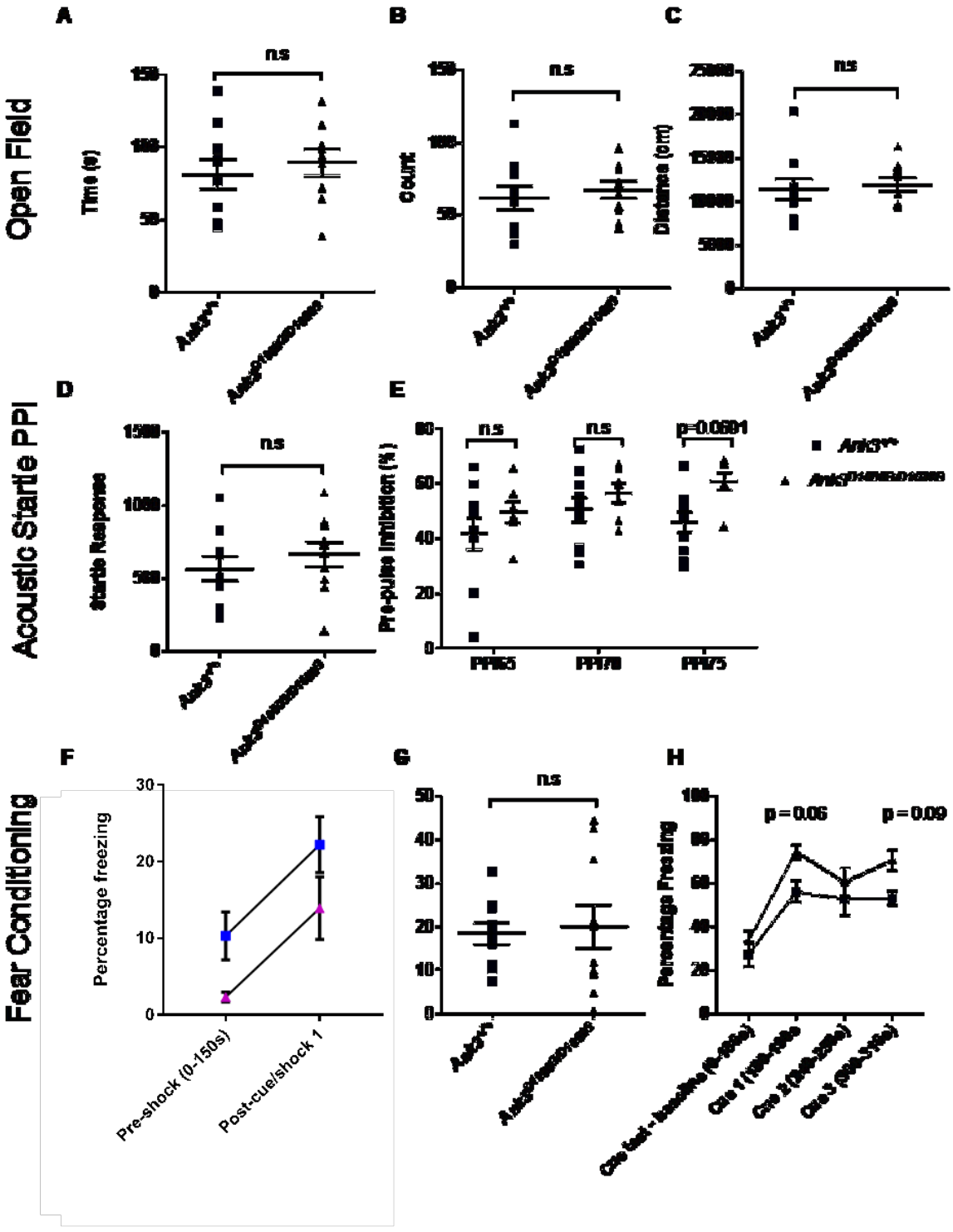

Figure 32 *Ank3*$^{D1056G/D1056G}$ mice do not show any behavioural differences.

Open Field: (A) Time spent in the centre; (B) Frequency of entries into the centre; (C) Total distance travelled. Acoustic startle PPI: (D) Startle response; (E) pre-pulse inhibition over three tests. Fear conditioning: (F)

Unconditioned freezing in the conditioning trial pre-shock and post-shock 1; (G) Difference in percentage freezing between baseline and context test; (H) Percentage freezing at baseline in a novel environment and after three cues in the cue-dependent test.

A

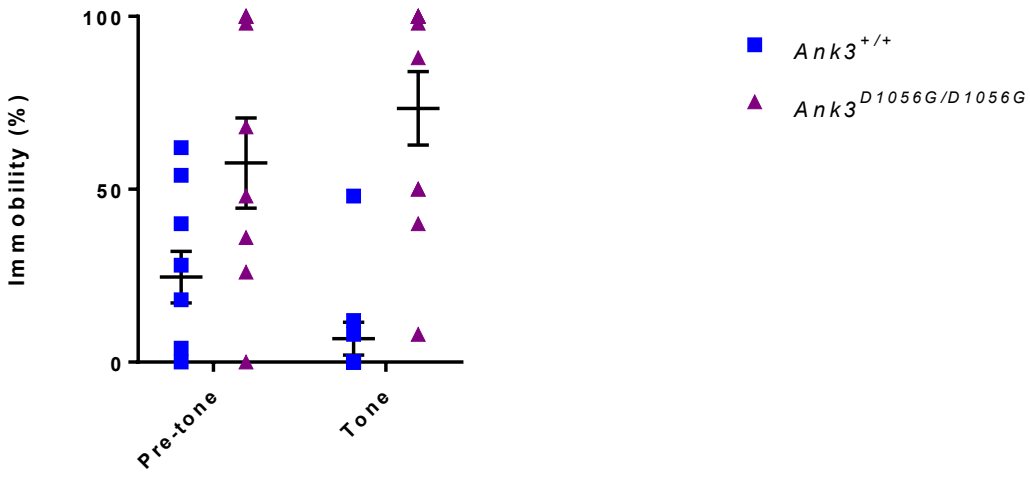

B

Source of Variation	% of total variation	P value	P value summary
Interaction	4.69	0.0629	ns
Time	0.01662	0.9074	ns
Genotype	41.21	0.0002	***
Subjects (matching)	32.6	0.1923	ns

Figure 33 Unconditioned response to the cue.

(A) Percentage of time spent immobile in the 5 seconds pre-tone and post-tone onset in the conditioning session. (B) 2-way RM ANOVA

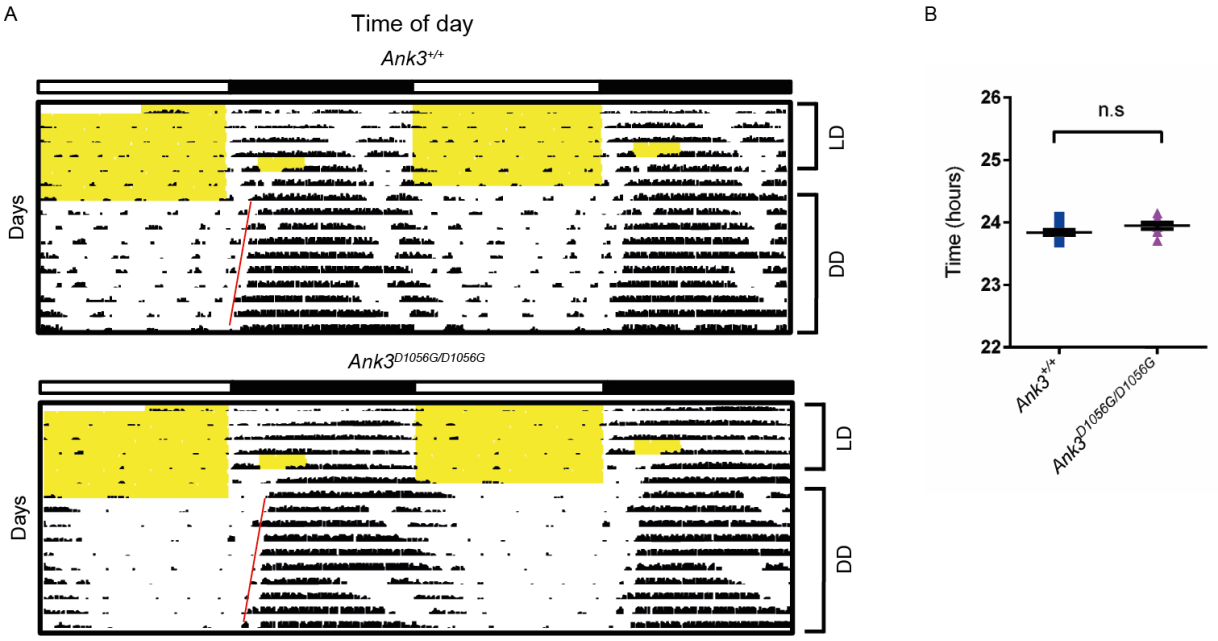

Figure 34 *Ank3*$^{D1056G/D1056G}$ mice show no change in circadian period or rhythmicity.

(A) Representative actograms showing activity in 12:12LD and DD with light periods indicated by yellow boxes. *Ank3*$^{+/+}$ (top) and *Ank3*$^{D1056G/D1056G}$ (bottom) mice entrain to light in LD. In DD, circadian period (tau) is depicted by a red line fitted to activity onsets on successive days and is the same in both cohorts. (B) Tau_{DD} is unchanged in *Ank3*$^{D1056G/D1056G}$.

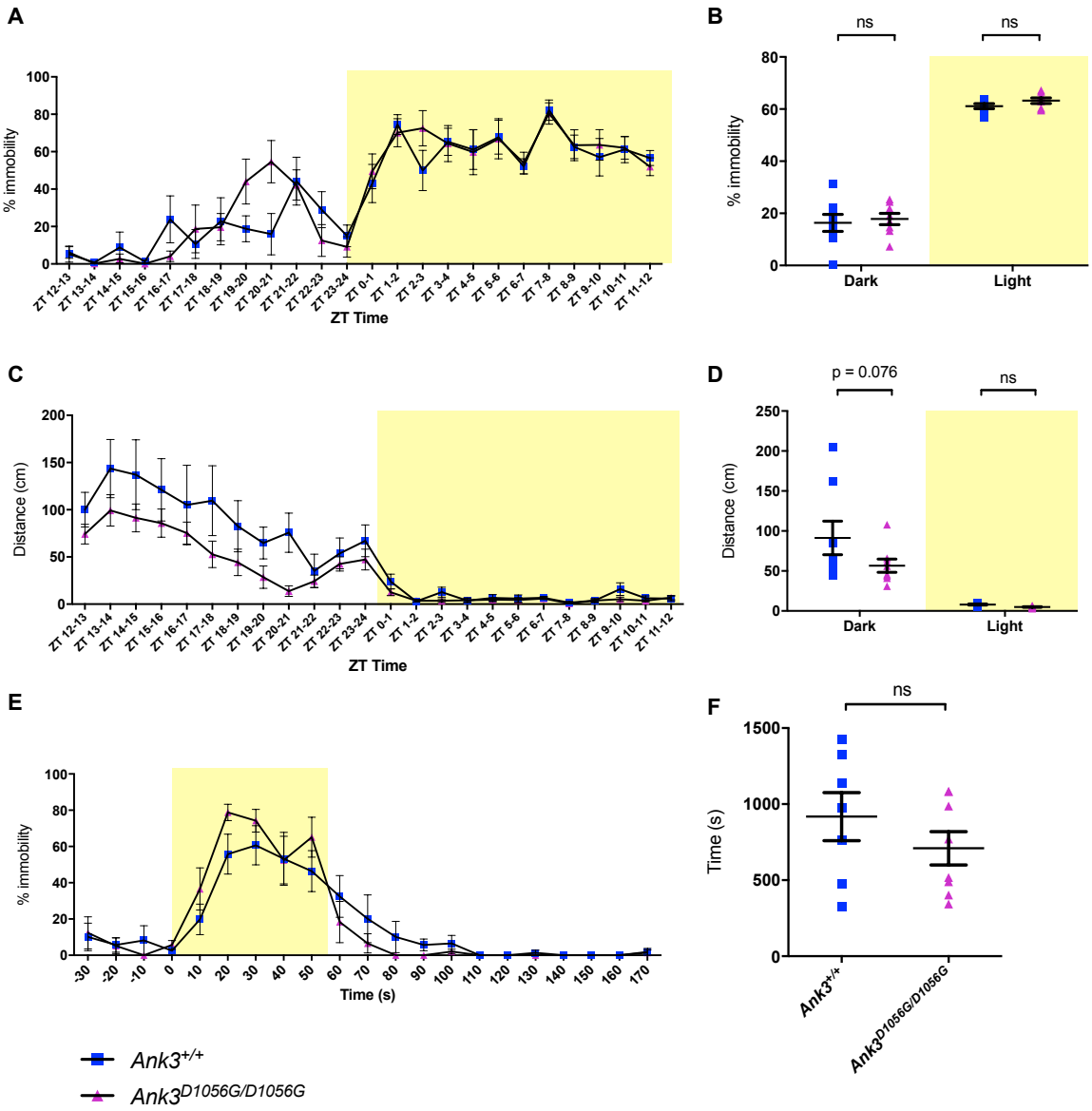

Figure 35 *Ank3*$^{D1056G/D1056G}$ mice show no differences in sleep screens.

(A) Percentage immobility over 24 hours, (B) Average hourly immobility in the dark and the light phase, (C) total distance travelled over 24 hours, (D) Average hourly distance travelled in the dark and the light phase,(E) percentage immobility during a light pulse (LP2) at ZT14, (F) Latency to immobility after onset of LP2.

3.4 Discussion

Multiple GWAS have associated SNPs in ANK3 with schizophrenia and bipolar disorder. In order to study the effects of single point mutations on ankyrin$_G$ function we generated and analysed adult mice from an ENU-mutagenised sample. ENU mutagenesis is an established method for producing point mutations and allelic series (Nolan et al., 2000a, Nolan et al., 2002) and a forward-genetics approach has been utilised previously to identify endophenotypes of schizophrenia and their causative mutations (for example in the *Blind-drunk* (*Bdr*) model)(Jeans et al., 2007). In this current study, we have instead used a reverse-genetics approach to finding mutations in multiple functional domains of *ANK3* before generating adult mice from one mutagenised sample for phenotyping.

Ank3^{D1056G} was selected for re-derivation based on *in silico* analysis as described above. The conservation of the βIV-spectrin-binding domain and the change in size and charge of the side change made this mutation a suitable candidate but unfortunately there was no phenotype observed in these animals. There were subtle trends towards a larger increase in freezing in the cue-dependent memory test, suggesting that these animals could potentially be making a stronger association between the cue and the shock. Only 10 animals and their controls were tested in this battery and it could be that with a higher-powered experiment and larger numbers this effect would be larger. It was also impossible to confirm that the animals could hear the cue in the conditioning trial, and we did not test whether mutant mice responded to the shock with the same burst activity as wild-type mice.

One reason for the lack of phenotype could be that the mutation simply has no effect and *Ank3*$^{D1056G/D1056G}$ mice have no defects in spectrin-binding or localisation of ankyrin$_G$ or channel proteins. There could also be some compensatory effects;

although ankyrin$_B$ (encoded by *Ank2*) is unable to compensate for the loss of ankyrin$_G$ and vice-versa there is some evidence that ankyrin$_R$ (encoded by *Ank1*) can compensate for the loss of ankyrin$_G$ in the PNS (Ho et al., 2014). It could also be that this mutation is present only in some splice isoforms and that others are present enough to compensate. There have been some rare cardiac isoforms identified that do not have the spectrin-binding domain (Yamankurt et al., 2015) so it may be that there is also a diverse population of splice isoforms in the brain allowing *Ank3*$^{D1056G/D1056G}$ mice to survive to adulthood with no defects.

If time and animal space allowed it would be interesting to age these mice to 6 and 12 months and re-test for cognitive and cardiac defects. Due to time constraints, other lines were prioritised as described in chapters 5 and 6.

4 *Tcf4*

4.1 Introduction

The transcription factor *TCF4* is involved in neurodevelopment. As introduced in section 1.8, TCF4 is a helix-loop-helix protein that forms heterodimers and binds E-box motifs to activate gene transcription. Common variants have been associated with schizophrenia and novel mutations were identified in murine *Tcf4* through screening of the ENU-mutagenised archive as described in 1.8.6. Briefly, two non-synonymous mutations were identified in *Tcf4* through screening as described previously (Parsons, unpublished data). Both mutations affect serine residues in a putative serine-rich region, which encompasses residues 181 - 371 (in mouse) in between the nuclear localisation signal (NLS) and transactivational domain 2 (TAD2), and is predicted by PROSITE (Sigrist et al., 2002, Sigrist et al., 2013). $Tcf4^{S189G}$ causes a serine-glycine substitution and $Tcf4^{S275R}$ causes a serine-arginine change.

We hypothesise that these residues may undergo post-translational phosphorylation and that their mutation will cause changes in dimerisation of TCF4 both alone and with heterodimer binding partners. Once prioritised and re-derived animals may show neurodevelopmental defects, potentially including severe psychomotor delay and morphological changes as in Pitt-Hopkins Syndrome. On the other hand, if they are a gain of function we may see defects in sensorimotor gating and fear-conditioned learning. Animals are also likely to have circadian defects if a mutation causes changes in circadian gene expression.

4.2 Results

4.2.1 *In vitro* prioritisation

4.2.1.1 Sequence conservation analysis

Sequences corresponding to mouse *Tcf4* residues 121-360 from vertebrates (mouse, rat, rabbit, human, chimp, gorilla, cat, dog and frog) were aligned using ClustalOmega and sequence conservation was visualised using JalView. From this, we can see that both serine mutations are at highly conserved positions (*Tcf4*^{S189G}: Figure 36A, *Tcf4*^{S275R}: Figure 36B). *Tcf4*^{S189G} causes a serine to glycine change, which decreases the size of the side chain and could cause it to become less polar (Figure 36C). *Tcf4*^{S275R} conversely causes a large increase in the size and charge of the side chain from a serine to arginine, which is positively charged (Figure 36D).

4.2.1.2 Predicted post-translational modification

Both S189 and S275 were predicted to be phosphorylated. The top hit for S189 (when corrected to cut-off) was casein kinase 1 isoform epsilon (CK1ε), which is a ubiquitous kinase that is involved in circadian rhythms. It binds and phosphorylates PER1 and PER2 (Takano et al., 2000), which increases their ubiquitination and degradation. Myotonin dystrophy protein kinase (DMPK) was also predicted to phosphorylate S189. Although the role of this kinase is not well-understood, there are suggestions that it may play a role in synaptic plasticity (Schulz et al., 2003). DUN1 is a damage response protein kinase that is involved in cell cycle checkpoint (Zhao and Rothstein, 2002).

S275 was predicted to be phosphorylated by G-protein coupled receptor kinase 6 (GPRK6), RAF kinase, mammalian Ste20 (MST) kinase and salt-inducible kinase

(SIK)-1 (Table 39). GPRK6 is involved in the acute inflammation response (Kavelaars et al., 2003) while RAF kinase is a MAP kinase kinase kinase (MAP3K) that targets MKK1 and MKK2 proteins (Catling et al., 1995). MST is a regulator of MAPK and is a component of the Hippo pathway, which restrains cell proliferation (Dan et al., 2001, Thompson and Sahai, 2015). PAK4 is another MST kinase, which is implicated in the organisation of the actin cytoskeleton and filopodia formation (Abo et al., 1998). Finally, SIK1 is a sodium-inducible kinase that is involved in regulation of the circadian clock (Jagannath et al., 2013a).

4.2.1.3 Tcf4wt construct requires a binding partner for transcriptional activation

A significant effect of binding partner on luciferase activity was observed on the ability of *Tcf4wt* to activate transcription (Figure 37). In the dual-luciferase reporter assay, $TCF4^{WT}$ construct alone was unable to cause transcriptional activation (normalised to negative control = 1). When transfected with a binding partner, in all cases there was an increase in transcriptional activation (2-way ANOVA with Sidak's test, summarised in Table 37). *Tcf12* co-transfection produced the most increase, and interestingly *Id1* and *Id3* co-transfections also produced an increase in luciferase activation akin to that seen in *Tcf3*, *Clock* and *Bmal1* co-transfections. While the reasons for this are unclear, there were striking and significant differences seen in co-transfections of both mutagenised constructs.

ANOVA table	SS	DF	MS	F (DFn, DFd)	P value
Interaction	21.61	5	4.322	F (5, 60) = 137.7	P<0.0001
Binding Partner	21.61	5	4.322	F (5, 60) = 137.7	P<0.0001
Dimer Type	67.07	1	67.07	F (1, 60) = 2137	P<0.0001
Residual	1.883	60	0.03139		

Table 37 2way ANOVA of TCF4wt homodimer vs heterodimers

4.2.1.4 Tcf4^{S189G} decreases transcriptional activation

When acting alone as a homodimer or with *Tcf4wt* construct, the *Tcf4*^{S189G} construct shows no difference in transcriptional activation (2-way ANOVA with Dunnett's test). When co-transfected with heteromeric binding partners, however, there was a consistent and significant reduction in normalised luciferase activation (Figure 37). This is particularly observed when co-transfected with *Tcf3* or *Tcf12*, two factors predicted to be involved in transcriptional activation. Therefore the *Tcf4*^{S189G} mutation appears to cause defects in heterodimerisation or DNA binding and transcriptional activation.

4.2.1.5 Tcf4^{S275R} shows contrasting effects on homodimerisation and heterodimerisation

When co-transfected with heteromeric binding partners, the *Tcf4*^{S275R} construct showed a significant decrease in transcriptional activation compared to *Tcf4wt*, similar to the effect seen with *Tcf4*^{S189G} (Figure 37). Again, the effect was most pronounced in co-transfections with *Tcf3* and *Tcf12*. Intriguingly, when transfected either alone or with *Tcf4wt* (and therefore presumably acting as a homodimer to activate transcription) *Tcf4*^{S275R} shows a significantly increased transcriptional activation of luciferase (Figure 37).

Based on these *in vitro* results, *Tcf4*^{S275R} was chosen as the mutation to be taken forward and re-derived. We predicted that the increase in activity as a homodimer combined with the decrease in heterodimerisation would produce mice with potential deficits in acoustic startle PPI and fear-conditioned memory.

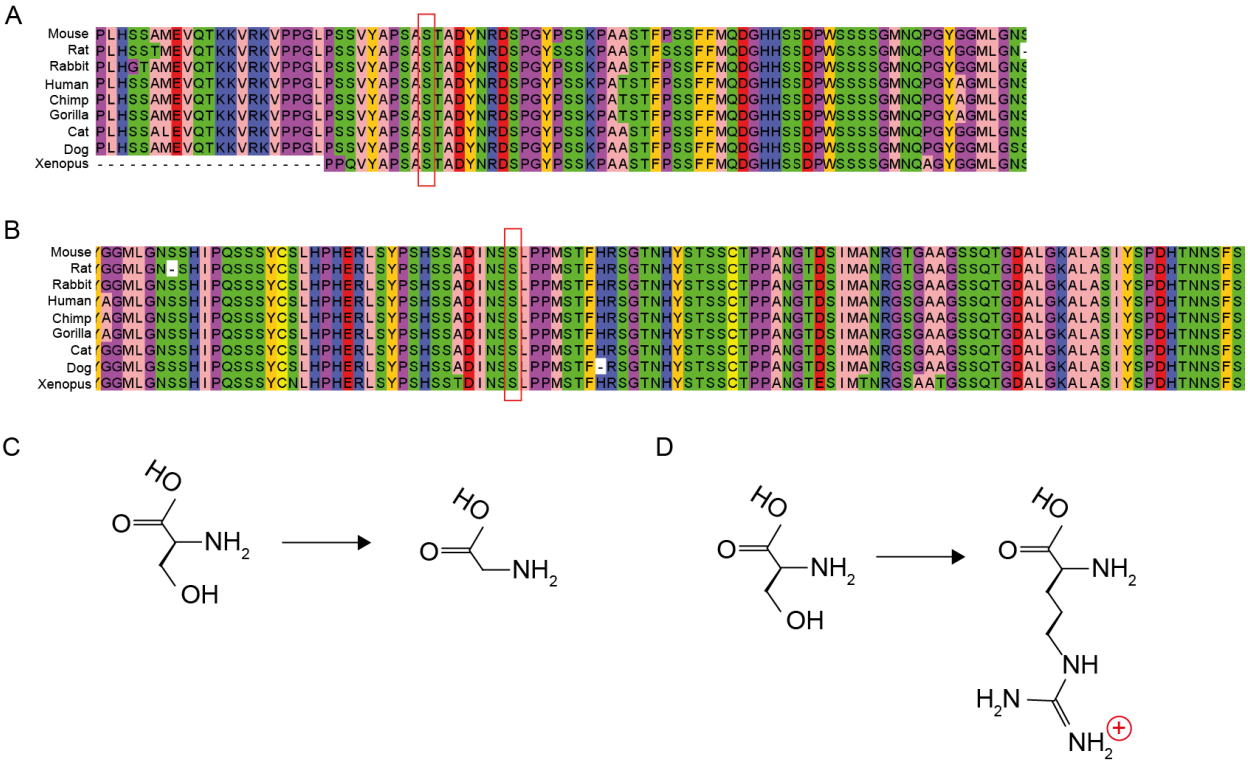

Figure 36 Sequence alignment of TCF4.

(A) Sequence alignment showing conservation of residue S189, (B) sequence alignment showing conservation of residue S275, (C) Skeletal formula of S189 and the ENU-induced change to glycine,(D) skeletal formula of S275R and the resulting arginine.

Position	Kinase	Score	Cutoff	Ratio	FPR
189	CK1/CK1/CK1-D/CK1e	12.176	6.526	1.865768	0.02
189	AGC/DMPK/GEK/DMPK	8	6.088	1.31406	0.02
189	CAMK/RAD53/DUN1	8.333	7.333	1.13637	0.02

Table 38 Phosphorylation predictions for Serine-189

Position	Kinase	Score	Cutoff	Ratio	FPR
275	AGC/GRK/GRK/GPRK6	8.429	3.086	2.731367	0.02
275	TKL/RAF	3.667	2.289	1.60201	0.02
275	STE/STE20/MST	15.026	9.532	1.576374	0.02
275	STE/STE20/PAKB/PAK4	7.667	5.333	1.437652	0.02
275	CAMK/CAMKL/QIK/SIK1	5.312	4.074	1.303878	0.02

Table 39 Phosphorylation predictions for Serine-275

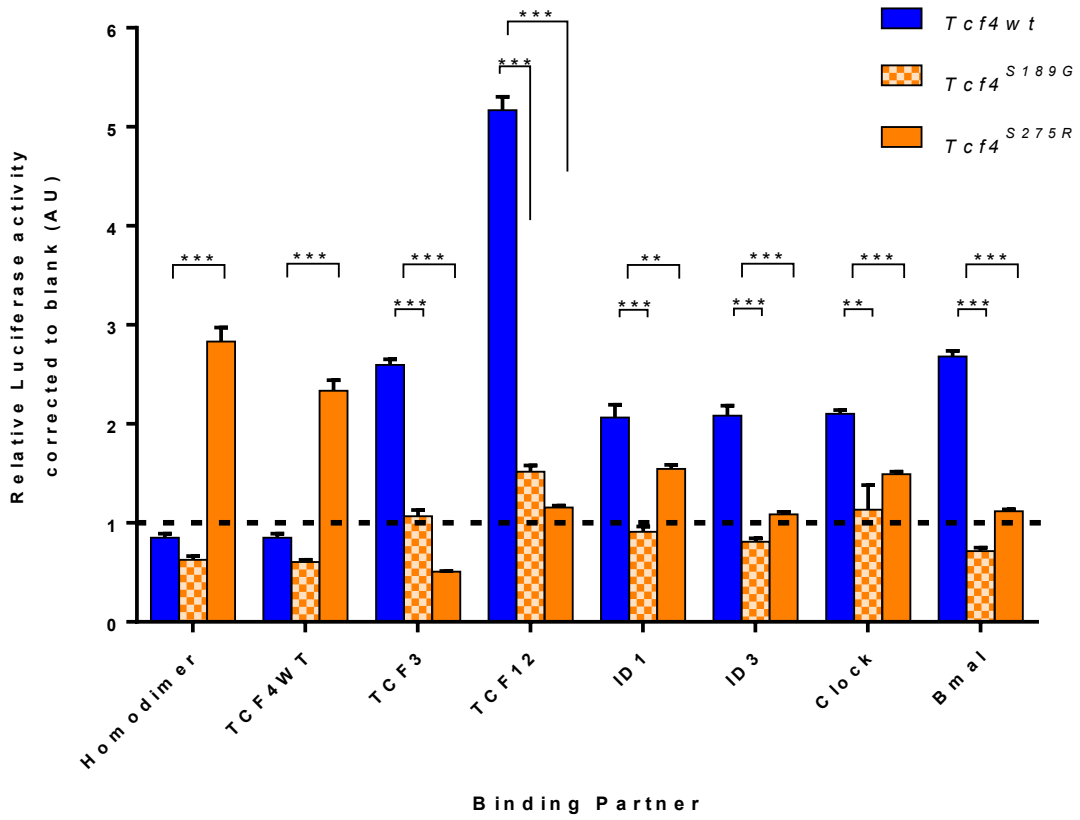

Figure 37 Dual-reporter gene assays show differences in transcriptional activation.

Graph of normalised luciferase activity corrected to the blank (Blank = 1, dotted line). Each binding partner (x-axis) was co-transfected with *Tcf4wt*, *Tcf4*^{S189G}, or *Tcf4*^{S275R} expression construct.

4.2.2 *Tcf4*$^{S275R/S275R}$ mice are viable to adulthood

At post-natal day 21 (P21), offspring from *Tcf4*$^{S275R/+}$ x *Tcf4*$^{S275R/+}$ intercross matings were weaned, biopsied and genotyped. There were 32 WT animals, 46 heterozygous *Tcf4*$^{S275R/+}$ animals and 24 homozygous *Tcf4*$^{S275R/S275R}$ animals recorded (Figure 38A). This is not significantly different to the expected Mendelian ratio (X^2=2.235, ns) (Figure 38B). The homozygous mutation is therefore not lethal, either pre-or post-natally, and appears to have no effect on survival to weaning age. There was no observation of abnormal survival post-weaning.

A

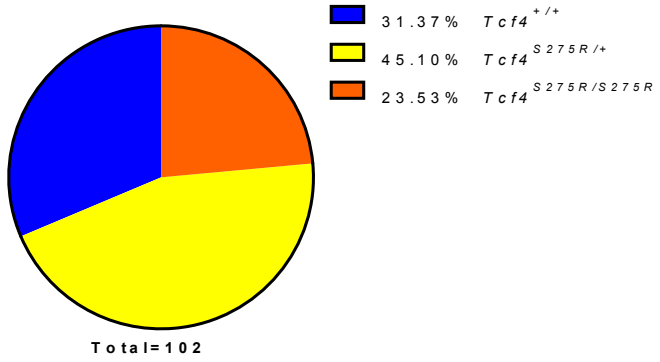

B

Chi-square	2.235
DF	2
P value (two-tailed)	0.3270
P value summary	ns

Figure 38 Survival of homozygous *Tcf4*$^{S275R/S275R}$ mice.

A) Observed genotype percentages at post-natal day 21. B) Chi-squared test

4.2.3 *Tcf4*$^{S275R/S275R}$ mice show no behavioural phenotype

4.2.3.1 SHIRPA

Tcf4$^{S275R/S275R}$ mice showed no obvious morphological or behavioural differences to *Tcf4*$^{+/+}$ animals. They also did not show any differences in transfer arousal or locomotor activity and did not display any limb grasping or trunk curl.

4.2.3.2 Open Field

Over the whole 30-minute trial *Tcf4*$^{S275R/S275R}$ mice showed no differences in duration spent in the centre (M = 60.2s ± 11.7, n=10) compared to *Tcf4*$^{+/+}$ mice (M = 85.9s ± 18.2, n=10), t(18)=1.189, ns (Figure 39A). There was no difference in frequency of entries into the centre between *Tcf4*$^{S275R/S275R}$ (M = 41 ± 7, n=10) and *Tcf4*$^{+/+}$ (M = 47 ± 7, n=10), t(18)=0.6493, ns) (Figure 39B). They also showed no difference in total distance travelled (*Tcf4*$^{S275R/S275R}$ M = 8781cm ± 528.4, n=10; *Tcf4*$^{+/+}$ M = 8823cm ± 516.5, n=10; t(18)=0.05671, ns) (Figure 39C).

4.2.3.3 Acoustic Startle PPI

There was a trend towards an increase in the startle response in *Tcf4*$^{S275R/S275R}$ (679.1 ± 81.3, n=10) compared to WT animals (M = 483.7 ± 65, n=10), t(18)=1.877), p = 0.077 (Figure 39D). There were no significant differences in the pre-pulse inhibition using the 65dB, 70dB, or 75dB pre-pulse (2-way RM ANOVA, Table 40, Figure 39E).

ANOVA table	SS	DF	MS	F (DFn, DFd)	P value
Interaction	102.1	2	51.06	F (2, 36) = 0.6931	P=0.5066
Pre-Pulse	517.6	2	258.8	F (2, 36) = 3.513	P=0.0404
Genotype	338.6	1	338.6	F (1, 18) = 0.3201	P=0.5786
Subjects (matching)	19044	18	1058	F (18, 36) = 14.36	P<0.0001
Residual	2652	36	73.68		

Table 40 2-way RM ANOVA of pre-pulse decibel level interaction with genotype

4.2.3.4 Fear Conditioning

A two-way ANOVA of genotype and time in the conditioning trial showed no differences in the unconditioned response between *Tcf4*$^{+/+}$ and *Tcf4*$^{S275R/S275R}$ mice after the first cue and shock (Table 41, Figure 39F). The ratio of context freezing percentage to baseline percentage showed no difference (*Tcf4*$^{+/+}$ M = 24.02 ± 3.861, n=9;*Tcf4*$^{S275R/S275R}$ M = 17.77 ± 2.81, n=10, t(18) =1.329, ns) (Figure 39G). Analysis

of the baseline freezing in a novel arena and response to cues 1, 2 and 3 in the cue-dependent memory test showed no difference (2-way RM ANOVA, Figure 39H), and there was no interaction between genotype and time (Table 42).

Unconditioned response to the cue appeared to be lower after tone onset (Figure 40A) although there were no effects of genotype (2-way RM ANOVA, Figure 40B).

ANOVA table	SS	DF	MS	F (DFn, DFd)	P value
Interaction	5.232	1	5.232	F (1, 18) = 0.1469	P=0.7060
Time	820.2	1	820.2	F (1, 18) = 23.02	P=0.0001
Genotype	168.4	1	168.4	F (1, 18) = 1.479	P=0.2396
Subjects (matching)	2049	18	113.8	F (18, 18) = 3.195	P=0.0090
Residual	641.2	18	35.62		

Table 41 2-way RM ANOVA measures of unconditioned response to freezing

ANOVA table	SS	DF	MS	F (DFn, DFd)	P value
Interaction	441.1	3	147	F (3, 54) = 1.019	P=0.3913
Time	24585	3	8195	F (3, 54) = 56.83	P<0.0001
Genotype	247.3	1	247.3	F (1, 18) = 0.366	P=0.5528
Subjects (matching)	12165	18	675.8	F (18, 54) = 4.687	P<0.0001
Residual	7787	54	144.2		

Table 42 2-way RM ANOVA of freezing in the cue-dependent test

4.2.3.5 Tcf4$^{S275R/S275R}$ mice do not show any circadian or sleep deficits

Both *Tcf4*$^{+/+}$ and *Tcf4*$^{S275R/S275R}$ female mice entrained to light in 12:12 LD showing that light input and response is intact (Figure 41A). Free-running period in DD (τ_{DD}) showed no difference between *Tcf4*$^{+/+}$ (M = 23.9 ± 0.05375, n=10) and *Tcf4*$^{S275R/S275R}$ (M = 23.87 ± 0.06333, n=10), t(18) = 0.3612, ns (Figure 41B).

In sleep screens, there were no significant differences seen in immobility (as a correlate of sleep) over 24 hours (2-way RM ANOVA, Table 43, Figure 42A), or averaged in the dark and light phase (Table 44, Figure 42B). There were also no differences in activity while the mice were awake shown by distance travelled over 24 hours (Table 45, Figure 42C) and averaged in each phase (Table 46, Figure 42D).

After a light pulse, both *Tcf4*$^{+/+}$ and *Tcf4*$^{S275R/S275R}$ mice showed an increase in immobility (Table 47, Figure 42E). Latency to immobility after the light pulse was also similar between *Tcf4*$^{+/+}$ (722.7 ± 82.43, n=9) and *Tcf4*$^{S275R/S275R}$ (M = 511.6 ± 137.8, n=7), t(14) = 1.382, ns (Figure 42F).

ANOVA table	SS	DF	MS	F (DFn, DFd)	P value
Interaction	10922	23	474.9	F (23, 368) = 0.8868	P=0.6169
Time	214813	23	9340	F (23, 368) = 17.44	**P<0.0001**
Genotype	142.3	1	142.3	F (1, 16) = 0.4387	P=0.5172
Subjects (matching)	5190	16	324.3	F (16, 368) = 0.6057	P=0.8795
Residual	197062	368	535.5		

Table 43 2-way RM ANOVA measures - % Immobility over 24 hours

ANOVA table	SS	DF	MS	F (DFn, DFd)	P value
Interaction	22	1	22	F (1, 16) = 0.6612	P=0.4281
Time	12471	1	12471	F (1, 16) = 374.8	**P<0.0001**
Genotype	11.87	1	11.87	F (1, 16) = 0.4392	P=0.5169
Subjects (matching)	432.5	16	27.03	F (16, 16) = 0.8124	P=0.6586
Residual	532.4	16	33.28		

Table 44 2-way RM ANOVA measures - % Immobility in Dark and Light phase

ANOVA table	SS	DF	MS	F (DFn, DFd)	P value
Interaction	8666	23	376.8	F (23, 368) = 0.2625	P=0.9998
Time	523271	23	22751	F (23, 368) = 15.85	**P<0.0001**
Genotype	3212	1	3212	F (1, 16) = 0.2646	P=0.6140
Subjects (matching)	194283	16	12143	F (16, 368) = 8.46	**P<0.0001**
Residual	528194	368	1435		

Table 45 2-way RM ANOVA measures - Distance travelled over 24 hours

ANOVA table	SS	DF	MS	F (DFn, DFd)	P value
Interaction	93.9	1	93.9	F (1, 16) = 0.1156	P=0.7383
Time	27783	1	27783	F (1, 16) = 34.2	**P<0.0001**
Genotype	267.6	1	267.6	F (1, 16) = 0.2645	P=0.6141
Subjects (matching)	16190	16	1012	F (16, 16) = 1.246	P=0.3328
Residual	12996	16	812.3		

Table 46 2-way RM ANOVA measures – Distance travelled in Dark and Light phase

ANOVA table	SS	DF	MS	F (DFn, DFd)	P value
Interaction	11861	20	593	F (20, 260) = 1.166	P=0.2845
Time	173163	20	8658	F (20, 260) = 17.02	**P<0.0001**
Column Factor	259.9	1	259.9	F (1, 13) = 0.2292	P=0.6401
Subjects (matching)	14739	13	1134	F (13, 260) = 2.228	**P=0.0089**
Residual	132285	260	508.8		

Table 47 2-way RM ANOVA measures – % Immobility after LP2

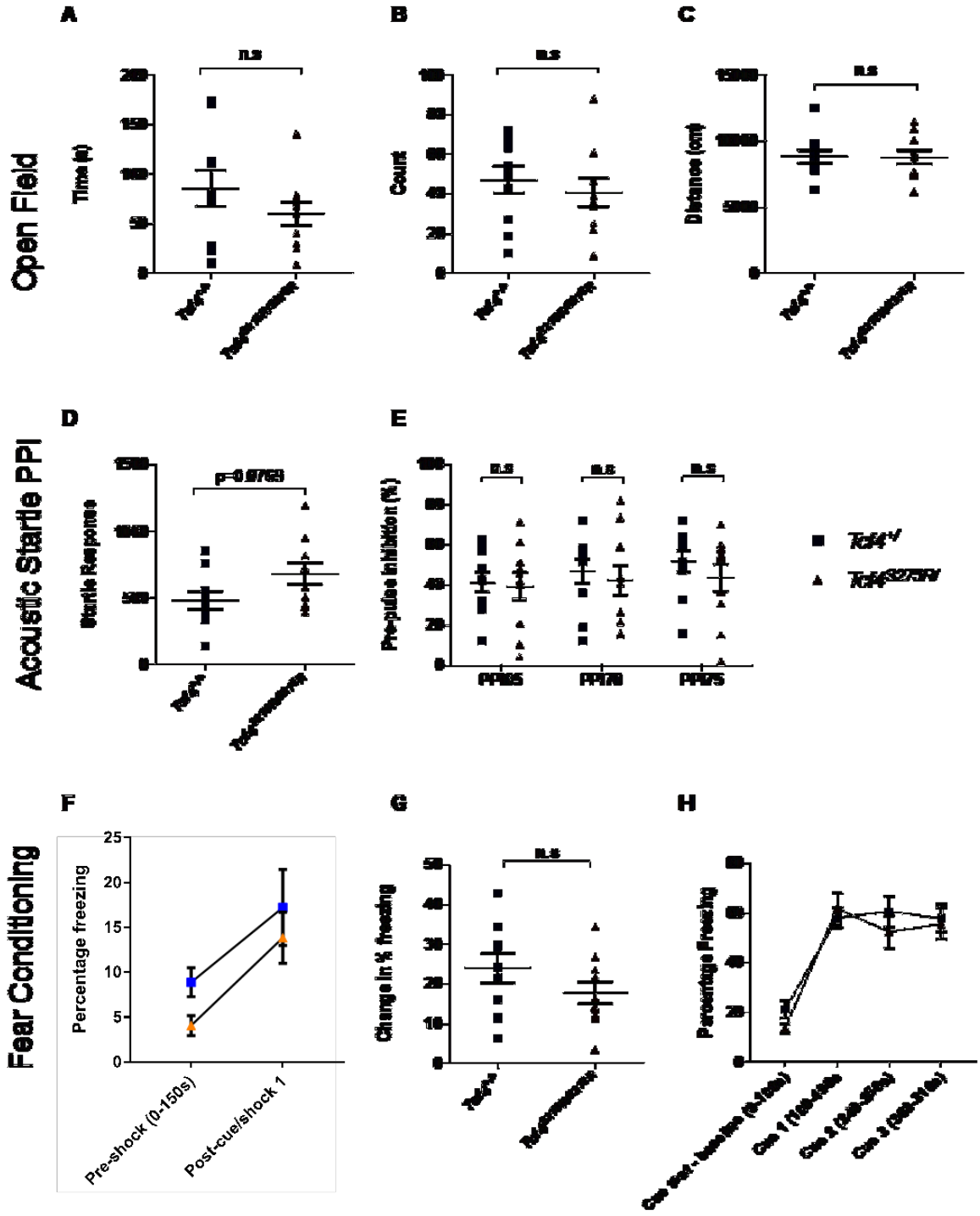

Figure 39 Behavioural Phenotyping of *Tcf4*$^{S275R/S275R}$ mice.

Open Field: (A) Time spent in the centre; (B) Frequency of entries into the centre; (C) Total distance travelled. Acoustic startle PPI: (D) Startle response; (E) pre-pulse inhibition over three tests. Fear conditioning: (F) Unconditioned freezing response in the conditioning trial pre-shock and post-first cue/shock; (G) Difference in

percentage freezing between baseline and context test; (H) Percentage freezing at baseline in a novel environment and after three cues in the cue-dependent test.

A

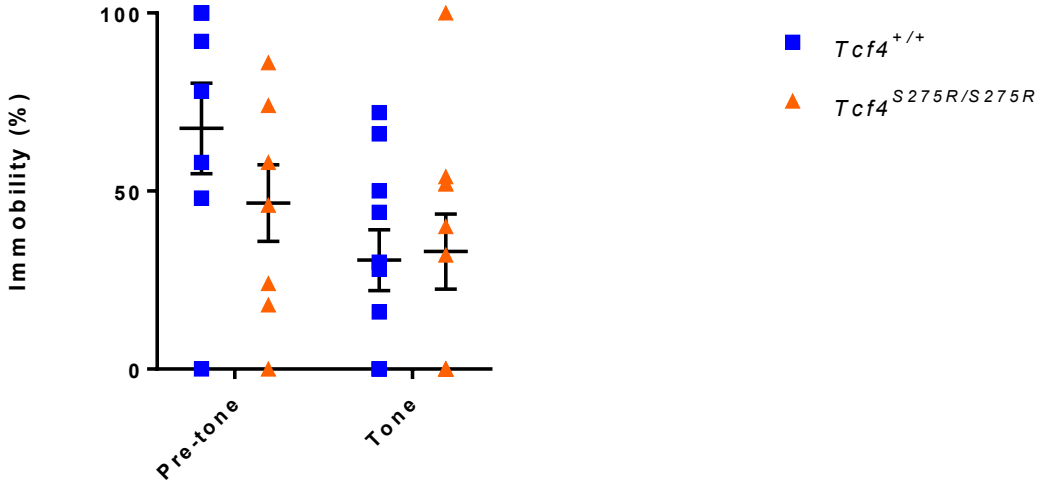

B

Source of Variation	% of total variation	P value	P value summary
Interaction	2.728	0.1119	ns
Time	12.76	0.0020	**
Genotype	1.724	0.4991	ns
Subjects (matching)	65.22	0.0040	**

Figure 40 Unconditioned response to the cue.

(A) Percentage of time spent immobile in the 5 seconds pre-tone and post-tone onset in the conditioning session. (B) 2-way RM ANOVA

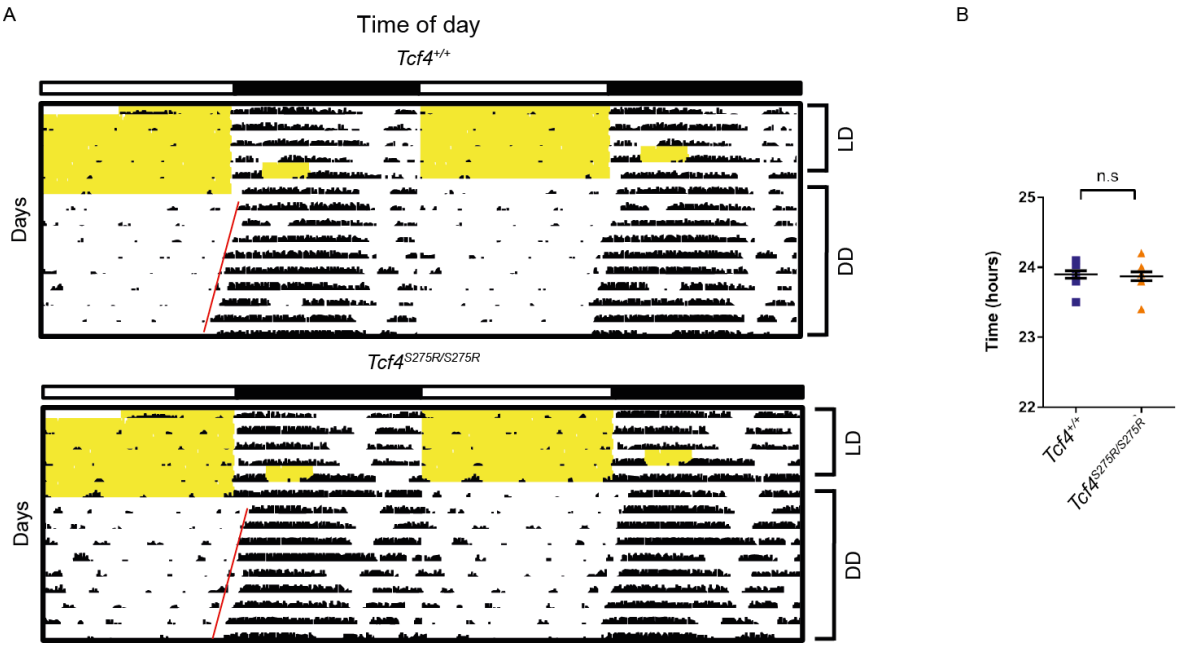

Figure 41 *Tcf4*$^{S275R/S275R}$ mice show no change in circadian period or rhythmicity.

(A) Representative actograms showing activity in 12:12LD and DD with light periods indicated by yellow boxes. *Tcf4*+/+ (top) and *Tcf4*$^{S275R/S275R}$ (bottom) mice entrain to light in LD. In DD, circadian period (tau) is depicted by a red line fitted to activity onsets on successive days and is the same in both cohorts. (B) Tau_{DD} is unchanged in *Tcf4*$^{S275R/S275R}$.

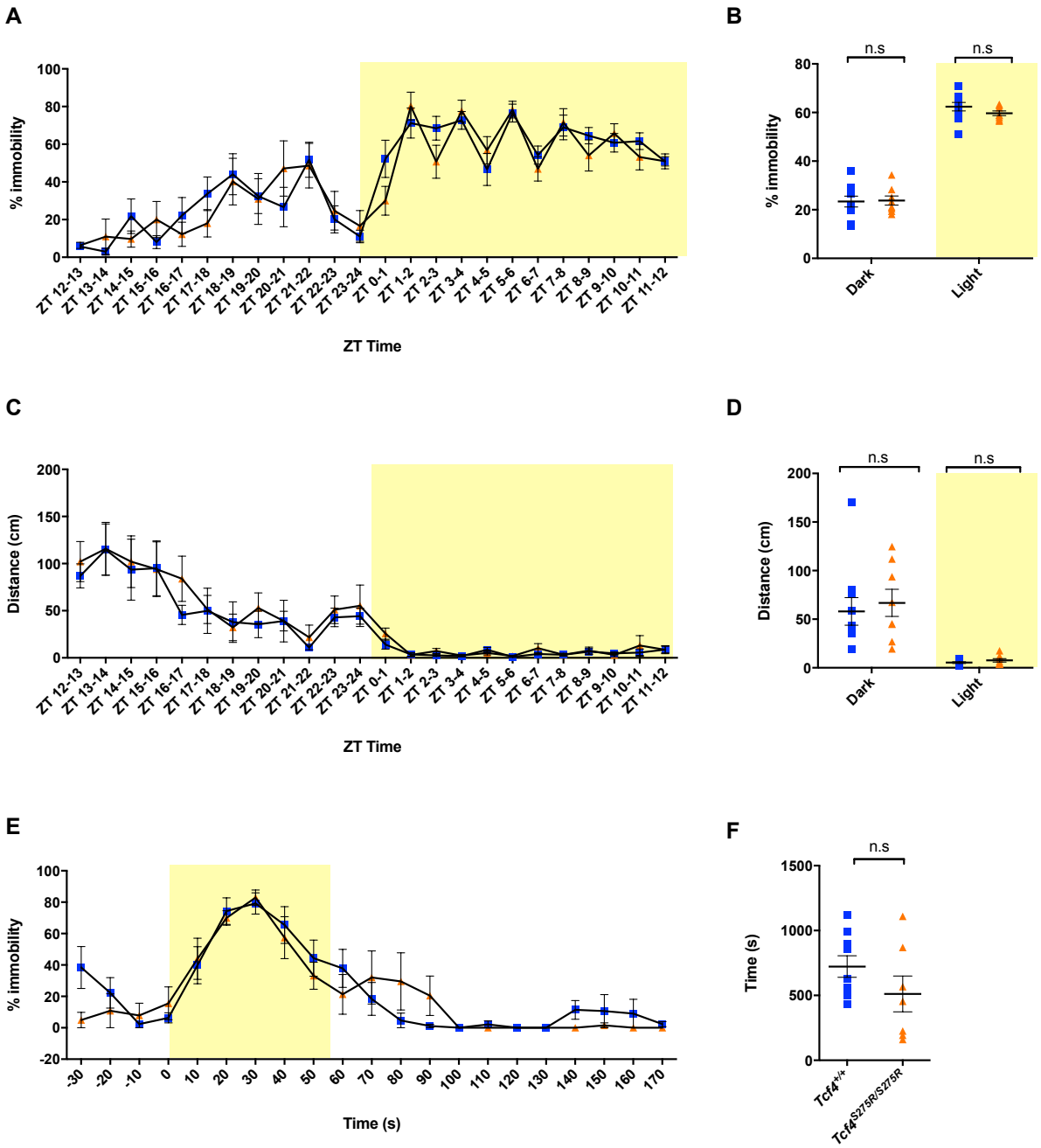

Figure 42 S *Tcf4*$^{S275R/S275R}$ mice show no differences in sleep screens.

(A) Percentage immobility over 24 hours, (B) Average hourly immobility in the dark and the light phase, (C) total distance travelled over 24 hours, (D) Average hourly distance travelled in the dark and the light phase,(E) percentage immobility during a light pulse (LP2) at ZT14, (F) Latency to immobility after onset of LP2.

4.3 Discussion

Mutations in *TCF4* have been associated with multiple neurodevelopmental disorders. Pitt-Hopkins Syndrome is caused by deletions and mutations that cause haploinsufficiency (Amiel et al., 2007, Zweier et al., 2007) while common variants have been associated with schizophrenia as detailed above. The causative effect of these common variants is still unclear, so *Tcf4* was chosen as a candidate gene for screening in the ENU archive. Two mutations, both of serine residues in the serine-rich region of *Tcf4*, were identified.

Little is known about the serine-rich region of TCF4. It is likely that it is post-translationally modified; serine residues can be phosphorylated (Prabakaran et al., 2012) which allows greater proteomic diversity. The region could, therefore, be involved in facilitating binding and transactivation. The prediction programme GPS3.0 produced a readout of kinases, which potentially phosphorylate S189 and S275.

Kinases predicted to phosphorylate S189 are involved in circadian rhythms, cell cycle checkpoint regulation and potentially synaptic plasticity, whereas S275 predictions included cell cycle regulators such as RAF and MST. S275 was also predicted to be phosphorylated by GPRK6 (an inflammatory response protein). This supports results of previous enrichment analyses and microarray analysis of TCF4 knockdown in cells that suggested a role for TCF4 in the inflammasome (Forrest et al., 2013). SIK1 is another kinase implicated in the regulation of circadian rhythms through negative feedback of CREB-regulated transcription coactivator 1 (CRTC1) (Jagannath et al., 2013a) and *de novo* mutations in SIK1 have been linked to developmental epilepsy (Hansen et al., 2015), suggesting that it may play a role in neurodevelopment. These predictions support the roles of TCF4 in the immune

system (Bergqvist et al., 2000), neurodevelopment (Flora et al., 2007, Ge et al., 2006), and circadian rhythm gene expression (Mullegama et al., 2014). TCF4 is expressed ubiquitously, and these kinases are likely to act in a tissue- or cell-specific manner to increase the proteomic diversity of TCF4 function (Johnson, 2009, Prabakaran et al., 2012). We did not test whether these residues are phosphorylated *in vitro* or *in vivo*. If the *Tcf4*^{S189G} mutation were derived, tissues or homogenates from different tissues could be examined for evidence of phosphorylation changes. Alongside this, an *in vitro* approach could also use the mutagenised *Tcf4* plasmid constructs, transfected alongside each predicted kinase in cell culture. We hypothesise that, due to the loss of the serine side chain in both mutants, there would be a loss of phosphorylation and this could lead to changes in transcriptional activation or dimerisation. In the case of *Tcf4*^{S275R}, we found that the mutation did not cause any significant behavioural phenotypes. Another approach to studying phosphorylation would be to mutate one or both serine residues, *in vivo* or *in vitro*, to a phosphomimetic residue such as aspartic acid or glutamic acid. The large negatively charged side chains of these residues are thought to mimic long-term phosphorylation of the residue (Maciejewski et al., 1995, Dissmeyer and Schnittger, 2011).

Changes in transcriptional activation were observed when the *Tcf4*^{S275R} construct was transfected *in vitro* but no *in vivo* phenotype was observed. This could be because the mutation is simply not drastic enough to cause any changes to the binding and transactivation in the mouse. Another explanation could be that the endogenous expression of genes in the cell line (HEK293T) somehow interfered with the expression of the plasmids *in vitro*; these cells contain the SV40 T antigen which promotes S-phase entry and cell division (Ahuja et al., 2005) which could somehow

perturb TCF4 (which promotes G_1 phase as described in 1.8.3). HEK293T cells also contain multiple copies of the genome and endogenous expression of TCF4 or its binding partners could have an effect, although we would expect this to be the same in all samples. This could have exacerbated a small effect of the mutation, leading to a false positive. It has also been shown that *in vitro* dimerisation is less efficient than *in vivo* (Goldfarb et al., 1998) and this could be reflected in the lack of phenotype.

In order to validate the mutations further, it would have been useful to study expression *in vitro* using immunohistochemistry or immunoblotting. This was attempted using a TCF4-B antibody (kindly provided by Dr Spengler, Max Planck Institute, Germany). Unfortunately, in our hands this antibody was unsuccessful and due to time constraints re-derivation went ahead. With more available time it would be interesting to re-derive and characterise the *Tcf4*^{S189G} mutation.

As in the case of *Ank3*^{D1056G}, it would have been interesting to age this cohort of *Tcf4*$^{S275/S275R}$ mice and examine their phenotype at a later stage but, due to time constraints, other lines were prioritised.

5 *Cacna1c*^{Q1625STOP}

5.1 Introduction

CACNA1C encodes $Ca_v1.2$, an α_1 subunit of the post-synaptic voltage-dependent calcium channel expressed in the brain and heart. $Ca_v1.2$ is responsible for the voltage-dependence, calcium specificity, and calcium-dependent inactivation of the channel, mediated by cytoplasmic N- and C-terminal domains and four transmembrane pore-forming regions.

The Harwell ENU-mutagenised archive was screened for mutations in *Cacna1c* and this identified *Cacna1c*^{Q1625STOP}, which causes a premature stop codon to replace the glutamine residue Q1625 (Figure 18). This is the 'Q' residue of the IQ motif in mouse $Ca_v1.2$ (ENSMUST00000078320) as described in 1.9.13.1.

As described previously, studies have indicated that truncations cause degradation of the protein and therefore we hypothesise that this mutation could cause loss of function and perinatal lethality when this allele is homozygous. As discussed in 1.9.14, we hypothesise that we will recapitulate endophenotypes observed in *Cacna1c* knock-out models, as well as potentially identifying sleep deficits.



Figure 43 The IQ Domain and *Cacna1c*^{Q1625STOP} mutation.

This causes a premature truncation at a glutamic acid residue.

5.2 Results

5.2.1 *Cacna1c*$^{Q1625STOP/Q1625STOP}$ animals die before weaning

At P21, offspring from *Cacna1c*$^{Q1625STOP/+}$ x *Cacna1c*$^{Q1625STOP/+}$ intercrosses were biopsied and genotyped. 66 wild-type and 139 heterozygous animals were identified, but no homozygous animals were alive at this time point (Figure 44A). This significantly differed from the expected Mendelian ratio (X^2 = 68.49, $p < 0.0001$) (Figure 44B). Timed matings dissected at 9.5dpc identified 3 wild-type, 5 *Cacna1c*$^{Q1625STOP/+}$, and 7 *Cacna1c*$^{Q1625STOP/Q1625STOP}$ animals (Figure 44C) which was not significantly different from the expected Mendelian ratio (X^2 = 3.8, ns) (Figure 44D). Further timed mates at 14.5dpc also identified 5 wild-type, 17 *Cacna1c*$^{Q1625STOP/+}$, and 7 *Cacna1c*$^{Q1625STOP/Q1625STOP}$ animals (X^2 = 1.138, ns) (Figure 44E-F). Therefore we predicted that homozygous lethality occurred between 14.5dpc and birth. Subsequently, behavioural phenotyping was carried out on wild-type and heterozygous animals only.

5.2.2 *Cacna1c*$^{Q1625STOP/+}$ animals show behavioural phenotypes

5.2.2.1 SHIRPA

SHIRPA was used to assess obvious morphological and behavioural characteristics as described in 2.2.1. *Cacna1c*$^{Q1625STOP/+}$ animals did not show any gross morphological differences to wild-type controls. They also did not display any differences in transfer arousal or gait and showed no evidence of trunk curl or limb grasping. Although locomotor activity over 30 seconds appeared to be reduced in *Cacna1c*$^{Q1625STOP/+}$ mice (Figure 45) this was not significant (*Cacna1c*$^{+/+}$ M = 15 ± 2, n=6; *Cacna1c*$^{Q1625STOP/+}$ 20 ± 1, n=6, t(10)=1.733, ns), probably due to low numbers and therefore low power in this test.

5.2.2.2 Open Field

Open Field was used as a primary test of locomotor activity and anxiety. Over the total 30 minutes, *Cacna1c*$^{Q1625STOP/+}$ mice spent more time in the periphery (M = 1565.2s ± 79.1, n=6) than *Cacna1c*$^{+/+}$ littermates (M = 1265.3s ± 103.6, n=6) t(10)= 2.301, $p < 0.05$ (Figure 46A). They also showed fewer entries into the periphery from the intermediate arena (*Cacna1c*$^{Q1625STOP/+}$ M = 97 ± 24, n=6; *Cacna1c*$^{+/+}$ M = 222 ± 28, n=6) t(10)= 3.382, $p < 0.01$ (Figure 46B). Total distance travelled was decreased in *Cacna1c*$^{Q1625STOP/+}$ (M = 6718cm ± 674.8, n=6) compared to *Cacna1c*$^{+/+}$ (M = 11170cm ± 453, n=6) t(10)=5.477, $p < 0.001$ (Figure 46C). To separate the effects on exploratory behaviour and anxiety, results were separated into the first 5-minute time bin (to study exploratory behaviour) and the remaining 25 minutes (to study anxiety).

5.2.2.3 Cacna1c$^{Q1625STOP/+}$ *animals show decreased exploratory behaviour*

From the start of the test to the end of the first 5-minute time bin, *Cacna1c*$^{Q1625STOP/+}$ animals had shorter path lengths, shown by fewer entries into the periphery (*Cacna1c*$^{Q1625STOP/+}$ M = 17 ± 4, n=6; *Cacna1c*$^{+/+}$ M = 43 ± 6, n=6) t(10)= 3.7, $p < 0.01$ (Figure 46E) although the difference in time spent in the periphery did not reach significance (M = 263.9s ± 12.5, n=6; M = 229.9s ± 16.1, n=6), t(10)= 1.671, ns (Figure 46D). During this time bin they also travelled less (*Cacna1c*$^{Q1625STOP/+}$ M = 1041cm ± 95.36, n=6; *Cacna1c*$^{+/+}$ M = 1885cm ± 201.4, n=6), t(10)=3.787, $p < 0.01$ (Figure 46F).

5.2.2.4 Cacna1c$^{Q1625STOP/+}$ *animals show increased anxiety*

In the remaining 25 minutes of the test, *Cacna1c*$^{Q1625STOP/+}$ animals continued to spend more time in the periphery (M = 1035.3s ± 58.3, n=6) compared to *Cacna1c*$^{+/+}$ (M = 834.5s ± 62.3, n=6) t(10)= 2.352, $p < 0.05$ (Figure 46G); entries into the periphery from the intermediate area were less frequent (*Cacna1c*$^{Q1625STOP/+}$ M = 67 ±

17, n=6; *Cacna1c*$^{+/+}$ M = 147 ± 17, n=6) t(10)= 3.31, p < 0.01 (Figure 46H); they also continued to travel less over the whole arena (*Cacna1c*$^{Q1625STOP/+}$ M = 455cm ± 479.9, n=6; *Cacna1c*$^{+/+}$ M = 7115cm ± 327.2, n=6) t(10)= 4.58, p = 0.0010 (Figure 46I).

In order to validate the anxiety phenotype a secondary cohort was put through Light-dark box and Elevated Nought Maze, as described in 2.3.

5.2.2.5 Light-Dark Box

When tested in Light-Dark box, *Cacna1c*$^{Q1625STOP/+}$ animals did not show a significant difference in time spent in light (*Cacna1c*$^{Q1625STOP/+}$ M = 40.5s ± 8.8, n=21; *Cacna1c*$^{+/+}$ = 56.6s ± 6.5, n=20) t(39)= 1.46, ns; or time in the dark (*Cacna1c*$^{Q1625STOP/+}$ M = 247.3s ± 11.5, n=21; *Cacna1c*$^{+/+}$ M = 224.9s ± 8.2, n=20) t(39)= 1.57, ns (Figure 47A). *Cacna1c*$^{Q1625STOP/+}$ also had an increased latency to light entry, and some heterozygous animals did not enter the light area at all during the test (Mann-Whitney non-parametric t-test, p < 0.05)(Figure 47B).

5.2.2.6 Elevated Nought Maze

Cacna1c$^{Q1625STOP/+}$ animals spent more time in the closed area (*Cacna1c*$^{Q1625STOP/+}$ M = 198.4s ± 8.1, n=21; *Cacna1c*$^{+/+}$ = 164.1s ± 7.5, n=21) t(40)= 3.10632, p < 0.01) and less time in the open area (*Cacna1c*$^{Q1625STOP/+}$ M = 101.7s ± 8.1, n=21; *Cacna1c*$^{+/+}$ M = 135.7s ± 7674, n=21) t(40)= 3.05736, p < 0.01 (Figure 47C). This test also validated the lower distance travelled by *Cacna1c*$^{Q1625STOP/+}$ mice (*Cacna1c*$^{Q1625STOP/+}$ M = 1274cm ± 83.79, n=21; *Cacna1c*$^{+/+}$ M = 1554cm ± 97.64, n=20) t(39)=2.183, p < 0.05 (Figure 47D).

A

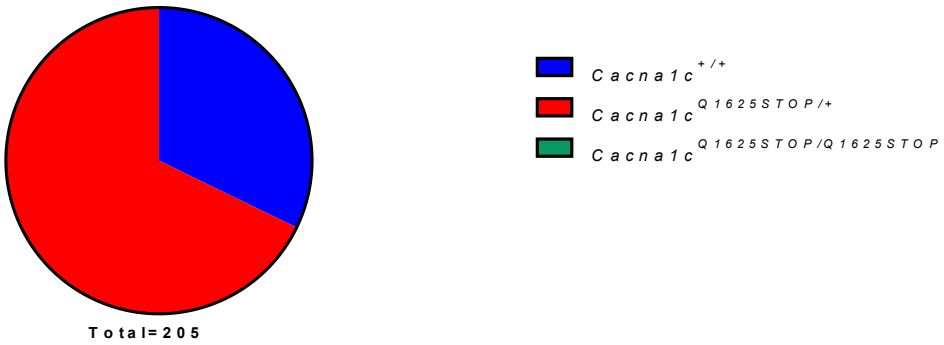

B

Chi-square test	
Chi-square	68.49
DF	2
P value (two-tailed)	<0.0001
P value summary	****

C

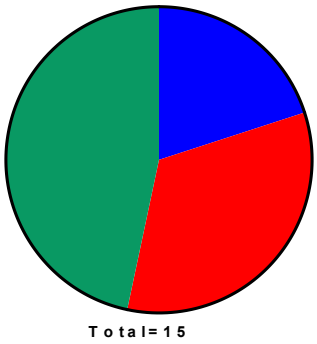

D

Chi-square test	
Chi-square	3.8
DF	2
P value (two-tailed)	0.1496
P value summary	ns

E

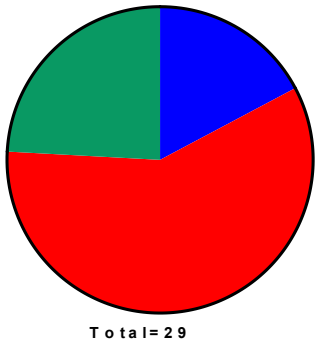

F

Chi-square test	
Chi-square	1.138
DF	2
P value (two-tailed)	0.5661
P value summary	ns

Figure 44 Homozygous *Cacna1c*$^{Q1625STOP/Q1625STOP}$ mice do not survive to weaning.

(A) At P21 no homozygotes were observed and this was significantly different to expected Mendelian ratio (B). (C) At 9.5dpc all three genotypes were observed, (D) Chi-squared test. (E) At 14.5dpc all three genotypes were observed, (F) Chi-squared test

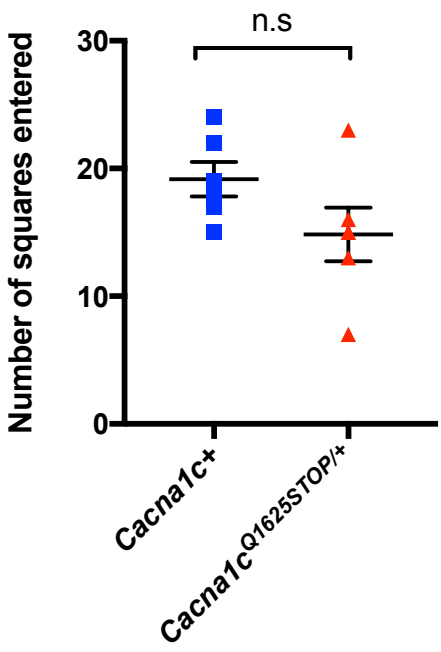

Figure 45 Locomotor activity in the SHIRPA test.

Number of squares entered in 30s.

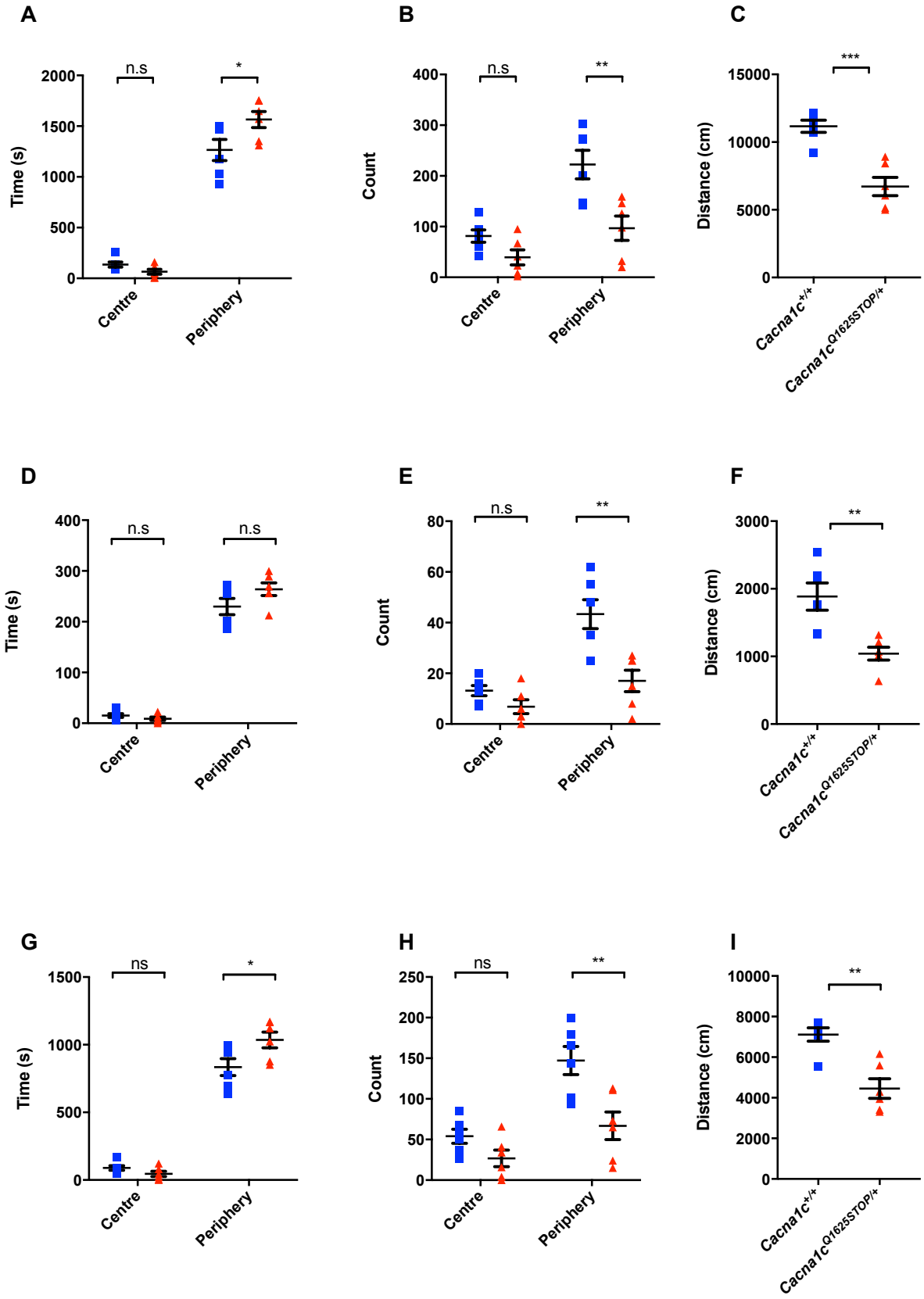
A
B
C
D
E
F
G
H
I
Time (s)
Count
Distance (cm)
n.s
ns
*
**
***
Centre
Periphery
Cacna1c+/+
Cacna1cQ1625STOP/+

Figure 46 *Cacna1c*$^{Q1625STOP/+}$ animals have increased anxiety and reduced exploratory behaviour.

(A)Time spent in centre and periphery over 30 minutes, (B) frequency of entries into centre and periphery from intermediate arena over 30 minutes, (C) total distance travelled in the whole arena over 30 minutes. (D)Time spent in centre and periphery over the first 5 minutes, (E) frequency of entries into centre and periphery from the intermediate arena in the first 5 minutes, (F) total distance travelled in the whole arena in the first five minutes. (G)Time spent in centre and periphery in the remaining 25 minutes, (H) frequency of entries into centre and periphery from the intermediate arena in the remaining 25 minutes, (I) total distance travelled in the whole arena in the remaining 25 minutes.

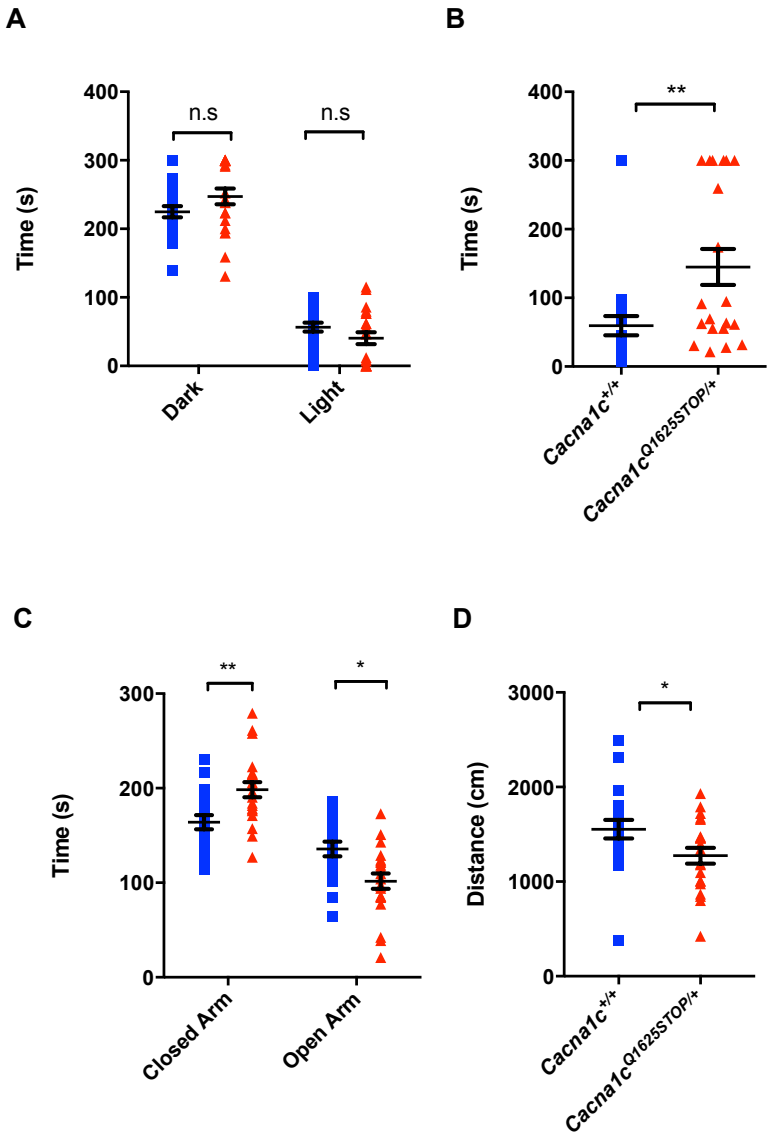

Figure 47 Light-Dark Box and Elevated Nought Maze validate the anxiety phenotype

(A) Time spent in dark or light area of the Light-Dark box over 5 minutes, (B) Latency to entry into the light area, (C) Time spent in the closed or open arms of the elevated nought maze over 5 minutes, (D) Total distance travelled in the whole maze over 5 minutes.

5.2.2.7 Acoustic Startle PPI

Cacna1c$^{Q1625STOP/+}$ mice displayed a mildly reduced startle response (M = 313.4 ± 21.38, n=20) compared to *Cacna1c*$^{+/+}$ (M = 420.8 ± 42.41, n=17), t(35)=2.367, p < 0.05 (Figure 48A). We considered that this may be due to a difference in weight but *Cacna1c*$^{Q1625STOP/+}$ animals (M=27.6g ± 0.9, n=21) showed no difference compared to *Cacna1c*$^{++}$ animals (M=27.0 ± 0.9, n=20) t(39)= t=0.5233, ns (Figure 48C). They did not show any significant changes in pre-pulse inhibition when corrected for multiple testing (Figure 48B, Table 48).

ANOVA table	SS	DF	MS	F (DFn, DFd)	P value
Interaction	200.7	2	100.4	F (2, 64) = 1.131	P=0.3289
Pre-Pulse	1094	2	547	F (2, 64) = 6.166	P=0.0036
Genotype	724.9	1	724.9	F (1, 32) = 1.024	P=0.3192
Subjects (matching)	22655	32	708	F (32, 64) = 7.98	P<0.0001
Residual	5678	64	88.71		

Table 48 2-way RM ANOVA of pre-pulse decibel level interaction with genotype

5.2.2.8 Fear Conditioning

On the first day of testing, all mice tested froze more after the conditioning tones and shocks (Figure 49A) but a 2-way ANOVA showed that there was significant variation between genotypes as well as by time (Figure 49B). When separated into pre-shock and post-shock by genotype, the pre-shock freezing is similar between genotypes but post-shocks *Cacna1c*$^{Q1625STOP/+}$ mice have a higher freezing percentage (M = 65.219 ± 3.42, n=14) compared to *Cacna1c*$^{+/+}$ (M = 47.967 ± 5.14,

n=14), t(26)= 2.796, p < 0.01 (Figure 49C). *Cacna1c*$^{Q1625STOP/+}$ mice had a higher unconditioned response to the first cue and shock (Figure 49D, 2-way RM ANOVA).

On the second day of testing, *Cacna1c*$^{Q1625STOP/+}$ mice froze more in context testing (corrected to baseline; M = 42.29 ± 4.538, n=14) compared to *Cacna1c*$^{+/+}$ (M = 18.99 ± 3.053, n=13) t(25)=4.193, p < 0.001 (Figure 49E). In the cue-dependent test on day 3, there was a significant effect of genotype but no interaction between genotype and time (2-way RM ANOVA, Table 49) and after corrections for multiple testing only one time-point was significant (Figure 49F).

The unconditioned response to cue, similar to previous tests described, did not show that animals could definitely hear the cue. Both *Cacna1*$^{Q1625STOP/+}$ and wild-type mice were immobile for less time after the tone onset (Figure 50A). This did not differ significantly by genotype (2-way RM ANOVA, Figure 50B).

ANOVA table	SS	DF	MS	F (DFn, DFd)	P value
Interaction	597.8	3	199.3	F (3, 78) = 0.6278	P=0.5992
Time	9019	3	3006	F (3, 78) = 9.471	P<0.0001
Genotype	8250	1	8250	F (1, 26) = 11.34	P=0.0024
Subjects (matching)	18910	26	727.3	F (26, 78) = 2.291	P=0.0027
Residual	24759	78	317.4		

Table 49 2-way RM ANOVA of freezing in the cue-dependent test

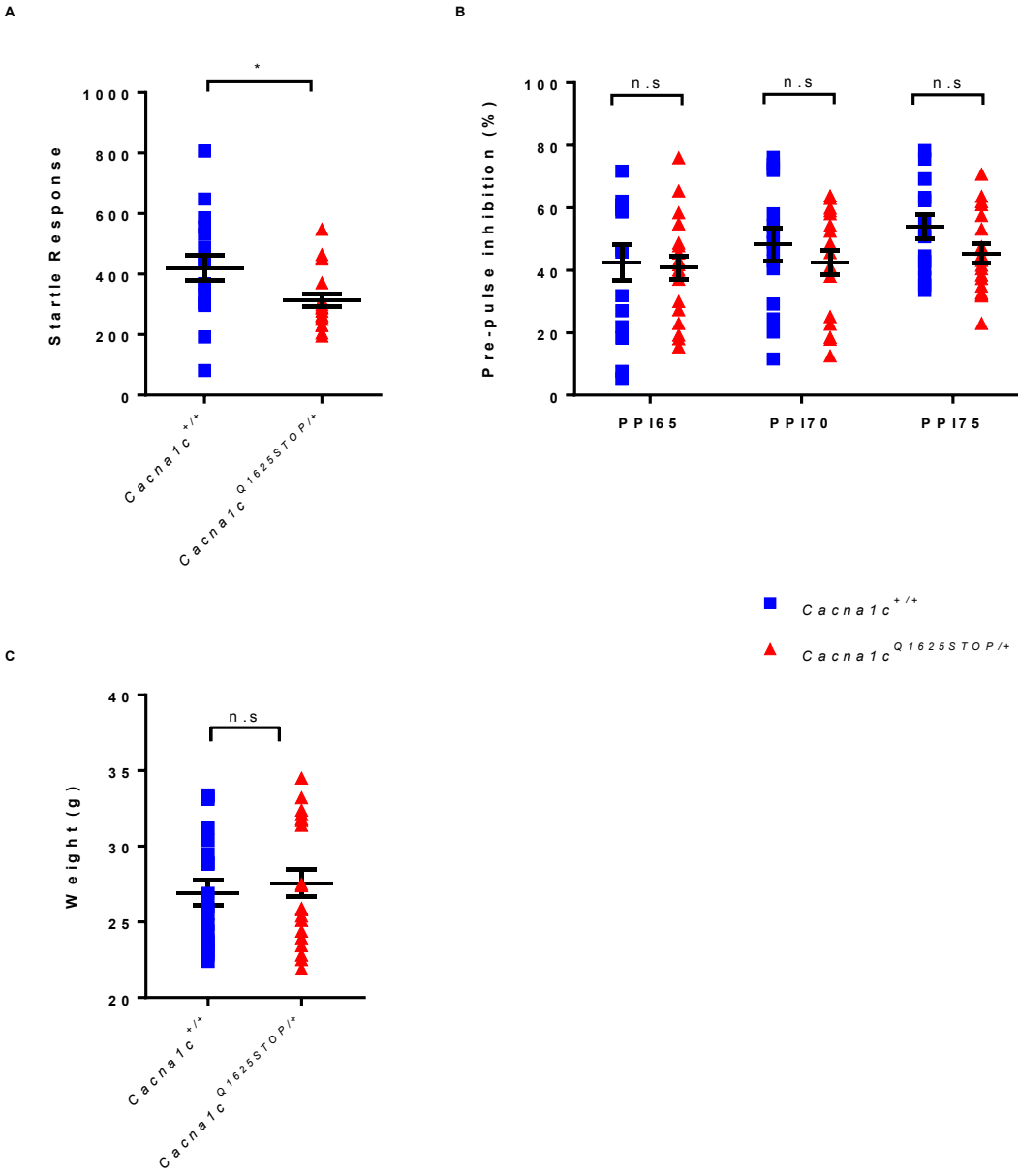

Figure 48 *Cacna1c*$^{Q1625STOP/+}$ animals show mild changes in startle response.

(A) Startle Response, (B) the percentage pre-pulse inhibition caused by pre-pulses of 65, 70 and 75 dB, (C) Body weights of the cohort.

A

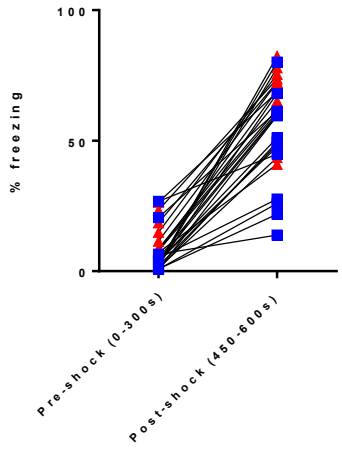

B

Source of Variation	% of total variation	P value	P value summary
Interaction	1.362	0.0518	ns
Time	75.41	<0.0001	****
Genotype	3.68	0.0067	**
Subjects (matching)	11.02	0.2587	ns

ANOVA table	SS	DF	MS	F (DFn, DFd)	P value
Interaction	596.3	1	596.3	F (1, 26) = 4.154	P=0.0518
Time	33006	1	33006	F (1, 26) = 229.9	P<0.0001
Genotype	1611	1	1611	F (1, 26) = 8.68	P=0.0067
Subjects (matching)	4825	26	185.6	F (26, 26) = 1.293	P=0.2587

C

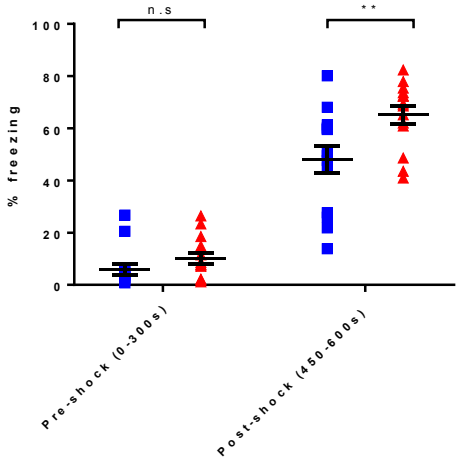

D

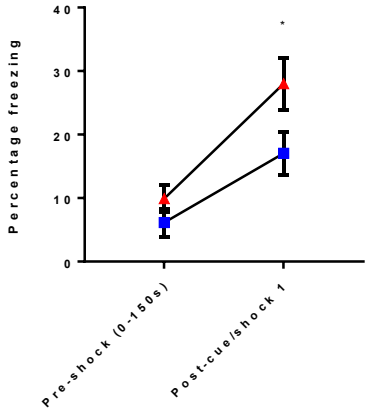

E

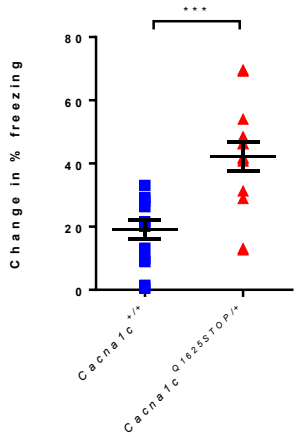

F

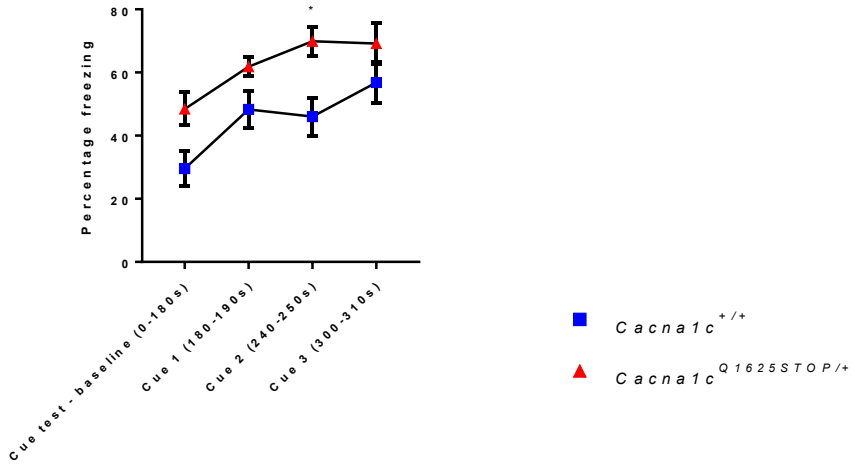

Figure 49 *Cacna1c*$^{Q1625STOP/+}$ mice show differences in freezing.

(A) Percentage freezing before any shocks and after three shocks on the first day of testing, (B) 2-way RM ANOVA table showing variation by genotype as well as time, (C) Percentage freezing before shocks and after shocks separated by genotype, (D) The unconditioned response to the first cue and shock, (E) Change in percentage freezing between conditioning baseline and context-dependent testing on day 2, (F) Percentage freezing at baseline and after three cues on day 3.

A

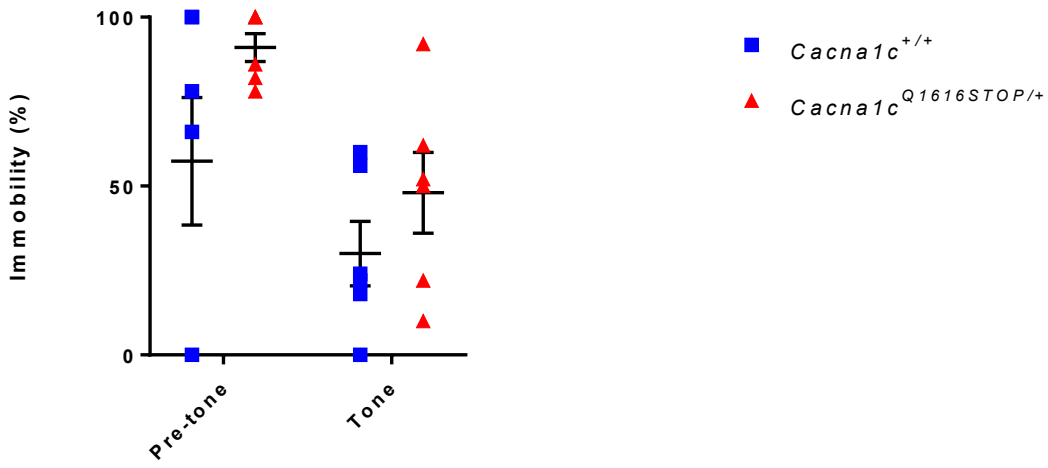

B

Source of Variation	% of total variation	P value	P value summary
Interaction	1.226	0.5338	ns
Time	24.72	0.0160	*
Genotype	13.34	0.0655	ns
Subjects (matching)	31.18	0.4665	ns

Figure 50 Unconditioned response to the cue.

(A) Percentage of time spent immobile in the 5 seconds pre-tone and post-tone onset in the conditioning session. (B) 2-way RM ANOVA

5.2.2.9 Cacna1c$^{Q1625STOP/+}$ *mice do not have any heart defects*

In an echocardiogram, *Cacna1c*$^{Q1625STOP/+}$ mice did not show any differences in thickness of the left ventricular posterior wall (Figure 51A), anterior wall (Figure 51B), interior diameter of the left ventricle (Figure 51C) or interior diameter (Figure 51D).

Means, SEM and t values are summarised in Table 50. This was not taken further due to the absence of phenotype. Mice were aged to one year and *Cacna1c*$^{Q1625STOP/+}$ animals lived as long as littermate controls with no deaths due to heart problems in aged mice.

		***Cacna1cQ1625STOP/+* n=6 M±SEM**	***Cacna1c+/+*n=5 M±SEM**	**df**	**t**	**p**
Left Ventricular Posterior Wall Thickness	Diastole	0.73 ± 0.027	0.84 ± 0.05	9	1.908	n.s
mm	Systole	1.01 ± 0.05	1.23 ± 0.11	9	1.874	n.s
Left Ventricular Anterior Wall Thickness	Diastole	0.81 ± 0.05	0.94 ± 0.08	9	1.475	n.s
mm	Systole	1.14 ± 0.07	1.33 ± 0.09	9	1.671	n.s
Left Ventricular Interior Diameter	Diastole	4.09 ± 0.17	4.41 ± 0.17	9	1.304	n.s
mm	Systole	3.17 ± 0.18	3.13 ± 0.19	9	0.139	n.s
Left Ventricular Volume	Diastole	74.83 ± 7.59	88.95 ±8.01	9	1.275	n.s
µl	Systole	41.00 ± 5.81	39.73 ± 5.85	9	0.153	n.s
Fractional Shortening		22.82 ± 1.694	28.92 ± 3.665	9	1.604	n.s

Table 50 Summary of echocardiogram data showing no changes in any parameters

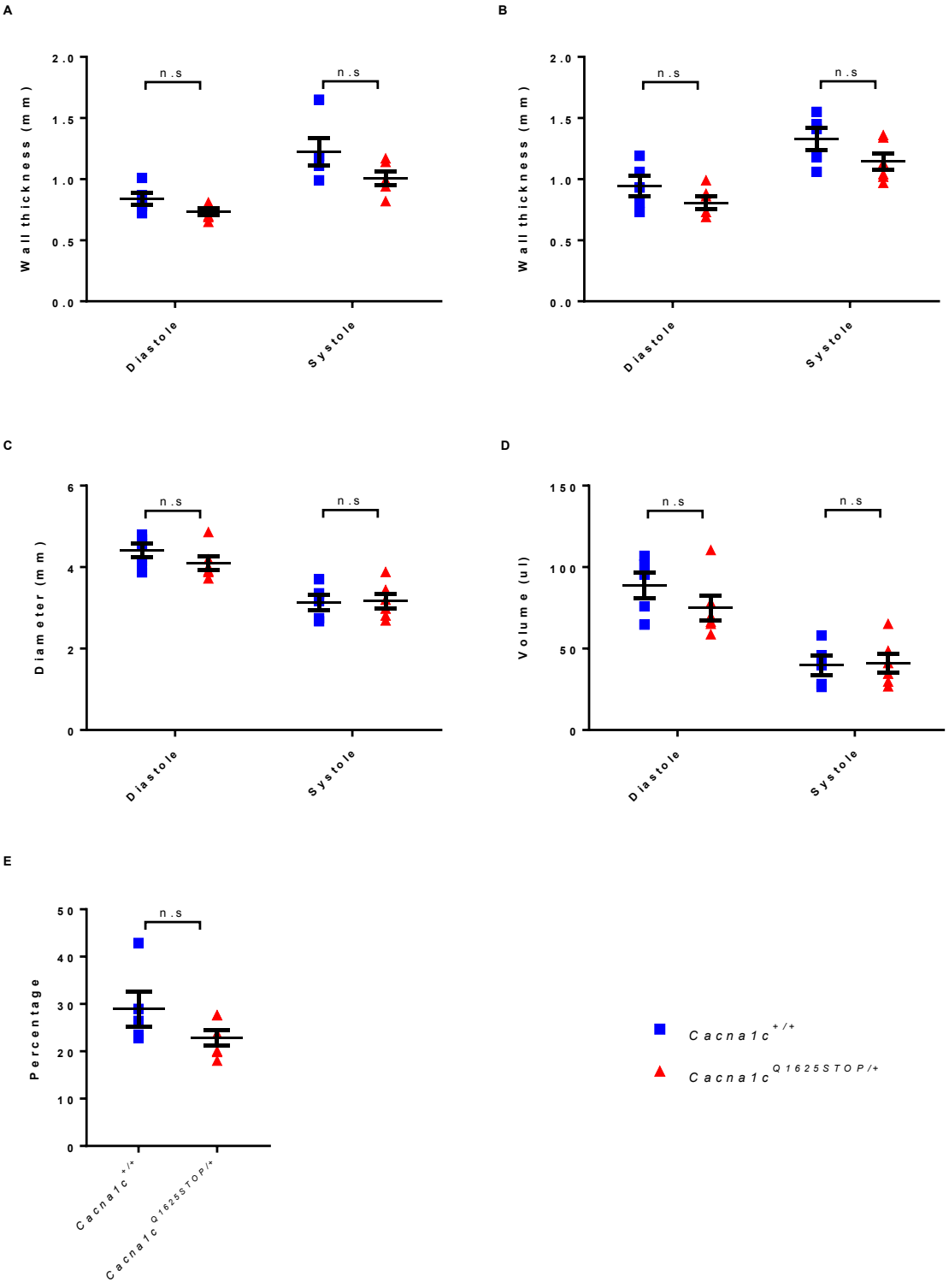

Figure 51 The *Cacna1c*^{Q1625STOP} mutation does not cause defects in heart function.

No differences were seen in (A) thickness of left ventricular posterior wall, (B) thickness of left anterior wall, (C) ventricular interior diameter, or (D) left ventricular volume. Correspondingly there was no difference in fractional shortening (E).

5.2.3 Circadian Rhythms and Sleep in *Cacna1c*$^{1625STOP/+}$ mice

5.2.3.1 Cacna1c$^{1625STOP/+}$ *mice show no differences in circadian period*

Cacna1c$^{1625STOP/+}$ female mice entrained to light in 12:12 LD (Figure 52A), showing that light input and response are normal. There was also no difference in free-running period in DD between *Cacna1c*$^{1625STOP/+}$ (M = 23.86 ± 0.02278, n=10) and *Cacna1c*$^{+/+}$ (M = 23.84 ± 0.05488, n=9) t(17)=0.3865, ns (Figure 52B).

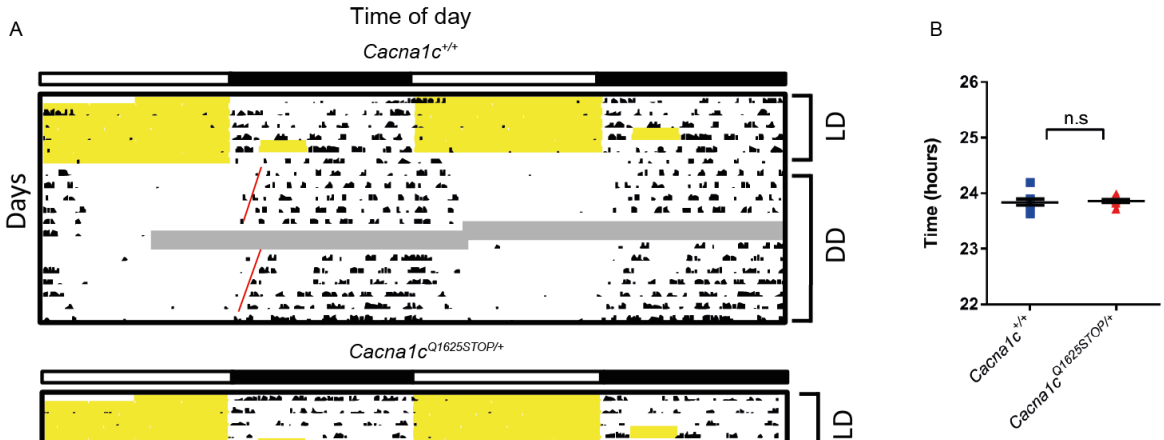

Figure 52 *Cacna1c*$^{Q1625STOP/+}$ mice show no difference in circadian period.

(A) Representative actograms from *Cacna1c*$^{+/+}$ (top) and *Cacna1c*$^{Q1625STOP/+}$ (bottom) mice showing activity in 12:12LD and DD with light periods indicated by yellow boxes. In DD, circadian period (tau) is depicted by a red line fitted to activity onsets on successive days and is the same in both cohorts. Grey bars indicate a period where there was a problem with the power supply so analysis does not include this time. (B) Tau_{DD} is unchanged in *Cacna1c*$^{Q1625STOP/+}$ mice.

5.2.3.2 Cacna1c$^{1625STOP/+}$ *mice show minor differences in mobility in the video-tracking Sleep Screen*

Female mice were singly housed and video-tracked as described in 2.2.6. *Cacna1c*$^{1625STOP/+}$ animals showed no difference in immobility over 24 hours (2way

RM ANOVA, Table 51, Figure 53A) or when averaged in the light and dark phase (Table 52, Figure 53B). At one time point in the dark phase between ZT17-18, *Cacna1c*$^{1625STOP/+}$ mice travelled less distance (M = 4.984 ± 1.418, n=8) than *Cacna1c*$^{+/+}$ (M = 19.38 ± 4.933, n=8) (Figure 53C) although this did not survive multiple testing (Table 53) and was not shown when averaged in dark and light (Table 54, Figure 53D). During a light pulse at ZT14, *Cacna1c*$^{1625STOP/+}$ showed a trend towards increased immobility compared to *Cacna1c*$^{+/+}$ although this is due to the *Cacna1c*$^{+/+}$ mice having a lower immobility than usually observed in wild-type animals during a light pulse (Figure 53E, Table 55). *Cacna1c*$^{Q1625STOP/+}$ animals showed no differences in latency to immobility after the light pulse (*Cacna1c*$^{Q1625STOP/+}$ M = 301.3 ± 144, n=8, *Cacna1c*$^{+/+}$ M = 475.6 ± 266.9, n=8, t(14) =0.5745, ns) (Figure 53F).

ANOVA table	SS	DF	MS	F (DFn, DFd)	P value
Interaction	6134	23	266.7	F (23, 322) = 0.6025	P=0.9267
Time	133416	23	5801	F (23, 322) = 13.1	P<0.0001
Genotype	193.7	1	193.7	F (1, 14) = 0.449	P=0.5137
Subjects (matching)	6038	14	431.3	F (14, 322) = 0.9744	P=0.4794
Residual	142531	322	442.6		

Table 51 2-way RM ANOVA measures - % Immobility over 24 hours

ANOVA table	SS	DF	MS	F (DFn, DFd)	P value
Interaction	6.364	1	6.364	F (1, 14) = 0.09185	P=0.7663
Time	7911	1	7911	F (1, 14) = 114.2	P<0.0001
Genotype	16.15	1	16.15	F (1, 14) = 0.4491	P=0.5137
Subjects (matching)	503.3	14	35.95	F (14, 14) = 0.5189	P=0.8840
Residual	970	14	69.28		

Table 52 2-way RM ANOVA measures - % Immobility in Dark and Light phase

ANOVA table	SS	DF	MS	F (DFn, DFd)	P value
Interaction	1424	23	61.93	F (23, 322) = 0.6507	P=0.8910
Time	26600	23	1157	F (23, 322) = 12.15	P<0.0001
Genotype	33.08	1	33.08	F (1, 14) = 0.06818	P=0.7978
Subjects (matching)	6792	14	485.1	F (14, 322) = 5.098	P<0.0001
Residual	30645	322	95.17		

Table 53 2-way RM ANOVA measures - Distance travelled over 24 hours

ANOVA table	SS	DF	MS	F (DFn, DFd)	P value
Interaction	0.0004	1	0.0004	F (1, 14) = 0	P=0.9974
Time	1381	1	1381	F (1, 14) = 39.63	P<0.0001
Genotype	2.744	1	2.744	F (1, 14) = 0.06786	P=0.7983
Subjects (matching)	566	14	40.43	F (14, 14) = 1.16	P=0.3924
Residual	487.8	14	34.84		

Table 54 2-way RM ANOVA measures – Distance travelled in Dark and Light phase

ANOVA table	SS	DF	MS	F (DFn, DFd)	P value
Interaction	31288	20	1564	F (20, 280) = 1.495	P=0.0819
Time	133430	20	6671	F (20, 280) = 6.375	P<0.0001
Genotype	1977	1	1977	F (1, 14) = 1.108	P=0.3104
Subjects (matching)	24993	14	1785	F (14, 280) = 1.706	P=0.0540
Residual	293029	280	1047		

Table 55 2-way RM ANOVA measures – % Immobility after LP2

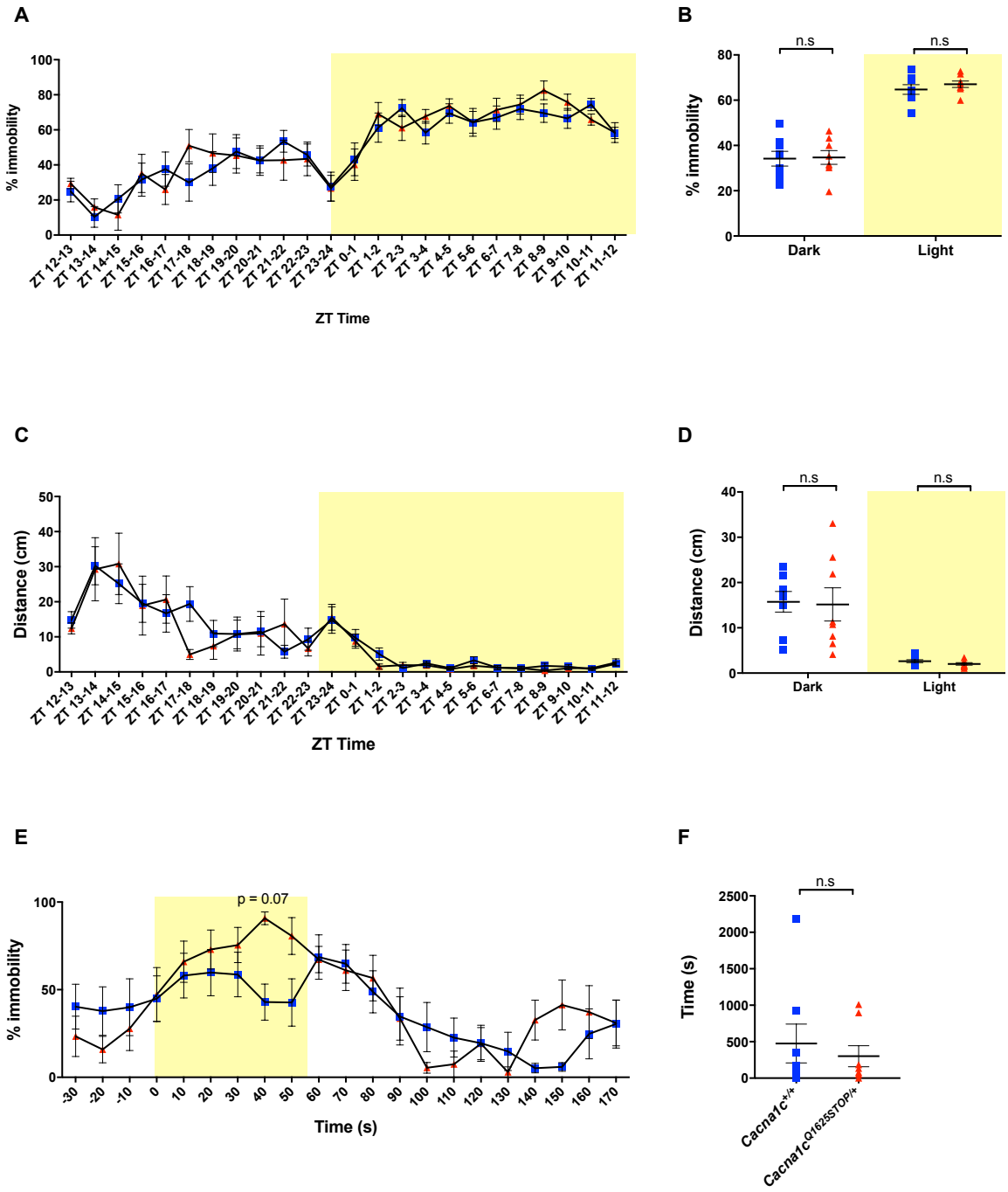

Figure 53 Minor differences in immobility revealed by a video-tracked Sleep Screen.

(A) Percentage immobility over 24 hours, (B)) Average hourly immobility in the dark and the light phase, (C) total distance travelled over 24 hours, (D) Average hourly distance travelled averaged in the dark and the light phase,(E) percentage immobility during a light pulse at ZT14, (F) Latency to immobility after onset of LP2

5.2.3.3 EEG recordings show a reduction in sleep pressure in *Cacna1c*$^{Q1625STOP/+}$ mice

In recordings of total sleep time per 2-hour time bins, *Cacna1c*$^{Q1625STOP/+}$ showed a trend to a higher amount of sleep at hour 22 (in the dark phase) and a lower amount of sleep at hour 14 after sleep deprivation; after correction for multiple testing, however, these differences were not significant (Figure 54A). Power spectra of total sleep in the light phase (Figure 54B), dark phase (Figure 54C) and after sleep deprivation (SD) (Figure 54D) showed a significant reduction of delta frequencies (0.1-3Hz) in *Cacna1c*$^{Q1625STOP/+}$ mice. This was due to a reduction in delta frequencies during NREM sleep (Figure 54E-G: light, dark, post-SD). In REM sleep (Figure 54H-J: light, dark, post-SD) there were no changes in delta frequencies but after sleep deprivation, there was a small reduction in theta frequencies (6-10Hz)(Figure 54J).

Delta power (a measure of sleep pressure) in NREM sleep was lower in *Cacna1c*$^{Q1625STOP/+}$ mice compared to *Cacna1c*$^{+/+}$ mice in both baseline and recovery post-SD recordings (two-way RM ANOVA; $p < 0.05$) (Figure 55A). After four hours SD, *Cacna1c*$^{+/+}$ mice showed a significant increase of delta power as expected, meaning that their sleep pressure had increased. Conversely *Cacna1c*$^{Q1625STOP/+}$ mice showed an attenuated delta power rebound. This is also shown by comparing delta power in the last hour of baseline (pre-SD) to delta power in the first hour of recovery (post-SD): *Cacna1c*$^{+/+}$ animals show a significant increase in delta power after SD ($M_1 = 1.501 \pm 0.1742$, n=7; $M_2 = 2.419 \pm 0.135$, n=7; $t(12)=4.162$, $p < 0.01$) whereas *Cacna1c*$^{Q1625STOP/+}$ show no difference ($M_1 = 1.35 \pm 0.1611$, n=8; $M_2 = 1.637 \pm 0.2102$, n=8; $t(14)=1.082$, ns)(Figure 55B).

These findings show that *Cacna1c*$^{Q1625STOP/+}$ mice have impaired sleep homoeostasis due to a reduction in delta frequencies during NREM sleep, both at baseline and following sleep deprivation, and therefore decreased sleep pressure. However, they do still sleep for the same amount of time as *Cacna1c*$^{+/+}$ animals, suggesting that there is a compensatory mechanism (for example the circadian machinery, which is intact) steering them towards a normal 12:12 sleep:wake cycle.

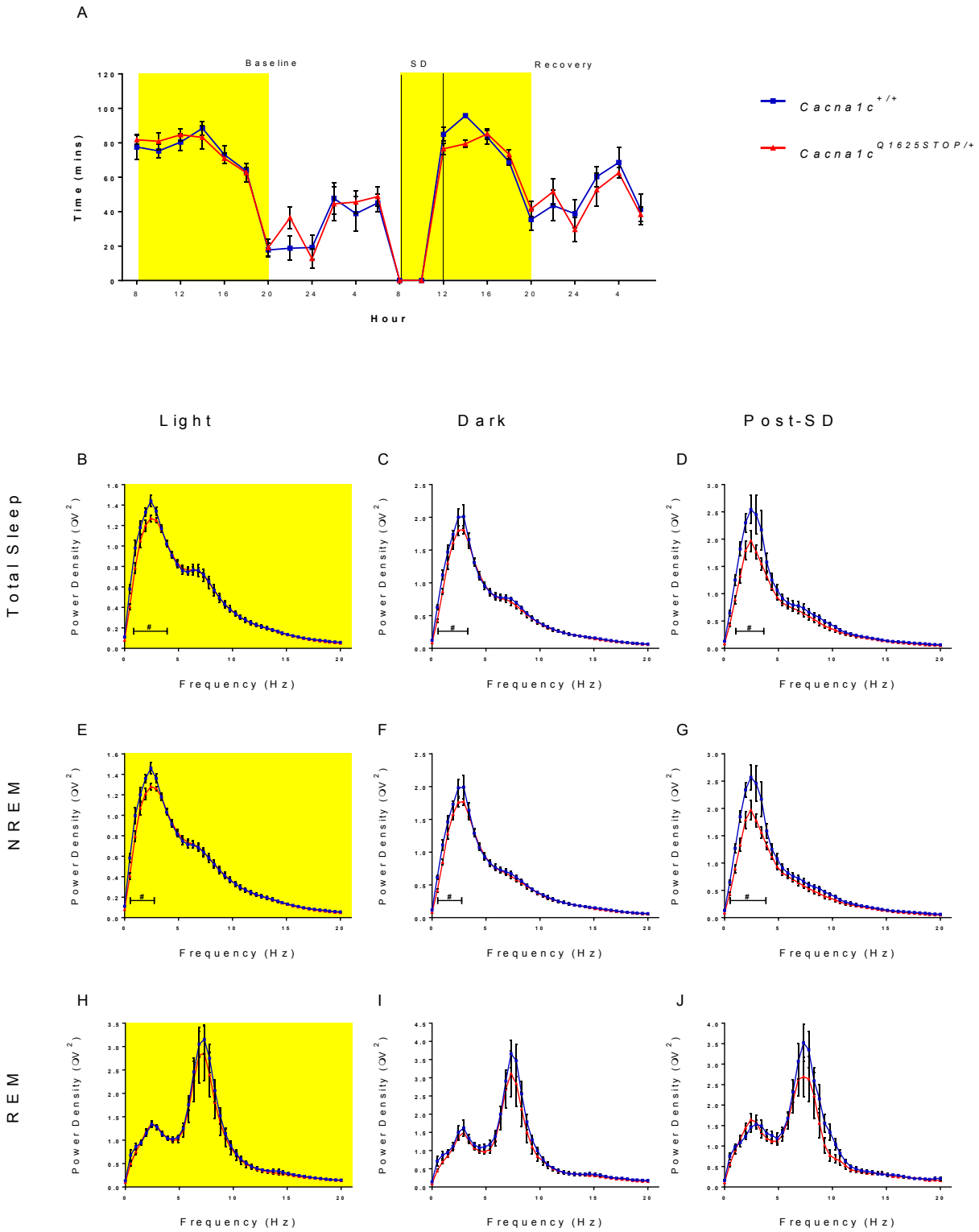

Figure 54 EEG Recordings show a reduction in delta frequencies in *Cacna1c*$^{Q1625STOP/+}$ mice.

(A) Total sleep during baseline light and dark, sleep deprivation (SD) and recovery. Total sleep power spectra during: (B) Light, (C) Dark, (D) after SD; NREM power spectra during: (E) Light, (F) Dark, (G) after SD; REM

power spectra during: (H) Light, (I) Dark, (J) after SD; Significance is indicated by # and lines indicate multiple significant points $p < 0.05$ (2-way RM ANOVA)

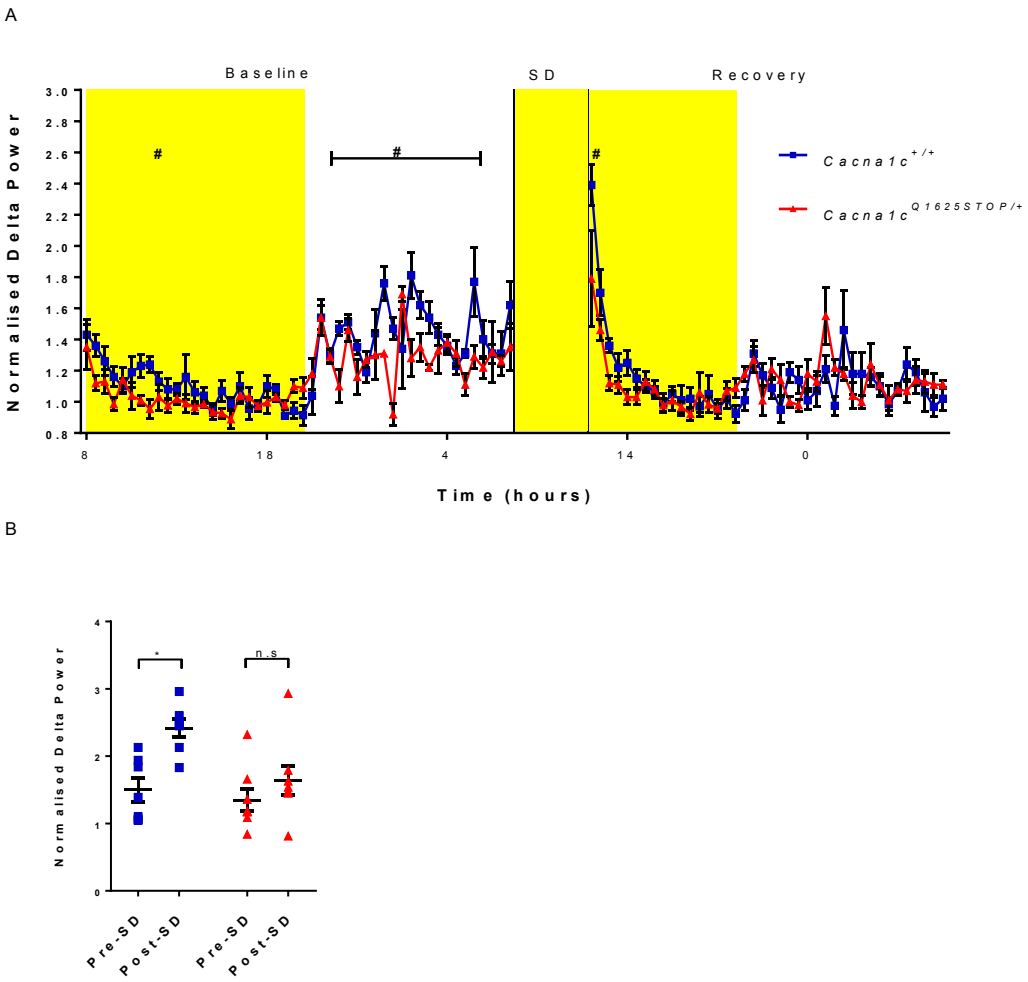

Figure 55 Delta power is decreased in *Cacna1c*$^{Q1625STOP/+}$ mice.

(A) Time course showing delta power normalised to baseline split into 30-min time bins during light and dark, and during recovery after sleep deprivation, (B) Normalised delta power in the final 30 minutes before SD and the first 30 minutes after SD. In (A) Significance is indicated by # and lines indicate multiple significant points $p < 0.05$ (2-way RM ANOVA)

5.3 Discussion

To give us new insights into the function of $Ca_v1.2$ and how it acts as a risk gene for schizophrenia and bipolar disorder, we generated and analysed *Cacna1c*$^{Q1625STOP/+}$ adult mice. This mutation was originally identified through screening of an ENU DNA and sperm archive.

Although there is post-natal lethality in this line, homozygous mice survive until 14.5dpc, while in complete knock-out models lethality occurs earlier at around 12.5dpc due to loss of cardiac function (Seisenberger et al., 2000). This could mean that the *Cacna1c*^{Q1625STOP} allele, when homozygous, maintains sufficient embryonic cardiac function beyond 14.5dpc. This could mean that it is a hypomorphic allele. Another possibility is that these differences are due to the genetic background; *Cacna1c*$^{+/-}$ mice were originally derived from (129X1/SvJ x 129S1/Sv)F1-*Kitl*$^{+}$-derived R1 embryonic stem cells and the colony was maintained on a mixed 129, C57BL/6 and FVB background (Seisenberger et al., 2000). It is unknown whether mice with an increasing proportion of C57BL/6J congenicity would be less susceptible to cardiac failure. That *Cacna1c*$^{Q1625STOP/+}$ mice show no differences in heart function is consistent with work carried out on *Cacna1c*$^{+/-}$ animals showing that they had no reduction in L-type Ca^{2+} current density in the heart even though mRNA expression was reduced by approximately 50% (Rosati et al., 2011). Further work on the *Cacna1c*^{Q1625STOP} line would be useful to quantify whether expression levels are changed by qRT-PCR using tissue from heart and brain – differences between these two tissues could be expected given that we observed a behavioural phenotype in *Cacna1c*$^{Q1625STOP/+}$ mice but no cardiac phenotype.

One effect of the *Cacna1c*$^{Q1625STOP/+}$ allele appears to be decreased startle reactivity in Acoustic Startle PPI (see 5.2.2.7). As the C57BL/6J strain is susceptible

to hearing loss and poor PPI (reviewed in Crawley et al. (1997)) we tested the auditory brainstem response of these mice (data not shown) but did not show any significant difference. All animals were age-matched so a similar reduction in wild-type animals would be expected if hearing loss were the cause; it has also been shown that hearing loss in C57BL/6J mice is associated with an increase in startle response (Ison et al., 2007) making it even more unlikely that *Cacna1c*$^{Q1625STOP/+}$ mice show increased hearing loss. As startle response correlates with body weight, it is important to consider that differences in weight between *Cacna1c*$^{+/+}$ and *Cacna1c*$^{Q1625STOP/+}$ mice could account for reduced startle in *Cacna1c*$^{Q1625STOP/+}$ animals. However, when these animals were weighed there was no difference observed in body weights. Therefore, we believe that this difference in startle response is associated with the *Cacna1c*$^{Q1625STOP/+}$ mutation.

In fear conditioning (5.2.2.8) *Cacna1c*$^{Q1625STOP/+}$ mice freeze more after the conditioning tones and shocks, and in particular displayed an increased unconditioned response. This increase in freezing at baseline makes it difficult to draw conclusions about the increase in freezing when returned to the context test 24h after conditioning. *Cacna1c*$^{Q1625STOP/+}$ mice could be showing an enhanced association of the context with the foot shock and therefore an over-activation of brain regions involved in context-dependent memory such as the hippocampus or amygdala (Maren et al., 2013). Deletion of $Ca_v1.2$ in the anterior cingulate cortex (ACC) causes reduced behavioural pain responses (Jeon et al., 2010) so *Cacna1c*^{Q1625STOP} could be having an effect on pain or mechanosensation. We did not measure the unconditioned response to the first shock in the conditioning session. This can be used as a measure of sensitivity to shock, and therefore we cannot rule out increased shock sensitivity in *Cacna1c*$^{Q1625STOP/+}$ mice. In order to

study this further, another cohort could be run through Fear Conditioning and burst activity (high-frequency activity) measured after the first shock. Mechanosensation in *Cacna1c*$^{Q1625STOP/+}$ mice could also be measured using the Von Frey test (Xie, 2010). We were also not able to definitively show that these animals can hear the cue tones. The unconditioned response to a tone is usually an increase in immobility immediately after tone onset, whereas in both wild-type and *Cacna1c*$^{Q1625STOP/+}$ mice we observed lower percentage immobility. As mice were able to hear a click box in the SHIRPA task and also showed no differences in ABR, it could be this is affected by background strain. The baseline period may also not be long enough for the mice to acclimatise to the chamber and reduce freezing behaviour. While *Cacna1c*$^{Q1625STOP/+}$ mice appear to show changes in memory it is difficult to pinpoint exactly what circuits are involved and whether these are true differences in learning and memory. Many studies do not report the post-conditioning stimulus freezing response or report absolute percentage freezing with no corrections to baseline, and this makes it difficult to compare results between studies and from novel models as in this work. In order to study memory without using the freezing response, a cohort of *Cacna1c*$^{Q1625STOP/+}$ animals could be tested using different paradigms. For example, spatial memory could be tested using Morris water maze or T-maze (or its variants) (Morris, 1984), or cognition can be assessed using positive reinforcement-based operant tests such as pairwise association (Brigman et al., 2006).

Taken together, Open Field and Elevated Nought Maze data from *Cacna1c*$^{Q1625STOP/+}$ suggest an increased anxiety and reduced exploratory phenotype in animals, reminiscent of the heterozygous null model (Dao et al., 2010). Data from SHIRPA tests did not show a significant difference in locomotor activity over 30 seconds, which could verify that the phenotype observed in Open Field was not due

to locomotor deficits. However, the numbers for this were very low and the test could be under-powered. The data from light-dark box was not so discriminatory in determining whether this was a generalised anxiety phenotype, although latency to light entry was increased. These tests indicate that this allele may cause a loss of function in $Ca_v1.2$ in the brain, similar to some knock-out models. Therefore, we can add this to the range of alleles already studied, which have shown varying phenotypes. For example, a CNS-specific knockout does not cause increased anxiety (Langwieser et al., 2010) but does cause reduced phase responsiveness to light pulses late at night (Schmutz et al., 2014) which was not seen in these models. A forebrain-specific conditional knockout results in increased anxiety (Lee et al., 2012) which implicates this region in the anxiogenic response.

Conditional knockouts are useful for narrowing down brain region-specific effects, but in human patients with psychiatric disorders mutations could affect multiple tissues and brain regions. The *Cacna1c*^{Q1625STOP} allele is present throughout development and in all tissues and this suggests that the increased anxiety seen in animals is more analogous to anxiety observed in humans carrying the risk allele at rs1006737 in *CACNA1C* (Roussos et al., 2011, Pasparakis et al., 2015). This locus is an eQTL for *CACNA1C* expression and in the superior temporal gyrus is associated with lower expression levels (Eckart et al., 2016). Additionally, the risk allele has been associated with high startle reactivity (Roussos et al., 2011) and impairments in logical memory, spatial working memory and facial recognition (Hori et al., 2012, Zhang et al., 2012, Soeiro-de-Souza et al., 2012). Given that anxiety, increased startle response, and potential memory deficits are observed in *Cacna1c*$^{Q1625STOP/+}$ mice, this shows more face validity for the rs1006737 risk allele compared to previous knock-out models. The rs1006737 risk allele has also been associated with increased

amygdala volume and reductions in hippocampal activation during memory recall (Lancaster et al., 2016, Erk et al., 2014b) and further structural studies of brains from *Cacna1c*$^{Q1625STOP/+}$ mice would reveal whether these mice also have changes in these brain areas. That there was no effect on sensorimotor gating in these animals (an endophenotype of schizophrenia) also ties in with human studies of rs1006737 showing that there is no reduction in prepulse inhibition in healthy volunteers carrying the risk allele (Roussos et al., 2011).

$Ca_V1.2$ is highly expressed in the hippocampus and thalamus (Obermair et al., 2004, Splawski et al., 2004), which are important for EEG rhythmic activity (Cantero et al., 2003, Steriade et al., 1993). We observed a significant decrease in delta frequencies (0.5-5Hz) in *Cacna1c*$^{Q1625STOP/+}$ mice during NREM bouts in light and dark phase and after 4 hours of sleep deprivation (described in 5.2.3.3). Delta waves are a signifier of slow wave activity (SWA) during NREM, and at a cellular level are caused by synchronised transitions in large populations of cortical pyramidal neurons between a depolarised UP and hyperpolarised DOWN state (reviewed in Deboer (2015)). Slow wave activity is cortically generated but maintained by the thalamus (David et al., 2013, Crunelli et al., 2015) and is thought to be important in sleep homoeostasis and plasticity (Halasz et al., 2014). Although the precise mechanism is not completely understood, a synaptic homoeostasis hypothesis has been proposed in which synaptic activity and connections during wake are modulated and consolidated during NREM (Tononi and Cirelli, 2006) and after longer periods of wake more SWA is observed (Mistlberger et al., 1987, Dijk and Czeisler, 1995). It has now also been shown that SWA in specific brain regions correlates with activation of specific circuits during wake (Vyazovskiy et al., 2004, Vyazovskiy et al., 2006, Vyazovskiy and Tobler, 2008). The decrease in delta frequencies and the attenuated

increase in delta power/SWA after sleep deprivation observed in *Cacna1c*$^{Q1625STOP/+}$ suggests that this allele causes an impairment in NREM sleep homoeostasis and could also mean that these mice consequently have defects in memory consolidation.

SWA deficits have been seen frequently in patients with schizophrenia (Feinberg et al., 1969, Kupfer et al., 1970, Traub, 1972, Poulin et al., 2003, Goder et al., 2004, Sekimoto et al., 2007, 2011) but are not consistently observed (Chouinard et al., 2004, Forest et al., 2007, Ferrarelli et al., 2010, Manoach et al., 2010, Chan et al., 2016). This may be due to variation in sample sizes, medication status of patients and study design differences, or it could reflect the heterogenous nature of the schizophrenia diagnosis. The effects of SNPs in *CACNA1C* on polysomnography have not been studied, although associations with narcolepsy and decreased sleep quality have been identified (Shimada et al., 2010, Parsons et al., 2013). Results from *Cacna1c*$^{Q1625STOP/+}$ mice suggest that a decrease in $Ca_v1.2$ function leads to defects in SWA. If schizophrenia-associated polymorphisms in *CACNA1C* cause a decrease in expression (as seen in some brain regions of rs1006737 carriers) this suggests a mechanism of disrupted SWA seen in some patients with schizophrenia.

Cacna1c$^{+/-}$ mice show a decreased EEG power over beta and gamma frequencies during wake and sleep but showed no change in delta frequencies. *Cacna1c*$^{+/-}$ mice also showed a normal increase in slow wave activity (SWA) in NREM after sleep deprivation and therefore a preserved NREM homoeostasis. (Kumar et al., 2015). This discrepancy could be due to the small but residual function of the *Cacna1c*^{Q1625STOP} allele. The effect could also be due to differences in background strain; in the previous study by Kumar et al. (2015) the *Cacna1c*$^{+/-}$ colony was maintained on a mixed 129S1/Sv × 129X1/SvJ × C57BL/6 background, whereas the *Cacna1c*$^{Q1625STOP/-}$ mice tested were derived onto C57BL/6J from a mutagenised

sperm sample from offspring of a BALB/c x C3H/HeH mating and the colony had been backcrossed seven times to C57BL/J. The presence of 129S1/Sv genomic regions in the original study could increase susceptibility to changes in high frequencies, and strain differences have been previously observed in EEG recording data (Franken et al., 1998, Huber et al., 2000). All 129 mouse substrains have also been shown to be homozygous for a deletion in the *Disc1* gene (Clapcote and Roder, 2006), which as discussed in 1.2.3.1 is a candidate gene for psychiatric disease. This mutation causes a premature stop codon and has been shown to perturb cortical development and working memory in mice (Kamiya et al., 2005, Koike et al., 2006), although it may only affect a percentage of DISC1 isoforms (Ishizuka et al., 2007). As Kumar *et al* did not genotype their colony for this mutation it is possible that the changes observed in *Cacna1c*$^{+/-}$ mice were influenced by defects in DISC1 function. A transgenic DISC1 overexpression *Drosophila* model has shown that nuclear-localised DISC1 affects CRE-mediated binding and sleep homoeostasis (Sawamura et al., 2008) and DISC1 has been shown to bind *CACNA1C* mRNA (Tsuboi et al., 2015). It would be useful to study the *Cacna1c*$^{+/-}$ heterozygous allele on a congenic C57BL/6J background in order to compare these phenotypes more closely.

Previous work has shown that mice with the distal C-terminus (DCT) truncated from residue G1706 die perinatally with cardiac hypertrophy, with death occurring between 15dpc and birth (Fu et al., 2011). A region between residues 1623-2024 (rabbit cardiac $Ca_v1.2$) has also been shown to be critical for membrane targeting of the channel and disruption results in loss of functional channels (Gao et al., 2000). The *Cacna1c*^{Q1625STOP} allele causes truncation and loss of this region and of the DCT as well as the death of embryos after 14.5dpc, leading to our hypothesis that this mutation causes a premature truncation and loss of trafficking, a loss of function and

perinatal death of homozygotes. While the anxiety phenotype indicates a loss of function, phenotypes observed in fear conditioning and EEG recordings suggest that there are some differences in function between *Cacna1c*^{Q1625STOP} and heterozygous null alleles.

As mentioned above, further behavioural phenotyping, including tests of cognition and social interaction, would give more insight into the function of the *Cacna1c*^{Q1625STOP} allele. In particular, tests that study endophenotypes of other psychiatric disorders would be enlightening; study of autism-related behaviours (asocial and repetitive behaviour)(Silverman et al., 2010) and depression (behavioural despair, anhedonia)(Hasler et al., 2004) would be an advantageous direction in which to continue as *CACNA1C* has also been associated with these disorders (Liu et al., 2011, Li et al., 2015a). Social behaviour and further study of sleep patterns could also be studied using home cage monitoring (Bains et al., 2016).

In order to study membrane expression, an antibody raised against an epitope of the $Ca_v1.2$ channel prior to the Q1625STOP truncation could be used to probe either *in vitro* cells using an expression construct, *ex vivo* primary neurons or brain slices, and would show how much functional $Ca_v1.2$ is successfully trafficked to the membrane. Alternatively or in combination with this an antibody against an epitope in the distal C-terminus (a region which should not be present in the truncated product) would show whether truncated $Ca_v1.2$ is trafficked to the membrane, if it gets retained in the endoplasmic reticulum as seen in previous work (Fu et al., 2011), or if it is degraded in some fashion by the cellular machinery, for example by nonsense-mediated decay.

Nonsense-mediated decay (NMD) is a pathway that reduces errors in gene transcription and selectively degrades proteins containing premature termination codons (Chang et al., 2007, Baker and Parker, 2004). The mechanism of NMD involves the interaction of the ribosome and the Exon Junction Complex (EJC), a protein complex that remains bound to exon-exon boundaries of mRNA after splicing. If the last exon of the mRNA contains a stop codon, the ribosome removes all EJCs in the first round of translation. If however there is a premature stop codon >50 bp upstream of the last codon the ribosome is prevented from traversing all the exon-exon boundaries and some EJC will remain bound. The EJC then acts as a signal to the degradation machinery (Shyu et al., 2008). Protein synthesis inhibitors such as cycloheximide have been used to demonstrate NMD; treatment of slices or primary cells with cycloheximide leads to an increase in the prematurely truncated mRNA that can be measured using qRT-PCR or Northern blotting (Busi and Cresteil, 2005). This approach could be used to test whether the product of the *Cacna1c*^{Q1625STOP} allele is degraded in slices or primary neurons of *Cacna1c*$^{Q1625STOP/+}$ animals. If *Cacna1c* were cloned into a plasmid containing a luciferase reporter, and site-directed mutagenesis used to reproduce the Q1625STOP truncation, a reporter assay could also be used in cell lines to study the translation of each allele *in vitro*.

Primary neurons could also be used to compare cellular morphology and co-localisation of $Ca_V1.2$ with dendritic or post-synaptic markers. L-type channel-specific blockers such as nifedipine or nimodipine or agonists such as FPL64176 could be used in primary neuronal cultures before assessment of activity-induced gene transcription. As well as this, a whole cell patch clamp approach could be used to study the L-type Ca^{2+} current in primary neurons from *Cacna1c*$^{Q1625STOP/+}$ mice or in

in vivo recordings coupled with agonists or antagonists to dissect the $Ca_v1.2$-specific current from other L-type channels (as in Evans et al. (2013)).

The rationale behind the use of ENU mutagenesis is to produce allelic series of mutations. It has been shown here that *Cacna1c*^{Q1625STOP} is a hypomorphic allele that causes a decrease in function. Point mutations resulting from ENU mutagenesis are not always loss-of-function, and one such allele is discussed in the next chapter.

6 *Cacna1c*^{G1616D}

6.1 Introduction

As described in the previous chapter, ENU mutagenesis and a reverse genetics approach can be utilised to produce hypomorphic alleles such as *Cacna1c*^{Q1625STOP}. A SNP in *CACNA1C* that has been associated with bipolar disorder, rs1006737, has been associated with reduced expression in some regions of the brain and this reduction may cause endophenotypes observed in carriers of the risk allele including increased anxiety and memory deficits as discussed in 1.9.10. Mutations in *CACNA1C* that cause a gain of function, on the other hand, cause long QT syndromes and are associated with autism (1.9.11). The rs1006737 SNP is also associated with a trend towards increased expression in the prefrontal cortex (Eckart et al., 2016), suggesting that it is not necessarily a global decrease in expression that increases risk for neuropsychiatric disease. An advantage of ENU mutagenesis is that it creates single point mutations that are not necessarily loss of function, and one such allele, *Cacna1c*^{G1616D}, is described in this chapter.

The G1616D allele was identified in an ENU archive screen as described in 1.9.13.2 by Dr Michael Parsons (unpublished data) and is predicted to cause a glycine to aspartic acid change within the IQ motif of murine $Ca_V1.2$ (ENSMUST00000078320) as shown in Figure 19A-B.

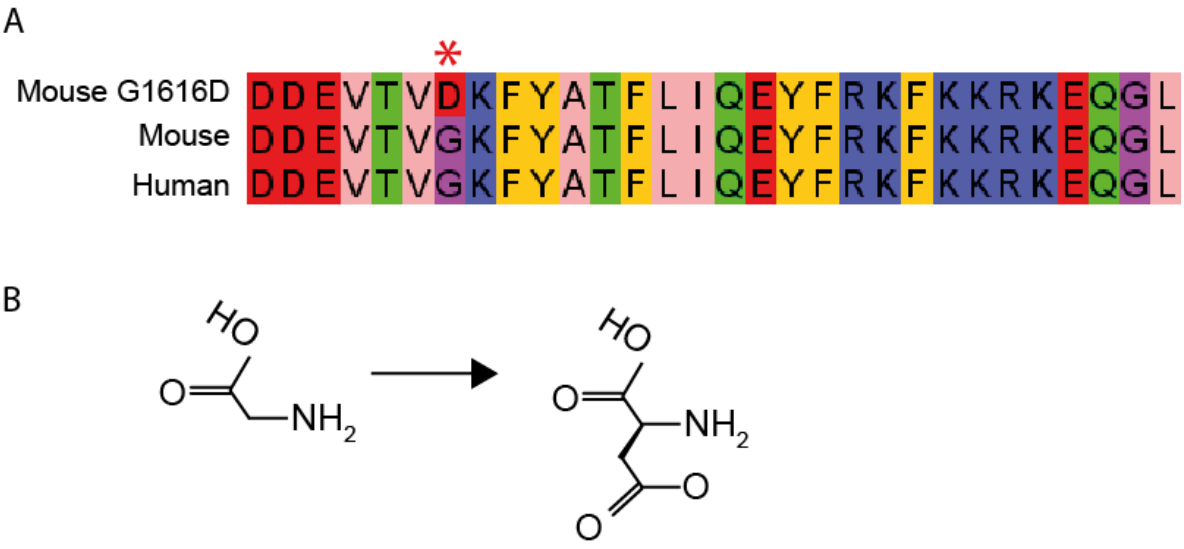

Figure 56 IQ domain of $Ca_v1.2$ and the *Cacna1c*^{G1616D} mutation.

(A) Alignment of the IQ domain from mouse and human $Ca_v1.2$ showing the location of the missense mutation G1616D. (B) Skeletal formula showing the amino acid structures of glycine and aspartic acid.

6.2 Results: *Cacna1c*^{G1616D}

6.2.1 *Cacna1c*$^{G1616D/G1616D}$ animals are viable to P21

Litters from *Cacna1c*$^{G1616D/+}$ x *Cacna1c*$^{G1616D/+}$ intercross matings were biopsied and genotyped at P21. 81 homozygous animals were observed, compared to 167 heterozygotes and 84 wild-types (Figure 57A). A X^2 test of these numbers showed that this did not significantly differ from the expected Mendelian ratio (X^2 = 0.06471, ns) (Figure 57B). Therefore, homozygous animals are viable at this age and were used for phenotyping.

A

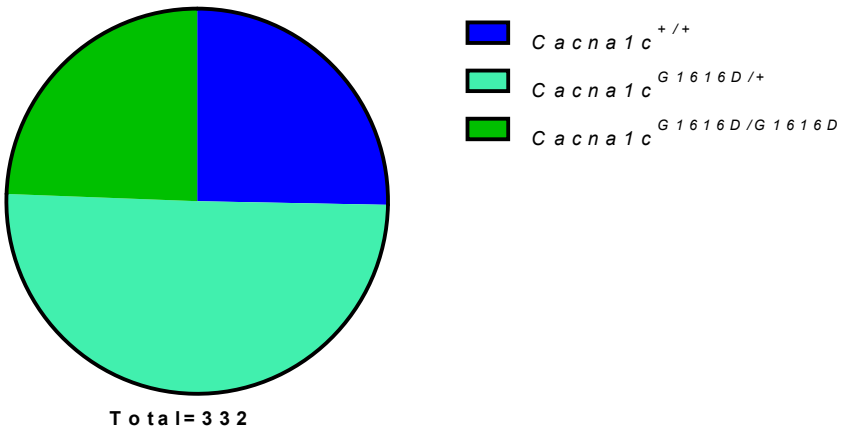

B

Chi-square test	
Chi-square	0.06627
DF	2
P value (two-tailed)	0.9674
P value summary	ns

Figure 57 *Cacna1c*$^{G1616D/G1616D}$ mice are viable to P21.

(A) Homozygous mice were observed at P21. (B) A Chi-squared test showed there was no difference to the expected Mendelian ratio.

6.2.2 *Cacna1c*$^{G1616D/G1616D}$ mice have changes in anxiety and learning

6.2.2.1 SHIRPA

Cacna1c$^{G1616D/G1616D}$ animals did not show any gross morphological differences to wild-type controls. They also did not display any differences in transfer arousal or gait . Locomotor activity was measured as the number of squares entered during 30s, and *Cacna1c*$^{G1616D/G1616D}$ (M = 14 ± 1, n=9) showed no difference to *Cacna1c*$^{+/+}$ mice (M = 11 ± 2, n=9) t(16)=1.616, ns (Figure 58), and these mice showed no evidence of trunk curl or limb grasping.

6.2.2.2 Open Field

Over 30 minutes, *Cacna1c*$^{G1616D/G1616D}$ mice spent less time in the periphery (M = 1417.9s ± 45.0, n=9) compared to *Cacna1c*$^{+/+}$ littermate controls (M = 1562.8s ± 45.3, n=9) t(16)= 2.266, $p < 0.05$ (Figure 59A). There was no difference in frequency of entries between zones (Figure 59B) or distance travelled (Figure 59C). As in 5.2.2.2, results were separated into Start-05:00 and 05:00-End time bins to investigate the exploratory versus anxiety phenotype.

6.2.2.2.1 Cacna1c$^{G1616D/G1616D}$ *mice explore more in the first five minutes*

From the start of the test to 05:00, *Cacna1c*$^{G1616D/G1616D}$ mice trended towards less time in the periphery (M = 253.2s ± 7.5, n=9) compared to *Cacna1c*$^{+/+}$ (M = 273.4s ± 6.1, n=9) t(16)= 2.095, $p = 0.052$ (Figure 59D), suggesting an increase in exploring outside the periphery (in the intermediate and centre areas). This was not reflected in frequency of entries (Figure 59E) or distance travelled (Figure 59F).

6.2.2.2.2 Cacna1c$^{G1616D/G1616D}$ mice show a mild decrease in anxiety

In the remaining time, *Cacna1c*$^{G1616D/G1616D}$ mice continued to trend towards less time in the periphery than *Cacna1c*$^{+/+}$ (*Cacna1c*$^{G1616D/G1616D}$ M = 939.8s ± 35.9, n=9; *Cacna1c*$^{+/+}$ M = 1027.4s ± 33.1, n=9; t(16)=1.795, p = 0.092) (Figure 59G). This is accompanied by increased entries into the centre (*Cacna1c*$^{G1616D/G1616D}$ M = 54 ± 8, n=9; *Cacna1c*$^{+/+}$ M = 29 ± 6, n=9; t(16)= 2.384, p < 0.05) (Figure 59H) but no difference in distance travelled (Figure 59I).

This decrease in anxiety and increase in exploratory behaviour is a hallmark of mania, an endophenotype of bipolar disorder. To investigate further, a secondary cohort was put through Light-dark box and Elevated Nought Maze similar to *Cacna1c*$^{G1616D/G1616D}$ mice, as described in 2.3.

6.2.2.3 Light-Dark Box

In Light-Dark Box, *Cacna1c*$^{G1616D/G1616D}$ mice showed a trend towards spending less time in the light area of the Light-Dark Box (M = 64.7s ± 7.3, n=17) compared to *Cacna1c*$^{+/+}$ (M = 81.3s ± 6.3, n=17) t(32)= 1.73, p = 0.093) (

Figure 60A). They also showed a trend towards increased latency to light entry (*Cacna1c*$^{G1616D/G1616D}$ M = 50.31 ± 5.265, n=17; *Cacna1c*$^{+/+}$ M = 35.4 ± 5.114, n=17; t(31.97)=2.031, p = 0.0506) (

Figure 60B).

6.2.2.4 Elevated Nought Maze

Similar to Light-Dark Box, in Elevated Nought Maze *Cacna1c*$^{G1616D/G1616D}$ animals showed a trend towards less time in the open arm (M = 111.8s ± 7.5, n = 21) compared to *Cacna1c*$^{+/+}$ (M = 135.0s ± 9.0, n = 17) t(72)= 1.989, p = 0.0504 (

Figure 60C). This was accompanied by a significant reduction in distance travelled (*Cacna1c*$^{G1616D/G1616D}$ M = 1491cm ± 64.97, n=21; *Cacna1c*$^{+/+}$ M = 1797cm ± 77.65, n=17; t(36)= 3.041, p < 0.01) (

Figure 60D).

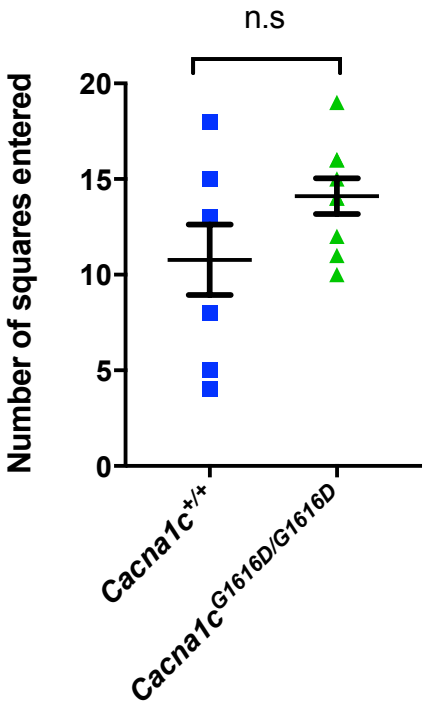

Figure 58 Locomotor activity in the SHIRPA test

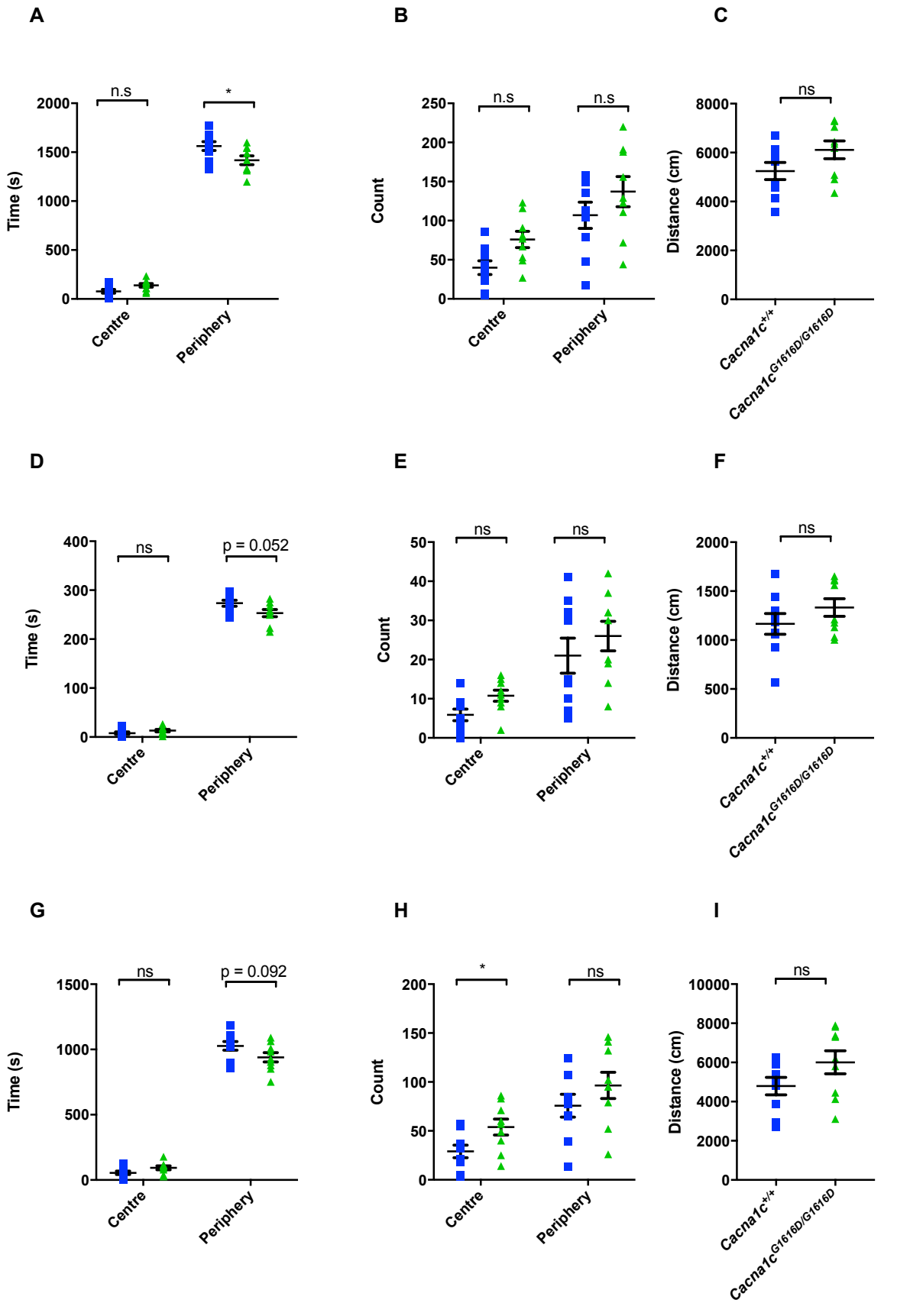
A
B
C
D
E
F
G
H
I
Time (s)
Count
Distance (cm)
n.s
*
ns
p = 0.052
p = 0.092
Centre
Periphery
Cacna1c+/+
Cacna1cG1616D/G1616D
Cacna1c+/+
Cacna1cG1616D/G1616D

Figure 59 *Cacna1c*$^{G1616D/G1616D}$ mice show mildly reduced anxiety in Open Field.

(A)Time spent in centre and periphery over 30 minutes, (B) frequency of entries into centre and periphery from intermediate arena over 30 minutes, (C) total distance travelled in the whole arena over 30 minutes. (D) Time spent in centre and periphery over the first 5 minutes, (E) frequency of entries into centre and periphery from the intermediate arena in the first 5 minutes, (F) total distance travelled in the whole arena in the first five minutes. (G)Time spent in centre and periphery in the remaining 25 minutes, (H) frequency of entries into centre and periphery from the intermediate arena in the remaining 25 minutes, (I) total distance travelled in the whole arena in the remaining 25 minutes.

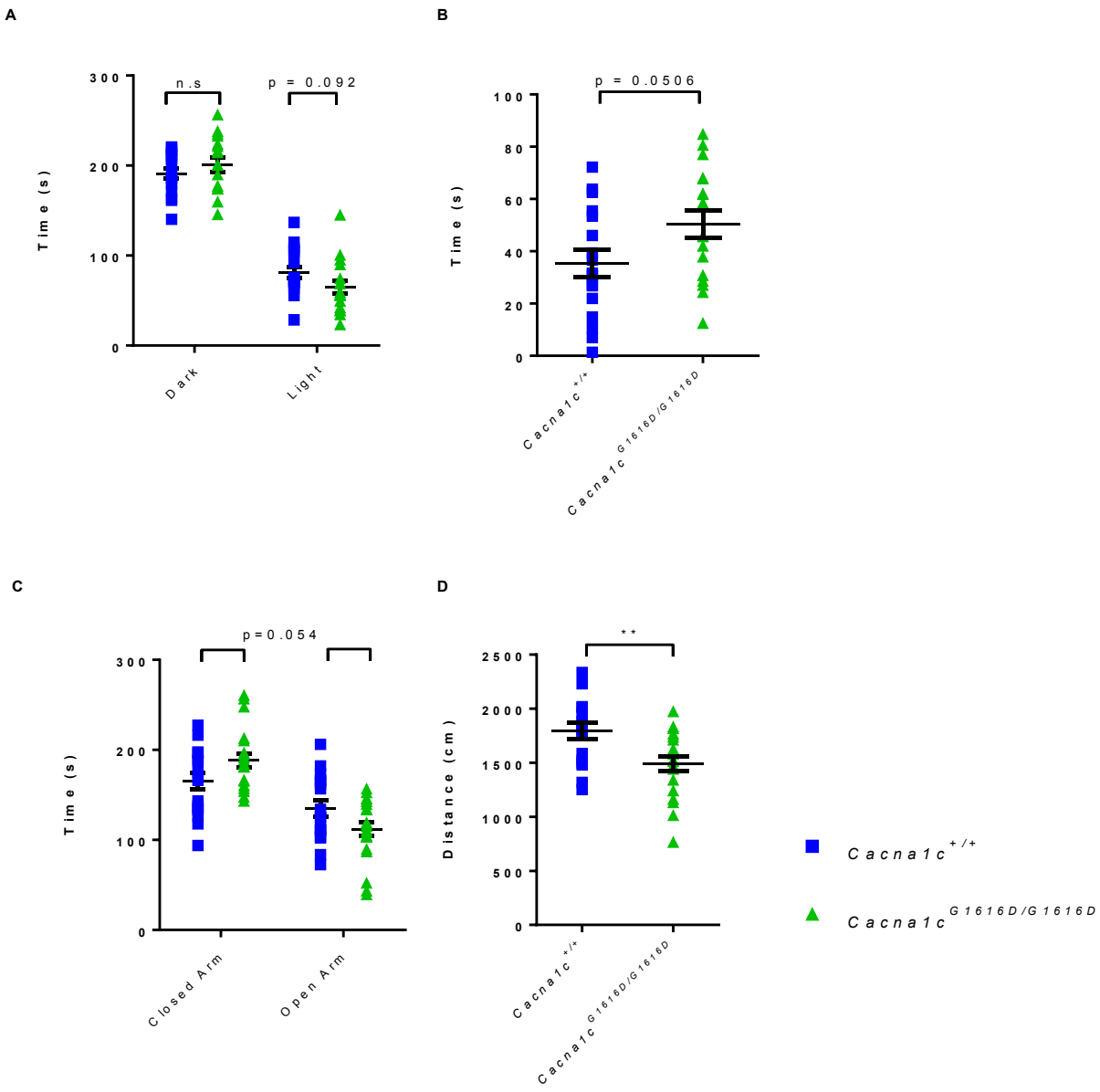

Figure 60 *Cacna1c*$^{G1616D/G1616D}$ mice show a trend towards increased anxiety in other tests of anxiety.

(A) Time spent in dark or light area of the Light-Dark box over 5 minutes, (B) Latency to entry into the light area, (C) Time spent in the closed or open arms of the elevated nought maze over 5 minutes, (D) Total distance travelled in the whole maze over 5 minutes.

6.2.2.5 Acoustic Startle PPI

Unlike *Cacna1c*$^{Q1625STOP/+}$ mice, *Cacna1c*$^{G1616D/G1616D}$ mice did not show any significant differences in startle response (M = 354.5 ± 27.57, n=19) compared to *Cacna1c*$^{+/+}$ (M = 319.6 ± 26.61, n=16) t(33)=0.9014, ns (Figure 61A). They also did not show any differences in pre-pulse inhibition (2-way RM ANOVA, ns) (Figure 61B)

6.2.2.6 Fear Conditioning

There were no differences in freezing observed between *Cacna1c*$^{G1616D/G1616D}$ and *Cacna1c*$^{+/+}$ mice either pre- or post-shocks during conditioning (Table 56, Figure 61C). The unconditioned response to shock was non-significant in both *Cacna1c*$^{+/+}$ and *Cacna1c*$^{G1616D/G1616D}$ (2-way RM ANOVA) but this is due to high levels of freezing pre-shock. There was no difference observed in context-dependent memory (Welch's t-test: *Cacna1c*$^{G1616D/G1616D}$ M = 31.14 ± 6.954, n=9; *Cacna1c*$^{+/+}$ M = 26.82 ± 3.149, n=8; t(11.09)=0.567, ns)(Figure 61E). Although *Cacna1c*$^{G1616D/G1616D}$ mice appear to freeze more in the novel environment during the cue-dependent test (Figure 61F), this is not significant (2-way RM ANOVA, Table 56).

We were unable to observe an unconditioned response to cue, similar to previous tests described. Neither wild-type nor *Cacna1c*$^{G1616D/G1616D}$ mice showed a difference in immobility during presentation of the first tone (Figure 62A). There was no effect of either time or genotype (2-way RM ANOVA, Figure 62B).

ANOVA table	SS	DF	MS	F (DFn, DFd)	P value
Interaction	11.82	1	11.82	F (1, 16) = 0.07539	P=0.7872
Time	13190	1	13190	F (1, 16) = 84.12	P<0.0001
Genotype	369.5	1	369.5	F (1, 16) = 1.098	P=0.3102
Subjects (matching)	5383	16	336.5	F (16, 16) = 2.146	P=0.0687
Residual	2509	16	156.8		

Table 56 2-way ANOVA of freezing pre- and post-shock in conditioning

ANOVA table	SS	DF	MS	F (DFn, DFd)	P value
Interaction	1715	3	571.7	F (3, 48) = 2.089	P=0.1141
Time	3911	3	1304	F (3, 48) = 4.763	P=0.0055
Genotype	285.3	1	285.3	F (1, 16) = 0.3342	P=0.5713
Subjects (matching)	13663	16	853.9	F (16, 48) = 3.12	P=0.0012
Residual	13139	48	273.7		

Table 57 2-way RM ANOVA of freezing in the cue-dependent test

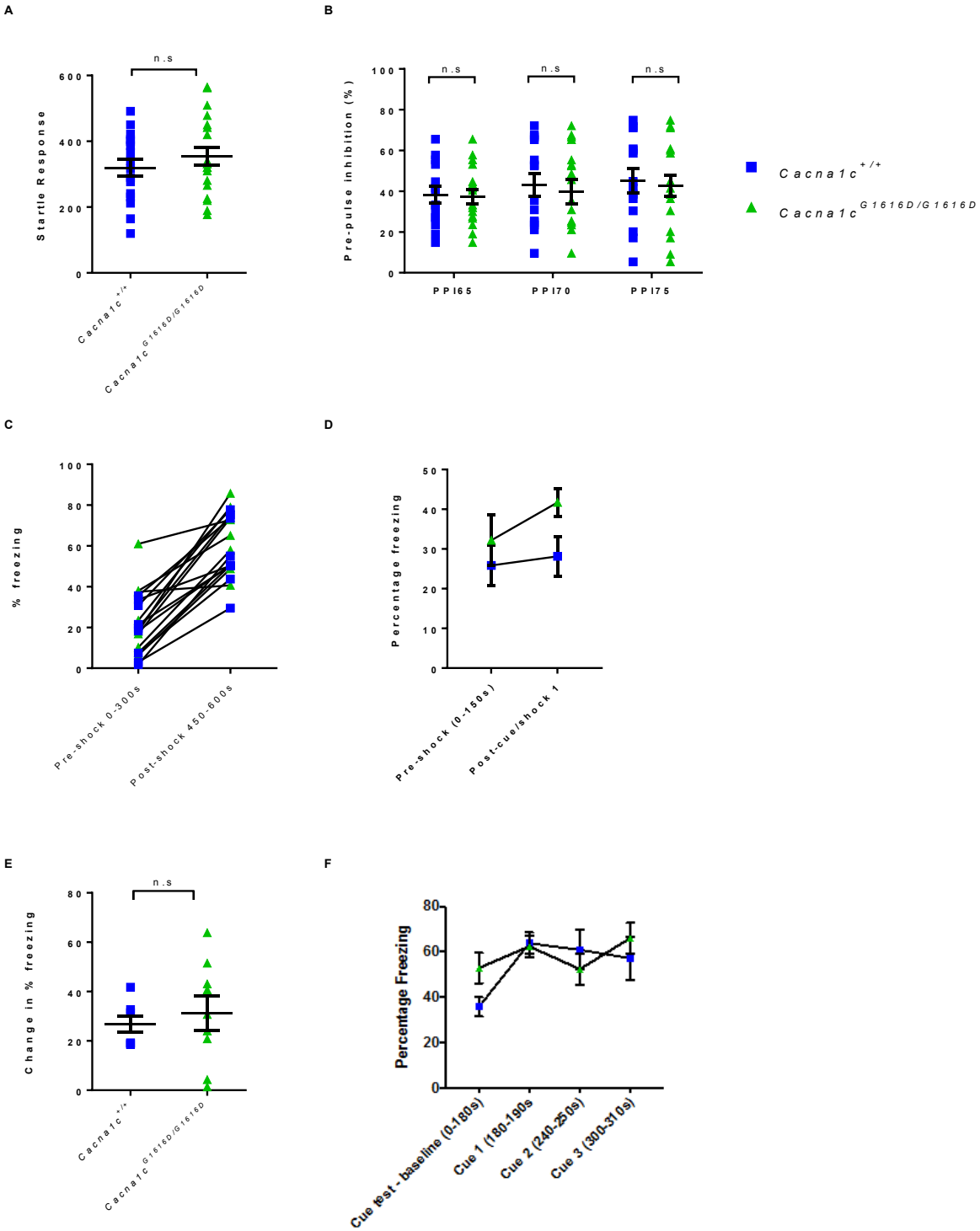

Figure 61 Acoustic Startle PPI and Fear Conditioning of *Cacna1c*$^{G1616D/G1616D}$ mice

(A) Startle Response, (B) the percentage pre-pulse inhibition caused by pre-pulses of 65, 70 and 75 dB, (C) Percentage freezing before any shocks and after three shocks on the first day of testing, (D) Unconditioned freezing response to the first cue and shock in conditioning, (E) Change in percentage freezing between

conditioning baseline and context-dependent testing on day 2, (F) Baseline freezing and cue-dependent freezing in the cue-dependent test.

A

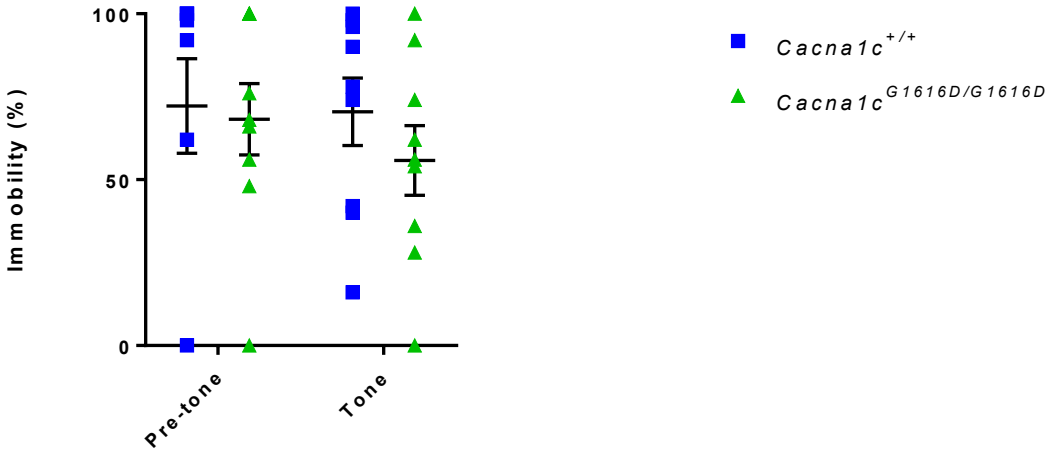

B

Source of Variation	% of total variation	P value	P value summary
Interaction	0.6444	0.6379	ns
Time	1.146	0.5315	ns
Genotype	1.973	0.4448	ns
Subjects (matching)	51.43	0.3931	ns

Figure 62 Unconditioned response to the cue.

(A) Percentage of time spent immobile in the 5 seconds pre-tone and post-tone onset in the conditioning session. (B) 2-way RM ANOVA

6.2.3 *Cacna1c*$^{G1616D/G1616D}$ mice display cardiac defects

6.2.3.1 Cacna1c$^{G1616D/G1616D}$ *mice have increased left ventricular diameter and volume and decreased fractional shortening*

Echocardiograms carried out on mice 3 months of age showed that there were no differences in the thickness of the left ventricular posterior or anterior wall (Figure 64A-B) in *Cacna1c*$^{G1616D/G1616D}$ mice. There was an increase in left ventricular diameter in both diastole ($p < 0.05$) and systole ($p < 0.01$) (Figure 64C) coupled with an increase in left ventricular volume in diastole ($p < 0.05$) and systole ($p < 0.01$) (Figure 64D). The enlarged ventricle phenotype leads to a decrease in fractional shortening ($p < 0.05$) (Figure 64E, Equation 1). Means are summarised in Table 58.

		Cacna1c$^{G1616D/G1616D}$ n=10 M±SEM	*Cacna1c+/+* n=10 M±SEM	df	t	p
Left Ventricular Posterior Wall Thickness	Diastole	0.77 ± 0.03	0.76 ± 0.03	18	0.192	n.s
mm	Systole	1.11 ± 0.04	1.06 ± 0.04	18	0.939	n.s
Left Ventricular Anterior Wall Thickness	Diastole	0.83 ± 0.04	0.81 ± 0.05	18	0.481	n.s
mm	Systole	1.17 ± 0.05	1.13 ± 0.06	18	0.522	n.s
Left Ventricular Interior Diameter	Diastole	4.20 ± 0.09	4.51 ± 0.10	18	2.311	**p < 0.05**
mm	Systole	3.05 ± 0.08	3.47 ± 3.47	18	3.213	**p < 0.01**
Left Ventricular Volume	Diastole	79.18 ± 3.83	93.29 ± 4.86	18	1.275	**p < 0.05**
µl	Systole	36.76 ± 2.54	50.35 ± 3.43	18	0.153	**p < 0.01**
Fractional Shortening		23.07 ± 1.33	27.44 ± 1.55	18	2.143	**p < 0.05**

Table 58 Summary of echocardiogram data.

$$FS\ (\%) = {(LVID^{D} - LVID^{S})}/{LVID^{D}} \times 100$$

Equation 1 Fractional Shortening.

$LVID^{D}$ = Left ventricular interior diameter at end of diastole; $LVID^{S}$ = Left ventricular interior diameter at end of systole

As we observed a phenotype in echocardiogram, a secondary cohort underwent an electrocardiogram (ECG) to study the heart's electrical activity.

6.2.3.2 Cacna1c$^{G1616D/G1616D}$ mice have a lengthened QT interval

Electrocardiogram data produces a wave that is divided into entities as shown in Figure 63. The QT interval is measured from the beginning of the QRS segment (representing the rapid depolarisation of the ventricles) to the end of the T wave (repolarisation of the ventricles) and is corrected by dividing by the square root of the RR interval (heart rate). ECG data showed that *Cacna1c*$^{G1616D/G1616D}$ animals had a lower heart rate (M = 494.2 ± 13.45, n=10) compared to *Cacna1c*$^{+/+}$ (M = 530.3 ± 6.315, n=9) $t(17) = 2.341$, $p < 0.05$ (Figure 64F), and this corresponded with a small but significant increase in QT interval (M = 48.58 ± 1.324, n=10) compared to *Cacna1c*$^{+/+}$ (M = 45.14 ± 0.6111, n=9) $t(17) = 2.267$, $p < 0.05$ (Figure 64G). Consistent with an enlarged left ventricle, the amplitude of the R wave was also increased in *Cacna1c*$^{G1616D/G1616D}$ (M = 1.044 ± 0.04656, n=10) compared to *Cacna1c*$^{+/+}$ (M = 0.8977 ± 0.04534, n=9) $t(17) = 2.244$, $p < 0.05$ (Figure 64H).

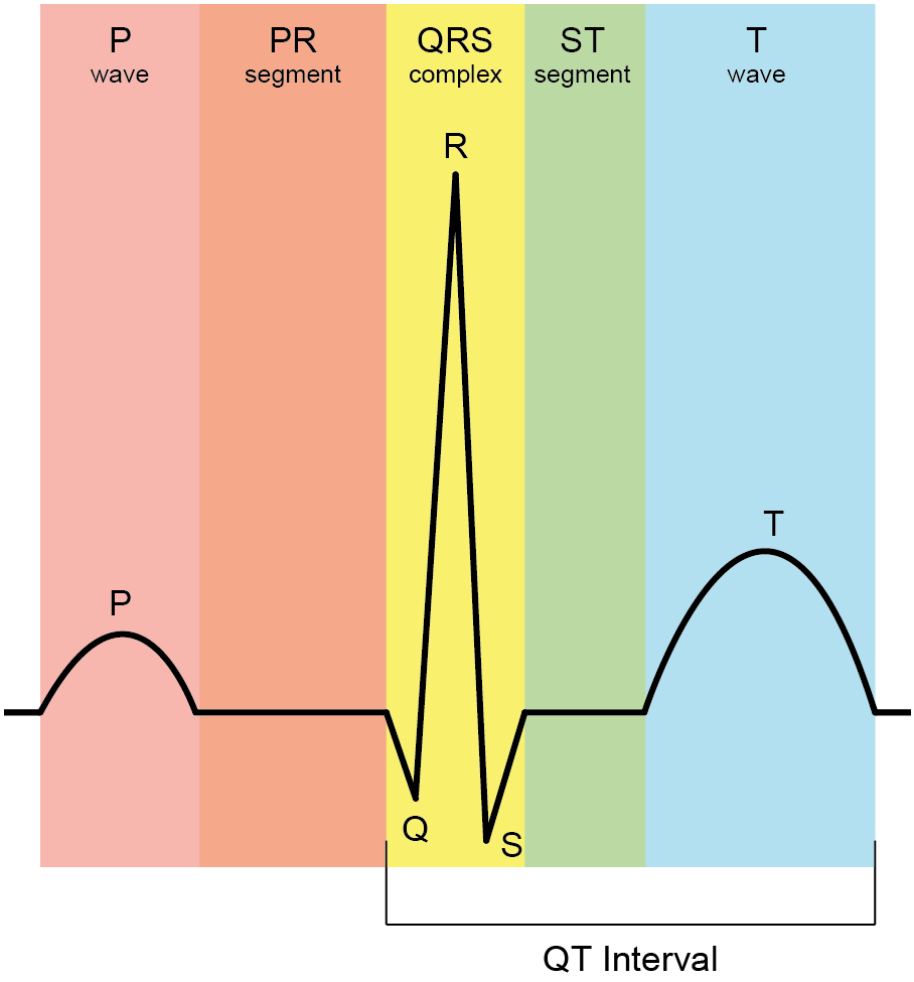

Figure 63 The ECG wave.

ECG of a human heart in normal sinus rhythm.

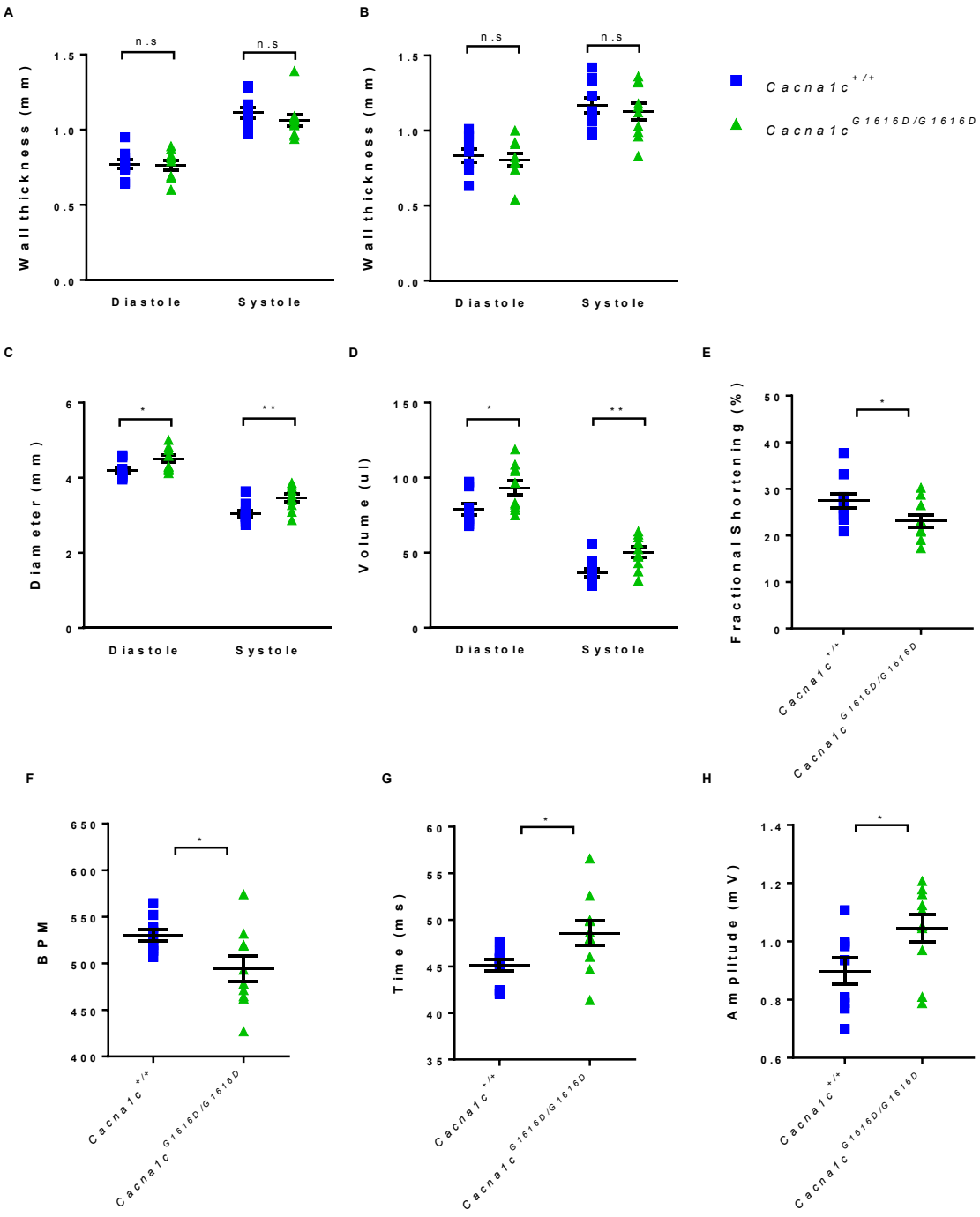

Figure 64 Heart defects in *Cacna1c*$^{G1616D/G1616D}$ revealed using echocardiogram and electrocardiogram.

Measures of echocardiography: (A) Thickness of left ventricular posterior wall and (B) left ventricular anterior wall, (C) left ventricular internal diameter, (D) left ventricular interior volume, and (E) percentage fractional shortening. Measures of ECG activity: (F) Heart rate, (G) QT interval corrected to heart rate, and (H) amplitude of the R-wave (see Figure 63).

6.2.4 Circadian Rhythms and Sleep in *Cacna1c*$^{1625STOP/G1616D}$ mice

6.2.4.1 Cacna1c$^{1625STOP/G1616D}$ *mice show no differences in circadian period*

Cacna1c$^{G1616D/G1616D}$ female mice entrained to light in 12:12 LD (Figure 65A), showing that light input and processing is intact in this line. Mice also showed no difference in free-running period in DD (*Cacna1c*$^{G1616D/G1616D}$ M = 23.64 ± 0.04978, n=8; *Cacna1c*$^{+/+}$ M = 23.71 ± 0.04795, n=8; t(14)= 1.085, ns) (Figure 65B).

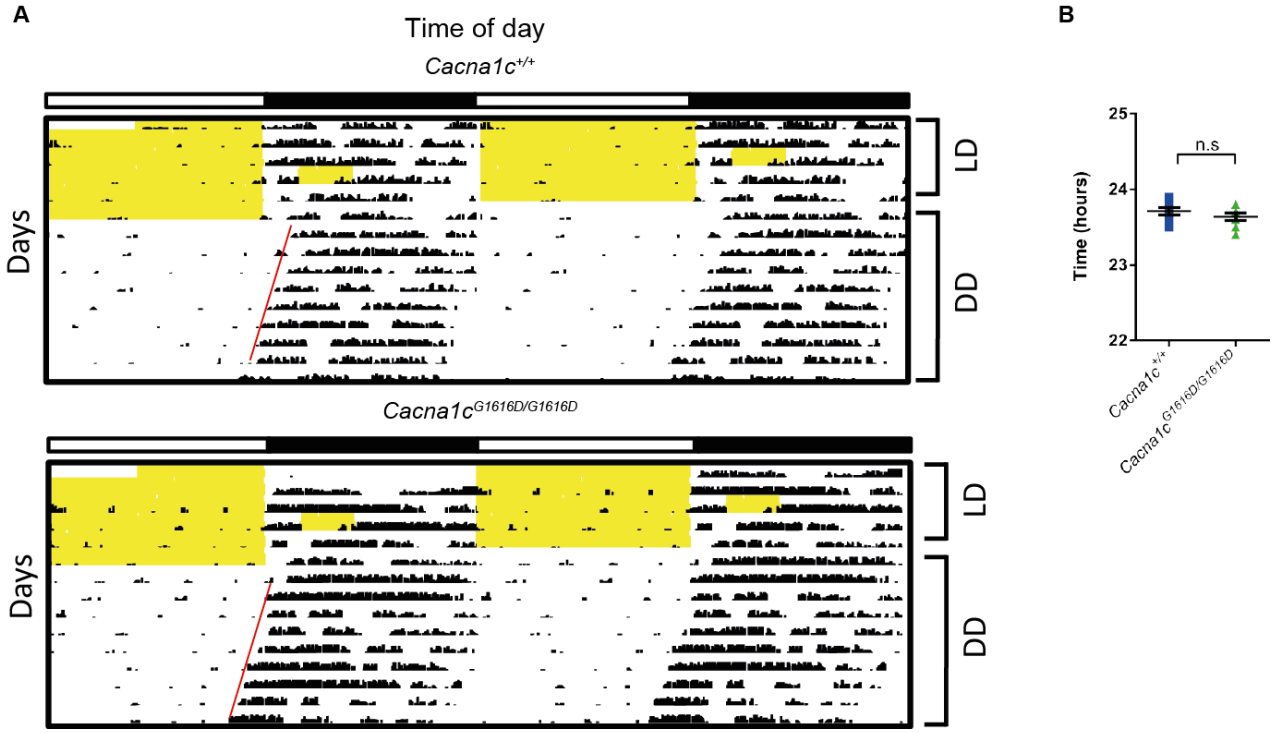

Figure 65 *Cacna1c*$^{G1616D/G1616D}$ mice have normal circadian rhythms.

(A) Representative actograms showing activity in 12:12LD and DD with light periods indicated by yellow boxes. *Cacna1c*$^{+/+}$ (top) and *Cacna1c*$^{G1616D/G1616D}$ (bottom) mice entrain to light in LD. In DD, circadian period (tau) is depicted by a red line fitted to activity onsets on successive days and is the same in both cohorts. (B) Tau_{DD} is unchanged in *Cacna1c*$^{G1616D/G1616D}$.

6.2.4.2 Cacna1c$^{G1616D/G1616D}$ mice respond more quickly to a light pulse in the video-tracked Sleep Screen

There were no differences observed in % immobility over 24 hours (2way RM ANOVA, Table 59, Figure 66A) or averaged over the dark and light phase (Table 60, Figure 66). There were also no significant differences in distance travelled over 24 hours (Table 61, Figure 66C) or when averaged in dark and light phase (Table 62, Figure 66D). After a light pulse at ZT14 (LP2), *Cacna1c*$^{G1616D/G1616D}$ mice showed a decreased latency to immobility after the light pulse onset compared to *Cacna1c*$^{+/+}$ (Table 63, Table 64, Figure 66E, Figure 66F: *Cacna1c*$^{G1616D/G1616D}$ M = 556 ± 68.72, n=8; *Cacna1c*$^{+/+}$ M = 1227 ± 149.3, n=8; t(14)= 4.082, p < 0.01).

ANOVA table	SS	DF	MS	F (DFn, DFd)	P value
Interaction	11920	23	518.3	F (23, 322) = 0.9535	P=0.5263
Time	223992	23	9739	F (23, 322) = 17.92	P<0.0001
Genotype	39.33	1	39.33	F (1, 14) = 0.09087	P=0.7675
Subjects (matching)	6060	14	432.9	F (14, 322) = 0.7964	P=0.6732
Residual	175018	322	543.5		

Table 59 Table 11 2-way RM ANOVA measures - % Immobility over 24 hours

ANOVA table	SS	DF	MS	F (DFn, DFd)	P value
Interaction	40.86	1	40.86	F (1, 14) = 0.8539	P=0.3711
Time	16423	1	16423	F (1, 14) = 343.2	P<0.0001
Genotype	3.29	1	3.29	F (1, 14) = 0.09121	P=0.7671
Subjects (matching)	504.9	14	36.07	F (14, 14) = 0.7537	P=0.6981
Residual	669.9	14	47.85		

Table 60 2-way RM ANOVA measures - % Immobility in Dark and Light phase

ANOVA table	SS	DF	MS	F (DFn, DFd)	P value
Interaction	25263	23	1098	F (23, 322) = 0.605	P=0.9251
Time	652817	23	28383	F (23, 322) = 15.63	P<0.0001
Genotype	1079	1	1079	F (1, 14) = 0.09127	P=0.7670
Subjects (matching)	165534	14	11824	F (14, 322) = 6.513	P<0.0001
Residual	584582	322	1815		

Table 61 2-way RM ANOVA measures - Distance travelled over 24 hours

ANOVA table	SS	DF	MS	F (DFn, DFd)	P value
Interaction	199.2	1	199.2	F (1, 14) = 0.2033	P=0.6590
Time	42930	1	42930	F (1, 14) = 43.83	P<0.0001
Genotype	90.01	1	90.01	F (1, 14) = 0.09136	P=0.7669
Subjects (matching)	13795	14	985.3	F (14, 14) = 1.006	P=0.4957
Residual	13714	14	979.6		

Table 62 2-way RM ANOVA measures – Distance travelled in Dark and Light phase

ANOVA table	SS	DF	MS	F (DFn, DFd)	P value
Interaction	23721	20	1186	F (20, 280) = 3.141	P<0.0001
Time	311808	20	15590	F (20, 280) = 41.29	P<0.0001
Genotype	1684	1	1684	F (1, 14) = 3.639	P=0.0772
Subjects (matching)	6478	14	462.7	F (14, 280) = 1.225	P=0.2559
Residual	105730	280	377.6		

Table 63 2-way RM ANOVA measures – % Immobility after LP2

Time	*Cacna1c*+/+ M	*Cacna1c*$^{G1616D/G1616D}$ M	t	DF	Adjusted P Value	
20	6.809	42.58	3.662	294	0.0062	**
30	38.19	84.03	4.692	294	<0.0001	****

Table 64 Adjusted P-values for significant differences in immobility after LP2

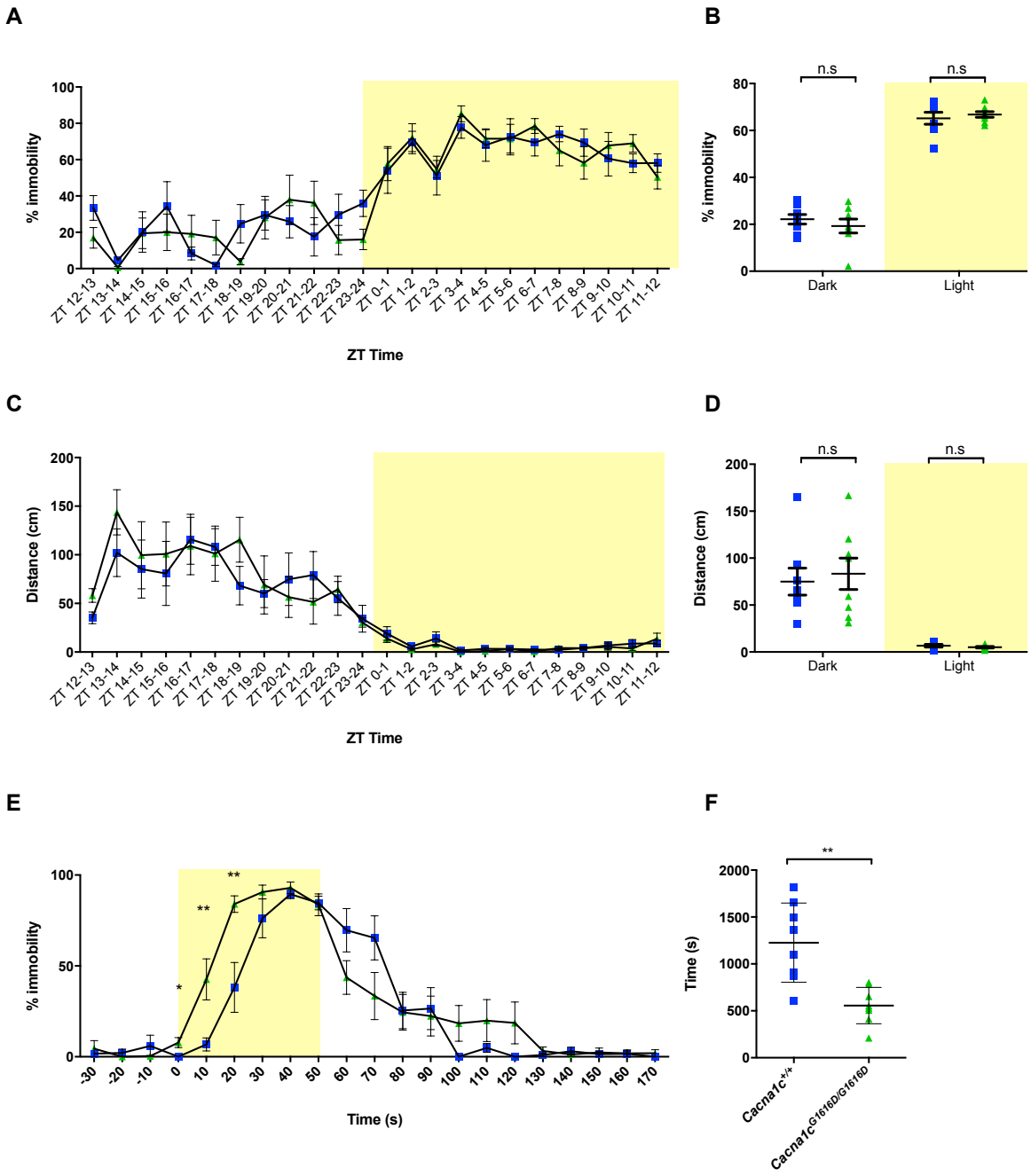

Figure 66 *Cacna1c*$^{G1616D/G1616D}$ mice have a shortened latency to immobility after LP2 onset.

(A) Percentage immobility over 24 hours, (B) Average hourly immobility in the dark and the light phase, (C) total distance travelled over 24 hours, (D) Average hourly distance travelled in the dark and the light phase, (E) percentage immobility during a light pulse (LP2) at ZT14, (F) Latency to immobility after onset of LP2.

6.2.4.3 Cacna1c$^{G1616D/G1616D}$ mice show a small but significant reduction in EEG theta frequencies

EEG recordings showed that *Cacna1c*$^{G1616D/G1616D}$ mice had no differences in time spent asleep (Figure 67A), consistent with results from Harwell Sleep Screen. Power spectra analysed from total sleep bouts identified a small but significant reduction in theta frequencies (5-9Hz) in light (Figure 67B) and dark (Figure 67C) but not after sleep deprivation (Figure 67D). This was also shown in NREM bouts during light and dark (Figure 67E-F) but not after SD (Figure 67G). During REM sleep bouts, there was a decrease in theta although this was less significant (Figure 67H: light; Figure 67I: dark) and again this was not seen after sleep deprivation (Figure 67J).

Cacna1c$^{G1616D/G1616D}$ mice showed no differences in delta power at baseline or after sleep deprivation (Figure 68A). Averaged delta power in the first hour after sleep deprivation showed no significant differences by genotype (Figure 68B).

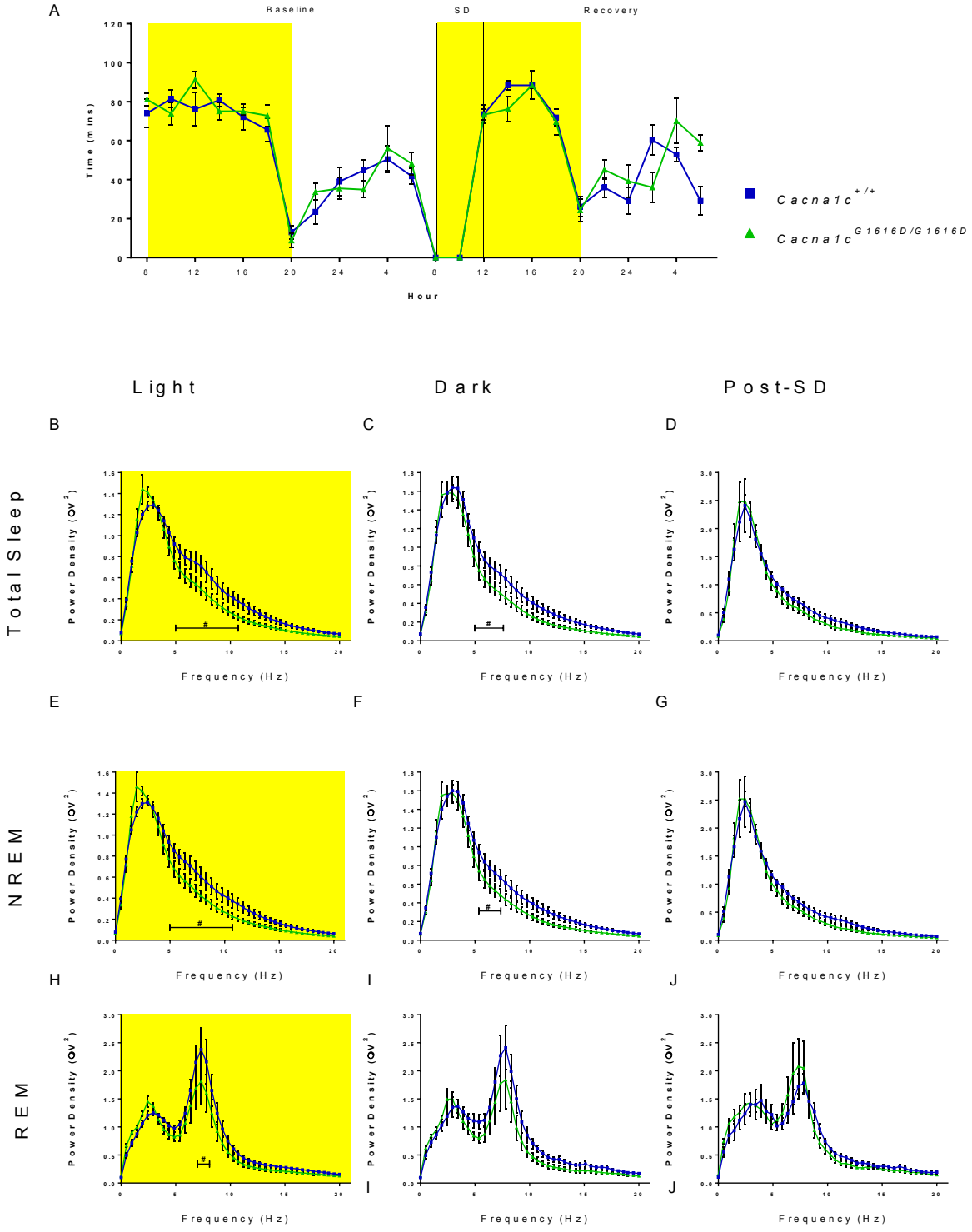

Figure 67 *Cacna1c*$^{G1616D/G1616D}$ mice have a small but significant decrease in theta frequencies.

(A) Total sleep during baseline light and dark, sleep deprivation (SD) and recovery. Total sleep power spectra during: (B) Light, (C) Dark, (D) after SD; NREM power spectra during: (E) Light, (F) Dark, (G) after SD; REM

power spectra during: (H) Light, (I) Dark, (J) after SD; Significance is indicated by # and lines indicate multiple significant points $p < 0.05$ (2-way RM ANOVA)

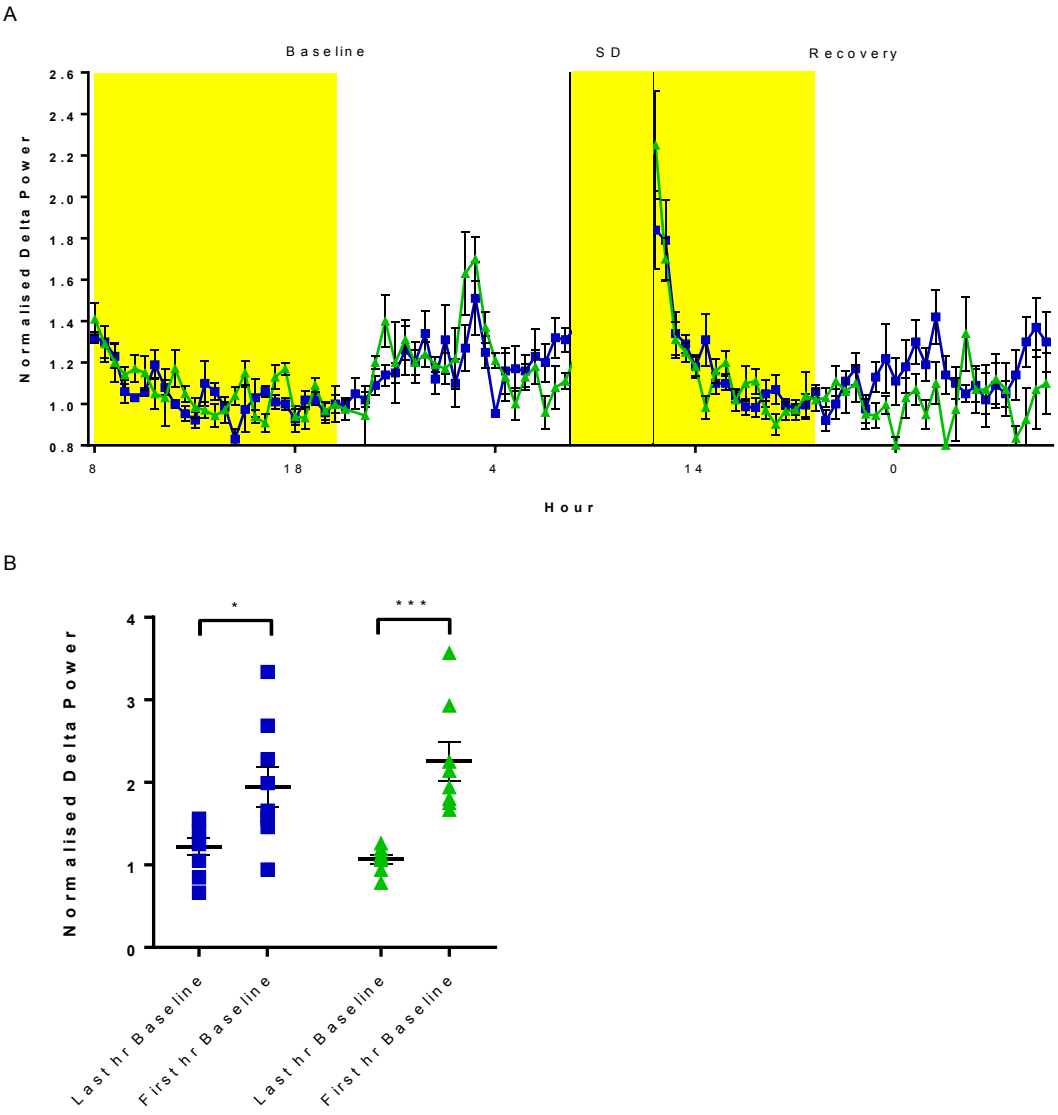

Figure 68 Delta power is normal in *Cacna1c*$^{G1616D/G1616D}$ mice.

(A) Time course showing delta power normalised to baseline split into 30-min time bins during light and dark, and during recovery after sleep deprivation, (B) Normalised delta power in the final 30 minutes before SD and the first 30 minutes after SD.

6.3 Discussion

Homozygous *Cacna1c*$^{G1616D/G1616D}$ mice survived to adulthood and did not show any premature lethality in aged mice (data not shown). This implies that this allele, when homozygous, does not cause gross cardiac dysfunction developmentally or with age.

Cacna1c$^{G1616D/G1616D}$ mice showed mixed results in tests of anxiety. In Open Field, *Cacna1c*$^{G1616D/G1616D}$ mice appeared to be less anxious than *Cacna1c*$^{+/+}$ littermate controls, as well as travelling a greater total distance. However, other tests of anxiety such as the light-dark box and elevated nought maze did not produce similar results; in these, *Cacna1c*$^{G1616D/G1616D}$ mice show a trend towards increased anxiety compared to littermate controls. This could be clarified by increasing the number of animals and repeating the experiments to increase the power.

Open Field, Light-Dark Box and Elevated mazes (Elevated Nought or Elevated Plus) are often used as a front-line test for anxiety-related behaviours in animals due to their relative simplicity of design and assumed face validity (reviewed in Cryan and Holmes (2005)). These tests are based on exploiting the conflict between the anxiety-induced avoidance of well-lit areas and the exploratory drive in mice (Holmes, 2001) and are often used to test potential anxiolytic drugs. There have been many differences observed between mouse strains, and the direction of difference is inconsistent between laboratory and between tests (Trullas and Skolnick, 1993). This could account for the inconsistencies in *Cacna1c*$^{G1616D/G1616D}$ results between Open Field, Light-Dark Box and Elevated Nought Maze; the secondary phenotyping cohort was derived from heterozygous parents that had been backcrossed eight times onto a C57BL/6J background whereas the primary phenotyping cohort had only been

backcrossed three times. As the original ENU-mutagenised sperm sample originated from male offspring of a BALB/c x C3H/HeH mating, there may have been genomic regions from C3H/HeH and BALB/c still present in the primary cohort that could affect anxiety.

More recently, the validity of these tests as true measures of anxiety has been called into question. As mice have no incentive or compulsion to enter the centre region or light areas, these tests could instead be measuring fear-induced escape or avoidance, or simply the mouse's natural preference for an unlit and protected space (Ennaceur, 2014, Ennaceur and Chazot, 2016). It is difficult to compare the results seen in *Cacna1c*$^{G1616D/G1616D}$ mice to previous studies to find examples where these tests have produced inconsistent results as there is no single index measure for anxiety – measures vary between studies and in some cases within the study to eliminate inconsistencies and present a unified phenotype, and the measure chosen is often not decided on before the test is carried out (Ennaceur and Chazot, 2016).

Attempts are now being made to create and validate new tests of anxiety that can be used to study mice, such as the 3D radial arm maze (a modification of the radial arm maze) which consists of a central area and nine arms which can be tilted upwards or downwards, and all areas are open (Ennaceur, 2014, Ennaceur and Chazot, 2016). This test is based on the supposition that in humans and animals, an ambiguous situation that is not easy to escape is a cause of anxiety and the motivation to escape provides the incentive to explore the surrounding area. Another method to try to reduce the effects of test batteries involves an integrated apparatus combining an interconnected Open Field arena, Elevated Plus maze and Light-Dark box. This has been put forward as a testing method that allows researchers to discern between anxiety and locomotor measures and eliminates the need for testing

batteries where mice are put through different phenotyping tests, each of which can increase variability due to differences in handling, time of day, or researcher (Ramos et al., 2008, Fraser et al., 2010). In future, as well as using Open Field as a first-stage phenotyping test it would be useful to validate one or both of these methods for identifying endophenotypes of psychiatric disease.

It is not yet clear how calcium influx through $Ca_v1.2$ affects anxiety. As discussed in 1.9.12, *Cacna1c*$^{+/-}$ and conditional forebrain-specific *Cacna1c*$^{-/-}$ mice show increased anxiety. The bipolar disorder risk allele SNP rs1006737 is also associated with decreased expression and anxiety, and together this suggests that it is a decrease in Ca^{2+} influx that correlates with anxiogenicity. On the other hand, pharmacological calcium channel blockers such as verapamil and nimodipine have been associated with anxiolytic properties in animal models (Moreno et al., 2014, Verma et al., 2016). Interestingly, one study has shown that this is dose-dependent; high doses of nifedipine or verapamil were anxiogenic while low doses of nifedipine had an anxiolytic effect, and the authors considered this to be produced by the opening of channels by nifedipine (Fulga and Stroescu, 1997) which would cause an increase in calcium influx. The decreased anxiety observed in *Cacna1c*$^{G1616D/G1616D}$ mice in Open Field could be due to the protein product of this allele taking slightly longer to inactivate following voltage-dependent activation and therefore increased calcium influx through $Ca_v1.2$. The anxiolytic phenotype seen in *Cacna1c*$^{G1616D/G1616D}$ mice alongside the anxiogenic phenotype seen in *Cacna1c*$^{Q1625STOP/+}$ is evidence that it is a decrease in Ca^{2+} influx through LTCC and specifically $Ca_v1.2$ that causes an increase in anxiety. $Ca_v1.2$ is, therefore, a target for drugs to alleviate anxiety disorders and in particular a target for the development of calcium channel agonists.

Cacna1c$^{G1616D/G1616D}$ mice also appear to have defects in cue-dependent learning. This is thought to be modulated by the amygdala (Phillips and LeDoux, 1992) and pharmacological blockade of L-type VGCC causes deficits in LTP (Bauer et al., 2002, Shinnick-Gallagher et al., 2003) and fear extinction, which we did not study in these mice (Davis and Bauer, 2012). On the other hand, in aged or brain-damaged rats, VGCC antagonists have been reported to enhance memory and learning (Levy et al., 1991, Levere and Walker, 1992). Together with the data from *Cacna1c*$^{G1616D/G1616D}$ mice, we can conclude that $Ca_v1.2$ is playing a role in LTP, although the exact effect and direction is yet to be specifically identified. Similar to the *Cacna1c*$^{Q1625STOP/+}$ cohort, we were not able to definitively show that these animals can hear the cue tones as well as wild-type controls (although as the mice responded to cues in the test sessions they must be able to hear at some level). The unconditioned response to a tone is usually an increase in immobility immediately after tone onset, whereas in both wild-type and *Cacna1c*$^{G1616D/G1616D}$ mice we observed no difference in percentage immobility. As mice were able to hear a click box in the SHIRPA task, it could be that this is affected by background strain, and again the baseline period may also not be long enough for the mice to acclimatise to the chamber and reduce freezing behaviour. Other studies that use this measure have much longer acclimatisation periods of up to 6 minutes, which may be long enough for mice to become acclimatised to the arena and freeze less at baseline. As well as this, we did not measure response to shock and cannot rule out changes in sensitivity.

Cacna1c$^{G1616D/G1616D}$ mice had a small but significant decrease in levels of theta frequencies during NREM and REM bouts (as described in 6.2.4.3). Theta waves have a frequency of 5-9Hz, a large amplitude and a sinusoidal rhythm, and brain

oscillations in this range are associated with memory formation and retrieval (Rutishauser et al., 2010). Theta oscillations are thought to originate in the medial septum and drive rhythms in the hippocampus, which co-ordinates further synchronisation between the medial pre-frontal cortex (mPFC) and amygdala (reviewed in Colgin (2013)). As discussed in 2.2.4 and 6.3, the amygdala and hippocampus are involved in memory formation and retrieval, and increases in theta synchronisation across these areas have been observed during cued and contextual memory retrieval (Seidenbecher et al., 2003, Pape et al., 2005, Lesting et al., 2011, Bazelot et al., 2015). Defects in cue-dependent memory retrieval observed in *Cacna1c*$^{G1616D/G1616D}$ mice could, therefore, correlate with decreased levels of theta frequencies. Further to this, theta synchronicity between the hippocampus and the mPFC correlates with avoidance of aversive compartments in tests of anxiety and are increased in 5-HT1A knockout mice (a model of anxiety) (Adhikari et al., 2010). The slight decrease in anxiety seen in *Cacna1c*$^{G1616D/G1616D}$ mice could correlate with decreased theta synchronicity. In order to test this further, *Cacna1c*$^{G1616D/G1616D}$ mice could be behaviourally phenotyped while EEG recordings are taken. The relevant tests would include Open Field and Elevated Nought Maze (as tests of anxiety) and tests of memory such as fear conditioning or operant conditioning, for example using an integrated touch screen apparatus (Hvoslef-Eide et al., 2015, Kwak et al., 2015).

SNPs in *CACNA1C* have been associated with cardiovascular disease (CVD) (Andreassen et al., 2013) and patients with schizophrenia have an increased risk of CVD due to both genetic factors and lifestyle factors including obesity and smoking (Correll et al., 2014). Increased LV volume and a small but significant decrease in fractional shortening in *Cacna1c*$^{G1616D/G1616D}$ mice may demonstrate an underlying cardiomyopathy that, with age or under stress, could predispose to the development

of CVD. An increased QT interval in these mice also indicates that this mutation may cause a gain of function, as gain of function mutations in patients have been shown to cause long-QT (Fukuyama et al., 2014, Wemhoner et al., 2015). Antipsychotics, the primary treatment for schizophrenia, have been associated with lengthened QT but their effects are unpredictable in any given individual (Zemrak and Kenna, 2008, Roden, 2004). A risk factor for increased QT after medication is an already-lengthened QT interval (Drew et al., 2010) and this work posits gain of function mutations in *CACNA1C* as potential mediators of this risk.

A specific mutation in *CACNA1C* causes Timothy Syndrome as discussed in 1.9.11. We considered that *Cacna1c*$^{G1616D/G1616D}$ may mimic some aspects of this syndrome but, while we observed a long QT which is similar to Timothy Syndrome, we did not observe any of the morphological differences which occur in patients such as syndactyly or facial dysmorphology (Splawski et al., 2004). Given that *Cacna1c*$^{G1616D/G1616D}$ mice also survive to adulthood with no reduction in survival or sudden cardiac failure, we suggest that it is a gain of function allele that is able to retain most of its normal inactivation (both voltage- and calcium-dependent). Another symptom in Timothy Syndrome patients who live long enough for evaluation is autism (Splawski et al., 2004). The causative mutation of Timothy Syndrome Type II (G406R) has been recapitulated in the mouse, and animals displayed autism-like behaviours including repetitive behaviour, altered social behaviour and vocalisation, and enhanced cued and contextual memory (Bader et al., 2011, Bett et al., 2012) although these studies did not report any cardiac phenotyping and did not observe any cardiac failure, even under high-stress conditions. They also did not report any facial deformities or syndactyly, two symptoms of Timothy Syndrome. The mechanism behind the autistic-like traits in these mice is, therefore, more complex

than a simple loss of inactivation of $Ca_v1.2$. Exon 8a (containing the mutation) also retained a neomycin cassette necessary for the survival of mice carrying the G406R mutation, which if it had enough effect on cardiac function to allow survival to adulthood may also have had an unknown effect in the brain. We did not study any autistic-like traits in either *Cacna1c* mouse line, but phenotyping tests such as marble burying (a test of repetitive behaviour), Morris water maze (to study perseverative behaviour) and social tests could be used in the future to assess whether *Cacna1c*$^{G1616D/G1616D}$ mice also have increases in these behaviours. Social dominance, social approach, and social preference tasks, such as the three-chamber task, would show whether *Cacna1c* mutations are associated with social defects (Silverman et al., 2010). Home cage monitoring would also give us insights into the reciprocal social behaviour of *Cacna1c*$^{G1616D/G1616D}$ mice within established social groups (Silverman et al., 2010, Bains et al., 2016) as well as more data about the locomotor activity and sleep patterns of these mice.

To conclude, the *Cacna1c*^{G1616D} allele is likely to be gain-of-function, causing a small but significant increase in QT interval and possibly mediating anxiety. As with *Cacna1c*^{Q1616STOP}, it would be very interesting to further test the cognition of *Cacna1c*$^{G1616D/G1616D}$ mice using Morris water maze or Y maze, or operant conditioning tests. The culture of primary hippocampal and cortical neurons from these animals could also be utilised both to study neuronal morphology and to look at calcium transients and current density. Activity-dependent gene transcription and Ca^{2+} currents could be analysed as described in 5.3, in order to study long-term effects such as LTP. In the next chapter, the validity of ENU mutagenesis as a model of psychiatric disease is evaluated.

7 Discussion

As discussed in section 1.3, mouse models of disease can be evaluated on their construct, face and predictive validity. For psychiatric disorders such as schizophrenia, there are specific considerations to take into account. Construct validity is difficult as the underlying genetic risk is made up of small variants that each cause an incremental increase in risk. Face validity is evaluated based on behavioural domains in the mouse that are then mapped onto human behavioural domains with deficits observed in patients, but these are not necessarily direct comparisons. Finally, predictive validity is difficult to achieve, as there are not many treatments that have a predictable and uniform outcome in human patients.

7.1 Validity of ENU-induced single point mutations

7.1.1 Construct validity

The polygenic risk burden in schizophrenia is mostly caused by single nucleotide polymorphisms (SNPs) – variations in a single base pair that have become common throughout the population because they do not affect fecundity (International Schizophrenia et al., 2009, Bundy et al., 2011, Kavanagh et al., 2015). Many of these SNPs are intronic or intergenic, making it difficult to predict exactly what effect they will have on gene function. As well as this, associated SNPs are not necessarily causal but may be in linkage disequilibrium with another SNP or group of SNPs (Kavanagh et al., 2015). ENU mutagenesis is useful in generating novel point mutations, as in this regard it models SNPs observed in patients with psychiatric disease although it does not recreate the exact polymorphism. Consequently, these models have moderate construct validity for behavioural deficits observed in patients with schizophrenia although, as noted previously, a mouse is extremely unlikely to

model schizophrenia as a disorder (1.3.2). ENU-induced single point mutations are advantageous as experimental tools, particularly as they can generate a series of alleles with varying functions including hypomorphic and gain-of-function.

7.1.1.1 Mutations in Cacna1c potentially model changes in protein levels and inactivation

Although we observed behavioural changes in *Cacna1c*$^{Q1625STOP/+}$ and *Cacna1c*$^{G1616D/G1616D}$ mice, we did not study the functional effect of the two mutations either *in vivo* or *in vitro*. Subsequently, we can only speculate on the changes that cause the differences in anxiety, memory and EEG spectra observed in these animals.

As discussed in chapter 5, *Cacna1c*$^{Q1625STOP/+}$ mice were more anxious in Open Field and Elevated Plus Maze, as well as having impairments in stimulus association, cue-dependent memory and context-dependent memory. This similarity in phenotype to heterozygous knock-out models (Seisenberger et al., 2000, Moosmang et al., 2005, Dao et al., 2010, Langwieser et al., 2010, Rosati et al., 2011, Lee et al., 2012) suggests that the *Cacna1c*^{Q1625STOP} mutation causes a decrease in expression or function as discussed in 5.3. Given that rs1006737, a SNP associated with schizophrenia and bipolar disorder, is an eQTL for $Ca_v1.2$ expression and has been associated with a reduced expression in some brain areas (Roussos et al., 2014, Eckart et al., 2016), this could suggest that a reduction in $Ca_v1.2$ causes deficits in specific behavioural domains. Interestingly, disruptive mutations in *CACNA1C* were identified in an exome-sequencing screen of patients with schizophrenia, and these mutations caused premature truncation of the protein (Purcell et al., 2014). The *Cacna1c*^{Q1625STOP} allele may then be modelling rare disruptive mutations in patients with schizophrenia.

Evidence of changes in $Ca_v1.2$ expression in patients with schizophrenia and bipolar disorder has been contradictory. In post-mortem brains, expression was increased in patients homozygous for the rs1006737 risk allele (Bigos et al., 2010) and this was also observed in neurons generated from induced pluripotent stem cells (iPSCs) (Yoshimizu et al., 2015). This implies that rs1006737 could be modulating expression of $Ca_v1.2$ in a region-specific manner, or that other factors in different regions or cell types are interacting to modulate expression or function. Although studies of human patients and healthy volunteers have associated the risk allele with increased anxiety, decreased startle reactivity and memory recall (Erk et al., 2010, Jogia et al., 2011, Roussos et al., 2011, Thimm et al., 2011, Hori et al., 2012, Soeiro-de-Souza et al., 2012, Erk et al., 2014a, Krug et al., 2014, Lancaster et al., 2014, Nieratschker et al., 2015, Pasparakis et al., 2015), no studies have associated behavioural effects with a particular direction of change in expression. This would be an interesting step to elucidate whether it is under- or over-expression that is associated with behavioural effects. This is likely to be difficult as there are multiple splice variants of $Ca_v1.2$, and they are expressed in a tissue-specific manner (Snutch et al., 1991, Tang et al., 2004, Lipscombe et al., 2013).

The *Cacna1c*^{G1616D} mutation, on the other hand, appears to phenocopy long-QT mutations (Wemhoner et al., 2015), suggesting it is a gain-of-function mutation. Defects in left ventricular function were observed in homozygous *Cacna1c*$^{G1616D/G1616D}$ animals, specifically increased left ventricular diameter, decreased posterior wall thickness, and decreased fractional shortening percentage (6.2.3). Although fractional shortening defects have not been associated with schizophrenia, one case study has identified a schizophrenic patient with dilated cardiomyopathy (Finsterer and Stollberger, 2016). As well as morphological changes,

Cacna1c$^{G1616D/G1616D}$ mice also had an increased QT interval. Specific heart defects are difficult to study in patients with psychosis but it is well-known that many antipsychotic drugs are cardiotoxic (Welch and Chue, 2000, Roden, 2004, Zemrak and Kenna, 2008) and that they can cause an elongated QT interval in some but not all cases (Roden, 2004, Zemrak and Kenna, 2008), and this depends on genetic predisposition. Although *CACNA1C* has not been associated with antipsychotic-induced QT interval elongation by GWAS (Aberg et al., 2012), it is possible that polymorphisms could slightly increase risk. Without GWAS of larger cohorts, we cannot assign construct validity to this mutation.

Both Timothy Syndrome and other long QT syndromes in human patients can be caused by gain-of-function mutations in *CACNA1C* (Splawski et al., 2004, Depil et al., 2011, Wemhoner et al., 2015). Calcium-imaging and electrophysiological experiments to assess calcium-dependent and voltage-dependent inactivation would allow us to confirm the effect of the mutation. If it were confirmed as a gain-of-function, this would increase the construct validity of the *Cacna1c*^{G1616D} mutation as a model for long QT disorders.

7.1.2 Face validity

As in all mouse models of psychiatric disease, ENU-induced mutations are unlikely to cause the full complement of schizophrenia phenotypes. As well as this, positive symptoms are only measurable as proxy behavioural manifestations such as defects in acoustic startle PPI and latent inhibition. These are hypothesised to be caused by misattribution of salience (Kapur, 2003, Turetsky et al., 2007, Howes and Nour, 2016).

A primary behavioural phenotyping battery was designed to assess endophenotypes that are commonly disturbed in psychiatric disease, including anxiety, locomotor activity, acoustic startle PPI, and fear conditioning. As sleep and circadian rhythm disorders are also often co-morbid with a psychiatric diagnosis (Martin et al., 2001, Cohrs, 2008, Krystal et al., 2008, Wulff et al., 2009, Wulff et al., 2010, Pritchett et al., 2012, Jagannath et al., 2013b), we also screened mutant lines for defects in these domains. This pipeline has been used previously in a forward-genetics approach to successfully identify behavioural changes caused by novel mutations (Nolan et al., 1997, Nolan et al., 2000b, Nolan et al., 2002, Jeans et al., 2007) and therefore we were confident that we would be able to observe changes in behaviour in experimental cohorts.

7.1.2.1 Mutations in Ank3 and Tcf4 do not affect behavioural domains

ENU-induced mutations in *Ank3* and *Tcf4* did not cause any effects that could be observed in the primary phenotyping screen (3.3.2 and 4.2.3). This suggests that these mutations have very little or no effect on behavioural domains in the mouse. Some potential reasons behind this are discussed in 3.4 and 4.3, but in summary, these mutations have no validity for psychiatric disorders.

Splice variants are one factor that may cause differences between *in vitro* and *in vivo* models. Both *Ank3* and *Tcf4* transcribe multiple splice variants as described in Chapter 1. All of the major *Ank3* isoforms contain the spectrin-binding domain and therefore we predicted that the $Ank3^{D1056G}$ mutation would affect spectrin binding in all isoforms throughout development. However, there are many processed $ankyrin_G$ transcripts with no known function, and the mutation may not have an effect in these variants. The 480-kDa isoform is not required for viability, although the loss of all isoforms causes perinatal lethality (Jenkins et al., 2015). This study also showed that

binding of βIV-spectrin was not disrupted by mutations in the canonical ZU5 spectrin binding domain (Jenkins et al., 2015), and so it is possible that the *Ank3*^{D1056G} mutation, although it is in the canonical spectrin-binding domain, has no effect on spectrin binding. With regards to *Tcf4*^{S275R}, although the 5' end of *Tcf4* undergoes complex splicing all *Tcf4* isoforms contain exon 11 (Sepp et al., 2011) and therefore this mutation should affect all transcripts. It is still possible that there are isoforms with unknown function that can compensate for a small effect caused by this mutation.

7.1.2.2 The Cacna1c^{Q1625STOP} *mutation affects behavioural domains associated with psychiatric disease*

Although we did not see differences in all behavioural domains, *Cacna1c*$^{Q1625STOP/+}$ mice displayed increased anxiety in Open Field and Elevated Plus Maze (5.2.2). This mirrors anxiety phenotypes observed in carriers of the rs1006737 risk allele (Erk et al., 2010, Roussos et al., 2011), suggesting that this mutation has face validity for this endophenotype. *Cacna1c*$^{Q1625STOP/+}$ mice also have a decreased proportion of delta frequencies during NREM sleep and defects in sleep homoeostasis, as shown by a decrease in delta power and slow-wave activity (5.2.3.3). SNPs in *CACNA1C* have been associated with increased sleep latency (Byrne et al., 2013) and sleep quality (Parsons et al., 2013) and although SWA has not been studied in relationship to *CACNA1C* genotype it could be that decreased sleep pressure and defects in homoeostasis are linked to sleep disruption. Decreased SWA has also been observed in patients with schizophrenia (Pritchett et al., 2012, Wulff et al., 2010, Wulff et al., 2006). Consequently, the *Cacna1c*^{Q1625STOP} allele has some face validity for this phenotype.

A decreased startle response was observed in *Cacna1c*$^{Q1625STOP/+}$ animals (5.2.2.7). Startle response is affected in carriers of the risk allele at rs1006737, although findings have been inconsistent in the direction of change (Dao et al., 2010, Roussos et al., 2011, Pasparakis et al., 2015). Heterozygous knockout in the mouse also causes a decrease in startle response (Dao et al., 2010), implying that decrease in $Ca_V1.2$ expression is correlated with a reduction in startle. It is difficult to evaluate the face validity of *Cacna1c*^{Q1625STOP} for startle reactivity, although this study supports the involvement of $Ca_V1.2$ in this domain.

Cacna1c$^{Q1625STOP/+}$ animals also had defects in stimulus association, shown by an increase in freezing after conditioning and in context (5.2.2.8). Although as discussed this cannot be definitively attributed to defects in memory, it could be an indication of misattributed salience and an increased association of the foot shock with the context. Aberrant salience is thought to be a behavioural measure of positive symptoms and psychosis (Kapur, 2003, Howes and Nour, 2016), and can be tested in the mouse using the Novel Object Recognition test, and it would be beneficial to carry this out to increase the validity of *Cacna1c*^{Q1625STOP} for aberrant salience. Further tests of cognition, such as the Morris water maze, could also increase the validity of *Cacna1c*^{Q1625STOP} for memory defects.

To summarise, the *Cacna1c*^{Q1625STOP} allele shows face validity for some behavioural domains that are affected in risk allele carriers and patients with schizophrenia.

7.1.2.3 The Cacna1c^{G1616D} mutation has a subtle effect on behavioural domains and heart function

Face validity of the *Cacna1c*^{G1616D} allele is more difficult to determine. This allele, when homozygous, is associated with a defect in cue-dependent recall. Memory

deficits are observed in patients with schizophrenia (Lencz et al., 2006, Trandafir et al., 2006, Dickinson et al., 2008, Ranganath et al., 2008, Galderisi et al., 2009) and particularly defects in extinction memory (Holt et al., 2009, Holt et al., 2012). While we did not test extinction memory, defects in conditioned memory suggest that *Cacna1c*^{G1616D} shows some face validity for memory defects in schizophrenia. Further tests of extinction memory and of other types of memory as described above would add validity to this model for cognitive deficits.

Defects in left ventricular function and an increased QT interval were observed as described above, and these are similar to the long QT observed in patients with mutations in *CACNA1C* (Fukuyama et al., 2014, Wemhoner et al., 2015), suggesting that *Cacna1c*$^{G1616D/G1616D}$ mice show some face validity for this phenotype. We considered that this model may have some face validity for Timothy Syndrome, which is characterised by syndactyly, facial deformities and autism spectrum disorders as well as a long QT interval (Splawski et al., 2004, Splawski et al., 2005, Bader et al., 2011) but we did not test any autism spectrum endophenotypes such as repetitive behaviour or social interaction. Without these tests, it is difficult to assign face validity to *Cacna1c*$^{G1616D/G1616D}$ mice as a model of Timothy Syndrome.

Cacna1c$^{G1616D/G1616D}$ mice also appear to have a slight decrease in anxiety when tested in Open Field (6.2.2.2). Conversely, in other tests of anxiety such as Light-Dark Box and Elevated Nought Maze, there was a trend towards higher anxiety. This may be due to differences in strain, and this limitation is discussed below.

In summary, *Cacna1c*$^{G1616D/G1616D}$ mice may be useful models for studying the genetic susceptibility to antipsychotic cardiotoxicity and shows some face validity for memory defects observed in patients with schizophrenia.

7.2 Limitations

7.2.1 Using the mouse to model psychiatric disorders

As previously discussed, the mouse is an extremely useful model organism to study human disease. Compared to higher mammals such as primates, mice are easy and quick to breed and maintain, and we are able to manipulate the mouse genome accurately and efficiently. Many behavioural and genetic models can be mapped directly onto their human counterparts. However, complex psychiatric traits are more difficult to translate into single measurable endophenotypes. Although many studies have evaluated the validity of endophenotypes such as acoustic startle PPI and fear conditioning as cross-species behaviours (Braff et al., 2001, Gottesman and Gould, 2003, Turetsky et al., 2007, Amann et al., 2010, Nestler and Hyman, 2010), there are still factors that have to be taken into account. It is difficult to state definitively that some behaviours in humans can be directly translated into the mouse. This particularly applies to behaviours such as anxiety and depression, which in humans are partly based on verbal reporting (American Psychiatric Association, 2013, Dickinson et al., 2008, Kirkpatrick et al., 2011). Another example is memory; there are many different types of memory (Braisby and Gellatly, 2012) and while there are well-established tests of non-declarative memory in rodents (Crawley, 2006) declarative memory is more difficult to study (Braisby and Gellatly, 2012). Some endophenotypes are now less well-validated than previously thought. For example, PPI can vary between sexes and depends on medication status (Braff et al., 2001, Turetsky et al., 2007) and may be state-dependent (Turetsky et al., 2007).

7.2.2 Impact of background strain and congenicity

A major issue in mouse genetics is the use and reporting of background strains. Inbred strains such as C57BL/6J are isogenic, and this genetic uniformity should lead

to phenotypic uniformity and therefore fewer animals can be used and statistical power is higher. There are also many resources available on the genetics and phenotypes of inbred strains. In this work, due to time constraints, re-derived lines were backcrossed only three times onto C57BL/6J as described in 2.2 before generating cohorts for phenotyping. This means that there may be some residual genomic regions from C3H/HeH x BALB/c as mutagenised sperm originated from this mixed background. Furthermore, as previously discussed, secondary cohorts of *Cacna1c*$^{G1616D/G1616D}$ failed to replicate the decrease in anxiety observed in the primary cohort. The primary cohort was derived from BC-3 mice while the secondary cohort was derived from BC-8, meaning that there may be effects of the mixed background. To control for the mixed background as much as possible, littermate controls were used. However, these will still potentially be slightly different even between siblings. Consequently, it is impossible to rule out background strain effects in this work. To remedy this, a full phenotyping battery would ideally be carried out on congenic C57BL/6J animals.

Strain differences also make it more difficult to compare across studies. As discussed in 5.3, *Cacna1c*$^{+/-}$ heterozygous mice have been maintained on a mixed 129S1/Sv × 129X1/SvJ × C57BL/6 background, which means that results from experiments on *Cacna1c*$^{+/-}$ mice and *Cacna1c* mutants in this thesis cannot be directly compared. The reason for this is not indicated in the literature, and again an ideal solution would be to generate a congenic *Cacna1c*$^{+/-}$ C57BL/6J line. This is a limitation of many genetic studies in the mouse. Alleles of interest can be maintained on a particular background for many reasons. Some background strains are more well-characterised, and for some phenotypes, certain backgrounds will display changes that are more robust. If alleles are transferred to a different background this

can confound results due to background alleles and modifier regions that may be present in the new background. This is already known to cause problems (Threadgill et al., 1997, Specht and Schoepfer, 2001, Wotjak, 2003) and there are undoubtedly such effects that have not been discovered or reported in the literature.

A recent study has shown that genetic background can limit generalisation of genotype-phenotype relationships, using *Cacna1c* as an example. The *Cacna1c* null allele was backcrossed onto C57BL/6J and *Cacna1c*$^{+/-}$ mice were found to be 99.8% identical to wild-type C57BL/6J using a SNP panel. Male heterozygous founders were then crossed to wild-type females from 30 commonly used inbred laboratory strains. F1 offspring were then behaviourally phenotyped. This work showed that differences in phenotype between heterozygous and wild-type animals can vary in degree and direction of effect, dependent on background strain (Sittig et al., 2016). There was also a small but significant effect of sex on some but not all phenotypes (Sittig et al., 2016). This shows that the reductionist approach of studying single genetic difference while holding all other genetic and environmental variables the same requires updating in order to observe potential phenotypes and to represent genetic variability in human disease more accurately.

Many resources are taking steps to improve control and reporting of background strain. Repositories and transgenic services such as The Jackson Laboratory now make information about background strain phenotype and genotype available online, as well as including the background of deposited mutants and providing materials to enable clear and consistent reporting of background strain. Other large-scale phenotyping initiatives, such as the International Mouse Phenotyping Consortium (IMPC) aim to generate knock-out models on a consistent congenic background, and these can easily be compared to coisogenic littermate controls. Again, results are

published online using ontological terms, reporting the exact background strain, and including information about the research centre that carried out the phenotyping (Koscielny et al., 2014). These centralised resources can be used by researchers to choose a background strain, predict effects of modifier regions, and accurately report the background strain used in experiments.

7.2.3 Predictive Validity

In this study, we did not examine the predictive validity of the *Cacna1c*^{Q1625STOP} or *Cacna1c*^{G1616D} mutations. Although, as discussed previously, antipsychotics are used to treat mainly positive symptoms of schizophrenia, it would be interesting to test whether they had any effect on the deficits observed in the two lines. It could be expected that they may worsen the QT lengthening in *Cacna1c*$^{G1616D/G1616D}$ as this has been shown in patients (Zemrak and Kenna, 2008). Other drug classes of interest would be anti-anxiety drugs such as benzodiazepines (Olkkola and Ahonen, 2008) and lithium, which is used to treat bipolar disorder (Ketter et al., 2016). Calcium-channel antagonists and agonists, combined with electrophysiological recordings, would also give more insight into the changes caused by each mutation (Foster, 2015).

7.3 Future Directions

There are still major inroads to be made into the genetic aetiology of psychiatric disorders. It has been shown that two novel mutations in *Cacna1c* can be used to form an allelic series and give us new insights into the function of $Ca_v1.2$ in psychiatric disease, cardiac function and the interplay between the two. Future directions may utilise next-generation mutagenesis to investigate the effect of SNPs on *CACNA1C* expression and function further, for example by recreating associated

SNPs *in vivo*. Targeted mutagenesis could also be used to induce *de novo* mutations identified through exome sequencing.

7.3.1 Gene editing

The CRISPR (clustered regularly interspaced short palindromic repeats)/Cas9 system has emerged as an efficient tool in genome editing (Ceasar et al., 2016, Gurumurthy et al., 2016). It allows targeted and precise alterations of the genome through the ability of the caspase Cas9 to cause double-stranded breaks in DNA after binding to guide RNA molecules. CRISPR/Cas9 can be used to insert or delete DNA sequences, or to change a base pair (Ceasar et al., 2016, Gurumurthy et al., 2016).

This approach could be used in mice to study the functional effect of single schizophrenia-associated SNPs. Effects on expression, behaviour, and mechanism would all increase knowledge of the contribution to disorders. On the other hand, many genetic variants are in non-coding regions (Schizophrenia Working Group of the Psychiatric Genomics, 2014) and while mice are homologous to humans in coding regions, conservation of non-coding regions is much lower (Batzoglou et al., 2000). Consequently, there is a possibility that there will be no observable change in phenotype.

Another approach using animal models is to recreate *de novo* mutations or CNVs that have been identified in exome screens of patients with psychiatric disease. A higher CNV burden is associated with schizophrenia (International Schizophrenia Consortium, 2008, Rees et al., 2011, Malhotra and Sebat, 2012) and modelling these in the mouse would give insight into the impact on behaviour. *De novo* mutations in a coding region of *ANK3* have been identified through exome screens of ASD patients,

and these would be ideal candidates for CRISPR particularly as they are at conserved residues (Bi et al., 2012).

Transgenic mouse models are extremely useful but cannot recapitulate the full genetic heterogeneity associated with schizophrenia. A different approach, which could be used in parallel, is patient-derived induced pluripotent stem cells (hiPSCs). These can then be differentiated into neuronal progenitors and neurons (Flaherty and Brennand, 2015). The advantage of using patient-derived cells is that they maintain the complete pattern of risk variants present in the patient, allowing the study of complex genetic interactions. CRISPR can then be used to add a SNP or alternatively to reverse a SNP, and then cellular phenotypes can be studied in the context of other risk alleles (Flaherty and Brennand, 2015).

7.3.2 Gene x environment interactions

While a substantial proportion of the risk of schizophrenia is genetic, environment is also important (Rapoport et al., 2012, Owen et al., 2016) The *Cacna1c*$^{Q1625STOP/+}$ and *Cacna1c*$^{G1616D/G1616D}$ mouse lines could be further utilised in a gene x environment study. This has been successfully carried out on another ENU mutant *Blind-drunk* (*Bdr*); the mutation (a dominant mutation in *Snap25*) caused sensorimotor gating deficits (Jeans et al., 2007) while variable prenatal stress (PNS) influenced anxiety-related behaviours (Oliver and Davies, 2009). When the influence of PNS on *Bdr* animals was assessed, the sensorimotor gating deficits were increased and social interaction abnormalities were observed only in *Bdr* animals from stressed dams (Oliver and Davies, 2009). This shows that the combination of a mouse point mutant with a prenatal stress paradigm produces both modified and previously unseen phenotypes, and this could also be the case in *Cacna1c* mutant lines.

7.4 Concluding Remarks

To conclude, ENU mutagenesis and a reverse genetics approach have produced novel models with potential construct validity and face validity for endophenotypes of schizophrenia and long QT syndromes. Although in some cases this approach ends with no observable phenotype (as in the case of *ANK3* and *TCF4*) we were able to generate two *Cacna1c* mutants which show varied phenotypes, and which are prospective experimental tools to link GWAS results to behavioural traits and cellular mechanisms.

8 Bibliography

Aberg, K, Adkins, DE, Liu, Y, McClay, JL, Bukszar, J, Jia, P, . . . van den Oord, EJ (2012). Genome-wide association study of antipsychotic-induced QTc interval prolongation. *Pharmacogenomics J,* 12**,** 165-72.

Aberg, KA, Liu, Y, Bukszar, J, McClay, JL, Khachane, AN, Andreassen, OA, . . . van den Oord, EJ (2013). A comprehensive family-based replication study of schizophrenia genes. *JAMA Psychiatry,* 70**,** 573-81.

Abo, A, Qu, J, Cammarano, MS, Dan, C, Fritsch, A, Baud, V, . . . Minden, A (1998). PAK4, a novel effector for Cdc42Hs, is implicated in the reorganization of the actin cytoskeleton and in the formation of filopodia. *EMBO J,* 17**,** 6527-40.

Adhikari, A, Topiwala, MA & Gordon, JA (2010). Synchronized activity between the ventral hippocampus and the medial prefrontal cortex during anxiety. *Neuron,* 65**,** 257-69.

Ahlijanian, MK, Westenbroek, RE & Catterall, WA (1990). Subunit structure and localization of dihydropyridine-sensitive calcium channels in mammalian brain, spinal cord, and retina. *Neuron,* 4**,** 819-32.

Ahuja, D, Saenz-Robles, MT & Pipas, JM (2005). SV40 large T antigen targets multiple cellular pathways to elicit cellular transformation. *Oncogene,* 24**,** 7729-45.

Amann, LC, Gandal, MJ, Halene, TB, Ehrlichman, RS, White, SL, McCarren, HS & Siegel, SJ (2010). Mouse behavioral endophenotypes for schizophrenia. *Brain Res Bull,* 83**,** 147-61.

American Psychiatric Association (2013). Schizophrenia Spectrum and Other Psychotic Disorders. *Diagnostic and Statistical Manual of Mental Disorders.* 5th ed. Washington, DC: http://dx.doi.org/10.1176/appi.books.9780890425596.dsm02.

Amiel, J, Rio, M, de Pontual, L, Redon, R, Malan, V, Boddaert, N, . . . Colleaux, L (2007). Mutations in TCF4, encoding a class I basic helix-loop-helix transcription factor, are responsible for Pitt-Hopkins syndrome, a severe epileptic encephalopathy associated with autonomic dysfunction. *Am J Hum Genet,* 80**,** 988-93.

Andreassen, OA, Djurovic, S, Thompson, WK, Schork, AJ, Kendler, KS, O'Donovan, MC, . . . Dale, AM (2013). Improved detection of common variants associated with schizophrenia by leveraging pleiotropy with cardiovascular-disease risk factors. *Am J Hum Genet,* 92**,** 197-209.

Arseneault, L, Cannon, M, Fisher, HL, Polanczyk, G, Moffitt, TE & Caspi, A (2011). Childhood trauma and children's emerging psychotic symptoms: A genetically sensitive longitudinal cohort study. *Am J Psychiatry,* 168**,** 65-72.

Athanasiu, L, Mattingsdal, M, Kahler, AK, Brown, A, Gustafsson, O, Agartz, I, . . . Andreassen, OA (2010). Gene variants associated with schizophrenia in a Norwegian genome-wide study are replicated in a large European cohort. *J Psychiatr Res,* 44**,** 748-53.

Babitch, J (1990). Channel hands. *Nature,* 346**,** 321-2.

Bader, PL, Faizi, M, Kim, LH, Owen, SF, Tadross, MR, Alfa, RW, . . . Shamloo, M (2011). Mouse model of Timothy syndrome recapitulates triad of autistic traits. *Proc Natl Acad Sci USA,* 108**,** 15432-7.

Bailey, KR & Crawley, JN 2009. Anxiety-Related Behaviors in Mice. *In:* BUCCAFUSCO, J. J. (ed.) *Methods of Behavior Analysis in Neuroscience.* 2nd ed. Boca Raton (FL).

Bailey, KRC, J. N. (2009). Anxiety-Related Behaviors in Mice. *In:* JJ, B. (ed.) *Methods of Behavior Analysis in Neuroscience.* 2nd ed. Boca Raton (FL): CRC Press/Taylor & Francis.

Bains, RS, Cater, HL, Sillito, RR, Chartsias, A, Sneddon, D, Concas, D, . . . Armstrong, JD (2016). Analysis of Individual Mouse Activity in Group Housed Animals of Different Inbred Strains using a Novel Automated Home Cage Analysis System. *Front Behav Neurosci,* 10**,** 106.

Baker, KE & Parker, R (2004). Nonsense-mediated mRNA decay: terminating erroneous gene expression. *Curr Opin Cell Biol,* 16**,** 293-9.

Banks, GT & Nolan, PM (2011). Assessment of Circadian and Light-Entrainable Parameters in Mice Using Wheel-Running Activity. *Curr Protoc Mouse Biol,* 1**,** 369-81.

Barch, DM & Smith, E (2008). The cognitive neuroscience of working memory: relevance to CNTRICS and schizophrenia. *Biol Psychiatry,* 64**,** 11-7.

Batzoglou, S, Pachter, L, Mesirov, JP, Berger, B & Lander, ES (2000). Human and mouse gene structure: comparative analysis and application to exon prediction. *Genome Res,* 10**,** 950-8.

Bauer, EP, Schafe, GE & LeDoux, JE (2002). NMDA receptors and L-type voltage-gated calcium channels contribute to long-term potentiation and different components of fear memory formation in the lateral amygdala. *J Neurosci,* 22**,** 5239-49.

Bauer, MS, Crits-Christoph, P, Ball, WA, Dewees, E, McAllister, T, Alahi, P, . . . Whybrow, PC (1991). Independent assessment of manic and depressive symptoms by self-rating. Scale characteristics and implications for the study of mania. *Arch Gen Psychiatry,* 48**,** 807-12.

Bazelot, M, Bocchio, M, Kasugai, Y, Fischer, D, Dodson, PD, Ferraguti, F & Capogna, M (2015). Hippocampal Theta Input to the Amygdala Shapes Feedforward Inhibition to Gate Heterosynaptic Plasticity. *Neuron,* 87**,** 1290-303.

Benca, RM, Gilliland, MA & Obermeyer, WH (1998). Effects of lighting conditions on sleep and wakefulness in albino Lewis and pigmented Brown Norway rats. *Sleep,* 21**,** 451-60.

Bender, KJ & Trussell, LO (2012). The physiology of the axon initial segment. *Annu Rev Neurosci,* 35**,** 249-65.

Benmocha Guggenheimer, A, Almagor, L, Tsemakhovich, V, Tripathy, DR, Hirsch, JA & Dascal, N (2016). Interactions between N and C termini of alpha1C subunit regulate inactivation of CaV1.2 L-type Ca(2+) channel. *Channels (Austin),* 10**,** 55-68.

Berghs, S, Aggujaro, D, Dirkx, R, Jr., Maksimova, E, Stabach, P, Hermel, JM, . . . Solimena, M (2000). betaIV spectrin, a new spectrin localized at axon initial segments and nodes of ranvier in the central and peripheral nervous system. *J Cell Biol,* 151**,** 985-1002.

Bergqvist, I, Eriksson, M, Saarikettu, J, Eriksson, B, Corneliussen, B, Grundstrom, T & Holmberg, D (2000). The basic helix-loop-helix transcription factor E2-2 is involved in T lymphocyte development. *Eur J Immunol,* 30**,** 2857-63.

Bertrand, N, Castro, DS & Guillemot, F (2002). Proneural genes and the specification of neural cell types. *Nat Rev Neurosci,* 3**,** 517-30.

Bett, GC, Lis, A, Wersinger, SR, Baizer, JS, Duffey, ME & Rasmusson, RL (2012). A Mouse Model of Timothy Syndrome: a Complex Autistic Disorder Resulting from a Point Mutation in Cav1.2. *N Am J Med Sci (Boston),* 5**,** 135-140.

Bi, C, Wu, J, Jiang, T, Liu, Q, Cai, W, Yu, P, . . . Sun, ZS (2012). Mutations of ANK3 identified by exome sequencing are associated with autism susceptibility. *Hum Mutat,* 33**,** 1635-8.

Biel, M, Ruth, P, Bosse, E, Hullin, R, Stuhmer, W, Flockerzi, V & Hofmann, F (1990). Primary structure and functional expression of a high voltage activated calcium channel from rabbit lung. *FEBS Lett,* 269**,** 409-12.

Bigos, KL, Mattay, VS, Callicott, JH, Straub, RE, Vakkalanka, R, Kolachana, B, . . . Weinberger, DR (2010). Genetic variation in CACNA1C affects brain circuitries related to mental illness. *Arch Gen Psychiatry,* 67**,** 939-45.

Blackwood, DH, Fordyce, A, Walker, MT, St Clair, DM, Porteous, DJ & Muir, WJ (2001). Schizophrenia and affective disorders--cosegregation with a translocation at chromosome 1q42 that directly disrupts brain-expressed genes: clinical and P300 findings in a family. *Am J Hum Genet,* 69**,** 428-33.

Bonoldi, I & Howes, OD (2013). The enduring centrality of dopamine in the pathophysiology of schizophrenia: in vivo evidence from the prodrome to the first psychotic episode. *Adv Pharmacol,* 68**,** 199-220.

Bourque, F, van der Ven, E & Malla, A (2011). A meta-analysis of the risk for psychotic disorders among first- and second-generation immigrants. *Psychol Med,* 41**,** 897-910.

Bouzidi, M, Tricaud, N, Giraud, P, Kordeli, E, Caillol, G, Deleuze, C, . . . Alcaraz, G (2002). Interaction of the Nav1.2a subunit of the voltage-dependent sodium channel with nodal ankyrinG. In vitro mapping of the interacting domains and association in synaptosomes. *J Biol Chem,* 277**,** 28996-9004.

Boydell, J, van Os, J, McKenzie, K, Allardyce, J, Goel, R, McCreadie, RG & Murray, RM (2001). Incidence of schizophrenia in ethnic minorities in London: ecological study into interactions with environment. *BMJ,* 323**,** 1336-8.

Braff, DL, Geyer, MA & Swerdlow, NR (2001). Human studies of prepulse inhibition of startle: normal subjects, patient groups, and pharmacological studies. *Psychopharmacology (Berl),* 156**,** 234-58.

Braga, RJ, Reynolds, GP & Siris, SG (2013). Anxiety comorbidity in schizophrenia. *Psychiatry Res,* 210**,** 1-7.

Braisby, N & Gellatly, A (2012). *Cognitive psychology,* Oxford, Oxford University Press.

Brandon, NJ, Millar, JK, Korth, C, Sive, H, Singh, KK & Sawa, A (2009). Understanding the role of DISC1 in psychiatric disease and during normal development. *J Neurosci,* 29**,** 12768-75.

Bresnahan, M, Begg, MD, Brown, A, Schaefer, C, Sohler, N, Insel, B, . . . Susser, E (2007). Race and risk of schizophrenia in a US birth cohort: another example of health disparity? *Int J Epidemiol,* 36**,** 751-8.

Brigman, JL, Padukiewicz, KE, Sutherland, ML & Rothblat, LA (2006). Executive functions in the heterozygous reeler mouse model of schizophrenia. *Behav Neurosci,* 120**,** 984-8.

Briskman, I, Bar, G, Boaz, M & Shargorodsky, M (2012). Impact of co-morbid mental illness on the diagnosis and management of patients hospitalized for medical conditions in a general hospital. *Int J Psychiatry Med,* 43**,** 339-48.

Brockschmidt, A, Todt, U, Ryu, S, Hoischen, A, Landwehr, C, Birnbaum, S, . . . Weber, RG (2007). Severe mental retardation with breathing abnormalities (Pitt-Hopkins syndrome) is caused by haploinsufficiency of the neuronal bHLH transcription factor TCF4. *Hum Mol Genet,* 16**,** 1488-94.

Brown, AS (2012). Epidemiologic studies of exposure to prenatal infection and risk of schizophrenia and autism. *Dev Neurobiol,* 72**,** 1272-6.

Brown, AS, Begg, MD, Gravenstein, S, Schaefer, CA, Wyatt, RJ, Bresnahan, M, . . . Susser, ES (2004). Serologic evidence of prenatal influenza in the etiology of schizophrenia. *Arch Gen Psychiatry,* 61**,** 774-80.

Brown, AS, Cohen, P, Harkavy-Friedman, J, Babulas, V, Malaspina, D, Gorman, JM & Susser, ES (2001). A.E. Bennett Research Award. Prenatal rubella, premorbid abnormalities, and adult schizophrenia. *Biol Psychiatry,* 49**,** 473-86.

Brown, AS, Schaefer, CA, Quesenberry, CP, Jr., Liu, L, Babulas, VP & Susser, ES (2005). Maternal exposure to toxoplasmosis and risk of schizophrenia in adult offspring. *Am J Psychiatry,* 162**,** 767-73.

Brown, AS, Vinogradov, S, Kremen, WS, Poole, JH, Bao, Y, Kern, D & McKeague, IW (2011). Association of maternal genital and reproductive infections with verbal memory and motor deficits in adult schizophrenia. *Psychiatry Res,* 188**,** 179-86.

Brzozka, MM, Radyushkin, K, Wichert, SP, Ehrenreich, H & Rossner, MJ (2010). Cognitive and sensorimotor gating impairments in transgenic mice overexpressing the schizophrenia susceptibility gene Tcf4 in the brain. *Biol Psychiatry,* 68**,** 33-40.

Brzozka, MM & Rossner, MJ (2013). Deficits in trace fear memory in a mouse model of the schizophrenia risk gene TCF4. *Behav Brain Res,* 237**,** 348-56.

Buckley, PF, Miller, BJ, Lehrer, DS & Castle, DJ (2009). Psychiatric Comorbidities and Schizophrenia. *Schizophrenia Bulletin,* 35**,** 383-402.

Bundy, H, Stahl, D & MacCabe, JH (2011). A systematic review and meta-analysis of the fertility of patients with schizophrenia and their unaffected relatives. *Acta Psychiatr Scand,* 123**,** 98-106.

Burns, JK, Tomita, A & Kapadia, AS (2014). Income inequality and schizophrenia: increased schizophrenia incidence in countries with high levels of income inequality. *Int J Soc Psychiatry,* 60**,** 185-96.

Burrows, EL, McOmish, CE & Hannan, AJ (2011). Gene-environment interactions and construct validity in preclinical models of psychiatric disorders. *Prog Neuropsychopharmacol Biol Psychiatry,* 35**,** 1376-82.

Busi, F & Cresteil, T (2005). CYP3A5 mRNA degradation by nonsense-mediated mRNA decay. *Mol Pharmacol,* 68**,** 808-15.

Bustillo, JR, Chen, H, Jones, T, Lemke, N, Abbott, C, Qualls, C, . . . Gasparovic, C (2014). Increased glutamine in patients undergoing long-term treatment for schizophrenia: a proton magnetic resonance spectroscopy study at 3 T. *JAMA Psychiatry,* 71**,** 265-72.

Bustillo, JR, Rowland, LM, Mullins, P, Jung, R, Chen, H, Qualls, C, . . . Lauriello, J (2010). 1H-MRS at 4 tesla in minimally treated early schizophrenia. *Mol Psychiatry,* 15**,** 629-36.

Byrne, EM, Gehrman, PR, Medland, SE, Nyholt, DR, Heath, AC, Madden, PA, . . . Chronogen, C (2013). A genome-wide association study of sleep habits and insomnia. *Am J Med Genet B Neuropsychiatr Genet,* 162B**,** 439-51.

Cannon, TD, Kaprio, J, Lonnqvist, J, Huttunen, M & Koskenvuo, M (1998). The genetic epidemiology of schizophrenia in a Finnish twin cohort. A population-based modeling study. *Arch Gen Psychiatry,* 55**,** 67-74.

Cano, A & Portillo, F (2010). An emerging role for class I bHLH E2-2 proteins in EMT regulation and tumor progression. *Cell Adh Migr,* 4**,** 56-60.

Cantero, JL, Atienza, M, Stickgold, R, Kahana, MJ, Madsen, JR & Kocsis, B (2003). Sleep-dependent theta oscillations in the human hippocampus and neocortex. *J Neurosci,* 23**,** 10897-903.

Cantor-Graae, E & Selten, JP (2005). Schizophrenia and migration: a meta-analysis and review. *Am J Psychiatry,* 162**,** 12-24.

Carbon, M & Correll, CU (2014). Thinking and acting beyond the positive: the role of the cognitive and negative symptoms in schizophrenia. *CNS Spectr,* 19 Suppl 1**,** 38-52; quiz 35-7, 53.

Cardno, AG, Marshall, EJ, Coid, B, Macdonald, AM, Ribchester, TR, Davies, NJ, . . . Murray, RM (1999). Heritability estimates for psychotic disorders: the Maudsley twin psychosis series. *Arch Gen Psychiatry,* 56**,** 162-8.

Carlsson, A & Lindqvist, M (1963). Effect of Chlorpromazine or Haloperidol on Formation of 3methoxytyramine and Normetanephrine in Mouse Brain. *Acta Pharmacol Toxicol (Copenh),* 20**,** 140-4.

Carlsson, A, Lindqvist, M & Magnusson, T (1957). 3,4-Dihydroxyphenylalanine and 5-hydroxytryptophan as reserpine antagonists. *Nature,* 180**,** 1200.

Catling, AD, Schaeffer, HJ, Reuter, CW, Reddy, GR & Weber, MJ (1995). A proline-rich sequence unique to MEK1 and MEK2 is required for raf binding and regulates MEK function. *Mol Cell Biol,* 15**,** 5214-25.

Catterall, WA (2000). Structure and regulation of voltage-gated Ca2+ channels. *Annu Rev Cell Dev Biol,* 16**,** 521-55.

Catterall, WA, Perez-Reyes, E, Snutch, TP & Striessnig, J (2005). International Union of Pharmacology. XLVIII. Nomenclature and structure-function relationships of voltage-gated calcium channels. *Pharmacol Rev,* 57**,** 411-25.

Cavalli-Sforza, LL (2005). The Human Genome Diversity Project: past, present and future. *Nat Rev Genet,* 6**,** 333-40.

Ceasar, SA, Rajan, V, Prykhozhij, SV, Berman, JN & Ignacimuthu, S (2016). Insert, remove or replace: A highly advanced genome editing system using CRISPR/Cas9. *Biochim Biophys Acta,* 1863**,** 2333-44.

Chadman, KK, Yang, M & Crawley, JN (2009). Criteria for validating mouse models of psychiatric diseases. *Am J Med Genet B Neuropsychiatr Genet,* 150B**,** 1-11.

Chadwick, P, Strauss, C, Jones, AM, Kingdon, D, Ellett, L, Dannahy, L & Hayward, M (2016). Group mindfulness-based intervention for distressing voices: A pragmatic randomised controlled trial. *Schizophr Res,* 175**,** 168-73.

Chan, MS, Chung, KF, Yung, KP & Yeung, WF (2016). Sleep in schizophrenia: A systematic review and meta-analysis of polysomnographic findings in case-control studies. *Sleep Med Rev.* Mar 10 2016 ed.

Chang, WC, Hui, CL, Tang, JY, Wong, GH, Chan, SK, Lee, EH & Chen, EY (2013). Impacts of duration of untreated psychosis on cognition and negative symptoms in first-episode schizophrenia: a 3-year prospective follow-up study. *Psychol Med,* 43**,** 1883-93.

Chang, YF, Imam, JS & Wilkinson, MF (2007). The nonsense-mediated decay RNA surveillance pathway. *Annu Rev Biochem,* 76**,** 51-74.

Chen, DT, Jiang, X, Akula, N, Shugart, YY, Wendland, JR, Steele, CJ, . . . Strauss, J (2013). Genome-wide association study meta-analysis of European and Asian-ancestry samples identifies three novel loci associated with bipolar disorder. *Mol Psychiatry,* 18**,** 195-205.

Chesney, E, Goodwin, GM & Fazel, S (2014). Risks of all-cause and suicide mortality in mental disorders: a meta-review. *World Psychiatry,* 13**,** 153-60.

Chouinard, S, Poulin, J, Stip, E & Godbout, R (2004). Sleep in untreated patients with schizophrenia: a meta-analysis. *Schizophr Bull,* 30**,** 957-67.
Chow, TJ, Tee, SF, Yong, HS & Tang, PY (2016). Genetic Association of TCF4 and AKT1 Gene Variants with the Age at Onset of Schizophrenia. *Neuropsychobiology,* 73**,** 233-240.
Chung, SH, Marzban, H, Aldinger, K, Dixit, R, Millen, K, Schuurmans, C & Hawkes, R (2011). Zac1 plays a key role in the development of specific neuronal subsets in the mouse cerebellum. *Neural Dev,* 6**,** 25.
Chwastiak, LA, Rosenheck, RA, McEvoy, JP, Stroup, TS, Swartz, MS, Davis, SM & Lieberman, JA (2009). The impact of obesity on health care costs among persons with schizophrenia. *Gen Hosp Psychiatry,* 31**,** 1-7.
Cisse, B, Caton, ML, Lehner, M, Maeda, T, Scheu, S, Locksley, R, . . . Reizis, B (2008). Transcription factor E2-2 is an essential and specific regulator of plasmacytoid dendritic cell development. *Cell,* 135**,** 37-48.
Clapcote, SJ & Roder, JC (2006). Deletion polymorphism of Disc1 is common to all 129 mouse substrains: implications for gene-targeting studies of brain function. *Genetics,* 173**,** 2407-10.
Coghill, EL, Hugill, A, Parkinson, N, Davison, C, Glenister, P, Clements, S, . . . Brown, SD (2002). A gene-driven approach to the identification of ENU mutants in the mouse. *Nat Genet,* 30**,** 255-6.
Cohrs, S (2008). Sleep disturbances in patients with schizophrenia : impact and effect of antipsychotics. *CNS Drugs,* 22**,** 939-62.
Colgin, LL (2013). Mechanisms and functions of theta rhythms. *Annu Rev Neurosci,* 36**,** 295-312.
Collins, AL, Kim, Y, Sklar, P, International Schizophrenia, C, O'Donovan, MC & Sullivan, PF (2012). Hypothesis-driven candidate genes for schizophrenia compared to genome-wide association results. *Psychol Med,* 42**,** 607-16.
Cooper, CL, Vandaele, S, Barhanin, J, Fosset, M, Lazdunski, M & Hosey, MM (1987). Purification and characterization of the dihydropyridine-sensitive voltage-dependent calcium channel from cardiac tissue. *J Biol Chem,* 262**,** 509-12.
Cooper, SJ, Reynolds, GP, With expert, c-a, Barnes, T, England, E, Haddad, PM, . . . Smith, J (2016). BAP guidelines on the management of weight gain, metabolic disturbances and cardiovascular risk associated with psychosis and antipsychotic drug treatment. *J Psychopharmacol,* 30**,** 717-48.
Correll, CU, Robinson, DG, Schooler, NR, Brunette, MF, Mueser, KT, Rosenheck, RA, . . . Kane, JM (2014). Cardiometabolic risk in patients with first-episode schizophrenia spectrum disorders: baseline results from the RAISE-ETP study. *JAMA Psychiatry,* 71**,** 1350-63.
Corvin, A, Craddock, N & Sullivan, PF (2010). Genome-wide association studies: a primer. *Psychol Med,* 40**,** 1063-77.
Craddock, N, O'Donovan, MC & Owen, MJ (2007). Phenotypic and genetic complexity of psychosis. Invited commentary on ... Schizophrenia: a common disease caused by multiple rare alleles. *Br J Psychiatry,* 190**,** 200-3.
Crawley, JN 2006. Learning and Memory. *What's Wrong With My Mouse?* : John Wiley & Sons, Inc.
Crawley, JN, Belknap, JK, Collins, A, Crabbe, JC, Frankel, W, Henderson, N, . . . Paylor, R (1997). Behavioral phenotypes of inbred mouse strains: implications and recommendations for molecular studies. *Psychopharmacology (Berl),* 132**,** 107-24.

Cross-Disorder Group of the Psychiatric Genomics, C (2013). Identification of risk loci with shared effects on five major psychiatric disorders: a genome-wide analysis. *Lancet,* 381**,** 1371-9.

Cross-Disorder Group of the Psychiatric Genomics, C, Lee, SH, Ripke, S, Neale, BM, Faraone, SV, Purcell, SM, . . . International Inflammatory Bowel Disease Genetics, C (2013). Genetic relationship between five psychiatric disorders estimated from genome-wide SNPs. *Nat Genet,* 45**,** 984-94.

Crump, SM, Andres, DA, Sievert, G & Satin, J (2013). The cardiac L-type calcium channel distal carboxy terminus autoinhibition is regulated by calcium. *Am J Physiol Heart Circ Physiol,* 304**,** H455-64.

Crunelli, V, David, F, Lorincz, ML & Hughes, SW (2015). The thalamocortical network as a single slow wave-generating unit. *Curr Opin Neurobiol,* 31**,** 72-80.

Crusio, WE (2004). Flanking gene and genetic background problems in genetically manipulated mice. *Biol Psychiatry,* 56**,** 381-5.

Cryan, JF & Holmes, A (2005). The ascent of mouse: advances in modelling human depression and anxiety. *Nat Rev Drug Discov,* 4**,** 775-90.

Cunha, SR & Mohler, PJ (2006). Cardiac ankyrins: Essential components for development and maintenance of excitable membrane domains in heart. *Cardiovasc Res,* 71**,** 22-9.

Cutajar, MC, Mullen, PE, Ogloff, JR, Thomas, SD, Wells, DL & Spataro, J (2010). Schizophrenia and other psychotic disorders in a cohort of sexually abused children. *Arch Gen Psychiatry,* 67**,** 1114-9.

Dan, I, Watanabe, NM & Kusumi, A (2001). The Ste20 group kinases as regulators of MAP kinase cascades. *Trends Cell Biol,* 11**,** 220-30.

Dao, DT, Mahon, PB, Cai, X, Kovacsics, CE, Blackwell, RA, Arad, M, . . . Gould, TD (2010). Mood disorder susceptibility gene CACNA1C modifies mood-related behaviors in mice and interacts with sex to influence behavior in mice and diagnosis in humans. *Biol Psychiatry,* 68**,** 801-10.

David, F, Schmiedt, JT, Taylor, HL, Orban, G, Di Giovanni, G, Uebele, VN, . . . Crunelli, V (2013). Essential thalamic contribution to slow waves of natural sleep. *J Neurosci,* 33**,** 19599-610.

Davis, JQ & Bennett, V (1994). Ankyrin binding activity shared by the neurofascin/L1/NrCAM family of nervous system cell adhesion molecules. *J Biol Chem,* 269**,** 27163-6.

Davis, JQ, Lambert, S & Bennett, V (1996). Molecular composition of the node of Ranvier: identification of ankyrin-binding cell adhesion molecules neurofascin (mucin+/third FNIII domain-) and NrCAM at nodal axon segments. *J Cell Biol,* 135**,** 1355-67.

Davis, JQ, McLaughlin, T & Bennett, V (1993). Ankyrin-binding proteins related to nervous system cell adhesion molecules: candidates to provide transmembrane and intercellular connections in adult brain. *J Cell Biol,* 121**,** 121-33.

Davis, SE & Bauer, EP (2012). L-type voltage-gated calcium channels in the basolateral amygdala are necessary for fear extinction. *J Neurosci,* 32**,** 13582-6.

de Jong, S, van Eijk, KR, Zeegers, DW, Strengman, E, Janson, E, Veldink, JH, . . . Consortium, PGCS (2012). Expression QTL analysis of top loci from GWAS meta-analysis highlights additional schizophrenia candidate genes. *Eur J Hum Genet,* 20**,** 1004-8.

De Jongh, KS, Colvin, AA, Wang, KK & Catterall, WA (1994). Differential proteolysis of the full-length form of the L-type calcium channel alpha 1 subunit by calpain. *J Neurochem,* 63**,** 1558-64.

de Leon, M, Wang, Y, Jones, L, Perez-Reyes, E, Wei, X, Soong, TW, . . . Yue, DT (1995). Essential Ca(2+)-binding motif for Ca(2+)-sensitive inactivation of L-type Ca2+ channels. *Science,* 270**,** 1502-6.

De Peri, L, Crescini, A, Deste, G, Fusar-Poli, P, Sacchetti, E & Vita, A (2012). Brain structural abnormalities at the onset of schizophrenia and bipolar disorder: a meta-analysis of controlled magnetic resonance imaging studies. *Curr Pharm Des,* 18**,** 486-94.

de Pontual, L, Mathieu, Y, Golzio, C, Rio, M, Malan, V, Boddaert, N, . . . Amiel, J (2009). Mutational, functional, and expression studies of the TCF4 gene in Pitt-Hopkins syndrome. *Hum Mutat,* 30**,** 669-76.

Deboer, T (2015). Behavioral and electrophysiological correlates of sleep and sleep homeostasis. *Curr Top Behav Neurosci,* 25**,** 1-24.

Del Rio, M, Imam, A, DeLeon, M, Gomez, G, Mishra, J, Ma, Q, . . . Devarajan, P (2004). The death domain of kidney ankyrin interacts with Fas and promotes Fas-mediated cell death in renal epithelia. *J Am Soc Nephrol,* 15**,** 41-51.

Delvecchio, G, Dima, D & Frangou, S (2015). The effect of ANK3 bipolar-risk polymorphisms on the working memory circuitry differs between loci and according to risk-status for bipolar disorder. *Am J Med Genet B Neuropsychiatr Genet,* 168B**,** 188-96.

Demjaha, A, Egerton, A, Murray, RM, Kapur, S, Howes, OD, Stone, JM & McGuire, PK (2014). Antipsychotic treatment resistance in schizophrenia associated with elevated glutamate levels but normal dopamine function. *Biol Psychiatry,* 75**,** e11-3.

Demjaha, A, Murray, RM, McGuire, PK, Kapur, S & Howes, OD (2012). Dopamine synthesis capacity in patients with treatment-resistant schizophrenia. *Am J Psychiatry,* 169**,** 1203-10.

Depil, K, Beyl, S, Stary-Weinzinger, A, Hohaus, A, Timin, E & Hering, S (2011). Timothy mutation disrupts the link between activation and inactivation in Ca(V)1.2 protein. *J Biol Chem,* 286**,** 31557-64.

Dick, IE, Tadross, MR, Liang, H, Tay, LH, Yang, W & Yue, DT (2008). A modular switch for spatial Ca2+ selectivity in the calmodulin regulation of CaV channels. *Nature,* 451**,** 830-4.

Dickinson, D, Ragland, JD, Gold, JM & Gur, RC (2008). General and specific cognitive deficits in schizophrenia: Goliath defeats David? *Biol Psychiatry,* 64**,** 823-7.

Dickinson, D, Ramsey, ME & Gold, JM (2007). Overlooking the obvious: a meta-analytic comparison of digit symbol coding tasks and other cognitive measures in schizophrenia. *Arch Gen Psychiatry,* 64**,** 532-42.

Dijk, DJ & Czeisler, CA (1995). Contribution of the circadian pacemaker and the sleep homeostat to sleep propensity, sleep structure, electroencephalographic slow waves, and sleep spindle activity in humans. *J Neurosci,* 15**,** 3526-38.

Dissmeyer, N & Schnittger, A (2011). Use of phospho-site substitutions to analyze the biological relevance of phosphorylation events in regulatory networks. *Methods Mol Biol,* 779**,** 93-138.

Dolmetsch, RE, Pajvani, U, Fife, K, Spotts, JM & Greenberg, ME (2001). Signaling to the nucleus by an L-type calcium channel-calmodulin complex through the MAP kinase pathway. *Science,* 294**,** 333-9.

Drew, BJ, Ackerman, MJ, Funk, M, Gibler, WB, Kligfield, P, Menon, V, . . . the American College of Cardiology, F (2010). Prevention of torsade de pointes in hospital settings: a scientific statement from the American Heart Association and the American College of Cardiology Foundation. *Circulation,* 121**,** 1047-60.

Dubreuil, RR, MacVicar, G, Dissanayake, S, Liu, C, Homer, D & Hortsch, M (1996). Neuroglian-mediated cell adhesion induces assembly of the membrane skeleton at cell contact sites. *J Cell Biol,* 133**,** 647-55.

Duffield, GE, Watson, NP, Mantani, A, Peirson, SN, Robles-Murguia, M, Loros, JJ, . . . Dunlap, JC (2009). A role for Id2 in regulating photic entrainment of the mammalian circadian system. *Curr Biol,* 19**,** 297-304.

Duncan, M, DiCicco-Bloom, EM, Xiang, X, Benezra, R & Chada, K (1992). The gene for the helix-loop-helix protein, Id, is specifically expressed in neural precursors. *Dev Biol,* 154**,** 1-10.

Durak, O, de Anda, FC, Singh, KK, Leussis, MP, Petryshen, TL, Sklar, P & Tsai, LH (2015). Ankyrin-G regulates neurogenesis and Wnt signaling by altering the subcellular localization of beta-catenin. *Mol Psychiatry,* 20**,** 388-97.

Eckart, N, Song, Q, Yang, R, Wang, R, Zhu, H, McCallion, AS & Avramopoulos, D (2016). Functional Characterization of Schizophrenia-Associated Variation in CACNA1C. *PLoS One,* 11**,** e0157086.

Eckert, R & Chad, JE (1984). Inactivation of Ca channels. *Prog Biophys Mol Biol,* 44**,** 215-67.

Egerton, A, Brugger, S, Raffin, M, Barker, GJ, Lythgoe, DJ, McGuire, PK & Stone, JM (2012). Anterior cingulate glutamate levels related to clinical status following treatment in first-episode schizophrenia. *Neuropsychopharmacology,* 37**,** 2515-21.

Egerton, A, Chaddock, CA, Winton-Brown, TT, Bloomfield, MA, Bhattacharyya, S, Allen, P, . . . Howes, OD (2013). Presynaptic striatal dopamine dysfunction in people at ultra-high risk for psychosis: findings in a second cohort. *Biol Psychiatry,* 74**,** 106-12.

Einarson, MB & Chao, MV (1995). Regulation of Id1 and its association with basic helix-loop-helix proteins during nerve growth factor-induced differentiation of PC12 cells. *Mol Cell Biol,* 15**,** 4175-83.

Einat, H (2006). Modelling facets of mania--new directions related to the notion of endophenotypes. *J Psychopharmacol,* 20**,** 714-22.

Ennaceur, A (2014). Tests of unconditioned anxiety - pitfalls and disappointments. *Physiol Behav,* 135**,** 55-71.

Ennaceur, A & Chazot, PL (2016). Preclinical animal anxiety research - flaws and prejudices. *Pharmacol Res Perspect,* 4**,** e00223.

Erk, S, Meyer-Lindenberg, A, Linden, DE, Lancaster, T, Mohnke, S, Grimm, O, . . . Walter, H (2014a). Replication of brain function effects of a genome-wide supported psychiatric risk variant in the CACNA1C gene and new multi-locus effects. *Neuroimage,* 94**,** 147-54.

Erk, S, Meyer-Lindenberg, A, Schmierer, P, Mohnke, S, Grimm, O, Garbusow, M, . . . Walter, H (2014b). Hippocampal and frontolimbic function as intermediate phenotype for psychosis: evidence from healthy relatives and a common risk variant in CACNA1C. *Biol Psychiatry,* 76**,** 466-75.

Erk, S, Meyer-Lindenberg, A, Schnell, K, Opitz von Boberfeld, C, Esslinger, C, Kirsch, P, . . . Walter, H (2010). Brain function in carriers of a genome-wide supported bipolar disorder variant. *Arch Gen Psychiatry,* 67**,** 803-11.

Ertel, EA, Campbell, KP, Harpold, MM, Hofmann, F, Mori, Y, Perez-Reyes, E, . . . Catterall, WA (2000). Nomenclature of voltage-gated calcium channels. *Neuron,* 25**,** 533-5.
Escudero, I & Johnstone, M (2014). Genetics of schizophrenia. *Curr Psychiatry Rep,* 16**,** 502.
Evans, MD, Sammons, RP, Lebron, S, Dumitrescu, AS, Watkins, TB, Uebele, VN, . . . Grubb, MS (2013). Calcineurin signaling mediates activity-dependent relocation of the axon initial segment. *J Neurosci,* 33**,** 6950-63.
Farah, MH, Olson, JM, Sucic, HB, Hume, RI, Tapscott, SJ & Turner, DL (2000). Generation of neurons by transient expression of neural bHLH proteins in mammalian cells. *Development,* 127**,** 693-702.
Featherstone, RE, Liang, Y, Saunders, JA, Tatard-Leitman, VM, Ehrlichman, RS & Siegel, SJ (2012). Subchronic ketamine treatment leads to permanent changes in EEG, cognition and the astrocytic glutamate transporter EAAT2 in mice. *Neurobiol Dis,* 47**,** 338-46.
Feinberg, I (1982). Schizophrenia: caused by a fault in programmed synaptic elimination during adolescence? *J Psychiatr Res,* 17**,** 319-34.
Feinberg, I, Braun, M, Koresko, RL & Gottlieb, F (1969). Stage 4 sleep in schizophrenia. *Arch Gen Psychiatry,* 21**,** 262-6.
Ferrarelli, F, Peterson, MJ, Sarasso, S, Riedner, BA, Murphy, MJ, Benca, RM, . . . Tononi, G (2010). Thalamic dysfunction in schizophrenia suggested by whole-night deficits in slow and fast spindles. *Am J Psychiatry,* 167**,** 1339-48.
Ferre-D'Amare, AR, Prendergast, GC, Ziff, EB & Burley, SK (1993). Recognition by Max of its cognate DNA through a dimeric b/HLH/Z domain. *Nature,* 363**,** 38-45.
Ferreira, MA, O'Donovan, MC, Meng, YA, Jones, IR, Ruderfer, DM, Jones, L, . . . Wellcome Trust Case Control, C (2008). Collaborative genome-wide association analysis supports a role for ANK3 and CACNA1C in bipolar disorder. *Nat Genet,* 40**,** 1056-8.
Finsterer, J & Stollberger, C (2016). Noncompaction and Dilated Cardiomyopathy in a Patient with Schizophrenia. *Case Rep Cardiol,* 2016**,** 7384264.
Fischer, M, Harvald, B & Hauge, M (1969). A Danish twin study of schizophrenia. *Br J Psychiatry,* 115**,** 981-90.
Fisher, SP, Godinho, SI, Pothecary, CA, Hankins, MW, Foster, RG & Peirson, SN (2012). Rapid assessment of sleep-wake behavior in mice. *J Biol Rhythms,* 27**,** 48-58.
Flaherty, EK & Brennand, KJ. (2015). Using hiPSCs to model neuropsychiatric copy number variations (CNVs) has potential to reveal underlying disease mechanisms. *Brain Res* [Online], 10.1016/j.brainres.2015.11.009. Available: http://www.ncbi.nlm.nih.gov/pubmed/26581337 [Accessed Nov 12].
Flora, A, Garcia, JJ, Thaller, C & Zoghbi, HY (2007). The E-protein Tcf4 interacts with Math1 to regulate differentiation of a specific subset of neuronal progenitors. *Proc Natl Acad Sci USA,* 104**,** 15382-7.
Foley, DL & Morley, KI (2011). Systematic review of early cardiometabolic outcomes of the first treated episode of psychosis. *Arch Gen Psychiatry,* 68**,** 609-16.
Forest, G, Poulin, J, Daoust, AM, Lussier, I, Stip, E & Godbout, R (2007). Attention and non-REM sleep in neuroleptic-naive persons with schizophrenia and control participants. *Psychiatry Res,* 149**,** 33-40.

Forrest, M, Chapman, RM, Doyle, AM, Tinsley, CL, Waite, A & Blake, DJ (2012). Functional analysis of TCF4 missense mutations that cause Pitt-Hopkins syndrome. *Hum Mutat,* 33**,** 1676-86.

Forrest, MP, Waite, AJ, Martin-Rendon, E & Blake, DJ (2013). Knockdown of human TCF4 affects multiple signaling pathways involved in cell survival, epithelial to mesenchymal transition and neuronal differentiation. *PLoS One,* 8**,** e73169.

Foster, RW (2015). *Basic pharmacology,* Amsterdam, Butterworth-Heinemann.

Franken, P, Malafosse, A & Tafti, M (1998). Genetic variation in EEG activity during sleep in inbred mice. *Am J Physiol,* 275**,** R1127-37.

Fraser, LM, Brown, RE, Hussin, A, Fontana, M, Whittaker, A, O'Leary, TP, . . . Ramos, A (2010). Measuring anxiety- and locomotion-related behaviours in mice: a new way of using old tests. *Psychopharmacology (Berl),* 211**,** 99-112.

Fromer, M, Pocklington, AJ, Kavanagh, DH, Williams, HJ, Dwyer, S, Gormley, P, . . . O'Donovan, MC (2014). De novo mutations in schizophrenia implicate synaptic networks. *Nature,* 506**,** 179-84.

Fu, Y, Westenbroek, RE, Yu, FH, Clark, JP, 3rd, Marshall, MR, Scheuer, T & Catterall, WA (2011). Deletion of the distal C terminus of CaV1.2 channels leads to loss of beta-adrenergic regulation and heart failure in vivo. *J Biol Chem,* 286**,** 12617-26.

Fukuyama, M, Wang, Q, Kato, K, Ohno, S, Ding, WG, Toyoda, F, . . . Horie, M (2014). Long QT syndrome type 8: novel CACNA1C mutations causing QT prolongation and variant phenotypes. *Europace,* 16**,** 1828-37.

Fulga, IG & Stroescu, V (1997). Experimental research on the effect of calcium channel blockers nifedipine and verapamil on the anxiety in mice. *Rom J Physiol,* 34**,** 127-36.

Fustin, JM, O'Neill, JS, Hastings, MH, Hazlerigg, DG & Dardente, H (2009). Cry1 circadian phase in vitro: wrapped up with an E-box. *J Biol Rhythms,* 24**,** 16-24.

Gagelin, C, Constantin, B, Deprette, C, Ludosky, MA, Recouvreur, M, Cartaud, J, . . . Kordeli, E (2002). Identification of Ank(G107), a muscle-specific ankyrin-G isoform. *J Biol Chem,* 277**,** 12978-87.

Galderisi, S, Davidson, M, Kahn, RS, Mucci, A, Boter, H, Gheorghe, MD, . . . group, E (2009). Correlates of cognitive impairment in first episode schizophrenia: the EUFEST study. *Schizophr Res,* 115**,** 104-14.

Galderisi, S, Mucci, A, Bitter, I, Libiger, J, Bucci, P, Fleischhacker, WW, . . . Eufest Study, G (2013). Persistent negative symptoms in first episode patients with schizophrenia: results from the European First Episode Schizophrenia Trial. *Eur Neuropsychopharmacol,* 23**,** 196-204.

Galiano, MR, Jha, S, Ho, TS, Zhang, C, Ogawa, Y, Chang, KJ, . . . Rasband, MN (2012). A distal axonal cytoskeleton forms an intra-axonal boundary that controls axon initial segment assembly. *Cell,* 149**,** 1125-39.

Gao, T, Bunemann, M, Gerhardstein, BL, Ma, H & Hosey, MM (2000). Role of the C terminus of the alpha 1C (CaV1.2) subunit in membrane targeting of cardiac L-type calcium channels. *J Biol Chem,* 275**,** 25436-44.

Gao, T, Cuadra, AE, Ma, H, Bunemann, M, Gerhardstein, BL, Cheng, T, . . . Hosey, MM (2001). C-terminal fragments of the alpha 1C (CaV1.2) subunit associate with and regulate L-type calcium channels containing C-terminal-truncated alpha 1C subunits. *J Biol Chem,* 276**,** 21089-97.

Gasser, A, Ho, TS, Cheng, X, Chang, KJ, Waxman, SG, Rasband, MN & Dib-Hajj, SD (2012). An ankyrinG-binding motif is necessary and sufficient for targeting

Nav1.6 sodium channels to axon initial segments and nodes of Ranvier. *J Neurosci,* 32**,** 7232-43.
Ge, W, He, F, Kim, KJ, Blanchi, B, Coskun, V, Nguyen, L, . . . Sun, YE (2006). Coupling of cell migration with neurogenesis by proneural bHLH factors. *Proc Natl Acad Sci USA,* 103**,** 1319-24.
Geddes, JR, Verdoux, H, Takei, N, Lawrie, SM, Bovet, P, Eagles, JM, . . . Murray, RM (1999). Schizophrenia and complications of pregnancy and labor: an individual patient data meta-analysis. *Schizophr Bull,* 25**,** 413-23.
Ghosh, HS, Cisse, B, Bunin, A, Lewis, KL & Reizis, B (2010). Continuous expression of the transcription factor e2-2 maintains the cell fate of mature plasmacytoid dendritic cells. *Immunity,* 33**,** 905-16.
Giedd, JN, Blumenthal, J, Jeffries, NO, Castellanos, FX, Liu, H, Zijdenbos, A, . . . Rapoport, JL (1999). Brain development during childhood and adolescence: a longitudinal MRI study. *Nat Neurosci,* 2**,** 861-3.
Gifford, JL, Walsh, MP & Vogel, HJ (2007). Structures and metal-ion-binding properties of the Ca2+-binding helix-loop-helix EF-hand motifs. *Biochem J,* 405**,** 199-221.
Gingrich, JA & Hen, R (2000). The broken mouse: the role of development, plasticity and environment in the interpretation of phenotypic changes in knockout mice. *Curr Opin Neurobiol,* 10**,** 146-52.
Girard, SL, Dion, PA & Rouleau, GA (2012). Schizophrenia genetics: putting all the pieces together. *Curr Neurol Neurosci Rep,* 12**,** 261-6.
Giugiario, M, Crivelli, B, Mingrone, C, Montemagni, C, Scalese, M, Sigaudo, M, . . . Rocca, P (2012). Cognitive function and competitive employment in schizophrenia: relative contribution of insight and psychopathology. *Soc Psychiatry Psychiatr Epidemiol,* 47**,** 553-61.
Goder, R, Boigs, M, Braun, S, Friege, L, Fritzer, G, Aldenhoff, JB & Hinze-Selch, D (2004). Impairment of visuospatial memory is associated with decreased slow wave sleep in schizophrenia. *J Psychiatr Res,* 38**,** 591-9.
Goldfarb, AN, Lewandowska, K & Pennell, CA (1998). Identification of a highly conserved module in E proteins required for in vivo helix-loop-helix dimerization. *J Biol Chem,* 273**,** 2866-73.
Gomez-Ospina, N, Panagiotakos, G, Portmann, T, Pasca, SP, Rabah, D, Budzillo, A, . . . Dolmetsch, RE (2013). A promoter in the coding region of the calcium channel gene CACNA1C generates the transcription factor CCAT. *PLoS One,* 8**,** e60526.
Gomez-Ospina, N, Tsuruta, F, Barreto-Chang, O, Hu, L & Dolmetsch, R (2006). The C terminus of the L-type voltage-gated calcium channel Ca(V)1.2 encodes a transcription factor. *Cell,* 127**,** 591-606.
Goold, CP & Nicoll, RA (2010). Single-cell optogenetic excitation drives homeostatic synaptic depression. *Neuron,* 68**,** 512-28.
Gordon, JW, Scangos, GA, Plotkin, DJ, Barbosa, JA & Ruddle, FH (1980). Genetic transformation of mouse embryos by microinjection of purified DNA. *Proc Natl Acad Sci U S A,* 77**,** 7380-4.
Gottesman, II & Gould, TD (2003). The endophenotype concept in psychiatry: etymology and strategic intentions. *Am J Psychiatry,* 160**,** 636-45.
Green, EK, Hamshere, M, Forty, L, Gordon-Smith, K, Fraser, C, Russell, E, . . . Craddock, N (2013). Replication of bipolar disorder susceptibility alleles and identification of two novel genome-wide significant associations in a new bipolar disorder case-control sample. *Mol Psychiatry,* 18**,** 1302-7.

Greenberg, ME, Thompson, MA & Sheng, M (1992). Calcium regulation of immediate early gene transcription. *J Physiol Paris,* 86**,** 99-108.
Grillon, C, Ameli, R, Charney, DS, Krystal, J & Braff, D (1992). Startle gating deficits occur across prepulse intensities in schizophrenic patients. *Biol Psychiatry,* 32**,** 939-43.
Grubb, MS & Burrone, J (2010a). Activity-dependent relocation of the axon initial segment fine-tunes neuronal excitability. *Nature,* 465**,** 1070-4.
Grubb, MS & Burrone, J (2010b). Building and maintaining the axon initial segment. *Curr Opin Neurobiol,* 20**,** 481-8.
Guan, F, Zhang, B, Yan, T, Li, L, Liu, F, Li, T, . . . Li, S (2014). MIR137 gene and target gene CACNA1C of miR-137 contribute to schizophrenia susceptibility in Han Chinese. *Schizophr Res,* 152**,** 97-104.
Gurumurthy, CB, Grati, M, Ohtsuka, M, Schilit, SL, Quadros, RM & Liu, XZ (2016). CRISPR: a versatile tool for both forward and reverse genetics research. *Hum Genet,* 135**,** 971-6.
Haeseleer, F, Imanishi, Y, Sokal, I, Filipek, S & Palczewski, K (2002). Calcium-binding proteins: intracellular sensors from the calmodulin superfamily. *Biochem Biophys Res Commun,* 290**,** 615-23.
Haijma, SV, Van Haren, N, Cahn, W, Koolschijn, PC, Hulshoff Pol, HE & Kahn, RS (2013). Brain volumes in schizophrenia: a meta-analysis in over 18 000 subjects. *Schizophr Bull,* 39**,** 1129-38.
Halasz, P, Bodizs, R, Parrino, L & Terzano, M (2014). Two features of sleep slow waves: homeostatic and reactive aspects--from long term to instant sleep homeostasis. *Sleep Med,* 15**,** 1184-95.
Hall, J, Trent, S, Thomas, KL, O'Donovan, MC & Owen, MJ (2015). Genetic risk for schizophrenia: convergence on synaptic pathways involved in plasticity. *Biol Psychiatry,* 77**,** 52-8.
Hall, MH, Levy, DL, Salisbury, DF, Haddad, S, Gallagher, P, Lohan, M, . . . Smoller, JW (2014). Neurophysiologic effect of GWAS derived schizophrenia and bipolar risk variants. *Am J Med Genet B Neuropsychiatr Genet,* 165B**,** 9-18.
Halling, DB, Aracena-Parks, P & Hamilton, SL (2006). Regulation of voltage-gated Ca2+ channels by calmodulin. *Sci STKE,* 2006**,** er1.
Hammond, JC, Shan, D, Meador-Woodruff, JH & McCullumsmith, RE 2014. Evidence of Glutamatergic Dysfunction in the Pathophysiology of Schizophrenia. *In:* POPOLI, M., DIAMOND, D. & SANACORA, G. (eds.) *Synaptic Stress and Pathogenesis of Neuropsychiatric Disorders.* New York, NY: Springer New York.
Hamshere, ML, Walters, JT, Smith, R, Richards, AL, Green, E, Grozeva, D, . . . O'Donovan, MC (2013). Genome-wide significant associations in schizophrenia to ITIH3/4, CACNA1C and SDCCAG8, and extensive replication of associations reported by the Schizophrenia PGC. *Mol Psychiatry,* 18**,** 708-12.
Hansen, J, Snow, C, Tuttle, E, Ghoneim, DH, Yang, CS, Spencer, A, . . . Paciorkowski, AR (2015). De novo mutations in SIK1 cause a spectrum of developmental epilepsies. *Am J Hum Genet,* 96**,** 682-90.
Hardin, PE (2004). Transcription regulation within the circadian clock: the E-box and beyond. *J Biol Rhythms,* 19**,** 348-60.
Harris, LW, Sharp, T, Gartlon, J, Jones, DN & Harrison, PJ (2003). Long-term behavioural, molecular and morphological effects of neonatal NMDA receptor antagonism. *Eur J Neurosci,* 18**,** 1706-10.

Hashemi, SM, Hund, TJ & Mohler, PJ (2009). Cardiac ankyrins in health and disease. *J Mol Cell Cardiol,* 47**,** 203-9.
Hasler, G, Drevets, WC, Manji, HK & Charney, DS (2004). Discovering endophenotypes for major depression. *Neuropsychopharmacology,* 29**,** 1765-81.
Hedstrom, KL, Ogawa, Y & Rasband, MN (2008). AnkyrinG is required for maintenance of the axon initial segment and neuronal polarity. *J Cell Biol,* 183**,** 635-40.
Hedstrom, KL & Rasband, MN (2006). Intrinsic and extrinsic determinants of ion channel localization in neurons. *J Neurochem,* 98**,** 1345-52.
Heise, I. (2015). *Characterisation of ENU induced mutations affecting sleep/wake behaviour in mice.* PhD, Open University.
Heise, I, Fisher, SP, Banks, GT, Wells, S, Peirson, SN, Foster, RG & Nolan, PM (2015). Sleep-like behavior and 24-h rhythm disruption in the Tc1 mouse model of Down syndrome. *Genes Brain Behav,* 14**,** 209-16.
Hell, JW, Westenbroek, RE, Breeze, LJ, Wang, KK, Chavkin, C & Catterall, WA (1996). N-methyl-D-aspartate receptor-induced proteolytic conversion of postsynaptic class C L-type calcium channels in hippocampal neurons. *Proc Natl Acad Sci USA,* 93**,** 3362-7.
Hell, JW, Westenbroek, RE, Warner, C, Ahlijanian, MK, Prystay, W, Gilbert, MM, . . . Catterall, WA (1993). Identification and differential subcellular localization of the neuronal class C and class D L-type calcium channel alpha 1 subunits. *J Cell Biol,* 123**,** 949-62.
Hennekens, CH, Hennekens, AR, Hollar, D & Casey, DE (2005). Schizophrenia and increased risks of cardiovascular disease. *Am Heart J,* 150**,** 1115-21.
Henry, JD & Crawford, JR (2005). A meta-analytic review of verbal fluency deficits in schizophrenia relative to other neurocognitive deficits. *Cogn Neuropsychiatry,* 10**,** 1-33.
Henthorn, P, Kiledjian, M & Kadesch, T (1990a). Two distinct transcription factors that bind the immunoglobulin enhancer microE5/kappa 2 motif. *Science,* 247**,** 467-70.
Henthorn, P, McCarrick-Walmsley, R & Kadesch, T (1990b). Sequence of the cDNA encoding ITF-2, a positive-acting transcription factor. *Nucleic Acids Res,* 18**,** 678.
Herbst, A & Kolligs, FT (2008). A conserved domain in the transcription factor ITF-2B attenuates its activity. *Biochem Biophys Res Commun,* 370**,** 327-31.
Heresco-Levy, U & Javitt, DC (2004). Comparative effects of glycine and D-cycloserine on persistent negative symptoms in schizophrenia: a retrospective analysis. *Schizophr Res,* 66**,** 89-96.
Ho, TS, Zollinger, DR, Chang, KJ, Xu, M, Cooper, EC, Stankewich, MC, . . . Rasband, MN (2014). A hierarchy of ankyrin-spectrin complexes clusters sodium channels at nodes of Ranvier. *Nat Neurosci,* 17**,** 1664-72.
Hofer, GF, Hohenthanner, K, Baumgartner, W, Groschner, K, Klugbauer, N, Hofmann, F & Romanin, C (1997). Intracellular Ca2+ inactivates L-type Ca2+ channels with a Hill coefficient of approximately 1 and an inhibition constant of approximately 4 microM by reducing channel's open probability. *Biophys J,* 73**,** 1857-65.
Holmes, A (2001). Targeted gene mutation approaches to the study of anxiety-like behavior in mice. *Neurosci Biobehav Rev,* 25**,** 261-73.

Holt, DJ, Coombs, G, Zeidan, MA, Goff, DC & Milad, MR (2012). Failure of neural responses to safety cues in schizophrenia. *Arch Gen Psychiatry,* 69**,** 893-903.

Holt, DJ, Lebron-Milad, K, Milad, MR, Rauch, SL, Pitman, RK, Orr, SP, . . . Goff, DC (2009). Extinction memory is impaired in schizophrenia. *Biol Psychiatry,* 65**,** 455-63.

Homayoun, H & Moghaddam, B (2007). NMDA receptor hypofunction produces opposite effects on prefrontal cortex interneurons and pyramidal neurons. *J Neurosci,* 27**,** 11496-500.

Hori, H, Yamamoto, N, Fujii, T, Teraishi, T, Sasayama, D, Matsuo, J, . . . Kunugi, H (2012). Effects of the CACNA1C risk allele on neurocognition in patients with schizophrenia and healthy individuals. *Sci Rep,* 2**,** 634.

Hortsch, M, Homer, D, Malhotra, JD, Chang, S, Frankel, J, Jefford, G & Dubreuil, RR (1998). Structural requirements for outside-in and inside-out signaling by Drosophila neuroglian, a member of the L1 family of cell adhesion molecules. *J Cell Biol,* 142**,** 251-61.

Howes, O, Bose, S, Turkheimer, F, Valli, I, Egerton, A, Stahl, D, . . . McGuire, P (2011a). Progressive increase in striatal dopamine synthesis capacity as patients develop psychosis: a PET study. *Mol Psychiatry,* 16**,** 885-6.

Howes, O, McCutcheon, R & Stone, J (2015). Glutamate and dopamine in schizophrenia: an update for the 21st century. *J Psychopharmacol,* 29**,** 97-115.

Howes, OD, Bose, SK, Turkheimer, F, Valli, I, Egerton, A, Valmaggia, LR, . . . McGuire, P (2011b). Dopamine synthesis capacity before onset of psychosis: a prospective [18F]-DOPA PET imaging study. *Am J Psychiatry,* 168**,** 1311-7.

Howes, OD, Egerton, A, Allan, V, McGuire, P, Stokes, P & Kapur, S (2009a). Mechanisms underlying psychosis and antipsychotic treatment response in schizophrenia: insights from PET and SPECT imaging. *Curr Pharm Des,* 15**,** 2550-9.

Howes, OD, Kambeitz, J, Kim, E, Stahl, D, Slifstein, M, Abi-Dargham, A & Kapur, S (2012). The nature of dopamine dysfunction in schizophrenia and what this means for treatment. *Arch Gen Psychiatry,* 69**,** 776-86.

Howes, OD, Montgomery, AJ, Asselin, MC, Murray, RM, Valli, I, Tabraham, P, . . . Grasby, PM (2009b). Elevated striatal dopamine function linked to prodromal signs of schizophrenia. *Arch Gen Psychiatry,* 66**,** 13-20.

Howes, OD & Murray, RM (2014). Schizophrenia: an integrated sociodevelopmental-cognitive model. *Lancet,* 383**,** 1677-87.

Howes, OD & Nour, MM (2016). Dopamine and the aberrant salience hypothesis of schizophrenia. *World Psychiatry,* 15**,** 3-4.

Hruz, T, Laule, O, Szabo, G, Wessendorp, F, Bleuler, S, Oertle, L, . . . Zimmermann, P (2008). Genevestigator v3: a reference expression database for the meta-analysis of transcriptomes. *Adv Bioinformatics,* 2008**,** 420747.

Huber, R, Deboer, T & Tobler, I (2000). Effects of sleep deprivation on sleep and sleep EEG in three mouse strains: empirical data and simulations. *Brain Res,* 857**,** 8-19.

Hvoslef-Eide, M, Mar, AC, Nilsson, SR, Alsio, J, Heath, CJ, Saksida, LM, . . . Bussey, TJ (2015). The NEWMEDS rodent touchscreen test battery for cognition relevant to schizophrenia. *Psychopharmacology (Berl),* 232**,** 3853-72.

Imredy, JP & Yue, DT (1994). Mechanism of Ca(2+)-sensitive inactivation of L-type Ca2+ channels. *Neuron,* 12**,** 1301-18.

Ingraham, LJ & Kety, SS (2000). Adoption studies of schizophrenia. *Am J Med Genet,* 97**,** 18-22.

International Schizophrenia, C, Purcell, SM, Wray, NR, Stone, JL, Visscher, PM, O'Donovan, MC, . . . Sklar, P (2009). Common polygenic variation contributes to risk of schizophrenia and bipolar disorder. *Nature,* 460**,** 748-52.

International Schizophrenia Consortium (2008). Rare chromosomal deletions and duplications increase risk of schizophrenia. *Nature,* 455**,** 237-41.

Iqbal, Z, Vandeweyer, G, van der Voet, M, Waryah, AM, Zahoor, MY, Besseling, JA, . . . Rooms, L (2013). Homozygous and heterozygous disruptions of ANK3: at the crossroads of neurodevelopmental and psychiatric disorders. *Hum Mol Genet,* 22**,** 1960-70.

Ishizuka, K, Chen, J, Taya, S, Li, W, Millar, JK, Xu, Y, . . . Sawa, A (2007). Evidence that many of the DISC1 isoforms in C57BL/6J mice are also expressed in 129S6/SvEv mice. *Mol Psychiatry,* 12**,** 897-9.

Ising, HK, Kraan, TC, Rietdijk, J, Dragt, S, Klaassen, RM, Boonstra, N, . . . van der Gaag, M (2016). Four-Year Follow-up of Cognitive Behavioral Therapy in Persons at Ultra-High Risk for Developing Psychosis: The Dutch Early Detection Intervention Evaluation (EDIE-NL) Trial. *Schizophr Bull.*

Ison, JR, Allen, PD & O'Neill, WE (2007). Age-related hearing loss in C57BL/6J mice has both frequency-specific and non-frequency-specific components that produce a hyperacusis-like exaggeration of the acoustic startle reflex. *J Assoc Res Otolaryngol,* 8**,** 539-50.

Jagannath, A, Butler, R, Godinho, SI, Couch, Y, Brown, LA, Vasudevan, SR, . . . Peirson, SN (2013a). The CRTC1-SIK1 pathway regulates entrainment of the circadian clock. *Cell,* 154**,** 1100-11.

Jagannath, A, Peirson, SN & Foster, RG (2013b). Sleep and circadian rhythm disruption in neuropsychiatric illness. *Curr Opin Neurobiol,* 23**,** 888-94.

Javitt, DC (2010). Glutamatergic theories of schizophrenia. *Isr J Psychiatry Relat Sci,* 47**,** 4-16.

Javitt, DC, Balla, A, Burch, S, Suckow, R, Xie, S & Sershen, H (2004). Reversal of phencyclidine-induced dopaminergic dysregulation by N-methyl-D-aspartate receptor/glycine-site agonists. *Neuropsychopharmacology,* 29**,** 300-7.

Jeans, AF, Oliver, PL, Johnson, R, Capogna, M, Vikman, J, Molnar, Z, . . . Davies, KE (2007). A dominant mutation in Snap25 causes impaired vesicle trafficking, sensorimotor gating, and ataxia in the blind-drunk mouse. *Proc Natl Acad Sci USA,* 104**,** 2431-6.

Jenkins, PM, Kim, N, Jones, SL, Tseng, WC, Svitkina, TM, Yin, HH & Bennett, V (2015). Giant ankyrin-G: a critical innovation in vertebrate evolution of fast and integrated neuronal signaling. *Proc Natl Acad Sci USA,* 112**,** 957-64.

Jenkins, PM, Vasavda, C, Hostettler, J, Davis, JQ, Abdi, K & Bennett, V (2013). E-cadherin polarity is determined by a multifunction motif mediating lateral membrane retention through ankyrin-G and apical-lateral transcytosis through clathrin. *J Biol Chem,* 288**,** 14018-31.

Jenkins, SM & Bennett, V (2001). Ankyrin-G coordinates assembly of the spectrin-based membrane skeleton, voltage-gated sodium channels, and L1 CAMs at Purkinje neuron initial segments. *J Cell Biol,* 155**,** 739-46.

Jeon, D, Kim, S, Chetana, M, Jo, D, Ruley, HE, Lin, SY, . . . Shin, HS (2010). Observational fear learning involves affective pain system and Cav1.2 Ca2+ channels in ACC. *Nat Neurosci,* 13**,** 482-8.

Jiang, H, Qiao, F, Li, Z, Zhang, Y, Cheng, Y, Xu, X & Yu, L (2015). Evaluating the association between CACNA1C rs1006737 and schizophrenia risk: A meta-analysis. *Asia Pac Psychiatry,* 7**,** 260-7.

Jogia, J, Ruberto, G, Lelli-Chiesa, G, Vassos, E, Maieru, M, Tatarelli, R, . . . Frangou, S (2011). The impact of the CACNA1C gene polymorphism on frontolimbic function in bipolar disorder. *Mol Psychiatry,* 16**,** 1070-1.

John, JP, Lukose, A, Bagepally, BS, Halahalli, HN, Moily, NS, Vijayakumari, AA & Jain, S (2015). A systematic examination of brain volumetric abnormalities in recent-onset schizophrenia using voxel-based, surface-based and region-of-interest-based morphometric analyses. *J Negat Results Biomed,* 14**,** 11.

Johnson, LN (2009). The regulation of protein phosphorylation. *Biochem Soc Trans,* 37**,** 627-41.

Jones, D (2011). Genetic engineering of a mouse: Dr. Frank Ruddle and somatic cell genetics. *Yale J Biol Med,* 84**,** 117-24.

Justice, MJ, Noveroske, JK, Weber, JS, Zheng, B & Bradley, A (1999). Mouse ENU mutagenesis. *Hum Mol Genet,* 8**,** 1955-63.

Kalscheuer, VM, Feenstra, I, Van Ravenswaaij-Arts, CM, Smeets, DF, Menzel, C, Ullmann, R, . . . Ropers, HH (2008). Disruption of the TCF4 gene in a girl with mental retardation but without the classical Pitt-Hopkins syndrome. *Am J Med Genet A,* 146A**,** 2053-9.

Kamiya, A, Kubo, K, Tomoda, T, Takaki, M, Youn, R, Ozeki, Y, . . . Sawa, A (2005). A schizophrenia-associated mutation of DISC1 perturbs cerebral cortex development. *Nat Cell Biol,* 7**,** 1167-78.

Kapur, S (2003). Psychosis as a state of aberrant salience: a framework linking biology, phenomenology, and pharmacology in schizophrenia. *Am J Psychiatry,* 160**,** 13-23.

Kavanagh, DH, Tansey, KE, O'Donovan, MC & Owen, MJ (2015). Schizophrenia genetics: emerging themes for a complex disorder. *Mol Psychiatry,* 20**,** 72-6.

Kavelaars, A, Vroon, A, Raatgever, RP, Fong, AM, Premont, RT, Patel, DD, . . . Heijnen, CJ (2003). Increased acute inflammation, leukotriene B4-induced chemotaxis, and signaling in mice deficient for G protein-coupled receptor kinase 6. *J Immunol,* 171**,** 6128-34.

Keefe, RS, Eesley, CE & Poe, MP (2005). Defining a cognitive function decrement in schizophrenia. *Biol Psychiatry,* 57**,** 688-91.

Kendler, KS & Robinette, CD (1983). Schizophrenia in the National Academy of Sciences-National Research Council Twin Registry: a 16-year update. *Am J Psychiatry,* 140**,** 1551-63.

Kenny, EM, Cormican, P, Furlong, S, Heron, E, Kenny, G, Fahey, C, . . . Morris, DW (2014). Excess of rare novel loss-of-function variants in synaptic genes in schizophrenia and autism spectrum disorders. *Mol Psychiatry,* 19**,** 872-9.

Keshavan, MS, Anderson, S & Pettegrew, JW (1994). Is schizophrenia due to excessive synaptic pruning in the prefrontal cortex? The Feinberg hypothesis revisited. *J Psychiatr Res,* 28**,** 239-65.

Keshavan, MS, Reynolds, CF, 3rd, Miewald, MJ, Montrose, DM, Sweeney, JA, Vasko, RC, Jr. & Kupfer, DJ (1998). Delta sleep deficits in schizophrenia: evidence from automated analyses of sleep data. *Arch Gen Psychiatry,* 55**,** 443-8.

Ketter, TA, Miller, S, Dell'Osso, B & Wang, PW (2016). Treatment of bipolar disorder: Review of evidence regarding quetiapine and lithium. *J Affect Disord,* 191**,** 256-73.

Kew, JN & Kemp, JA (2005). Ionotropic and metabotropic glutamate receptor structure and pharmacology. *Psychopharmacology (Berl),* 179**,** 4-29.
Kim, AH, Parker, EK, Williamson, V, McMichael, GO, Fanous, AH & Vladimirov, VI (2012). Experimental validation of candidate schizophrenia gene ZNF804A as target for hsa-miR-137. *Schizophr Res,* 141**,** 60-4.
Kim, E, Howes, OD, Turkheimer, FE, Kim, BH, Jeong, JM, Kim, JW, . . . Kwon, JS (2013). The relationship between antipsychotic D2 occupancy and change in frontal metabolism and working memory : A dual [(11)C]raclopride and [(18) F]FDG imaging study with aripiprazole. *Psychopharmacology (Berl),* 227**,** 221-9.
Kim, SY, Lee, H, Kim, HJ, Bang, E, Lee, SH, Lee, DW, . . . Choe, BY (2011). In vivo and ex vivo evidence for ketamine-induced hyperglutamatergic activity in the cerebral cortex of the rat: Potential relevance to schizophrenia. *NMR Biomed,* 24**,** 1235-42.
Kirkbride, JB, Errazuriz, A, Croudace, TJ, Morgan, C, Jackson, D, Boydell, J, . . . Jones, PB (2012). Incidence of schizophrenia and other psychoses in England, 1950-2009: a systematic review and meta-analyses. *PLoS One,* 7**,** e31660.
Kirkbride, JB, Fearon, P, Morgan, C, Dazzan, P, Morgan, K, Tarrant, J, . . . Jones, PB (2006). Heterogeneity in incidence rates of schizophrenia and other psychotic syndromes: findings from the 3-center AeSOP study. *Arch Gen Psychiatry,* 63**,** 250-8.
Kirkpatrick, B, Strauss, GP, Nguyen, L, Fischer, BA, Daniel, DG, Cienfuegos, A & Marder, SR (2011). The brief negative symptom scale: psychometric properties. *Schizophr Bull,* 37**,** 300-5.
Ko, CH & Takahashi, JS (2006). Molecular components of the mammalian circadian clock. *Hum Mol Genet,* 15 Spec No 2**,** R271-7.
Koike, H, Arguello, PA, Kvajo, M, Karayiorgou, M & Gogos, JA (2006). Disc1 is mutated in the 129S6/SvEv strain and modulates working memory in mice. *Proc Natl Acad Sci USA,* 103**,** 3693-7.
Komada, M & Soriano, P (2002). [Beta]IV-spectrin regulates sodium channel clustering through ankyrin-G at axon initial segments and nodes of Ranvier. *J Cell Biol,* 156**,** 337-48.
Kordeli, E, Lambert, S & Bennett, V (1995). AnkyrinG. A new ankyrin gene with neural-specific isoforms localized at the axonal initial segment and node of Ranvier. *J Biol Chem,* 270**,** 2352-9.
Koscielny, G, Yaikhom, G, Iyer, V, Meehan, TF, Morgan, H, Atienza-Herrero, J, . . . Parkinson, H (2014). The International Mouse Phenotyping Consortium Web Portal, a unified point of access for knockout mice and related phenotyping data. *Nucleic Acids Res,* 42**,** D802-9.
Krug, A, Witt, SH, Backes, H, Dietsche, B, Nieratschker, V, Shah, NJ, . . . Kircher, T (2014). A genome-wide supported variant in CACNA1C influences hippocampal activation during episodic memory encoding and retrieval. *Eur Arch Psychiatry Clin Neurosci,* 264**,** 103-10.
Krystal, AD, Thakur, M & Roth, T (2008). Sleep disturbance in psychiatric disorders: effects on function and quality of life in mood disorders, alcoholism, and schizophrenia. *Ann Clin Psychiatry,* 20**,** 39-46.
Krystal, JH, Karper, LP, Seibyl, JP, Freeman, GK, Delaney, R, Bremner, JD, . . . Charney, DS (1994). Subanesthetic effects of the noncompetitive NMDA

antagonist, ketamine, in humans. Psychotomimetic, perceptual, cognitive, and neuroendocrine responses. *Arch Gen Psychiatry,* 51**,** 199-214.
Kumar, D, Dedic, N, Flachskamm, C, Voule, S, Deussing, JM & Kimura, M (2015). Cacna1c (Cav1.2) Modulates Electroencephalographic Rhythm and Rapid Eye Movement Sleep Recovery. *Sleep,* 38**,** 1371-80.
Kupfer, DJ, Wyatt, RJ, Scott, J & Snyder, F (1970). Sleep disturbance in acute schizophrenic patients. *Am J Psychiatry,* 126**,** 1213-23.
Kwak, C, Lim, CS & Kaang, BK (2015). Development of a touch-screen-based paradigm for assessing working memory in the mouse. *Exp Neurobiol,* 24**,** 84-9.
Kwon, E, Wang, W & Tsai, LH (2013). Validation of schizophrenia-associated genes CSMD1, C10orf26, CACNA1C and TCF4 as miR-137 targets. *Mol Psychiatry,* 18**,** 11-2.
Kyriakopoulos, M & Frangou, S (2007). Pathophysiology of early onset schizophrenia. *Int Rev Psychiatry,* 19**,** 315-24.
Lacinova, L, Moosmang, S, Langwieser, N, Hofmann, F & Kleppisch, T (2008). Cav1.2 calcium channels modulate the spiking pattern of hippocampal pyramidal cells. *Life Sci,* 82**,** 41-9.
Lahti, AC, Holcomb, HH, Medoff, DR & Tamminga, CA (1995a). Ketamine activates psychosis and alters limbic blood flow in schizophrenia. *Neuroreport,* 6**,** 869-72.
Lahti, AC, Koffel, B, LaPorte, D & Tamminga, CA (1995b). Subanesthetic doses of ketamine stimulate psychosis in schizophrenia. *Neuropsychopharmacology,* 13**,** 9-19.
Lambert, S, Davis, JQ & Bennett, V (1997). Morphogenesis of the node of Ranvier: co-clusters of ankyrin and ankyrin-binding integral proteins define early developmental intermediates. *J Neurosci,* 17**,** 7025-36.
Lambert, S, Yu, H, Prchal, JT, Lawler, J, Ruff, P, Speicher, D, . . . Palek, J (1990). cDNA sequence for human erythrocyte ankyrin. *Proc Natl Acad Sci U S A,* 87**,** 1730-4.
Lancaster, TM, Foley, S, Tansey, KE, Linden, DE & Caseras, X (2016). CACNA1C risk variant is associated with increased amygdala volume. *Eur Arch Psychiatry Clin Neurosci,* 266**,** 269-75.
Lancaster, TM, Heerey, EA, Mantripragada, K & Linden, DE (2014). CACNA1C risk variant affects reward responsiveness in healthy individuals. *Transl Psychiatry,* 4**,** e461.
Langwieser, N, Christel, CJ, Kleppisch, T, Hofmann, F, Wotjak, CT & Moosmang, S (2010). Homeostatic switch in hebbian plasticity and fear learning after sustained loss of Cav1.2 calcium channels. *J Neurosci,* 30**,** 8367-75.
Laruelle, M (2014). Schizophrenia: from dopaminergic to glutamatergic interventions. *Curr Opin Pharmacol,* 14**,** 97-102.
Laruelle, M, Abi-Dargham, A, Gil, R, Kegeles, L & Innis, R (1999). Increased dopamine transmission in schizophrenia: relationship to illness phases. *Biol Psychiatry,* 46**,** 56-72.
Laursen, TM, Munk-Olsen, T & Vestergaard, M (2012). Life expectancy and cardiovascular mortality in persons with schizophrenia. *Curr Opin Psychiatry,* 25**,** 83-8.
Laursen, TM, Nordentoft, M & Mortensen, PB (2014). Excess early mortality in schizophrenia. *Annu Rev Clin Psychol,* 10**,** 425-48.

Lee, AS, De Jesus-Cortes, H, Kabir, ZD, Knobbe, W, Orr, M, Burgdorf, C, . . . Pieper, AA (2016). The Neuropsychiatric Disease-Associated Gene cacna1c Mediates Survival of Young Hippocampal Neurons. *eNeuro,* 3.

Lee, AS, Ra, S, Rajadhyaksha, AM, Britt, JK, De Jesus-Cortes, H, Gonzales, KL, . . . Rajadhyaksha, AM (2012). Forebrain elimination of cacna1c mediates anxiety-like behavior in mice. *Mol Psychiatry,* 17**,** 1054-5.

Lee, KY & Chung, HJ (2014). NMDA receptors and L-type voltage-gated Ca(2)(+) channels mediate the expression of bidirectional homeostatic intrinsic plasticity in cultured hippocampal neurons. *Neuroscience,* 277**,** 610-23.

Lencz, T, Smith, CW, McLaughlin, D, Auther, A, Nakayama, E, Hovey, L & Cornblatt, BA (2006). Generalized and specific neurocognitive deficits in prodromal schizophrenia. *Biol Psychiatry,* 59**,** 863-71.

Lennertz, L, Rujescu, D, Wagner, M, Frommann, I, Schulze-Rauschenbach, S, Schuhmacher, A, . . . Mossner, R (2011). Novel schizophrenia risk gene TCF4 influences verbal learning and memory functioning in schizophrenia patients. *Neuropsychobiology,* 63**,** 131-6.

Lesting, J, Narayanan, RT, Kluge, C, Sangha, S, Seidenbecher, T & Pape, HC (2011). Patterns of coupled theta activity in amygdala-hippocampal-prefrontal cortical circuits during fear extinction. *PLoS One,* 6**,** e21714.

Leussis, MP, Berry-Scott, EM, Saito, M, Jhuang, H, de Haan, G, Alkan, O, . . . Petryshen, TL (2013). The ANK3 bipolar disorder gene regulates psychiatric-related behaviors that are modulated by lithium and stress. *Biol Psychiatry,* 73**,** 683-90.

Levere, TE & Walker, A (1992). Old age and cognition: enhancement of recent memory in aged rats by the calcium channel blocker nimodipine. *Neurobiol Aging,* 13**,** 63-6.

Levy, A, Kong, RM, Stillman, MJ, Shukitt-Hale, B, Kadar, T, Rauch, TM & Lieberman, HR (1991). Nimodipine improves spatial working memory and elevates hippocampal acetylcholine in young rats. *Pharmacol Biochem Behav,* 39**,** 781-6.

Li, J, Chen, Z, Wang, F, Ouyang, Y, Zhang, N, Yang, M, . . . Jin, T (2016). Polymorphisms of the TCF4 gene are associated with the risk of schizophrenia in the Han Chinese. *Am J Med Genet B Neuropsychiatr Genet,* 10.1002/ajmg.b.32449.

Li, J, Zhao, L, You, Y, Lu, T, Jia, M, Yu, H, . . . Wang, L (2015a). Schizophrenia Related Variants in CACNA1C also Confer Risk of Autism. *PLoS One,* 10**,** e0133247.

Li, T, Li, Z, Chen, P, Zhao, Q, Wang, T, Huang, K, . . . Shi, Y (2010). Common variants in major histocompatibility complex region and TCF4 gene are significantly associated with schizophrenia in Han Chinese. *Biol Psychiatry,* 68**,** 671-3.

Li, Z, Xiang, Y, Chen, J, Li, Q, Shen, J, Liu, Y, . . . Shi, Y (2015b). Loci with genome-wide associations with schizophrenia in the Han Chinese population. *Br J Psychiatry,* 207**,** 490-4.

Liao, BY & Zhang, J (2007). Mouse duplicate genes are as essential as singletons. *Trends Genet,* 23**,** 378-81.

Liao, BY & Zhang, J (2008). Null mutations in human and mouse orthologs frequently result in different phenotypes. *Proc Natl Acad Sci U S A,* 105**,** 6987-92.

Linden, DE (2012). The challenges and promise of neuroimaging in psychiatry. *Neuron,* 73**,** 8-22.

Linke, J, Witt, SH, King, AV, Nieratschker, V, Poupon, C, Gass, A, . . . Wessa, M (2012). Genome-wide supported risk variant for bipolar disorder alters anatomical connectivity in the human brain. *Neuroimage,* 59**,** 3288-96.

Linn, GS, O'Keeffe, RT, Lifshitz, K, Schroeder, C & Javitt, DC (2007). Behavioral effects of orally administered glycine in socially housed monkeys chronically treated with phencyclidine. *Psychopharmacology (Berl),* 192**,** 27-38.

Lipscombe, D, Andrade, A & Allen, SE (2013). Alternative splicing: functional diversity among voltage-gated calcium channels and behavioral consequences. *Biochim Biophys Acta,* 1828**,** 1522-9.

Lipscombe, D, Helton, TD & Xu, W (2004). L-type calcium channels: the low down. *J Neurophysiol,* 92**,** 2633-41.

Liu, Y, Blackwood, DH, Caesar, S, de Geus, EJ, Farmer, A, Ferreira, MA, . . . Wellcome Trust Case-Control, C (2011). Meta-analysis of genome-wide association data of bipolar disorder and major depressive disorder. *Mol Psychiatry,* 16**,** 2-4.

Liu, Y, Zhang, Y & Wang, JH (2014). Crystal structure of human Ankyrin G death domain. *Proteins,* 82**,** 3476-82.

Liu, Z, Wang, Y, Cheng, H, Deng, W, Pan, Z, Ullah, S, . . . Xue, Y (2015). GPS 3.0: web servers for the prediction of protein post-translational modification sites. Unpub.

Loveys, DA, Streiff, MB & Kato, GJ (1996). E2A basic-helix-loop-helix transcription factors are negatively regulated by serum growth factors and by the Id3 protein. *Nucleic Acids Res,* 24**,** 2813-20.

Lumey, LH, Stein, AD & Susser, E (2011). Prenatal famine and adult health. *Annu Rev Public Health,* 32**,** 237-62.

Luo, SX & Huang, EJ (2016). Dopaminergic Neurons and Brain Reward Pathways: From Neurogenesis to Circuit Assembly. *Am J Pathol,* 186**,** 478-88.

Lupi, D, Oster, H, Thompson, S & Foster, RG (2008). The acute light-induction of sleep is mediated by OPN4-based photoreception. *Nat Neurosci,* 11**,** 1068-73.

Lyon, GJ, Abi-Dargham, A, Moore, H, Lieberman, JA, Javitch, JA & Sulzer, D (2011). Presynaptic regulation of dopamine transmission in schizophrenia. *Schizophr Bull,* 37**,** 108-17.

Lyu, H, Hu, M, Eyler, LT, Jin, H, Wang, J, Ou, J, . . . Guo, W (2015). Regional white matter abnormalities in drug-naive, first-episode schizophrenia patients and their healthy unaffected siblings. *Aust N Z J Psychiatry,* 49**,** 246-54.

Maciejewski, PM, Peterson, FC, Anderson, PJ & Brooks, CL (1995). Mutation of serine 90 to glutamic acid mimics phosphorylation of bovine prolactin. *J Biol Chem,* 270**,** 27661-5.

Malhotra, AK, Pinals, DA, Weingartner, H, Sirocco, K, Missar, CD, Pickar, D & Breier, A (1996). NMDA receptor function and human cognition: the effects of ketamine in healthy volunteers. *Neuropsychopharmacology,* 14**,** 301-7.

Malhotra, D & Sebat, J (2012). CNVs: harbingers of a rare variant revolution in psychiatric genetics. *Cell,* 148**,** 1223-41.

Manoach, DS, Thakkar, KN, Stroynowski, E, Ely, A, McKinley, SK, Wamsley, E, . . . Stickgold, R (2010). Reduced overnight consolidation of procedural learning in chronic medicated schizophrenia is related to specific sleep stages. *J Psychiatr Res,* 44**,** 112-20.

Maren, S, Phan, KL & Liberzon, I (2013). The contextual brain: implications for fear conditioning, extinction and psychopathology. *Nat Rev Neurosci,* 14**,** 417-28.

Marenco, S & Weinberger, DR (2000). The neurodevelopmental hypothesis of schizophrenia: following a trail of evidence from cradle to grave. *Dev Psychopathol,* 12**,** 501-27.
Martin, J, Jeste, DV, Caliguiri, MP, Patterson, T, Heaton, R & Ancoli-Israel, S (2001). Actigraphic estimates of circadian rhythms and sleep/wake in older schizophrenia patients. *Schizophr Res,* 47**,** 77-86.
Martin, JL, Jeste, DV & Ancoli-Israel, S (2005). Older schizophrenia patients have more disrupted sleep and circadian rhythms than age-matched comparison subjects. *J Psychiatr Res,* 39**,** 251-9.
Massari, ME, Grant, PA, Pray-Grant, MG, Berger, SL, Workman, JL & Murre, C (1999). A conserved motif present in a class of helix-loop-helix proteins activates transcription by direct recruitment of the SAGA complex. *Mol Cell,* 4**,** 63-73.
McCarthy, MJ, Le Roux, MJ, Wei, H, Beesley, S, Kelsoe, JR & Welsh, DK (2016). Calcium channel genes associated with bipolar disorder modulate lithium's amplification of circadian rhythms. *Neuropharmacology,* 101**,** 439-48.
McCarthy, MJ, Wei, H, Marnoy, Z, Darvish, RM, McPhie, DL, Cohen, BM & Welsh, DK (2013). Genetic and clinical factors predict lithium's effects on PER2 gene expression rhythms in cells from bipolar disorder patients. *Transl Psychiatry,* 3**,** e318.
McCullumsmith, RE, Hammond, J, Funk, A & Meador-Woodruff, JH (2012). Recent advances in targeting the ionotropic glutamate receptors in treating schizophrenia. *Curr Pharm Biotechnol,* 13**,** 1535-42.
McGrath, J, Saha, S, Chant, D & Welham, J (2008). Schizophrenia: a concise overview of incidence, prevalence, and mortality. *Epidemiol Rev,* 30**,** 67-76.
McWilliam, H, Li, W, Uludag, M, Squizzato, S, Park, YM, Buso, N, . . . Lopez, R (2013). Analysis Tool Web Services from the EMBL-EBI. *Nucleic Acids Res,* 41**,** W597-600.
Megna, JL, Schwartz, TL, Siddiqui, UA & Herrera Rojas, M (2011). Obesity in adults with serious and persistent mental illness: a review of postulated mechanisms and current interventions. *Ann Clin Psychiatry,* 23**,** 131-40.
Mestas, J & Hughes, CC (2004). Of mice and not men: differences between mouse and human immunology. *J Immunol,* 172**,** 2731-8.
Michaely, P & Bennett, V (1992). The ANK repeat: a ubiquitous motif involved in macromolecular recognition. *Trends Cell Biol,* 2**,** 127-9.
Millar, JK, Wilson-Annan, JC, Anderson, S, Christie, S, Taylor, MS, Semple, CA, . . . Porteous, DJ (2000). Disruption of two novel genes by a translocation co-segregating with schizophrenia. *Hum Mol Genet,* 9**,** 1415-23.
Mistlberger, RE, Bergmann, BM & Rechtschaffen, A (1987). Relationships among wake episode lengths, contiguous sleep episode lengths, and electroencephalographic delta waves in rats with suprachiasmatic nuclei lesions. *Sleep,* 10**,** 12-24.
Mitchell, AJ & Malone, D (2006). Physical health and schizophrenia. *Curr Opin Psychiatry,* 19**,** 432-7.
Mohler, PJ, Gramolini, AO & Bennett, V (2002a). The ankyrin-B C-terminal domain determines activity of ankyrin-B/G chimeras in rescue of abnormal inositol 1,4,5-trisphosphate and ryanodine receptor distribution in ankyrin-B (-/-) neonatal cardiomyocytes. *J Biol Chem,* 277**,** 10599-607.
Mohler, PJ, Gramolini, AO & Bennett, V (2002b). Ankyrins. *J Cell Sci,* 115**,** 1565-6.

Mohler, PJ, Yoon, W & Bennett, V (2004). Ankyrin-B targets beta2-spectrin to an intracellular compartment in neonatal cardiomyocytes. *J Biol Chem,* 279**,** 40185-93.

Moosmang, S, Haider, N, Klugbauer, N, Adelsberger, H, Langwieser, N, Muller, J, . . . Kleppisch, T (2005). Role of hippocampal Cav1.2 Ca2+ channels in NMDA receptor-independent synaptic plasticity and spatial memory. *J Neurosci,* 25**,** 9883-92.

Moreno, LC, da Silva Oliveira, GZ, Cavalcanti, IM, Santos-Magalhaes, NS, Rolim, HM & de Freitas, RM (2014). Development and evaluation of liposomal formulation containing nimodipine on anxiolytic activity in mice. *Pharmacol Biochem Behav,* 116**,** 64-8.

Morgan, C, Charalambides, M, Hutchinson, G & Murray, RM (2010). Migration, ethnicity, and psychosis: toward a sociodevelopmental model. *Schizophr Bull,* 36**,** 655-64.

Morgan, C & Gayer-Anderson, C (2016). Childhood adversities and psychosis: evidence, challenges, implications. *World Psychiatry,* 15**,** 93-102.

Morris, R (1984). Developments of a water-maze procedure for studying spatial learning in the rat. *J Neurosci Methods,* 11**,** 47-60.

Morrison, AP, Burke, E, Murphy, E, Pyle, M, Bowe, S, Varese, F, . . . Wood, LJ (2016). Cognitive therapy for internalised stigma in people experiencing psychosis: A pilot randomised controlled trial. *Psychiatry Res,* 240**,** 96-102.

Mortensen, PB, Norgaard-Pedersen, B, Waltoft, BL, Sorensen, TL, Hougaard, D, Torrey, EF & Yolken, RH (2007). Toxoplasma gondii as a risk factor for early-onset schizophrenia: analysis of filter paper blood samples obtained at birth. *Biol Psychiatry,* 61**,** 688-93.

Mortimer, AM, Singh, P, Shepherd, CJ & Puthiryackal, J (2010). Clozapine for treatment-resistant schizophrenia: National Institute of Clinical Excellence (NICE) guidance in the real world. *Clin Schizophr Relat Psychoses,* 4**,** 49-55.

Mullegama, SV, Pugliesi, L, Burns, B, Tahir, R, Shah, Z, Gu, Y, . . . Elsea, SH (2014). Disruption of FMR1, RAI1, MBD5, and TCF4 results in abnormal expression of circadian rhythm genes and sleep disturbances in fragile X, Smith-Magenis, 2q23.1 deletion, and Pitt-Hopkins syndromes. (Abstract 3029M). *64th Annual Meeting of The American Society of Human Genetics.* San Diego, CA, USA.

Murakami, M, Kataoka, K, Tominaga, J, Nakagawa, O & Kurihara, H (2004). Differential cooperation between dHAND and three different E-proteins. *Biochem Biophys Res Commun,* 323**,** 168-74.

Murphy, BP, Chung, YC, Park, TW & McGorry, PD (2006). Pharmacological treatment of primary negative symptoms in schizophrenia: a systematic review. *Schizophr Res,* 88**,** 5-25.

Murphy, TH, Worley, PF & Baraban, JM (1991). L-type voltage-sensitive calcium channels mediate synaptic activation of immediate early genes. *Neuron,* 7**,** 625-35.

Murre, C, Bain, G, van Dijk, MA, Engel, I, Furnari, BA, Massari, ME, . . . Stuiver, MH (1994). Structure and function of helix-loop-helix proteins. *Biochim Biophys Acta,* 1218**,** 129-35.

Murre, C, McCaw, PS & Baltimore, D (1989a). A new DNA binding and dimerization motif in immunoglobulin enhancer binding, daughterless, MyoD, and myc proteins. *Cell,* 56**,** 777-83.

Murre, C, McCaw, PS, Vaessin, H, Caudy, M, Jan, LY, Jan, YN, . . . et al. (1989b). Interactions between heterologous helix-loop-helix proteins generate

complexes that bind specifically to a common DNA sequence. *Cell,* 58**,** 537-44.
Neely, A, Olcese, R, Wei, X, Birnbaumer, L & Stefani, E (1994). Ca(2+)-dependent inactivation of a cloned cardiac Ca2+ channel alpha 1 subunit (alpha 1C) expressed in Xenopus oocytes. *Biophys J,* 66**,** 1895-903.
Nestler, EJ & Hyman, SE (2010). Animal models of neuropsychiatric disorders. *Nat Neurosci,* 13**,** 1161-9.
Neuman, T, Keen, A, Zuber, MX, Kristjansson, GI, Gruss, P & Nornes, HO (1993). Neuronal expression of regulatory helix-loop-helix factor Id2 gene in mouse. *Dev Biol,* 160**,** 186-95.
Newcomer, JW (2007). Metabolic syndrome and mental illness. *Am J Manag Care,* 13**,** S170-7.
Nguyen, D & Xu, T (2008). The expanding role of mouse genetics for understanding human biology and disease. *Dis Model Mech,* 1**,** 56-66.
NICE (2014). Psychosis and schizophrenia in adults: prevention and management. Retrieved from https://www.nice.org.uk/guidance/cg178.
Nie, F, Wang, X, Zhao, P, Yang, H, Zhu, W, Zhao, Y, . . . Ma, J (2015). Genetic analysis of SNPs in CACNA1C and ANK3 gene with schizophrenia: A comprehensive meta-analysis. *Am J Med Genet B Neuropsychiatr Genet,* 168**,** 637-48.
Nieratschker, V, Bruckmann, C & Plewnia, C (2015). CACNA1C risk variant affects facial emotion recognition in healthy individuals. *Sci Rep,* 5**,** 17349.
Nolan, PM, Hugill, A & Cox, RD (2002). ENU mutagenesis in the mouse: application to human genetic disease. *Brief Funct Genomic Proteomic,* 1**,** 278-89.
Nolan, PM, Kapfhamer, D & Bucan, M (1997). Random mutagenesis screen for dominant behavioral mutations in mice. *Methods,* 13**,** 379-95.
Nolan, PM, Peters, J, Strivens, M, Rogers, D, Hagan, J, Spurr, N, . . . Hunter, J (2000a). A systematic, genome-wide, phenotype-driven mutagenesis programme for gene function studies in the mouse. *Nat Genet,* 25**,** 440-3.
Nolan, PM, Peters, J, Vizor, L, Strivens, M, Washbourne, R, Hough, T, . . . Brown, SD (2000b). Implementation of a large-scale ENU mutagenesis program: towards increasing the mouse mutant resource. *Mamm Genome,* 11**,** 500-6.
Normand, EA & Rasband, MN (2015). Subcellular patterning: axonal domains with specialized structure and function. *Dev Cell,* 32**,** 459-68.
Noveroske, JK, Weber, JS & Justice, MJ (2000). The mutagenic action of N-ethyl-N-nitrosourea in the mouse. *Mamm Genome,* 11**,** 478-83.
O'Donnell, L, Soileau, B, Heard, P, Carter, E, Sebold, C, Gelfond, J, . . . Cody, JD (2010). Genetic determinants of autism in individuals with deletions of 18q. *Hum Genet,* 128**,** 155-64.
Obermair, GJ, Szabo, Z, Bourinet, E & Flucher, BE (2004). Differential targeting of the L-type Ca2+ channel alpha 1C (CaV1.2) to synaptic and extrasynaptic compartments in hippocampal neurons. *Eur J Neurosci,* 19**,** 2109-22.
Olde Loohuis, NF, Nadif Kasri, N, Glennon, JC, van Bokhoven, H, Hebert, SS, Kaplan, BB, . . . Aschrafi, A (2016). The schizophrenia risk gene MIR137 acts as a hippocampal gene network node orchestrating the expression of genes relevant to nervous system development and function. *Prog Neuropsychopharmacol Biol Psychiatry.*
Oliver, PL & Davies, KE (2009). Interaction between environmental and genetic factors modulates schizophrenic endophenotypes in the Snap-25 mouse mutant blind-drunk. *Hum Mol Genet,* 18**,** 4576-89.

Olkkola, KT & Ahonen, J (2008). Midazolam and other benzodiazepines. *Handb Exp Pharmacol,* 10.1007/978-3-540-74806-9_16**,** 335-60.
Onstad, S, Skre, I, Torgersen, S & Kringlen, E (1991). Twin concordance for DSM-III-R schizophrenia. *Acta Psychiatr Scand,* 83**,** 395-401.
Otto, E, Kunimoto, M, McLaughlin, T & Bennett, V (1991). Isolation and characterization of cDNAs encoding human brain ankyrins reveal a family of alternatively spliced genes. *J Cell Biol,* 114**,** 241-53.
Owen, MJ, O'Donovan, MC, Thapar, A & Craddock, N (2011). Neurodevelopmental hypothesis of schizophrenia. *Br J Psychiatry,* 198**,** 173-5.
Owen, MJ, Sawa, A & Mortensen, PB (2016). Schizophrenia. *Lancet,* 388**,** 86-97.
Paez-Gonzalez, P, Abdi, K, Luciano, D, Liu, Y, Soriano-Navarro, M, Rawlins, E, . . . Kuo, CT (2011). Ank3-dependent SVZ niche assembly is required for the continued production of new neurons. *Neuron,* 71**,** 61-75.
Pan, Z, Kao, T, Horvath, Z, Lemos, J, Sul, JY, Cranstoun, SD, . . . Cooper, EC (2006). A common ankyrin-G-based mechanism retains KCNQ and NaV channels at electrically active domains of the axon. *J Neurosci,* 26**,** 2599-613.
Pape, HC, Narayanan, RT, Smid, J, Stork, O & Seidenbecher, T (2005). Theta activity in neurons and networks of the amygdala related to long-term fear memory. *Hippocampus,* 15**,** 874-80.
Parsons, MJ, Lester, KJ, Barclay, NL, Nolan, PM, Eley, TC & Gregory, AM (2013). Replication of Genome-Wide Association Studies (GWAS) loci for sleep in the British G1219 cohort. *Am J Med Genet B Neuropsychiatr Genet,* 162B**,** 431-8.
Parwani, A, Weiler, MA, Blaxton, TA, Warfel, D, Hardin, M, Frey, K & Lahti, AC (2005). The effects of a subanesthetic dose of ketamine on verbal memory in normal volunteers. *Psychopharmacology (Berl),* 183**,** 265-74.
Pasparakis, E, Koiliari, E, Zouraraki, C, Tsapakis, EM, Roussos, P, Giakoumaki, SG & Bitsios, P (2015). The effects of the CACNA1C rs1006737 A/G on affective startle modulation in healthy males. *Eur Psychiatry,* 30**,** 492-8.
Patterson, PH (2009). Immune involvement in schizophrenia and autism: etiology, pathology and animal models. *Behav Brain Res,* 204**,** 313-21.
Paus, T (2005). Mapping brain maturation and cognitive development during adolescence. *Trends Cogn Sci,* 9**,** 60-8.
Paus, T, Keshavan, M & Giedd, JN (2008). Why do many psychiatric disorders emerge during adolescence? *Nat Rev Neurosci,* 9**,** 947-57.
Pedersen, CB & Mortensen, PB (2001). Evidence of a dose-response relationship between urbanicity during upbringing and schizophrenia risk. *Arch Gen Psychiatry,* 58**,** 1039-46.
Pedersen, MG, Stevens, H, Pedersen, CB, Norgaard-Pedersen, B & Mortensen, PB (2011). Toxoplasma infection and later development of schizophrenia in mothers. *Am J Psychiatry,* 168**,** 814-21.
Peen, J, Schoevers, RA, Beekman, AT & Dekker, J (2010). The current status of urban-rural differences in psychiatric disorders. *Acta Psychiatr Scand,* 121**,** 84-93.
Perez-Reyes, E, Kim, HS, Lacerda, AE, Horne, W, Wei, XY, Rampe, D, . . . Birnbaumer, L (1989). Induction of calcium currents by the expression of the alpha 1-subunit of the dihydropyridine receptor from skeletal muscle. *Nature,* 340**,** 233-6.
Perry, W, Minassian, A, Feifel, D & Braff, DL (2001). Sensorimotor gating deficits in bipolar disorder patients with acute psychotic mania. *Biol Psychiatry,* 50**,** 418-24.

Perry, W, Minassian, A, Henry, B, Kincaid, M, Young, JW & Geyer, MA (2010). Quantifying over-activity in bipolar and schizophrenia patients in a human open field paradigm. *Psychiatry Res,* 178**,** 84-91.

Peters, LL, John, KM, Lu, FM, Eicher, EM, Higgins, A, Yialamas, M, . . . Lux, SE (1995). Ank3 (epithelial ankyrin), a widely distributed new member of the ankyrin gene family and the major ankyrin in kidney, is expressed in alternatively spliced forms, including forms that lack the repeat domain. *J Cell Biol,* 130**,** 313-30.

Peterson, BZ, Lee, JS, Mulle, JG, Wang, Y, de Leon, M & Yue, DT (2000). Critical determinants of Ca(2+)-dependent inactivation within an EF-hand motif of L-type Ca(2+) channels. *Biophys J,* 78**,** 1906-20.

Phillips, RG & LeDoux, JE (1992). Differential contribution of amygdala and hippocampus to cued and contextual fear conditioning. *Behav Neurosci,* 106**,** 274-85.

Piper, M, Beneyto, M, Burne, TH, Eyles, DW, Lewis, DA & McGrath, JJ (2012). The neurodevelopmental hypothesis of schizophrenia: convergent clues from epidemiology and neuropathology. *Psychiatr Clin North Am,* 35**,** 571-84.

Pitt, D & Hopkins, I (1978). A syndrome of mental retardation, wide mouth and intermittent overbreathing. *Aust Paediatr J,* 14**,** 182-4.

Pitt, GS, Zuhlke, RD, Hudmon, A, Schulman, H, Reuter, H & Tsien, RW (2001). Molecular basis of calmodulin tethering and Ca2+-dependent inactivation of L-type Ca2+ channels. *J Biol Chem,* 276**,** 30794-802.

Pittenger, C, Adams, TG, Jr., Gallezot, JD, Crowley, MJ, Nabulsi, N, James, R, . . . Carson, RE (2016). OCD is associated with an altered association between sensorimotor gating and cortical and subcortical 5-HT1b receptor binding. *J Affect Disord,* 196**,** 87-96.

Pletnikov, MV, Ayhan, Y, Nikolskaia, O, Xu, Y, Ovanesov, MV, Huang, H, . . . Ross, CA (2008). Inducible expression of mutant human DISC1 in mice is associated with brain and behavioral abnormalities reminiscent of schizophrenia. *Mol Psychiatry,* 13**,** 173-86, 115.

Podgorski, A, Alster, P & Elbaum, D (1988). Interactions among red cell membrane proteins. *Biochemistry,* 27**,** 609-14.

Poulin, J, Daoust, AM, Forest, G, Stip, E & Godbout, R (2003). Sleep architecture and its clinical correlates in first episode and neuroleptic-naive patients with schizophrenia. *Schizophr Res,* 62**,** 147-53.

Pouretemad, HR, Thompson, PJ & Fenwick, PB (1998). Impaired sensorimotor gating in patients with non-epileptic seizures. *Epilepsy Res,* 31**,** 1-12.

Powell, LM & Jarman, AP (2008). Context dependence of proneural bHLH proteins. *Curr Opin Genet Dev,* 18**,** 411-7.

Prabakaran, S, Lippens, G, Steen, H & Gunawardena, J (2012). Post-translational modification: nature's escape from genetic imprisonment and the basis for dynamic information encoding. *Wiley Interdiscip Rev Syst Biol Med,* 4**,** 565-83.

Pritchett, D, Wulff, K, Oliver, PL, Bannerman, DM, Davies, KE, Harrison, PJ, . . . Foster, RG (2012). Evaluating the links between schizophrenia and sleep and circadian rhythm disruption. *J Neural Transm (Vienna),* 119**,** 1061-75.

Prut, L & Belzung, C (2003). The open field as a paradigm to measure the effects of drugs on anxiety-like behaviors: a review. *Eur J Pharmacol,* 463**,** 3-33.

Pscherer, A, Dorflinger, U, Kirfel, J, Gawlas, K, Ruschoff, J, Buettner, R & Schule, R (1996). The helix-loop-helix transcription factor SEF-2 regulates the activity of

a novel initiator element in the promoter of the human somatostatin receptor II gene. *EMBO J,* 15**,** 6680-90.

Psychiatric GWAS Consortium Bipolar Disorder Working Group, G (2011). Large-scale genome-wide association analysis of bipolar disorder identifies a new susceptibility locus near ODZ4. *Nat Genet,* 43**,** 977-83.

Purcell, SM, Moran, JL, Fromer, M, Ruderfer, D, Solovieff, N, Roussos, P, . . . Sklar, P (2014). A polygenic burden of rare disruptive mutations in schizophrenia. *Nature,* 506**,** 185-90.

Quednow, BB, Brinkmeyer, J, Mobascher, A, Nothnagel, M, Musso, F, Grunder, G, . . . Winterer, G (2012). Schizophrenia risk polymorphisms in the TCF4 gene interact with smoking in the modulation of auditory sensory gating. *Proc Natl Acad Sci U S A,* 109**,** 6271-6.

Quednow, BB, Ettinger, U, Mossner, R, Rujescu, D, Giegling, I, Collier, DA, . . . Kumari, V (2011). The schizophrenia risk allele C of the TCF4 rs9960767 polymorphism disrupts sensorimotor gating in schizophrenia spectrum and healthy volunteers. *J Neurosci,* 31**,** 6684-91.

Quintana, J, Wong, T, Ortiz-Portillo, E, Marder, SR & Mazziotta, JC (2004). Anterior cingulate dysfunction during choice anticipation in schizophrenia. *Psychiatry Res,* 132**,** 117-30.

Quong, MW, Massari, ME, Zwart, R & Murre, C (1993). A new transcriptional-activation motif restricted to a class of helix-loop-helix proteins is functionally conserved in both yeast and mammalian cells. *Mol Cell Biol,* 13**,** 792-800.

Quong, MW, Romanow, WJ & Murre, C (2002). E protein function in lymphocyte development. *Annu Rev Immunol,* 20**,** 301-22.

Quwailid, MM, Hugill, A, Dear, N, Vizor, L, Wells, S, Horner, E, . . . Cox, RD (2004). A gene-driven ENU-based approach to generating an allelic series in any gene. *Mamm Genome,* 15**,** 585-91.

Rabinowitz, J, Berardo, CG, Bugarski-Kirola, D & Marder, S (2013). Association of prominent positive and prominent negative symptoms and functional health, well-being, healthcare-related quality of life and family burden: a CATIE analysis. *Schizophr Res,* 150**,** 339-42.

Ramos, A, Pereira, E, Martins, GC, Wehrmeister, TD & Izidio, GS (2008). Integrating the open field, elevated plus maze and light/dark box to assess different types of emotional behaviors in one single trial. *Behav Brain Res,* 193**,** 277-88.

Rampon, C, Tang, YP, Goodhouse, J, Shimizu, E, Kyin, M & Tsien, JZ (2000). Enrichment induces structural changes and recovery from nonspatial memory deficits in CA1 NMDAR1-knockout mice. *Nat Neurosci,* 3**,** 238-44.

Ranganath, C, Minzenberg, MJ & Ragland, JD (2008). The cognitive neuroscience of memory function and dysfunction in schizophrenia. *Biol Psychiatry,* 64**,** 18-25.

Rannals, MD, Hamersky, GR, Page, SC, Campbell, MN, Briley, A, Gallo, RA, . . . Maher, BJ (2016). Psychiatric Risk Gene Transcription Factor 4 Regulates Intrinsic Excitability of Prefrontal Neurons via Repression of SCN10a and KCNQ1. *Neuron,* 90**,** 43-55.

Rapoport, JL, Giedd, JN & Gogtay, N (2012). Neurodevelopmental model of schizophrenia: update 2012. *Mol Psychiatry,* 17**,** 1228-38.

Rasmussen, HB, Frokjaer-Jensen, C, Jensen, CS, Jensen, HS, Jorgensen, NK, Misonou, H, . . . Schmitt, N (2007). Requirement of subunit co-assembly and ankyrin-G for M-channel localization at the axon initial segment. *J Cell Sci,* 120**,** 953-63.

Ravasi, T, Suzuki, H, Cannistraci, CV, Katayama, S, Bajic, VB, Tan, K, . . . Hayashizaki, Y (2010). An atlas of combinatorial transcriptional regulation in mouse and man. *Cell,* 140**,** 744-52.

Rees, E, Moskvina, V, Owen, MJ, O'Donovan, MC & Kirov, G (2011). De novo rates and selection of schizophrenia-associated copy number variants. *Biol Psychiatry,* 70**,** 1109-14.

Rees, E, Walters, JT, Georgieva, L, Isles, AR, Chambert, KD, Richards, AL, . . . Kirov, G (2014). Analysis of copy number variations at 15 schizophrenia-associated loci. *Br J Psychiatry,* 204**,** 108-14.

Reichenberg, A & Harvey, PD (2007). Neuropsychological impairments in schizophrenia: Integration of performance-based and brain imaging findings. *Psychol Bull,* 133**,** 833-58.

Remington, G, Kapur, S, Foussias, G, Agid, O, Mann, S, Borlido, C, . . . Javaid, N (2012). Tetrabenazine augmentation in treatment-resistant schizophrenia: a 12-week, double-blind, placebo-controlled trial. *J Clin Psychopharmacol,* 32**,** 95-9.

Rhoads, AR & Friedberg, F (1997). Sequence motifs for calmodulin recognition. *FASEB J,* 11**,** 331-40.

Ripke, S, O'Dushlaine, C, Chambert, K, Moran, JL, Kahler, AK, Akterin, S, . . . Sullivan, PF (2013). Genome-wide association analysis identifies 13 new risk loci for schizophrenia. *Nat Genet,* 45**,** 1150-9.

Risch, NJ (2000). Searching for genetic determinants in the new millennium. *Nature,* 405**,** 847-56.

Roden, DM (2004). Drug-induced prolongation of the QT interval. *N Engl J Med,* 350**,** 1013-22.

Rogers, DC, Fisher, EM, Brown, SD, Peters, J, Hunter, AJ & Martin, JE (1997). Behavioral and functional analysis of mouse phenotype: SHIRPA, a proposed protocol for comprehensive phenotype assessment. *Mamm Genome,* 8**,** 711-3.

Rosati, B, Yan, Q, Lee, MS, Liou, SR, Ingalls, B, Foell, J, . . . McKinnon, D (2011). Robust L-type calcium current expression following heterozygous knockout of the Cav1.2 gene in adult mouse heart. *J Physiol,* 589**,** 3275-88.

Rosenheck, R, Leslie, D, Keefe, R, McEvoy, J, Swartz, M, Perkins, D, . . . Group, CSI (2006). Barriers to employment for people with schizophrenia. *Am J Psychiatry,* 163**,** 411-7.

Rosenthal, N & Brown, S (2007). The mouse ascending: perspectives for human-disease models. *Nat Cell Biol,* 9**,** 993-9.

Ross, SE, Greenberg, ME & Stiles, CD (2003). Basic helix-loop-helix factors in cortical development. *Neuron,* 39**,** 13-25.

Roussos, P, Giakoumaki, SG, Georgakopoulos, A, Robakis, NK & Bitsios, P (2011). The CACNA1C and ANK3 risk alleles impact on affective personality traits and startle reactivity but not on cognition or gating in healthy males. *Bipolar Disord,* 13**,** 250-9.

Roussos, P, Mitchell, AC, Voloudakis, G, Fullard, JF, Pothula, VM, Tsang, J, . . . Sklar, P (2014). A role for noncoding variation in schizophrenia. *Cell Rep,* 9**,** 1417-29.

Rubtsov, AM & Lopina, OD (2000). Ankyrins. *FEBS Lett,* 482**,** 1-5.

Ruderfer, DM, Fanous, AH, Ripke, S, McQuillin, A, Amdur, RL, Schizophrenia Working Group of Psychiatric Genomics, C, . . . Kendler, KS (2014). Polygenic

dissection of diagnosis and clinical dimensions of bipolar disorder and schizophrenia. *Mol Psychiatry,* 19**,** 1017-24.
Rutishauser, U, Ross, IB, Mamelak, AN & Schuman, EM (2010). Human memory strength is predicted by theta-frequency phase-locking of single neurons. *Nature,* 464**,** 903-7.
Saha, S, Chant, D & McGrath, J (2007). A systematic review of mortality in schizophrenia: is the differential mortality gap worsening over time? *Arch Gen Psychiatry,* 64**,** 1123-31.
Saha, S, Chant, D, Welham, J & McGrath, J (2005). A systematic review of the prevalence of schizophrenia. *PLoS Med,* 2**,** e141.
Salzer, JL (1997). Clustering sodium channels at the node of Ranvier: close encounters of the axon-glia kind. *Neuron,* 18**,** 843-6.
Santos, MC, Tegge, AN, Correa, BR, Mahesula, S, Kohnke, LQ, Qiao, M, . . . Penalva, LO (2016). miR-124, -128, and -137 Orchestrate Neural Differentiation by Acting on Overlapping Gene Sets Containing a Highly Connected Transcription Factor Network. *Stem Cells,* 34**,** 220-32.
Sawamura, N, Ando, T, Maruyama, Y, Fujimuro, M, Mochizuki, H, Honjo, K, . . . Sawa, A (2008). Nuclear DISC1 regulates CRE-mediated gene transcription and sleep homeostasis in the fruit fly. *Mol Psychiatry,* 13**,** 1138-48, 1069.
Schizophrenia Psychiatric Genome-Wide Association Study, C (2011). Genome-wide association study identifies five new schizophrenia loci. *Nat Genet,* 43**,** 969-76.
Schizophrenia Working Group of the Psychiatric Genomics, C (2014). Biological insights from 108 schizophrenia-associated genetic loci. *Nature,* 511**,** 421-7.
Schmidt-Edelkraut, U, Daniel, G, Hoffmann, A & Spengler, D (2014). Zac1 regulates cell cycle arrest in neuronal progenitors via Tcf4. *Mol Cell Biol,* 34**,** 1020-30.
Schmutz, I, Chavan, R, Ripperger, JA, Maywood, ES, Langwieser, N, Jurik, A, . . . Albrecht, U (2014). A specific role for the REV-ERBalpha-controlled L-Type Voltage-Gated Calcium Channel CaV1.2 in resetting the circadian clock in the late night. *J Biol Rhythms,* 29**,** 288-98.
Schulz, PE, McIntosh, AD, Kasten, MR, Wieringa, B & Epstein, HF (2003). A role for myotonic dystrophy protein kinase in synaptic plasticity. *J Neurophysiol,* 89**,** 1177-86.
Schulze, TG, Detera-Wadleigh, SD, Akula, N, Gupta, A, Kassem, L, Steele, J, . . . McMahon, FJ (2009). Two variants in Ankyrin 3 (ANK3) are independent genetic risk factors for bipolar disorder. *Mol Psychiatry,* 14**,** 487-91.
Schwab, MH, Bartholomae, A, Heimrich, B, Feldmeyer, D, Druffel-Augustin, S, Goebbels, S, . . . Nave, KA (2000). Neuronal basic helix-loop-helix proteins (NEX and BETA2/Neuro D) regulate terminal granule cell differentiation in the hippocampus. *J Neurosci,* 20**,** 3714-24.
Scott, LJ, Muglia, P, Kong, XQ, Guan, W, Flickinger, M, Upmanyu, R, . . . Boehnke, M (2009). Genome-wide association and meta-analysis of bipolar disorder in individuals of European ancestry. *Proc Natl Acad Sci U S A,* 106**,** 7501-6.
Sedgwick, SG & Smerdon, SJ (1999). The ankyrin repeat: a diversity of interactions on a common structural framework. *Trends Biochem Sci,* 24**,** 311-6.
Seidenbecher, T, Laxmi, TR, Stork, O & Pape, HC (2003). Amygdalar and hippocampal theta rhythm synchronization during fear memory retrieval. *Science,* 301**,** 846-50.
Seisenberger, C, Specht, V, Welling, A, Platzer, J, Pfeifer, A, Kuhbandner, S, . . . Hofmann, F (2000). Functional embryonic cardiomyocytes after disruption of

the L-type alpha1C (Cav1.2) calcium channel gene in the mouse. *J Biol Chem,* 275**,** 39193-9.

Sekimoto, M, Kato, M, Watanabe, T, Kajimura, N & Takahashi, K (2007). Reduced frontal asymmetry of delta waves during all-night sleep in schizophrenia. *Schizophr Bull,* 33**,** 1307-11.

Sekimoto, M, Kato, M, Watanabe, T, Kajimura, N & Takahashi, K (2011). Cortical regional differences of delta waves during all-night sleep in schizophrenia. *Schizophr Res,* 126**,** 284-90.

Sepp, M, Kannike, K, Eesmaa, A, Urb, M & Timmusk, T (2011). Functional diversity of human basic helix-loop-helix transcription factor TCF4 isoforms generated by alternative 5' exon usage and splicing. *PLoS One,* 6**,** e22138.

Sham, PC, MacLean, CJ & Kendler, KS (1994). A typological model of schizophrenia based on age at onset, sex and familial morbidity. *Acta Psychiatr Scand,* 89**,** 135-41.

Sheng, M, McFadden, G & Greenberg, ME (1990). Membrane depolarization and calcium induce c-fos transcription via phosphorylation of transcription factor CREB. *Neuron,* 4**,** 571-82.

Shenton, ME, Dickey, CC, Frumin, M & McCarley, RW (2001). A review of MRI findings in schizophrenia. *Schizophr Res,* 49**,** 1-52.

Shimada, M, Miyagawa, T, Kawashima, M, Tanaka, S, Honda, Y, Honda, M & Tokunaga, K (2010). An approach based on a genome-wide association study reveals candidate loci for narcolepsy. *Hum Genet,* 128**,** 433-41.

Shinnick-Gallagher, P, McKernan, MG, Xie, J & Zinebi, F (2003). L-type voltage-gated calcium channels are involved in the in vivo and in vitro expression of fear conditioning. *Ann N Y Acad Sci,* 985**,** 135-49.

Shyu, AB, Wilkinson, MF & van Hoof, A (2008). Messenger RNA regulation: to translate or to degrade. *EMBO J,* 27**,** 471-81.

Sieradzka, D, Power, RA, Freeman, D, Cardno, AG, McGuire, P, Plomin, R, . . . Ronald, A (2014). Are genetic risk factors for psychosis also associated with dimension-specific psychotic experiences in adolescence? *PLoS One,* 9**,** e94398.

Sievers, F, Wilm, A, Dineen, D, Gibson, TJ, Karplus, K, Li, W, . . . Higgins, DG (2011). Fast, scalable generation of high-quality protein multiple sequence alignments using Clustal Omega. *Mol Syst Biol,* 7**,** 539.

Sigrist, CJ, Cerutti, L, Hulo, N, Gattiker, A, Falquet, L, Pagni, M, . . . Bucher, P (2002). PROSITE: a documented database using patterns and profiles as motif descriptors. *Brief Bioinform,* 3**,** 265-74.

Sigrist, CJ, de Castro, E, Cerutti, L, Cuche, BA, Hulo, N, Bridge, A, . . . Xenarios, I (2013). New and continuing developments at PROSITE. *Nucleic Acids Res,* 41**,** D344-7.

Silverman, JL, Yang, M, Lord, C & Crawley, JN (2010). Behavioural phenotyping assays for mouse models of autism. *Nat Rev Neurosci,* 11**,** 490-502.

Simeone, JC, Ward, AJ, Rotella, P, Collins, J & Windisch, R (2015). An evaluation of variation in published estimates of schizophrenia prevalence from 1990-2013: a systematic literature review. *BMC Psychiatry,* 15**,** 193.

Simms, BA, Souza, IA & Zamponi, GW (2014). A novel calmodulin site in the Cav1.2 N-terminus regulates calcium-dependent inactivation. *Pflugers Arch,* 466**,** 1793-803.

Siskind, D, McCartney, L, Goldschlager, R & Kisely, S. (2016). Clozapine v. first- and second-generation antipsychotics in treatment-refractory schizophrenia:

systematic review and meta-analysis. *Br J Psychiatry* [Online], 10.1192/bjp.bp.115.177261. Available: http://www.ncbi.nlm.nih.gov/pubmed/27388573 [Accessed Jul 7 2016].

Sittig, LJ, Carbonetto, P, Engel, KA, Krauss, KS, Barrios-Camacho, CM & Palmer, AA (2016). Genetic Background Limits Generalizability of Genotype-Phenotype Relationships. *Neuron,* 91**,** 1253-1259.

Sklar, P, Smoller, JW, Fan, J, Ferreira, MA, Perlis, RH, Chambert, K, . . . Purcell, SM (2008). Whole-genome association study of bipolar disorder. *Mol Psychiatry,* 13**,** 558-69.

Smith, EN, Bloss, CS, Badner, JA, Barrett, T, Belmonte, PL, Berrettini, W, . . . Kelsoe, JR (2009). Genome-wide association study of bipolar disorder in European American and African American individuals. *Mol Psychiatry,* 14**,** 755-63.

Smith, KR, Kopeikina, KJ, Fawcett-Patel, JM, Leaderbrand, K, Gao, R, Schurmann, B, . . . Penzes, P (2014). Psychiatric risk factor ANK3/ankyrin-G nanodomains regulate the structure and function of glutamatergic synapses. *Neuron,* 84**,** 399-415.

Smith, MJ, Barch, DM, Thompson, PA & Csernansky, JG (2008). Subclinical expression of schizophrenia-like symptoms in non-psychotic siblings of individuals with schizophrenia. *Schizophr Res,* 103**,** 324-5.

Snutch, TP, Leonard, JP, Gilbert, MM, Lester, HA & Davidson, N (1990). Rat brain expresses a heterogeneous family of calcium channels. *Proc Natl Acad Sci U S A,* 87**,** 3391-5.

Snutch, TP, Tomlinson, WJ, Leonard, JP & Gilbert, MM (1991). Distinct calcium channels are generated by alternative splicing and are differentially expressed in the mammalian CNS. *Neuron,* 7**,** 45-57.

Sobotzik, JM, Sie, JM, Politi, C, Del Turco, D, Bennett, V, Deller, T & Schultz, C (2009). AnkyrinG is required to maintain axo-dendritic polarity in vivo. *Proc Natl Acad Sci U S A,* 106**,** 17564-9.

Soeiro-de-Souza, MG, Otaduy, MC, Dias, CZ, Bio, DS, Machado-Vieira, R & Moreno, RA (2012). The impact of the CACNA1C risk allele on limbic structures and facial emotions recognition in bipolar disorder subjects and healthy controls. *J Affect Disord,* 141**,** 94-101.

Song, AH, Wang, D, Chen, G, Li, Y, Luo, J, Duan, S & Poo, MM (2009). A selective filter for cytoplasmic transport at the axon initial segment. *Cell,* 136**,** 1148-60.

Specht, CG & Schoepfer, R (2001). Deletion of the alpha-synuclein locus in a subpopulation of C57BL/6J inbred mice. *BMC Neurosci,* 2**,** 11.

Splawski, I, Timothy, KW, Decher, N, Kumar, P, Sachse, FB, Beggs, AH, . . . Keating, MT (2005). Severe arrhythmia disorder caused by cardiac L-type calcium channel mutations. *Proc Natl Acad Sci U S A,* 102**,** 8089-96; discussion 8086-8.

Splawski, I, Timothy, KW, Sharpe, LM, Decher, N, Kumar, P, Bloise, R, . . . Keating, MT (2004). Ca(V)1.2 calcium channel dysfunction causes a multisystem disorder including arrhythmia and autism. *Cell,* 119**,** 19-31.

Sporn, AL, Greenstein, DK, Gogtay, N, Jeffries, NO, Lenane, M, Gochman, P, . . . Rapoport, JL (2003). Progressive brain volume loss during adolescence in childhood-onset schizophrenia. *Am J Psychiatry,* 160**,** 2181-9.

Srinivasan, Y, Elmer, L, Davis, J, Bennett, V & Angelides, K (1988). Ankyrin and spectrin associate with voltage-dependent sodium channels in brain. *Nature,* 333**,** 177-80.

Stefansson, H, Ophoff, RA, Steinberg, S, Andreassen, OA, Cichon, S, Rujescu, D, . . . Collier, DA (2009). Common variants conferring risk of schizophrenia. *Nature,* 460**,** 744-7.

Steinberg, S, de Jong, S, Irish Schizophrenia Genomics, C, Andreassen, OA, Werge, T, Borglum, AD, . . . Stefansson, K (2011). Common variants at VRK2 and TCF4 conferring risk of schizophrenia. *Hum Mol Genet,* 20**,** 4076-81.

Steriade, M, McCormick, DA & Sejnowski, TJ (1993). Thalamocortical oscillations in the sleeping and aroused brain. *Science,* 262**,** 679-85.

Sullivan, PF, Kendler, KS & Neale, MC (2003). Schizophrenia as a complex trait: evidence from a meta-analysis of twin studies. *Arch Gen Psychiatry,* 60**,** 1187-92.

Susser, E, Neugebauer, R, Hoek, HW, Brown, AS, Lin, S, Labovitz, D & Gorman, JM (1996). Schizophrenia after prenatal famine. Further evidence. *Arch Gen Psychiatry,* 53**,** 25-31.

Susuki, K, Chang, KJ, Zollinger, DR, Liu, Y, Ogawa, Y, Eshed-Eisenbach, Y, . . . Rasband, MN (2013). Three mechanisms assemble central nervous system nodes of Ranvier. *Neuron,* 78**,** 469-82.

Swerdlow, NR, Benbow, CH, Zisook, S, Geyer, MA & Braff, DL (1993). A preliminary assessment of sensorimotor gating in patients with obsessive compulsive disorder. *Biol Psychiatry,* 33**,** 298-301.

Swerdlow, NR, Paulsen, J, Braff, DL, Butters, N, Geyer, MA & Swenson, MR (1995). Impaired prepulse inhibition of acoustic and tactile startle response in patients with Huntington's disease. *J Neurol Neurosurg Psychiatry,* 58**,** 192-200.

Szeszko, PR, Bilder, RM, Lencz, T, Ashtari, M, Goldman, RS, Reiter, G, . . . Lieberman, JA (2000). Reduced anterior cingulate gyrus volume correlates with executive dysfunction in men with first-episode schizophrenia. *Schizophr Res,* 43**,** 97-108.

Takano, A, Shimizu, K, Kani, S, Buijs, RM, Okada, M & Nagai, K (2000). Cloning and characterization of rat casein kinase 1epsilon. *FEBS Lett,* 477**,** 106-12.

Talkowski, ME, Rosenfeld, JA, Blumenthal, I, Pillalamarri, V, Chiang, C, Heilbut, A, . . . Gusella, JF (2012). Sequencing chromosomal abnormalities reveals neurodevelopmental loci that confer risk across diagnostic boundaries. *Cell,* 149**,** 525-37.

Tanabe, T, Takeshima, H, Mikami, A, Flockerzi, V, Takahashi, H, Kangawa, K, . . . Numa, S (1987). Primary structure of the receptor for calcium channel blockers from skeletal muscle. *Nature,* 328**,** 313-8.

Tandon, N, Bolo, NR, Sanghavi, K, Mathew, IT, Francis, AN, Stanley, JA & Keshavan, MS (2013a). Brain metabolite alterations in young adults at familial high risk for schizophrenia using proton magnetic resonance spectroscopy. *Schizophr Res,* 148**,** 59-66.

Tandon, R, Gaebel, W, Barch, DM, Bustillo, J, Gur, RE, Heckers, S, . . . Carpenter, W (2013b). Definition and description of schizophrenia in the DSM-5. *Schizophr Res,* 150**,** 3-10.

Tandon, R, Nasrallah, HA & Keshavan, MS (2009). Schizophrenia, "just the facts" 4. Clinical features and conceptualization. *Schizophr Res,* 110**,** 1-23.

Tang, ZZ, Liang, MC, Lu, S, Yu, D, Yu, CY, Yue, DT & Soong, TW (2004). Transcript scanning reveals novel and extensive splice variations in human l-type voltage-gated calcium channel, Cav1.2 alpha1 subunit. *J Biol Chem,* 279**,** 44335-43.

Tao, X, Finkbeiner, S, Arnold, DB, Shaywitz, AJ & Greenberg, ME (1998). Ca2+ influx regulates BDNF transcription by a CREB family transcription factor-dependent mechanism. *Neuron,* 20**,** 709-26.

Tao, X, West, AE, Chen, WG, Corfas, G & Greenberg, ME (2002). A calcium-responsive transcription factor, CaRF, that regulates neuronal activity-dependent expression of BDNF. *Neuron,* 33**,** 383-95.

Tarantino, LM, Gould, TJ, Druhan, JP & Bucan, M (2000). Behavior and mutagenesis screens: the importance of baseline analysis of inbred strains. *Mamm Genome,* 11**,** 555-64.

Tarricone, I, Boydell, J, Kokona, A, Triolo, F, Gamberini, L, Sutti, E, . . . Berardi, D (2016). Risk of psychosis and internal migration: Results from the Bologna First Episode Psychosis study. *Schizophr Res,* 173**,** 90-3.

Tesli, M, Koefoed, P, Athanasiu, L, Mattingsdal, M, Gustafsson, O, Agartz, I, . . . Andreassen, OA (2011). Association analysis of ANK3 gene variants in nordic bipolar disorder and schizophrenia case-control samples. *Am J Med Genet B Neuropsychiatr Genet,* 156B**,** 969-74.

Tesli, M, Skatun, KC, Ousdal, OT, Brown, AA, Thoresen, C, Agartz, I, . . . Andreassen, OA (2013). CACNA1C risk variant and amygdala activity in bipolar disorder, schizophrenia and healthy controls. *PLoS One,* 8**,** e56970.

The Schizophrenia Commission (2012). The abandoned illness: a report from the Schizophrenia Commission. London: Rethink Mental Illness.

Thimm, M, Kircher, T, Kellermann, T, Markov, V, Krach, S, Jansen, A, . . . Krug, A (2011). Effects of a CACNA1C genotype on attention networks in healthy individuals. *Psychol Med,* 41**,** 1551-61.

Thoma, P & Daum, I (2013). Comorbid substance use disorder in schizophrenia: a selective overview of neurobiological and cognitive underpinnings. *Psychiatry Clin Neurosci,* 67**,** 367-83.

Thompson, BJ & Sahai, E (2015). MST kinases in development and disease. *J Cell Biol,* 210**,** 871-82.

Thornicroft, G, Tansella, M, Becker, T, Knapp, M, Leese, M, Schene, A, . . . Group, ES (2004). The personal impact of schizophrenia in Europe. *Schizophr Res,* 69**,** 125-32.

Thornton, CE, Brown, SD & Glenister, PH (1999). Large numbers of mice established by in vitro fertilization with cryopreserved spermatozoa: implications and applications for genetic resource banks, mutagenesis screens, and mouse backcrosses. *Mamm Genome,* 10**,** 987-92.

Threadgill, DW, Yee, D, Matin, A, Nadeau, JH & Magnuson, T (1997). Genealogy of the 129 inbred strains: 129/SvJ is a contaminated inbred strain. *Mamm Genome,* 8**,** 390-3.

Tononi, G & Cirelli, C (2006). Sleep function and synaptic homeostasis. *Sleep Med Rev,* 10**,** 49-62.

Tortelli, A, Errazuriz, A, Croudace, T, Morgan, C, Murray, RM, Jones, PB, . . . Kirkbride, JB (2015). Schizophrenia and other psychotic disorders in Caribbean-born migrants and their descendants in England: systematic review and meta-analysis of incidence rates, 1950-2013. *Soc Psychiatry Psychiatr Epidemiol,* 50**,** 1039-55.

Trandafir, A, Meary, A, Schurhoff, F, Leboyer, M & Szoke, A (2006). Memory tests in first-degree adult relatives of schizophrenic patients: a meta-analysis. *Schizophr Res,* 81**,** 217-26.

Traub, AC (1972). Sleep stage deficits in chronic schizophrenia. *Psychol Rep,* 31**,** 815-20.
Trullas, R & Skolnick, P (1993). Differences in fear motivated behaviors among inbred mouse strains. *Psychopharmacology (Berl),* 111**,** 323-31.
Tsai, J & Rosenheck, RA (2013). Psychiatric comorbidity among adults with schizophrenia: A latent class analysis. *Psychiatry Research,* 210**,** 16-20.
Tse, WT, Menninger, JC, Yang-Feng, TL, Francke, U, Sahr, KE, Lux, SE, . . . Forget, BG (1991). Isolation and chromosomal localization of a novel nonerythroid ankyrin gene. *Genomics,* 10**,** 858-66.
Tsuboi, D, Kuroda, K, Tanaka, M, Namba, T, Iizuka, Y, Taya, S, . . . Kaibuchi, K (2015). Disrupted-in-schizophrenia 1 regulates transport of ITPR1 mRNA for synaptic plasticity. *Nat Neurosci,* 18**,** 698-707.
Tuckwell, HC (2012). Quantitative aspects of L-type Ca2+ currents. *Prog Neurobiol,* 96**,** 1-31.
Turetsky, BI, Calkins, ME, Light, GA, Olincy, A, Radant, AD & Swerdlow, NR (2007). Neurophysiological endophenotypes of schizophrenia: the viability of selected candidate measures. *Schizophr Bull,* 33**,** 69-94.
Ucok, A & Gaebel, W (2008). Side effects of atypical antipsychotics: a brief overview. *World Psychiatry,* 7**,** 58-62.
Ueki, A, Goto, K, Sato, N, Iso, H & Morita, Y (2006). Prepulse inhibition of acoustic startle response in mild cognitive impairment and mild dementia of Alzheimer type. *Psychiatry Clin Neurosci,* 60**,** 55-62.
Umbricht, D, Schmid, L, Koller, R, Vollenweider, FX, Hell, D & Javitt, DC (2000). Ketamine-induced deficits in auditory and visual context-dependent processing in healthy volunteers: implications for models of cognitive deficits in schizophrenia. *Arch Gen Psychiatry,* 57**,** 1139-47.
Umeda-Yano, S, Hashimoto, R, Yamamori, H, Weickert, CS, Yasuda, Y, Ohi, K, . . . Takeda, M (2014). Expression analysis of the genes identified in GWAS of the postmortem brain tissues from patients with schizophrenia. *Neurosci Lett,* 568**,** 12-6.
Untergasser, A, Nijveen, H, Rao, X, Bisseling, T, Geurts, R & Leunissen, JA (2007). Primer3Plus, an enhanced web interface to Primer3. *Nucleic Acids Res,* 35**,** W71-4.
van der Gaag, M, Nieman, DH, Rietdijk, J, Dragt, S, Ising, HK, Klaassen, RM, . . . Linszen, DH (2012). Cognitive behavioral therapy for subjects at ultrahigh risk for developing psychosis: a randomized controlled clinical trial. *Schizophr Bull,* 38**,** 1180-8.
van der Werf, M, Hanssen, M, Kohler, S, Verkaaik, M, Verhey, FR, Investigators, R, . . . Allardyce, J (2014). Systematic review and collaborative recalculation of 133,693 incident cases of schizophrenia. *Psychol Med,* 44**,** 9-16.
van Os, J & Kapur, S (2009). Schizophrenia. *Lancet,* 374**,** 635-45.
van Os, J, Kenis, G & Rutten, BP (2010). The environment and schizophrenia. *Nature,* 468**,** 203-12.
Varese, F, Smeets, F, Drukker, M, Lieverse, R, Lataster, T, Viechtbauer, W, . . . Bentall, RP (2012). Childhood adversities increase the risk of psychosis: a meta-analysis of patient-control, prospective- and cross-sectional cohort studies. *Schizophr Bull,* 38**,** 661-71.
Venter, JC, Adams, MD, Myers, EW, Li, PW, Mural, RJ, Sutton, GG, . . . Zhu, X (2001). The sequence of the human genome. *Science,* 291**,** 1304-51.

Verma, M, Bali, A, Singh, N & Jaggi, AS (2016). Investigating the role of nisoldipine in foot-shock-induced post-traumatic stress disorder in mice. *Fundam Clin Pharmacol,* 30**,** 128-36.

Vinogradov, S & Schulz, SC (2016). Behavioral and emerging pharmacologic treatment options for cognitive impairment in schizophrenia. *J Clin Psychiatry,* 77 Suppl 2**,** 12-6.

Vita, A, De Peri, L, Deste, G, Barlati, S & Sacchetti, E (2015). The Effect of Antipsychotic Treatment on Cortical Gray Matter Changes in Schizophrenia: Does the Class Matter? A Meta-analysis and Meta-regression of Longitudinal Magnetic Resonance Imaging Studies. *Biol Psychiatry,* 78**,** 403-12.

Vita, A, De Peri, L, Deste, G & Sacchetti, E (2012). Progressive loss of cortical gray matter in schizophrenia: a meta-analysis and meta-regression of longitudinal MRI studies. *Transl Psychiatry,* 2**,** e190.

Vita, A, Dieci, M, Giobbio, GM, Tenconi, F & Invernizzi, G (1997). Time course of cerebral ventricular enlargement in schizophrenia supports the hypothesis of its neurodevelopmental nature. *Schizophr Res,* 23**,** 25-30.

Voronova, A & Baltimore, D (1990). Mutations that disrupt DNA binding and dimer formation in the E47 helix-loop-helix protein map to distinct domains. *Proc Natl Acad Sci U S A,* 87**,** 4722-6.

Vyazovskiy, VV, Ruijgrok, G, Deboer, T & Tobler, I (2006). Running wheel accessibility affects the regional electroencephalogram during sleep in mice. *Cereb Cortex,* 16**,** 328-36.

Vyazovskiy, VV & Tobler, I (2008). Handedness leads to interhemispheric EEG asymmetry during sleep in the rat. *J Neurophysiol,* 99**,** 969-75.

Vyazovskiy, VV, Welker, E, Fritschy, JM & Tobler, I (2004). Regional pattern of metabolic activation is reflected in the sleep EEG after sleep deprivation combined with unilateral whisker stimulation in mice. *Eur J Neurosci,* 20**,** 1363-70.

Walsh, T, McClellan, JM, McCarthy, SE, Addington, AM, Pierce, SB, Cooper, GM, . . . Sebat, J (2008). Rare structural variants disrupt multiple genes in neurodevelopmental pathways in schizophrenia. *Science,* 320**,** 539-43.

Wang, C, Wei, Z, Chen, K, Ye, F, Yu, C, Bennett, V & Zhang, M (2014). Structural basis of diverse membrane target recognitions by ankyrins. *Elife,* 3.

Wang, C, Yu, C, Ye, F, Wei, Z & Zhang, M (2012). Structure of the ZU5-ZU5-UPA-DD tandem of ankyrin-B reveals interaction surfaces necessary for ankyrin function. *Proc Natl Acad Sci U S A,* 109**,** 4822-7.

Waterhouse, AM, Procter, JB, Martin, DM, Clamp, M & Barton, GJ (2009). Jalview Version 2--a multiple sequence alignment editor and analysis workbench. *Bioinformatics,* 25**,** 1189-91.

Weinberger, DR (1987). Implications of normal brain development for the pathogenesis of schizophrenia. *Arch Gen Psychiatry,* 44**,** 660-9.

Welch, R & Chue, P (2000). Antipsychotic agents and QT changes. *J Psychiatry Neurosci,* 25**,** 154-60.

Wemhoner, K, Friedrich, C, Stallmeyer, B, Coffey, AJ, Grace, A, Zumhagen, S, . . . Decher, N (2015). Gain-of-function mutations in the calcium channel CACNA1C (Cav1.2) cause non-syndromic long-QT but not Timothy syndrome. *J Mol Cell Cardiol,* 80**,** 186-95.

Westenbroek, RE, Ahlijanian, MK & Catterall, WA (1990). Clustering of L-type Ca2+ channels at the base of major dendrites in hippocampal pyramidal neurons. *Nature,* 347**,** 281-4.

Whalley, HC, Harris, JC & Lawrie, SM (2007). The neurobiological underpinnings of risk and conversion in relatives of patients with schizophrenia. *Int Rev Psychiatry,* 19**,** 383-97.

Wheeler, DG, Barrett, CF, Groth, RD, Safa, P & Tsien, RW (2008). CaMKII locally encodes L-type channel activity to signal to nuclear CREB in excitation-transcription coupling. *J Cell Biol,* 183**,** 849-63.

White, T, Langen, C, Schmidt, M, Hough, M & James, A (2015). Comparative neuropsychiatry: white matter abnormalities in children and adolescents with schizophrenia, bipolar affective disorder, and obsessive-compulsive disorder. *Eur Psychiatry,* 30**,** 205-13.

Whiteford, HA, Degenhardt, L, Rehm, J, Baxter, AJ, Ferrari, AJ, Erskine, HE, . . . Vos, T (2013). Global burden of disease attributable to mental and substance use disorders: findings from the Global Burden of Disease Study 2010. *Lancet,* 382**,** 1575-86.

Williams, HJ, Craddock, N, Russo, G, Hamshere, ML, Moskvina, V, Dwyer, S, . . . O'Donovan, MC (2011). Most genome-wide significant susceptibility loci for schizophrenia and bipolar disorder reported to date cross-traditional diagnostic boundaries. *Hum Mol Genet,* 20**,** 387-91.

Wirgenes, KV, Sonderby, IE, Haukvik, UK, Mattingsdal, M, Tesli, M, Athanasiu, L, . . . Andreassen, OA (2012). TCF4 sequence variants and mRNA levels are associated with neurodevelopmental characteristics in psychotic disorders. *Transl Psychiatry,* 2**,** e112.

Wirgenes, KV, Tesli, M, Inderhaug, E, Athanasiu, L, Agartz, I, Melle, I, . . . Djurovic, S (2014). ANK3 gene expression in bipolar disorder and schizophrenia. *Br J Psychiatry,* 205**,** 244-5.

Wittwer, CT, Reed, GH, Gundry, CN, Vandersteen, JG & Pryor, RJ (2003). High-resolution genotyping by amplicon melting analysis using LCGreen. *Clin Chem,* 49**,** 853-60.

Wolke, D, Lereya, ST, Fisher, HL, Lewis, G & Zammit, S (2014). Bullying in elementary school and psychotic experiences at 18 years: a longitudinal, population-based cohort study. *Psychol Med,* 44**,** 2199-211.

Wotjak, CT (2003). C57BLack/BOX? The importance of exact mouse strain nomenclature. *Trends Genet,* 19**,** 183-4.

Wright, C, Calhoun, VD, Ehrlich, S, Wang, L, Turner, JA & Bizzozero, NI (2015). Meta gene set enrichment analyses link miR-137-regulated pathways with schizophrenia risk. *Front Genet,* 6**,** 147.

Wright, C, Turner, JA, Calhoun, VD & Perrone-Bizzozero, N (2013). Potential Impact of miR-137 and Its Targets in Schizophrenia. *Front Genet,* 4**,** 58.

Wulff, K, Gatti, S, Wettstein, JG & Foster, RG (2010). Sleep and circadian rhythm disruption in psychiatric and neurodegenerative disease. *Nat Rev Neurosci,* 11**,** 589-99.

Wulff, K, Joyce, E, Middleton, B, Dijk, DJ & Foster, RG (2006). The suitability of actigraphy, diary data, and urinary melatonin profiles for quantitative assessment of sleep disturbances in schizophrenia: a case report. *Chronobiol Int,* 23**,** 485-95.

Wulff, K, Porcheret, K, Cussans, E & Foster, RG (2009). Sleep and circadian rhythm disturbances: multiple genes and multiple phenotypes. *Curr Opin Genet Dev,* 19**,** 237-46.

Xia, S, Zhou, X, Wang, T, Zhang, Q, Li, Q, Liu, Y, . . . Zhao, X (2015). Experimental validation of candidate schizophrenia gene CALN1 as a target for microRNA-137. *Neurosci Lett,* 602**,** 110-4.

Xie, W 2010. Assessment of Pain in Animals. *Animal Models of Pain.*

Xiong, L, Kleerekoper, QK, He, R, Putkey, JA & Hamilton, SL (2005). Sites on calmodulin that interact with the C-terminal tail of Cav1.2 channel. *J Biol Chem,* 280**,** 7070-9.

Xu, B, Roos, JL, Levy, S, van Rensburg, EJ, Gogos, JA & Karayiorgou, M (2008). Strong association of de novo copy number mutations with sporadic schizophrenia. *Nat Genet,* 40**,** 880-5.

Xu, MQ, Sun, WS, Liu, BX, Feng, GY, Yu, L, Yang, L, . . . He, L (2009). Prenatal malnutrition and adult schizophrenia: further evidence from the 1959-1961 Chinese famine. *Schizophr Bull,* 35**,** 568-76.

Xue, Y, Liu, Z, Cao, J, Ma, Q, Gao, X, Wang, Q, . . . Ren, J (2011). GPS 2.1: enhanced prediction of kinase-specific phosphorylation sites with an algorithm of motif length selection. *Protein Eng Des Sel,* 24**,** 255-60.

Yamankurt, G, Wu, HC, McCarthy, M & Cunha, SR (2015). Exon organization and novel alternative splicing of Ank3 in mouse heart. *PLoS One,* 10**,** e0128177.

Yang, Y, Ogawa, Y, Hedstrom, KL & Rasband, MN (2007). betaIV spectrin is recruited to axon initial segments and nodes of Ranvier by ankyrinG. *J Cell Biol,* 176**,** 509-19.

Yin, L, Wang, J, Klein, PS & Lazar, MA (2006). Nuclear receptor Rev-erbalpha is a critical lithium-sensitive component of the circadian clock. *Science,* 311**,** 1002-5.

Yoshimizu, T, Pan, JQ, Mungenast, AE, Madison, JM, Su, S, Ketterman, J, . . . Tsai, LH (2015). Functional implications of a psychiatric risk variant within CACNA1C in induced human neurons. *Mol Psychiatry,* 20**,** 162-9.

Yoshimura, T & Rasband, MN (2014). Axon initial segments: diverse and dynamic neuronal compartments. *Curr Opin Neurobiol,* 27**,** 96-102.

Yuan, A, Yi, Z, Wang, Q, Sun, J, Li, Z, Du, Y, . . . Yu, S (2012). ANK3 as a risk gene for schizophrenia: new data in Han Chinese and meta analysis. *Am J Med Genet B Neuropsychiatr Genet,* 159B**,** 997-1005.

Yue, F, Cheng, Y, Breschi, A, Vierstra, J, Wu, W, Ryba, T, . . . Mouse, EC (2014). A comparative encyclopedia of DNA elements in the mouse genome. *Nature,* 515**,** 355-64.

Zemrak, WR & Kenna, GA (2008). Association of antipsychotic and antidepressant drugs with Q-T interval prolongation. *Am J Health Syst Pharm,* 65**,** 1029-38.

Zhang, Q, Shen, Q, Xu, Z, Chen, M, Cheng, L, Zhai, J, . . . Chen, C (2012). The effects of CACNA1C gene polymorphism on spatial working memory in both healthy controls and patients with schizophrenia or bipolar disorder. *Neuropsychopharmacology,* 37**,** 677-84.

Zhang, X & Bennett, V (1996). Identification of O-linked N-acetylglucosamine modification of ankyrinG isoforms targeted to nodes of Ranvier. *J Biol Chem,* 271**,** 31391-8.

Zhang, X & Bennett, V (1998). Restriction of 480/270-kD ankyrin G to axon proximal segments requires multiple ankyrin G-specific domains. *J Cell Biol,* 142**,** 1571-81.

Zhang, X, Davis, JQ, Carpenter, S & Bennett, V (1998). Structural requirements for association of neurofascin with ankyrin. *J Biol Chem,* 273**,** 30785-94.

Zhang, XY, Fan, FM, Chen, DC, Tan, YL, Tan, SP, Hu, K, . . . Soares, JC (2016). Extensive white matter abnormalities and clinical symptoms in drug-naive patients with first-episode schizophrenia: a voxel-based diffusion tensor imaging study. *J Clin Psychiatry,* 77**,** 205-11.

Zhao, X & Rothstein, R (2002). The Dun1 checkpoint kinase phosphorylates and regulates the ribonucleotide reductase inhibitor Sml1. *Proc Natl Acad Sci U S A,* 99**,** 3746-51.

Zhou, D, Lambert, S, Malen, PL, Carpenter, S, Boland, LM & Bennett, V (1998). AnkyrinG is required for clustering of voltage-gated Na channels at axon initial segments and for normal action potential firing. *J Cell Biol,* 143**,** 1295-304.

Zhou, J, Olcese, R, Qin, N, Noceti, F, Birnbaumer, L & Stefani, E (1997). Feedback inhibition of Ca^{2+} channels by Ca^{2+} depends on a short sequence of the C terminus that does not include the Ca^{2+}-binding function of a motif with similarity to Ca^{2+}-binding domains. *Proc Natl Acad Sci U S A,* 94**,** 2301-5.

Zhuang, Y, Cheng, P & Weintraub, H (1996). B-lymphocyte development is regulated by the combined dosage of three basic helix-loop-helix genes, E2A, E2-2, and HEB. *Mol Cell Biol,* 16**,** 2898-905.

Zühlke, RD, Pitt, GS, Deisseroth, K, Tsien, RW & Reuter, H (1999). Calmodulin supports both inactivation and facilitation of L-type calcium channels. *Nature,* 399**,** 159-62.

Zühlke, RD, Pitt, GS, Tsien, RW & Reuter, H (2000). Ca^{2+}-sensitive inactivation and facilitation of L-type Ca^{2+} channels both depend on specific amino acid residues in a consensus calmodulin-binding motif in the alpha1C subunit. *J Biol Chem,* 275**,** 21121-9.

Zühlke, RD & Reuter, H (1998). Ca2+-sensitive inactivation of L-type Ca2+ channels depends on multiple cytoplasmic amino acid sequences of the alpha1C subunit. *Proc Natl Acad Sci U S A,* 95**,** 3287-94.

Zweier, C, Peippo, MM, Hoyer, J, Sousa, S, Bottani, A, Clayton-Smith, J, . . . Rauch, A (2007). Haploinsufficiency of TCF4 causes syndromal mental retardation with intermittent hyperventilation (Pitt-Hopkins syndrome). *Am J Hum Genet,* 80**,** 994-1001.